

IMAGING THE VISUAL PATHWAY IN HUMAN ALBINISM



**This thesis is submitted for the degree of
Doctor of Philosophy at the University of Leicester**

By

Dr Sarim Ather BSc. (Hons.) MBChB (Hons.)

Ophthalmology Group

University of Leicester

June 2016

In loving memory of my late grandfather

Muhammad Naseer Ahsan

Former Auditor General of Pakistan

and my inspiration in life

ABSTRACT

Dr Sarim Ather BSc (Hons) MBChB (Hons)

Albinism refers to a group of genetic abnormalities that are associated with profound defects throughout the visual pathway. These include foveal hypoplasia, optic nerve anomalies, chiasmal misrouting, visual cortex reorganisation, and nystagmus. This study utilises optical coherence tomography and magnetic resonance imaging to assess the visual pathway in a large cohort of patients.

We find that in albinism, there is maldevelopment of the fovea, with a continuation of the inner retinal layers and a failure of the photoreceptor layers to specialize. The latter abnormality is the biggest contributor to reduced visual acuity seen in albinism.

The optic nerve head is characterized by presence of excess glial tissue within the optic rim indicating incomplete maturation. In addition, there is reduced peripapillary retinal nerve fibre layer thickness consistent with previous histology reports of reduced ganglion cell numbers in albinism.

We demonstrate the ability of diffusion tractography to quantify abnormal chiasmal decussation for the first time. Moreover, we find that cortical abnormalities are related to melanin levels within the retinal pigment epithelium and axonal disorganisation.

Our results show that nystagmus severity is related to the degree of foveal maldevelopment. This finding adds credence to the increasing recognition of the importance of sensory abnormalities in generating nystagmus.

In conclusion, we find that in albinism, normal development of the visual pathway appears to have halted prior to reaching completion. Patients with albinism show a spectrum of anomalies ranging from resembling normality to being grossly atypical. This spectrum closely resembles stages in normal visual development.

Our findings represent a step forward in the scientific understanding of visual deficits associated with albinism and are likely to aid clinicians in the management of affected patients.

ACKNOWLEDGEMENTS

This work would not have been possible without the generosity of many volunteers who chose to give up their time to take part in this study.

I would like to express gratitude to my two principle supervisors Professor Irene Gottlob and Dr Frank Proudlock for providing me the opportunity to undertake this research. I could not have imagined having better mentors to help me navigate past the multiple obstacles that I encountered along the way.

Alongside them, I would also like to thank all my collaborators and the staff working within the Ophthalmology group at the University of Leicester. In particular Mr Viral Sheth who was helped with recruitment of participants and Dr Rebecca McLean who guided me through the acquisition and analysis of the eye movement recordings. In addition, there are a number of ophthalmologists and orthoptists working at the Leicester Royal Infirmary whose clinical proficiency was vital in assessment of the study participants.

At the University of Nottingham, Dr Robert Dineen was always pillar of strength. His enthusiasm and expertise were vital at every step from getting the MRI study off the ground to its completion. Credit also goes to the staff at the Sir Peter Mansfield Magnetic Resonance Centre for their help with acquisition of the MRI scans.

Thanks to the Wolfson and Medisearch foundations for providing me financial support to complete this study and staff at the Leicester Medical School who allowed me to take time out of my medical training to embark on this research.

Finally, and most importantly, I would like to make a special mention of my wife Talia, parents Salik and Saadia and sisters Soofia, Fatima and Nabeeha for their patience, understanding and support through the course of this research.

CONTENTS

CHAPTER 1 INTRODUCTION	13
1.1 OPTICAL COHERENCE TOMOGRAPHY.....	15
1.1.1 Background.....	15
1.1.2 Principles behind OCT.....	16
1.2 MRI.....	18
1.2.1 Background.....	18
1.2.2 Principles behind MRI.....	18
1.2.3 Diffusion tensor imaging	20
1.3 ALBINISM	22
1.3.1 Genetic Basis Of Albinism	22
1.4 VISUAL PATHWAY ABNORMALITIES IN ALBINISM	30
1.4.1 Iris Transillumination.....	30
1.4.2 Refractive Errors	33
1.4.3 Strabismus.....	33
1.4.4 Macular Transparency.....	34
1.4.5 Foveal Abnormalities.....	35
1.4.6 Optic Nerve Abnormalities.....	43
1.4.7 Chiasmal abnormalities.....	49
1.4.8 Lateral Geniculate Nucleus.....	55
1.4.9 Visual Cortex Abnormalities.....	56
1.4.10 Nystagmus.....	63
1.5 AIMS.....	75
1.5.1 Overview.....	75
1.5.2 Specific Aims.....	76
CHAPTER 2 METHODS.....	80
2.1 RECRUITMENT OF VOLUNTEERS	81
2.1.1 Albinism Group.....	81
2.1.2 Control Group.....	81
2.1.3 Inclusion and Exclusion Criteria.....	82
2.1.4 Ethical Approval and Consent.....	82
2.2 OCT SCANNING.....	83
2.2.1 Scan acquisition	83
2.2.2 Data Analysis.....	86
MRI SCANNING.....	97

2.2.3	Scan Acquisiiton.....	97
2.3	EYE MOVEMENT RECORDING.....	105
2.3.1	Data Acquisition.....	105
2.3.2	Data Analysis.....	107
2.4	VISUAL EVOKED POTENTIALS	111
2.4.1	Data Acquisition.....	111
2.4.2	Data Analysis.....	113
2.5	STATISTICAL ANALYSES.....	115
CHAPTER 3 RESULTS & DISCUSSION		116
3.1	CLINICAL FEATURES.....	117
3.2	FOVEA.....	120
3.2.1	Background.....	120
3.2.2	Summary of Aims.....	120
3.2.3	Findings.....	120
3.2.4	Dicussion	130
3.3	OPTIC NERVE	136
3.3.1	Background.....	136
3.3.2	Summary of aims	136
3.3.3	Findings.....	136
3.3.4	Discussion	150
3.4	OPTIC CHIASM.....	157
3.4.1	Background.....	157
3.4.2	Summary of Aims.....	157
3.4.3	Findings.....	158
3.4.4	Discussion	170
3.5	CORTEX.....	174
3.5.1	Background.....	174
3.5.2	Summary of aims	174
3.5.3	Findings.....	175
3.5.4	Discussion	182
3.6	NYSTAGMUS.....	185
3.6.1	Background.....	185
3.6.2	Findings.....	185
3.6.3	Discussion	192
CHAPTER 4 CONCLUSION		196
4.1	SUMMARY OF FINDINGS.....	197
4.1.1	Comparison of Ocular and Post-Orbital Structures.....	200

4.1.2	<i>Comparison Of Anatomical and Functional Measurements</i>	202
4.2	SCIENTIFIC IMPACT	204
4.3	CLINICAL IMPLICATIONS.....	205
4.4	LIMITATIONS AND FUTURE WORK.....	207
4.5	FINAL CONCLUSION.....	208
CHAPTER 5	APPENDICES	242

LIST OF TABLES

TABLE 1-1: INNERVATION AND ACTIONS OF THE SIX EXTRAOCULAR MUSCLES.....	63
TABLE 3-1: SUMMARY DEMOGRAPHICS OF ALBINISM PATIENTS TAKING PART IN THE STUDY	119
TABLE 3-2: COMPARISON OF RETINAL LAYER THICKNESS BETWEEN THE LEFT AND RIGHT EYES OF THE ALBINISM AND CONTROL GROUPS.....	123
TABLE 3-3: COMPARISON OF BCVA FOVEAL MEASURES IN ALBINISM.	127
TABLE 3-4: COMPARISON OF VEP ASYMMETRY WITH FOVEAL PARAMETERS IN ALBINISM	128
TABLE 3-5: INTRA-CLASS CORRELATION COEFFICIENTS FROM TEST-RETEST ANALYSIS	137
TABLE 3-6:. DISC, CUP AND RIM AREAS AND PP RNFL THICKNESS COMPARED BETWEEN THE TWO EYES.	138
TABLE 3-7: COMPARISON OF ONH, FOVEAL AND CLINICAL MEASURES.....	149
TABLE 3-8: OPTIC NERVE, TRACT AND CHIASM COMPARISON BETWEEN THE ALBINISM AND CONTROL GROUPS.	159
TABLE 3-9: COMPARISON OF FOVEAL DEVELOPMENT WITH MRI AND DTI MEASUREMENTS	165
TABLE 3-10: COMPARISON OF ONH MORPHOLOGY WITH MRI AND DTI MEASUREMENTS	167
TABLE 3-11: COMPARISON OF BEST-CORRECTED VISUAL ACUITY (BCVA) WITH OPTIC NERVE, TRACT AND CHIASM AREAS MEASURED USING MRI AND DIFFUSION TRACTOGRAPHY DATA.....	169
TABLE 3-12: COMPARISON OF PHOTORECEPTOR LAYER THICKNESS, PROCESSING LAYER THICKNESS AND FOVEAL DEVELOPMENT INDEX (FDI) WITH CORTICAL THICKNESS AND VOLUME AT THE OCCIPITAL POLE.....	176
TABLE 3-13: COMPARISON OF OPTIC DISC, CUP AND RIM AREAS MEASURED USING OCT WITH CORTICAL THICKNESS AND VOLUME	177
TABLE 3-14: COMPARISON OF CORTICAL THICKNESS AND VOLUME WITH PP RNFL THICKNESS	179
TABLE 3-15: COMPARISON OF NYSTAGMUS SEVERITY WITH FOVEAL DEVELOPMENT.....	187
TABLE 3-16: COMPARISON OF NYSTAGMUS SEVERITY WITH ONH MORPHOLOGY	189
TABLE 3-17: COMPARISON OF NYSTAGMUS SEVERITY VEP ASYMMETRY	190
TABLE 4-1 SUMMARY OF KEY ANATOMICAL ABNORMALITIES FOUND IN ALBINISM AT THE LEVEL OF THE FOVEA, OPTIC NERVE HEAD, OPTIC CHIASM AND VISUAL CORTEX.....	197
TABLE 4-2: SUMMARY OF KEY FINDINGS WHILE COMPARING FOVEAL AND OPTIC NERVE HEAD ABNORMALITIES WITH POST-ORBITAL OPTIC NERVES, OPTIC CHIASM, OPTIC TRACTS AND THE VISUAL CORTEX.	200
TABLE 4-3: COMPARISON OF ANATOMICAL ABNORMALITIES AT THE FOVEA, OPTIC NERVE HEAD, OPTIC CHIASM AND VISUAL CORTEX WITH NYSTAGMUS, BEST CORRECTED VISUAL ACUITY AND VEP ASYMMETRY.....	203

LIST OF FIGURES

FIGURE 1-1: SCHEMATIC DIAGRAM OF AN OCT SET UP.	17
FIGURE 1-2 ILLUSTRATION OF THE BEHAVIOUR OF SPINS IN ABSENCE (A) AND PRESENCE (B) OF A STRONG MAGNETIC FIELD B_0	18
FIGURE 1-3 ILLUSTRATION OF ISOTROPIC AND ANISOTROPIC DIFFUSION.....	20
FIGURE 1-4 SCHEMATIC SHOWING ANISOTROPIC DIFFUSION.....	21
FIGURE 1-5: EFFECT OF KNOWN GENETIC DEFECTSON STAGES OF MELANIN SYNTHESIS.....	23
FIGURE 1-6: HISTOLOGICAL APPEARANCE OF THE IRIS.....	30
FIGURE 1-7: SUMMERS' CLASSIFICATION FOR IRIS TRANSILLUMINATION.....	31
FIGURE 1-8 COMPARISON OF OPTICAL COHERENCE TOMOGRAPHY IMAGES OF THE IRIS FROM HEALTHY CONTROL AND PATIENT WITH ALBINISM	31
FIGURE 1-9: COMPARISON OF MEAN IRIS LAYER THICKNESS IN ALBINISM PATIENTS AND HEALTHY CONTROLS AVERAGED BETWEEN LEFT AND RIGHT EYES.	32
FIGURE 1-10: SCHEMATIC DIAGRAM ILLUSTRATING HOW ANGLE KAPPA IS CALCULATED.....	33
FIGURE 1-11: GRADING SYSTEM FOR MACULAR TRANSPARENCY.....	34
FIGURE 1-12: SCHEMATIC DIAGRAM ILLUSTRATING THE SYNAPSES BETWEEN CELLS WITHIN THE DIFFERENT LAYERS OF THE RETINA.....	35
FIGURE 1-13: CROSS-SECTIONAL HISTOLOGY OF THE FOVEA	38
FIGURE 1-14: FUNDUS PHOTOGRAPH OF A HEALTHY OPTIC DISC	44
FIGURE 1-15: SCHEMATIC DIAGRAM OF THE OPTIC NERVE HEAD.....	45
FIGURE 1-16: FUNDUS PHOTOGRAPH SHOWING AN OPTIC NERVE HEAD WITH BERGMEISTER PAPILLA.....	45
FIGURE 1-17: SCHEMATIC DIAGRAM SHOWING THE DIFFERENCE IN THE ORGANISATION OF UNCROSSED FIBRES IN NORMALLY PIGMENTED RODENTS AND PRIMATES.....	50
FIGURE 1-18: SCHEMATIC COMPARING NORMAL VISUAL PATHWAYS AND MISROUTING SEEN IN ALBINISM	53
FIGURE 1-19: COMPARISON OF MRI IMAGES OF THE OPTIC CHIASM IN AN INDIVIDUAL WITH ALBINISM AND HEALTHY VOLUNTEER	54
FIGURE 1-20: SCHEMATICS DIAGRAM OF THE OCULOMOTOR COMMAND SYSTEM.....	66
FIGURE 1-21: CLASSIFICATION OF INFANTILE NYSTAGMUS	68
FIGURE 1-22: NYSTAGMUS CHARACTERISTICS.....	69
FIGURE 1-23: NYSTAGMUS WAVEFORMS AS CLASSIFIED BY DELL'OSSO AND DAROFF	70
FIGURE 1-24: ILLUSTRATION OF FOVEATION PERIODS.....	71
FIGURE 1-25: CHANGE IN NYSTAGMUS WAVEFORMS AT VARIOUS GAZE POSITIONS	71
FIGURE 2-1: A 3-DIMENSIONAL SCAN OUTLINING THE DIMENSIONS OF THE OCT SCAN	84
FIGURE 2-2: SOCT COPERNICUS HR DEVICE THAT WAS USED FOR THIS STUDY.....	85
FIGURE 2-3: DEVELOPMENT SIGNS USED TO IDENTIFY THE FOVEA IN THE OCT SCAN OF PATIENTS WITH ALBINISM	86
FIGURE 2-4: GRADING SYSTEM FOR ASSESSMENT OF FOVEAL HYPOPLASIA IN ALBINISM.....	88
FIGURE 2-5: FOVEAL B-SCAN PRE-FLATTENING (LEFT) AND POST-FLATTENING (RIGHT)	89
FIGURE 2-6: FIGURE ILLUSTRATING THE BOUNDARIES USED TO DIFFERENTIATE RETINAL LAYERS	90

FIGURE 2-7: COMPARISON OF FOVEAL RPE COMPLEX IN HEALTHY CONTROL (LEFT) AND ALBINISM (RIGHT).....	92
FIGURE 2-8: RE-ALIGNMENT OF B-SCANS TO CORRECT MOTION ARTEFACTS CAUSED BY NYSTAGMUS	93
FIGURE 2-9: METHOD FOR ESTIMATING DISC, RIM AND CUP DIMENSIONS.....	94
FIGURE 2-10: THE 3T SCANNER AT SPMMRC USED FOR THIS STUDY.	98
FIGURE 2-11: SCHEMATIC SHOWING HOW OPTIC NERVE, CHIASM AND TRACT DIMENSIONS WERE ACQUIRED.....	99
FIGURE 2-12: EXAMPLE DTI DATA STREAMLINE DATA FROM ALBINISM AND CONTROL VOLUNTEERS	102
FIGURE 2-13: MRI IMAGE PRE AND POST SKULL STRIPPING.....	103
FIGURE 2-14: SCHEMATIC SHOWING HOW CORTICAL THICKNESS IS MEASURED USING FREESURFER	104
FIGURE 2-15: THE EYE MOVEMENT RECORDING SETUP.....	105
FIGURE 2-16: DIAGRAM INDICATING THE DISTANCE BETWEEN THE PATIENTS AND THE PROJECTOR SCREEN.....	106
FIGURE 2-17: FOVEATION DATA PRE-CALIBRATION AND POST-CALIBRATION	107
FIGURE 2-18: CALIBRATION OF DATA.....	108
FIGURE 2-19: SCREENSHOT OF MICROSOFT EXCEL SPREADSHEET WITH VALUES FOR NYSTAGMUS PARAMETERS AND THEIR GRAPHICAL REPRESENTATION.....	110
FIGURE 2-20: ELECTRODES POSITIONS USED FOR VEP MEASUREMENTS	111
FIGURE 2-21: PATIENT UNDERGOING VISUAL EVOKED RESPONSE TESTING	112
FIGURE 2-22: EXAMPLE VEP TRACES FROM A NORMALLY PIGMENTED AND ALBINISM VOLUNTEERS	113
FIGURE 2-23: QUANTIFICATION OF VEP RESPONSE LATERALISATION.....	114
FIGURE 3-1: DEGREE OF FOVEAL HYPOPLASIA SEEN IN ALBINISM PATIENTS.....	121
FIGURE 3-2: COMPARISON OF OCT APPEARANCE OF THE FOVEA IN A HEALTHY CONTROL.....	122
FIGURE 3-3: BAR CHART ILLUSTRATING THE MEAN THICKNESS OF EACH RETINAL LAYER AT THE FOVEA IN BOTH ALBINISM AND CONTROL GROUPS	124
FIGURE 3-4: PLOT OF TOTAL PHOTORECEPTOR LAYER THICKNESS AGAINST PROCESSING LAYER THICKNESS AT THE FOVEA FOR 47 PATIENTS WITH ALBINISM.....	125
FIGURE 3-5: BAR CHART ILLUSTRATING THE CONTRIBUTION OF PROCESSING LAYERS (RED COLOURS) AND PHOTORECEPTOR LAYERS (BLUE COLOURS) TO OVERALL RETINAL THICKNESS.....	126
FIGURE 3-6: COMPARISON OF BCVA WITH FOVEAL MEASUREMENTS	129
FIGURE 3-7: COMPARISON OF OPTIC NERVE OCT SCANS OF THE RIGHT EYES FROM AN ALBINISM PATIENT AND A HEALTHY VOLUNTEER.....	140
FIGURE 3-8: COMPARISON OF FUNDUS PHOTOGRAPHS AND B SCAN CROSS-SECTIONAL IMAGES OF LEFT EYES THROUGH THE DEEPEST PART OF THE CUP FOR FOUR PATIENTS WITH ALBINISM.....	141
FIGURE 3-9: SCHEMATIC DIAGRAMS COMPARING THE MEDIAN DIMENSIONS OF ALBINISM AND CONTROL VOLUNTEERS FOR DISC, RIM AND CUP IN EN-FACE VIEW	142
FIGURE 3-10: CROSS SECTIONAL SCHEMATIC DIAGRAM OF OPTIC NERVE HEAD.....	144
FIGURE 3-11: A. OPTIC DISC TORSION (CALCULATED FROM THE EN-FACE VIEW), B. OPTIC DISC TILT AND DISC EDGE DISTORTION (CALCULATED FROM THE CROSS SECTIONAL VIEW).....	146
FIGURE 3-12: PERCENTAGE DIFFERENCE IN MEAN PERIPAPILLARY RETINAL NERVE FIBRE LAYER (PPRNFL) THICKNESS BETWEEN PARTICIPANTS WITH ALBINISM AND CONTROLS.....	147

FIGURE 3-13: COMPARISON OF LEFT EYE OPTIC NERVE HEAD OCT SCANS FROM PATIENTS WITH PERSISTENT HYALOID ARTERY AND OUR ALBINISM COHORT..	152
FIGURE 3-14 : COMPARISON OF THE OPTIC NERVE, TRACT AND CHIASM WIDTH AND AREA DIFFERENCES BETWEEN ALBINISM AND CONTROL GROUPS	160
FIGURE 3-15: COMPARISON OF TOTAL NUMBER OF STREAMLINE (LOG_{10}) BETWEEN OPTIC NERVE AND OPTIC TRACT ROIs	161
FIGURE 3-16 : COMPARISON OF THE STREAMLINE DECUSSATION INDEX BETWEEN ALBINISM AND CONTROL GROUPS	162
FIGURE 3-17 COMPARISON OF CROSS-HEMISPHERIC CONNECTIVITY AT THE CHIASM MEASURED USING DTI AND VEP ASYMMETRY SEEN IN PATIENTS WITH ALBINISM.....	163
FIGURE 3-18: COMPARISON OF TOTAL CONNECTIVITY AT THE CHIASM ESTIMATED USING DTI WITH FOVEAL DEVELOPMENT INDEX IN ALBINISM.	164
FIGURE 3-19: COMPARISON OF TEMPORAL PPRNFL THICKNESS MEASURED USING OCT WITH THE IPSI LATERAL OPTIC NERVE (A) AND CONTRALATERAL OPTIC TRACT (B) AREA MEASURED USING MRI.....	168
FIGURE 3-20: COMPARISON OF OCCIPITAL POLE THICKNESS AND VOLUME AVERAGED ACROSS BOTH HEMISPHERES BETWEEN THE ALBINISM AND CONTROL GROUPS.....	175
FIGURE 3-21: COMPARISON OF FOVEAL RETINAL PIGMENT EPITHELIUM (RPE) THICKNESS MEASURED USING OCT WITH THE CORTICAL THICKNESS IN THE CONTRALATERAL (LEFT) AND IPSILATERAL (RIGHT) OCCIPITAL POLE.	176
FIGURE 3-22: COMPARISON OF CORTICAL THICKNESS AT THE OCCIPITAL POLE WITH OPTIC DISC (A) AND RIM (B) AREAS AVERAGED ACROSS BOTH EYES OF PATIENTS WITH ALBINISM.....	178
FIGURE 3-23: COMPARISON OF SUPERIOR (A) AND NASAL (B) PPRNFL THICKNESS OF EACH EYE IN THE ALBINISM GROUP WITH CORTICAL THICKNESS AT THE OCCIPITAL POLE OF THE CONTRALATERAL HEMISPHERE.	180
FIGURE 3-24: COMPARISON OF MEAN CORTICAL THICKNESS AT THE OCCIPITAL POLE, WITH CHIASM AREA IN ALBINISM PATIENTS	181
FIGURE 3-25: COMPARISON OF NYSTAGMUS AMPLITUDE WITH FOVEAL DEVELOPMENT, PHOTORECEPTOR AND PROCESSING LAYERS.....	188
FIGURE 3-26: COMPARISON OF NYSTAGMUS CHARACTERISTICS OF AMPLITUDE WITH FOVEAL DEVELOPMENT INDEX AND VISUAL EVOKED POTENTIAL ASYMMETRY	191

LIST OF ABBREVIATIONS

BCVA	=	Best corrected visual acuity
CSF	=	Cerebrospinal fluid
DTI	=	Diffusion tensor imaging
EMR	=	Eye movement recordings
FAZ	=	Foveal avascular zone
GCL	=	Ganglion cell layer
IPL	=	Inner plexiform layer
IN	=	Infantile nystagmus
INL	=	Inner nuclear layer
IS	=	Inner segment (photoreceptor)
LGN	=	Lateral geniculate nucleus
logMAR	=	logarithm of the minimum angle of resolution
MRI	=	Magnetic resonance imaging
NAFX	=	Extended nystagmus acuity function
OCT	=	Optical coherence tomography
OPL	=	Outer plexiform layer
ONH	=	Optic nerve head
OS	=	Outer segment (photoreceptor)
ppRNFL	=	Peripapillary retinal nerve fibre layer
RNFL	=	Retinal nerve fibre layer
RPE	=	Retinal pigment epithelium
TD-OCT	=	Time domain optical coherence tomography
SBA	=	Surface based analysis
SD-OCT	=	Spectral domain OCT
VBM	=	Voxel based morphometry
VEP	=	Visual evoked potential

LIST OF PUBLICATIONS ARISING FROM THIS THESIS

Published papers:

Mohammad S, Gottlob I, Kumar A, Thomas M, Degg C, Sheth V, Proudlock FA. "The Functional Significance of Foveal Abnormalities in Albinism Measured Using Spectral-Domain Optical Coherence Tomography." *Ophthalmology*, 2011 Aug; 118(8):1645-52.

Mohammad S, Gottlob I, Sheth V, Pilat A, Lee H, Pollheimer E, Proudlock FA. "Characterization of Abnormal Optic Nerve Head Morphology in Albinism Using Optical Coherence Tomography." *Invest Ophthalmol Vis Sci*. 2015 July; 56(8):4611-8.

Published abstracts:

Mohammad S. et al. Comparison of retina and optic nerve head structure in Albinism imaged using OCT with the post orbital visual pathway imaged using MRI. *Invest. Ophthalmol. Vis. Sci*. 2014 55: E-Abstract 5100

Mohammad S. et al. "Association between retinal abnormalities and Null-region characteristics in Albinism" *Invest. Ophthalmol. Vis. Sci*. 2012 53: E-Abstract 3935

Mohammad S. et al. "The functional significance of foveal abnormalities in albinism measured using SD-OCT." *Invest. Ophthalmol. Vis. Sci*. 2011 52: E-Abstract 2989

Mohammad S. et al. "Evaluation of the retinal pigment epithelium in human albinism." *Invest. Ophthalmol. Vis. Sci*. 2010 51: E-Abstract 4407

CHAPTER 1

INTRODUCTION

This chapter provides a brief overview of optical coherence tomography (OCT) and magnetic resonance imaging (MRI), which were the two main imaging techniques employed in this study. It also details the current knowledge regarding the genetic basis of albinism and their impact on the visual pathway. In addition, the anatomy and embryological development of the normal visual pathway, and how this goes wrong in albinism is discussed. Finally, the chapter lists the specific aims for each part of the study.

1.1 OPTICAL COHERENCE TOMOGRAPHY

1.1.1 BACKGROUND

Optical coherence tomography is a non-invasive imaging technique that can generate high-resolution cross-sectional and three-dimensional images of optical scattering media such as biological tissue. It was first described by Huang et al in 1991¹ and the first in-vivo study was carried out by Fercher et al. in 1996.² Since then, OCT has been used in a range of diverse scenarios such as imaging airways,³ coronary arteries,⁴ monitoring growth of small tumours,⁵ and as an adjuvant to endoscopy.⁶

The essentially transparent nature of ocular media means that light is transmitted through it with minimal interference. As a result, optical coherence tomography is an ideal way to image the retina as it provides micrometre resolution *in-vivo* images that closely resemble histological sections.⁷ Image analysis software, often provided by the OCT manufacturers, allow qualitative and quantitative assessment of the retina as well as the optic nerve.⁸

These properties have meant that the use of OCT imaging has increased exponentially over the past few years and become part of routine assessment in ophthalmology clinics.

1.1.2 PRINCIPLES BEHIND OCT

OCT operates by measuring the difference in time delay of light reflected back by the various retinal layers. Figure 1-1 illustrates a schematic diagram of a time domain OCT (TD-OCT) setup. At the most basic level, this comprises of a light source (usually a super-luminescent diode), a reference mirror and a Michelson interferometer.

The light beam is split into a reference arm that is shone on to a mirror and a test arm that is directed towards an object under test. The test object can absorb, scatter or reflect back the light. In human tissue, absorption of light occurs between 200-600 nm by haemoglobin and above 1000 nm by water. Meanwhile, light scatter increases with decreasing wavelength. Therefore, in most OCT devices, the super-luminescent diode emits low-coherence near infrared light at a wavelength of around 830nm that achieves optimum balance between light scatter and absorption.⁹

Light that is reflected back to the interferometer with the same coherence is combined with the reference arm. Interaction between the reference and test beams produces an interference pattern, which is measured by a photodetector to produce an axial reflectivity profile or A-scan. Multiple A-scans can be combined to provide a B-scan and multiple B-scans can be combined to provide a 3-D image.¹⁰ The various layers within the retina and the boundaries between them have different optical properties that allow them to be visualised separately on the OCT scan.^{11, 12}

In TD-OCT, the reference mirror moves to be able to calculate the difference in the echo time delay of the light reflected by different layers of the retina. This means that a standard TD-OCT device can acquire approximately 400 B-scans per second.¹³ This makes TD-OCT prone to movement artefacts in imaging patients with nystagmus whose eye movements are larger than the transverse resolution of the OCT device.^{14, 15}

Figure removed from online version to avoid copyright infringement

Figure 1-1: Schematic diagram of an OCT set up. OS=optical source, BS=beam splitter, OUT=Object under test.

In 2002, Wojtowski et al. introduced spectral domain OCT (SD-OCT) where the interferometer is replaced by a spectrometer. In this setup, the reference mirror is static and allows OCT signal from different axial depths in the retina to be interpreted simultaneously which speeds up the scan acquisition and minimises motion artefact. This has allowed reliable measurements of retinal layer thickness in patients with nystagmus.¹⁶ Therefore, this was our choice of imaging modality for studying the fovea and optic nerve in albinism.

1.2 MRI

1.2.1 BACKGROUND

Magnetic resonance imaging (MRI) is a medical imaging technique, which due to its ability to offer soft tissue differentiation in multiple planes, has become almost ubiquitous in the in-vivo study of the brain since its development in the 1970s.¹⁷

1.2.2 PRINCIPLES BEHIND MRI

Due to the abundance of water in the human body, it contains a large number of charged hydrogen atoms. The positively charged nuclei of these atoms spin about their axis producing a local magnetic field parallel to this axis. However, due to the random distribution of the spin, their individual magnetic fields do not amount to any net magnetisation. When placed in an external magnetic field (B_0), the magnetic moment of the nuclei can align either in the same (parallel) or opposite (anti-parallel) direction as B_0 . (Figure 1-2) The parallel direction has a lower energy state; hence, there is a slight bias towards this orientation leading to a net magnetization in the direction of B_0 . The difference between the energy levels, and therefore the magnitude of net magnetization, depends on the field strength B_0 .¹⁸

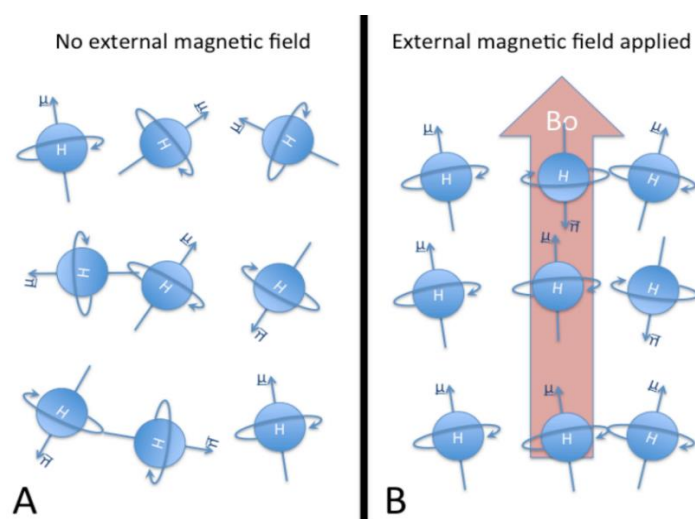


Figure 1-2 Illustration of the behaviour of spins in absence (A) and presence (B) of a strong magnetic field B_0 ¹⁹

The interaction between B_0 and the spinning positive charge of the nuclei causes them to rotate about the axis of B_0 ; this movement is known as precession. The frequency of this precession (ω_0) is proportional to the strength of the magnetic field and is expressed by the Larmor equation where γ is a known constant, the gyroscopic ratio.

$$\omega_0 = \gamma B_0$$

Application of an appropriate radiofrequency (RF) pulse generates an oscillating electromagnetic field (B_1), perpendicular to B_0 that excites the protons inside causing them to precess in phase. As the RF pulse continues the net magnetisation vector tips from the being parallel to B_0 to being parallel to B_1 . This energy interaction between the spinning nuclei and the electromagnetic RF pulse is known as magnetic resonance and it disturbs the original equilibrium.²⁰

As the protons precess in phase, their combined magnetic field induces a current in the receiver coil placed perpendicular to the transverse plane as per Faraday's law of Induction. This induced voltage, the MR signal, is known as the free induction decay (FID).

When the pulse is discontinued, the system returns from this state of imbalance via two independent forms of energy loss. During T1 relaxation, energy is transferred to the surrounding lattice and during T2 relaxation, energy exchange occurs between nuclei in the high and low energy state. As the protons give up their energy, they lose coherence leading to reduction of FID. The MRI signal provides information about proton density and difference in relaxation times between various tissues, which leads to the contrast seen in MR images.²¹

1.2.3 DIFFUSION TENSOR IMAGING

Diffusion tensor imaging (DTI) is a technique that measures the movement of water molecules in tissue to provide information regarding the structure of white matter bundles *in-vivo*.²² In a barrier-free environment, water molecules follow Brownian motion and move in a random fashion with equal displacement in all directions. This is known as isotropic diffusion. However, introduction of a barrier, such as within the highly organised axon bundles of cerebral white matter, molecular movement is greatest parallel to the long axis of the axons and is therefore anisotropic.²³ Figure 1-3 provides a schematic illustration of isotropic and anisotropic diffusion.

Figure removed from online version to avoid copyright infringement

Figure 1-3 Illustration of (a) isotropic and (b) anisotropic diffusion²⁴

Diffusion tensor imaging relies on measuring the diffusion parameters from multiple directions to construct a diffusion tensor that describes the orientation and magnitude of diffusion in each voxel.²² Figure 1-4 shows that the tensor can be visualised as an ellipsoid with three eigenvectors ϵ_1 , ϵ_2 , ϵ_3 representing the direction of the three axes of the ellipsoid and three eigenvalues λ_1 , λ_2 , λ_3 representing their magnitude.²⁵ The principle eigenvector ϵ_1 of a voxel represents the estimate of the dominant orientation of fibre bundles within it. This information is used to reconstruct white bundle tracts through the brain – a process called tractography.²⁶

Figure removed from online version to avoid copyright infringement

The algorithms for DTI tractography can be divided into deterministic and probabilistic methods. In deterministic tractography, the algorithm traces out a fibre streamline by following the primary diffusion direction from one voxel to the next. The tract terminates if it reaches a voxel with low anisotropy or if a sharp bend occurs. The two thresholds can be manually defined to ensure that the reconstruction is anatomically plausible and manually drawn regions of interest (ROIs) can be used to exclude streamlines that may stray into undesired locations.²⁶

Patient movement and imaging artefacts can affect estimation of the main diffusion direction and fibre orientation leading to inaccuracies in the deterministic fibre tracking models.²⁷ Probabilistic tractography accounts for these uncertainties, by producing a matrix of multiple possible fibre orientations at each voxel and assessing the likelihood of fibres following a particular path.²⁸

A number of studies have utilised DTI to map out the visual pathway in humans and in our study, we utilise it to investigate the abnormal chiasmal connectivity seen in albinism.²⁹⁻³⁴

1.3 ALBINISM

Albinism is a term derived from the Latin word for white, “Albus”.³⁵ It refers to a group of genetic mutations that lead to abnormalities in the melanin synthesis and transport pathway.³⁶ It manifests itself as a reduction or absence of tissue melanin and is also associated with a number of characteristic anomalies in the visual pathway that are discussed later in section 1.4.³⁷

In the UK, albinism affects around one in 4000 people.³⁸ Worldwide the prevalence has been reported to vary from one in 1000 in some parts of Africa³⁹ to 1 in 37000 in the United States.⁴⁰ The condition is currently classified into two broad categories of oculocutaneous (OCA) and ocular albinism (OA) based on the cutaneous appearance of the affected individuals. In OCA, there is a reduction or absence of melanin in the hair, skin and eyes whereas in OA, the melanin deficiency is limited to the eyes.⁴¹

1.3.1 GENETIC BASIS OF ALBINISM

Genetic analysis allows fine classification of albinism based on the mutation causing the condition. The step at which the melanin synthesis pathway is disrupted determines the presence of any residual tyrosinase activity and therefore the phenotypical characteristics displayed by the affected individual.⁴² Tyrosinase (TYR) is an enzyme which catalyses the first two steps in the melanin biosynthesis pathway, converting tyrosine to L- DOPA and subsequently to L-Dopaquinone.⁴³

Until recently, only four genes were shown to be associated with albinism.⁴⁴ Figure 1-5 shows what part of the melanin synthesis pathway these mutations influence. Over the last few years further mutations have been identified and these are detailed in subsequent sections.

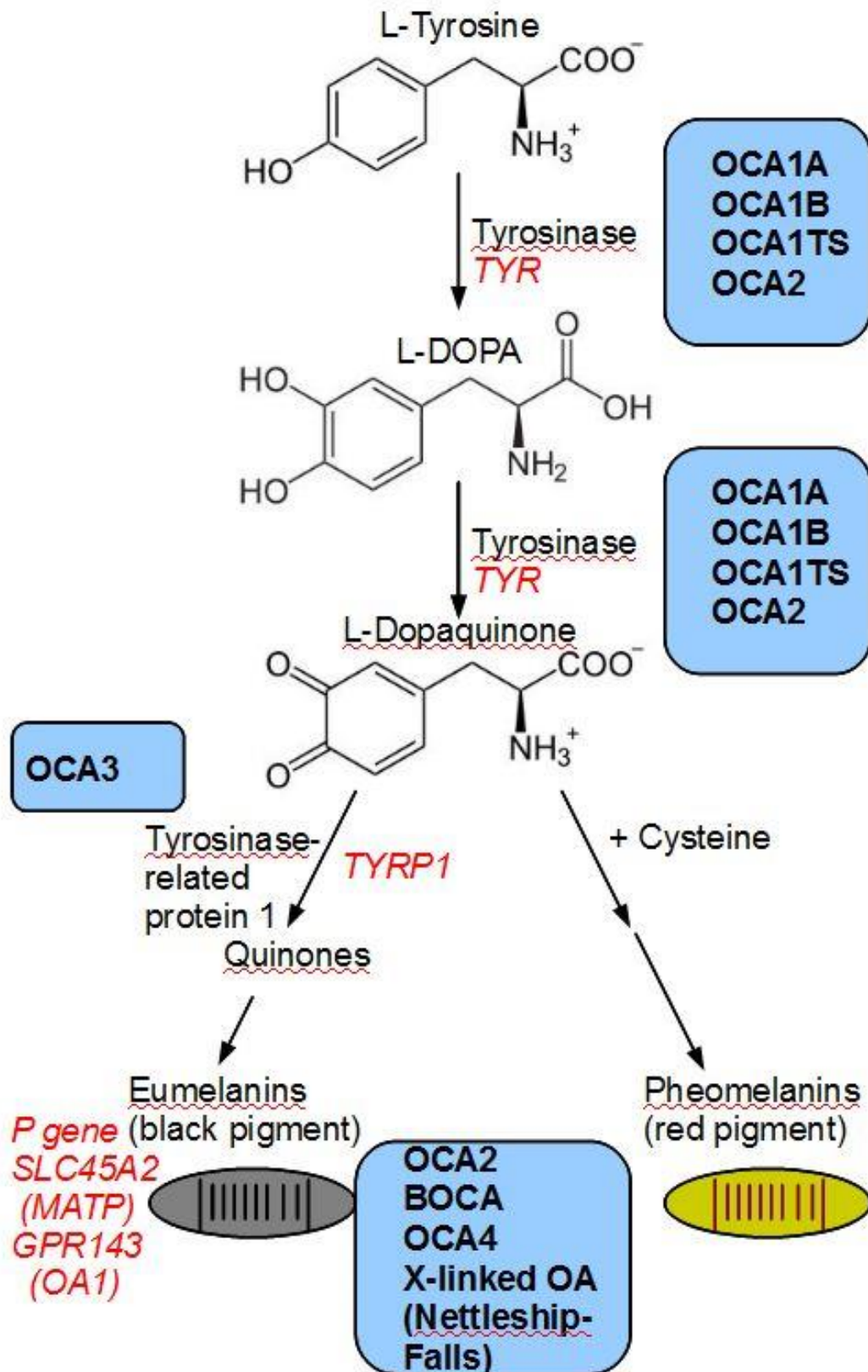


Figure 1-5: Effect of known genetic defects (red text) on stages of melanin synthesis (blue boxes). OCA 1-4 =oculocutaneous albinism type 1 -4, TS = temperature-sensitive, BOCA=brown OCA, OA=ocular albinism. ⁴⁵

1.3.1.1 OCULOCUTANEOUS ALBINISM

So far, mutations in seven genes have been implicated in causing OCA and they all display an autosomal recessive inheritance pattern.⁴⁴ The associated phenotype varies based on where in the melanin synthesis pathway the mutation occurs.

OCA 1

Oculocutaneous albinism type 1 (OCA1) is caused by mutations in the tyrosinase gene on chromosome 11q14.3.⁴⁶ Individuals with OCA1 are typically born with white hair at birth. Those with an OCA1A mutation, which completely eliminates the tyrosine activity, do not develop melanin pigment in their hair, skin or eyes at any point during their lifetimes. Individuals with OCA1B mutations have some residual enzyme activity and therefore may develop some melanin pigment in their lashes and hair by the age of three years.

OCA1TS is the temperature sensitive variant of OCA1 where tyrosinase activity is inversely proportional to skin temperature. Affected individuals display higher pigmentation levels on the cooler extremities but areas near the body core such as the axilla, pubic area, and scalp remain pale.³⁷

OCA 2

Oculocutaneous albinism type 2 (OCA2) is caused by mutation in the P-gene located at 15q12-q13.1.⁴⁷ The OCA2 protein is involved in the synthesis of melanosomes and maintaining an acidic pH within them,⁴⁸ as well as processing and transport of the tyrosinase enzyme.⁴⁹⁻⁵¹

OCA2 is the commonest type of OCA in Africa.⁵² Patients' phenotype can vary from the classic (blond hair, fair skin, blue irides) to near normal pigmentation.⁵³ Brown Albinism (BOCA) is a part of the clinical spectrum of OCA2 that was initially identified in

people of Nigerian and Ghanaian origin and is so called due to the light brown hair and skin in affected patients.⁵⁴

OCA 3

Oculocutaneous albinism type 3 (OCA3) is caused by mutations in tyrosinase related protein 1 (TYRP1) located on 9p23. This is an enzyme involved in catalysing the oxidation of 5,6-dihydroxyindole-2-carboxylic acid (DHICA) monomers to form melanin.^{55, 56}

OCA3 is rare in white Europeans but in Africans, it leads to the appearance of red skin and reddish brown hair and hence is also termed “rufous” or “red” albinism.⁵⁷

OCA 4

Oculocutaneous albinism type 4 (OCA 4) is caused by mutations in the membrane associated transporter protein gene (MATP).⁵⁸ The function of MATP is yet unknown and the clinical appearance and the phenotype varies from complete absence of pigment to some pigmentation with brown hair and irides. The gene is located on chromosome 5p13.2.⁵⁹

OCA 5

In 2012, a group of Pakistani researchers discovered a novel mutation on chromosome 4q24 in a consanguineous family with OCA. Affected individuals from this family possessed golden coloured hair and white skin regardless of their sex and age. However, the gene associated with this mutation remains unidentified and more work needs to be done to characterise this mutation and its associated phenotype.⁶⁰

OCA 6

In 2013, Wei Li et al. reported that mutations in SLC24A5 were associated with a new form of OCA.⁶¹ This gene is located at 15q21.1 and codes for a membrane transporter that is involved in calcium homeostasis within melanosomes. It is thought to play a role in melanocyte maturation.^{62, 63}

The patients with the OCA6 mutation presented with light hair that darkened with age as well as ocular features typical of albinism.⁶¹

OCA 7

The gene C10ORF11 was found to be associated with OCA amongst individuals from Faroe Islands and was named OCA7. The gene is located at 10q22.2-q22.3 and it has been suggested that it plays a role in melanocyte differentiation.⁶⁴

1.3.1.2 OCULAR ALBINISM

As the name suggests, hypopigmentation in ocular albinism (OA) is limited to the eyes.^{57, 65} OA is caused by mutations of the GPR143 gene, localized to Xp22.32.⁶⁶⁻⁶⁹ This codes for a G-protein coupled receptor that controls the melanosome transport in pigment cells.^{70, 71} The mutation displays an X-linked recessive inheritance pattern and affects 1/60,000 live births.⁷²

Individuals with OA often display normal or slightly reduced skin pigment; however, the associated ocular abnormality may be profound.⁷³ Carrier females do not show any visual abnormalities, but due to random X-inactivation, may display a characteristic mud splattered fundus and iris transillumination.^{74, 75}

1.3.1.3 SYNDROMIC ALBINISM

Albinism is also associated with some syndromes of defective packaging and transport of intracellular proteins that include melanin.⁷⁶

Hermansky-Pudlak Syndrome

Hermansky-Pudlak Syndrome (HPS) is an autosomal recessive disorder of lysosome-associated organelles such as platelet-dense granules leading to a bleeding tendency, melanosomes causing albinism and secretory lysosomes resulting ceroid deposition that can lead to pulmonary fibrosis, cardiomyopathy and colitis.⁷⁷ There are currently nine genes found to be associated with HPS.⁷⁸

Chediak-Higashi Syndrome

Chediak-Higashi syndrome (CHS) is a rare autosomal recessive disorder caused by a mutation in the CHS1 gene. Histologically, it is identified via the presence of enlarged intracellular lysosomal vesicles.⁷⁹

Clinically it is characterized by immunodeficiency, bleeding tendency and peripheral neuropathy alongside variable hypopigmentation. It is also associated with haemophagocytic lymphohistiocytosis (HLH), which is a lymphocytic infiltration of the major organs of the body known as the 'accelerated phase'.^{80, 81}

Griscelli Syndrome

Griscelli Syndrome (GS) is an extremely rare condition with only around 30 cases reported in literature since it was first described in 1978.⁸² Most of these cases have been described on the Turkish and Mediterranean populations.⁸³

GS has three subtypes based on the mutation causing the syndrome and this determines the clinical phenotype and severity. GS1 is caused by mutations in the MYO5A gene, and leads to pigment deficiency and neurological problems.⁸⁴ Children with GS2 present similarly to CHS with silvery grey hair, recurrent infections and HLH in majority of cases.⁸⁵ It is caused by mutations in the RAB27A gene.⁸⁶ The GS3 phenotype is restricted to skin and hair hypopigmentation and is caused by mutations in the MLPH gene.⁸⁷

1.3.1.4 FOVEAL HYPOPLASIA WITHOUT ALBINISM

Although foveal hypoplasia is a hallmark of the albinotic phenotype, there are certain mutations that can lead to foveal hypoplasia and on occasions chiasmal misrouting in the absence of albinism. The most well-known of these is aniridia which is caused by aberrations in the PAX6 gene and is associated malformation of the iris in addition to foveal hypoplasia.^{88, 89} Al-Araimi and colleagues have described the autosomal recessive FHONDA syndrome which comprises of foveal hypoplasia, optic nerve decussation defects and anterior segment abnormalities that is caused by a mutation in the SLC38A8 gene on chromosome 16q23.3–24.1.^{90, 91}

1.4 VISUAL PATHWAY ABNORMALITIES IN ALBINISM

In the eye, melanin is found in both the neural crest derived uveal melanocytes, as well as the retinal pigment epithelium (RPE) derived from neuroectoderm.⁹² Compounds associated with the melanin synthesis pathway within the RPE play a crucial part in the development of the neural retina. L-dopa for example, regulates the speed of the cell cycle and its absence leads to abnormal cellular proliferation and death.^{93, 94}

The disruption of melanin synthesis leads to a number of anomalies the visual pathway of patients with albinism.^{37, 95}

1.4.1 IRIS TRANSILLUMINATION

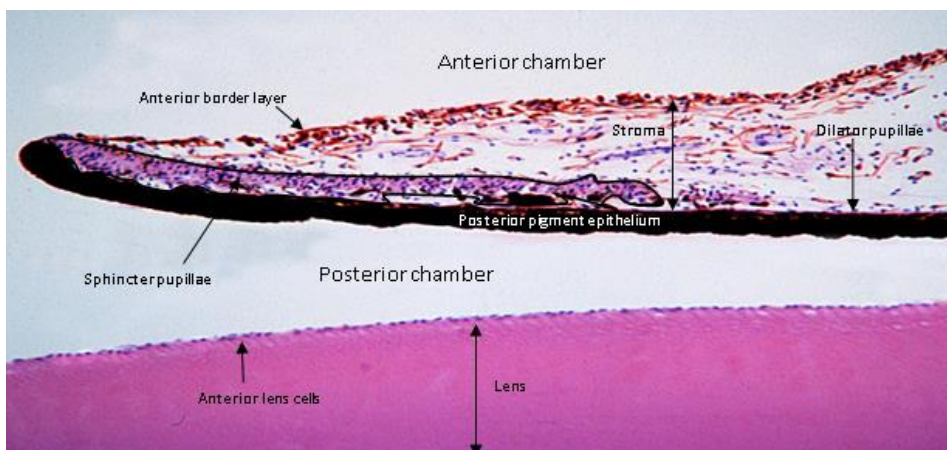


Figure 1-6: Histological appearance of the iris. ⁹⁶

Figure 1-6 shows a histological section of the iris. Its posterior pigmented epithelium contains large highly pigmented melanocytes that usually block any light from entering the eye except at the pupil.^{97, 98}

However, the melanin deficiency in albinism means that the iris does not filter light. As a result, there is intraocular light scattering, which leads to impairment of vision and photophobia. Clinically, this is seen as iris transillumination because the light reflected from the fundus can be seen through the iris. The severity of

transillumination can be graded one to four based on Summers' classification. (Figure 1-7)⁹⁹

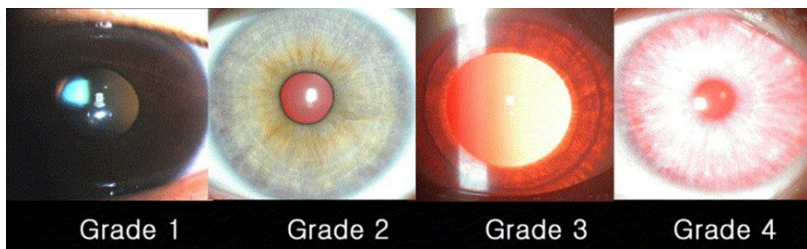


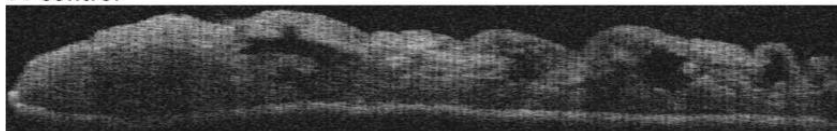
Figure 1-7: Summers' classification for iris transillumination. Class 4 represents the most severe end of the spectrum

The author of this thesis has recently contributed to a study that characterised the iris structure in patients with albinism using an anterior segment optical coherence tomography (OCT). The main findings of this study were that patients with albinism have a thinner iris. The thickness of the iris was related to other phenotypic features of albinism such as cutaneous pigmentation, nystagmus intensity and visual acuity.

Figure 1-8 compares the OCT appearance of an iris from an albinism patient and a healthy control while Figure 1-9 compares the average thickness of the iris between the two groups.

We also found that anterior segment OCT could be used as a tool in diagnosing albinism with a high degree of sensitivity (85%) and specificity (78%).¹⁰⁰ The role of the author in this study was to obtain some of the OCT scans as well as collecting phenotypical characteristics such as skin colour, hair colour and visual acuity. A copy of the paper is included in the appendix. (page **Error! Bookmark not defined.**)

A Control



B Albinism

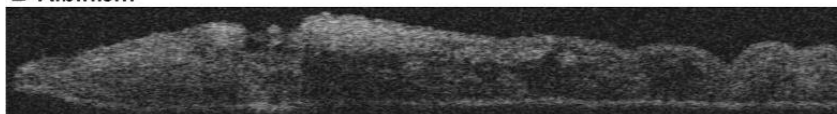


Figure 1-8 Comparison of optical coherence tomography images of the iris from (A) healthy control and (B) patient with albinism¹⁰⁰

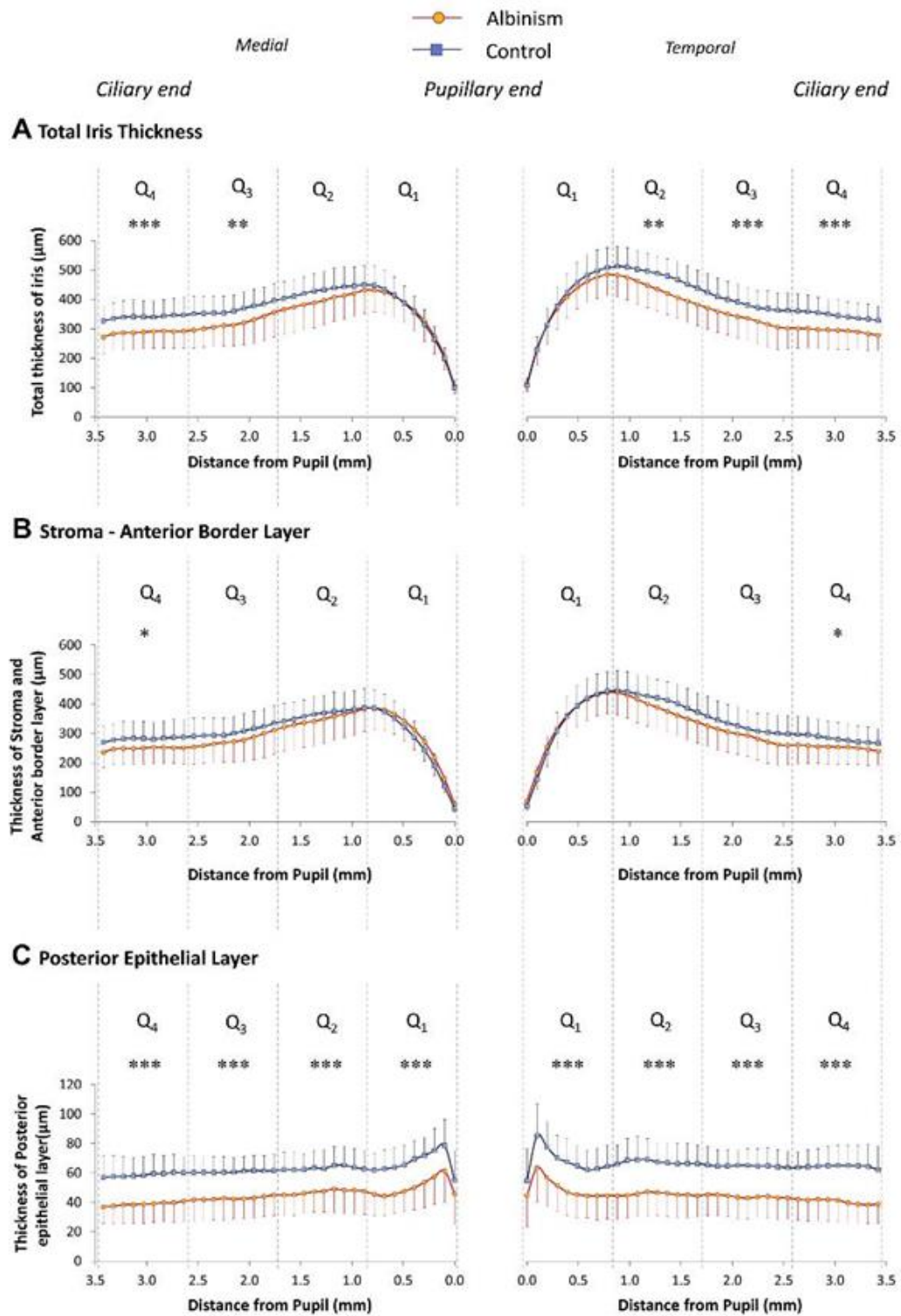


Figure 1-9: Comparison of mean iris layer thickness in albinism patients and healthy controls averaged between left and right eyes. (A) Shows total thickness, (B) shows stromal and anterior border layer thickness and (C) shows the posterior epithelial layer thickness. The medial aspect values are on the left and temporal aspect on the right. Each aspect is divided into four quartiles by dashed grey lines with Q₁ being the quartile at the pupillary end while Q₄ being closest to the ciliary apparatus. The number of asterisks above each quartile represent the level of significance (* $p < 0.05$, ** $p < 0.01$, *** $p < 0.001$)¹⁰⁰

1.4.2 REFRACTIVE ERRORS

Patients with albinism frequently display both spherical and cylindrical refractive errors.¹⁰¹⁻¹⁰³ Astigmatism is predominantly with the rule in nature.¹⁰⁴⁻¹⁰⁷ It has been suggested that this may be due to corneal moulding of lids in patients with horizontal nystagmus.^{102, 108, 109}

Hypermetropia is the predominant spherical abnormality although patients may also display high degree of myopia.^{102, 105, 110}

1.4.3 STRABISMUS

Strabismus refers to a misalignment between the two eyes. The misalignments in albinism are mainly horizontal but vertical misalignments have also been reported.¹¹¹ Brodsky et al. noted that 95% of patients display an abnormally positive angle kappa, which refers to an excessive nasal displacement of the pupillary reflex.(Figure 1-10) They suggested that this might reflect a compensation for the increased chiasmal decussation of axons originating in the temporal hemi-retina.¹¹²

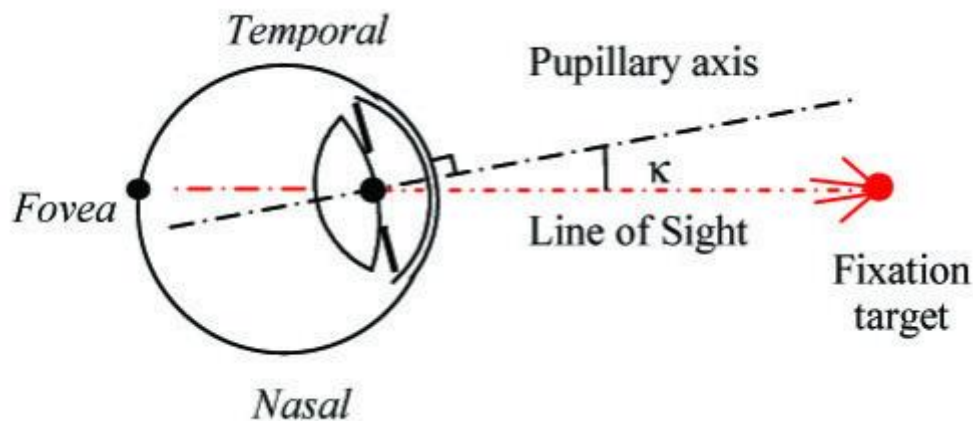


Figure 1-10: Schematic diagram illustrating how angle kappa is calculated. Angle kappa refers to the relationship between the pupillary axis (black dotted line), defined as a line passing through the centre of the pupil perpendicular to the cornea, and the visual axis (red dotted line) which is the line of sight connecting the fovea with a fixation target.¹¹³

1.4.4 MACULAR TRANSPARENCY

Lack of melanin in the RPE and choroid of individuals affected by albinism leads to the observation of a “blond” fundus. Figure 1-11 shows the Summers’ classification for macular transparency that has three grades based on how easily visible the choroidal vessels are.¹¹⁴ In addition, it has also been reported that patients with albinism lack macular pigment, which is usually found in the photoreceptor axons, inner plexiform layer and to a lesser extent in the photoreceptor outer segments and RPE.¹¹⁵⁻¹¹⁷

While the function of macular pigment is uncertain, it has been suggested that the pigment helps reduce chromatic aberration and to improve visual acuity. In addition, it has antioxidant capabilities, which alongside their ability to trap short-wavelength light may serve to protect the outer retina, retinal pigment epithelium, and choriocapillaris from oxidative damage.¹¹⁸

Figure removed from online version to avoid copyright infringement

Figure 1-11: Grading system for macular transparency. Grade 1 is the most severe

1.4.5 FOVEAL ABNORMALITIES

1.4.5.1 THE NORMAL RETINA

The retina is an intricate structure made up of a variety of cell types arranged in layers that work together to convert light striking the retina into electrical impulses. In this thesis, the cells within the retina will be divided into two broad categories of photoreceptor and processing cells based on their location and function. The arrangement of retinal layers is outlined in Figure 1-12.

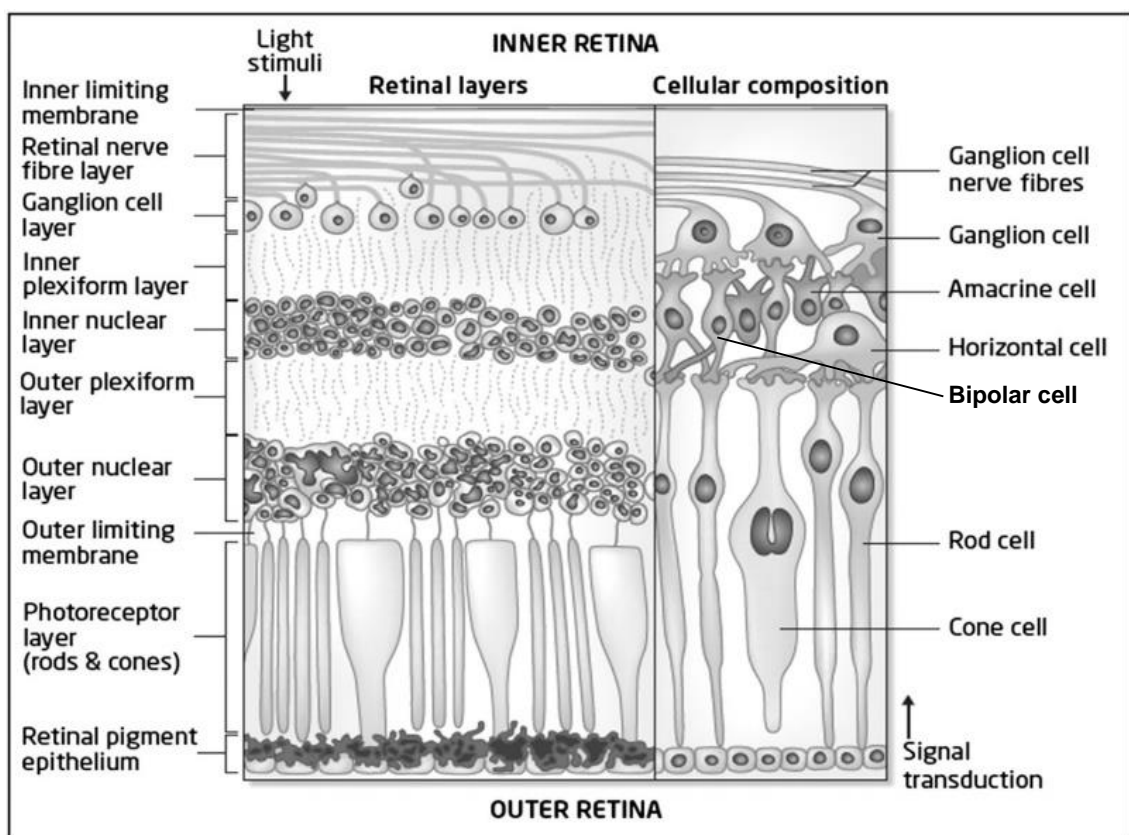


Figure 1-12: Schematic diagram illustrating the synapses (left) between cells within the different layers of the retina (right)¹¹⁹

Photoreceptor cells

Like any other sensory organ in the body, the retina comprises of specialised receptors, which in this case, are the photosensitive rod and cone cells.

The rods are situated mainly in the peripheral retina, and are sensitive enough to respond to a single photon of light. Convergence of multiple rods to a single interneuron amplifies their sensitivity. Hence, they are useful for vision at low levels of light, and are almost entirely responsible for night vision. However, they have only one type of light-sensitive pigment, and therefore play little role in colour vision. In addition, signal convergence from multiple rods to single interneuron reduces their spatial resolution. They also lack the ability to sense temporal changes due to their slow response time (around 100ms).¹²⁰

By contrast, cone photoreceptors are found primarily in the central retina. Three different types of cone cells exist and these are capable of responding to different wavelengths of light. They are called short or blue, middle or green, and long or red cones and difference in the signals they generate allows the brain to perceive a continuous range of colours. They also have higher spatial and temporal resolution.

The photoreceptors are organised in three layers within the retina. Their cell bodies and nuclei form the outer nuclear layer and their inner and outer segments form inner and outer segment layers, respectively. These three layers will collectively be referred to as the “photoreceptor” layers in this thesis.

Processing cells

The outer plexiform layer (OPL) is the region in which the photoreceptors synapse with bipolar cells whose cell bodies sit in the inner nuclear layer (INL). The INL also contains bodies of horizontal and amacrine cells. Bipolar cells relay electrical impulses from the photoreceptors to the ganglion cells in the ganglion cell layer (GCL). The signals can pass through direct synapses or via amacrine cells that modulate and integrate signals from bipolar cells before synapsing with the retinal ganglion cells. Horizontal cells are

laterally connecting interneurons that help regulate input from multiple photoreceptors. The synapses between cells from the INL and GCL occur in the inner plexiform layer (IPL). Their axonal processes also contribute to the inner and outer plexiform layers.

On average, each retinal ganglion cell receives inputs from about 100 photoreceptor cells. However, these numbers can vary greatly from the fovea, where a ganglion cell may receive input from few as five photoreceptors, to the extreme periphery where a single ganglion cell will communicate with thousands of photoreceptors.^{120, 121}

Based on their function, retinal ganglion cells can be divided into three main classes. Midget or P-cells form the largest class, making up around 80% of ganglion cells. They specialise in high spatial acuity, fine stereopsis and colour vision.^{122, 123} Parasol or M-cells, form around 10% of retinal ganglion cell population and are distributed mainly in the peripheral retina. They receive input from multiple bipolar cells and therefore have a larger receptive field but lower spatial resolution compared to the P-cells. Their anatomy means that M-cells specialise in low spatial resolution, motion detection, and coarse stereopsis.¹²⁴

Bistratified cells make up the majority of the remaining 10% of the retinal ganglion cells. Their small size has meant that these cells have only recently been identified. They receive input from intermediate numbers of rods and cones and have moderate spatial resolution.^{125, 126}

A small subset of retinal ganglion cells, are sensitive to light. While they do not contribute to vision, they play a role in regulating circadian rhythms and modulating the pupillary light reflex.¹²⁷

Ganglion cell axons form the nerve fibre layer (NFL) at the vitreal surface of the retina. The NFL, GCL, IPL, INL and OPL will be referred to as the “processing” layers in this thesis.

Fovea

In the central retina, an extrusion of the processing layers creates a pit around round 400 μ m wide.¹²⁰ This region of the central retina is known as the fovea centralis. (Figure 1-13)

Presence of the pit means, that light has to travel through fewer layers to reach the photoreceptors.¹²⁸ The pit also serves a refractive role by locally magnifying the retinal image onto the foveal cone mosaic.¹²⁹

In addition, the photoreceptor distribution and morphology at the fovea also differs from the rest of the retina. There is an absence of rod cells and the cone cells are thin and elongated allowing for high-density packing of cones at the fovea.¹³⁰ The foveal pit and high density of cones combine to ensure that the fovea is the region of the highest visual acuity in the retina.¹³¹

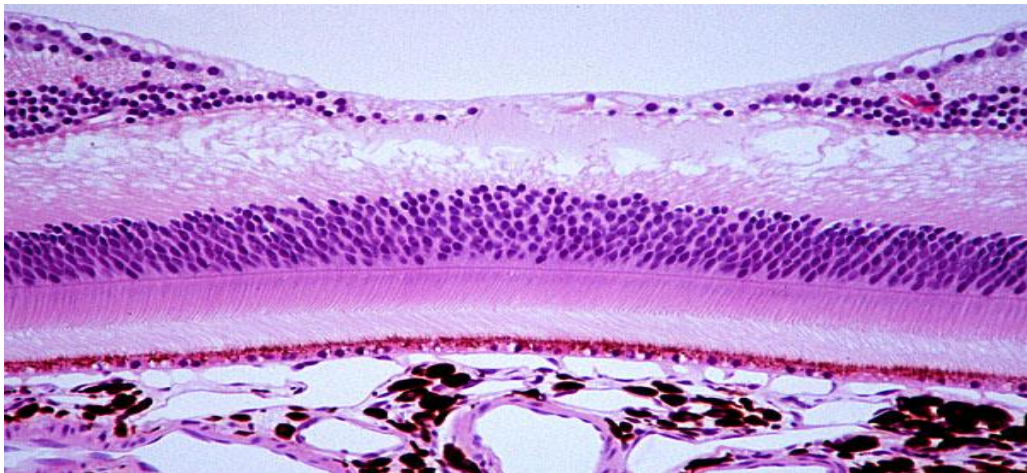


Figure 1-13: Cross-sectional histology of the fovea⁹⁶

1.4.5.2 RETINA IN ALBINISM

Clinical examination of the macula in albinism patients shows an absence of the annular and foveal reflexes.⁹⁹ Post-mortem histological studies of human eyes affected by albinism demonstrated a diminished foveal pit along with continuation of the inner retinal layers through the fovea.¹³²⁻¹³⁶ However, these histological studies have been few in number, and as a result, it had been difficult to determine the full picture of retinal deficits present in albinism.

OCT imaging in albinism

Over the last 15 years, deployment of optical coherence tomography has allowed real time in-vivo imaging of the retina and to date, various studies have looked at the retinal architecture in patients with albinism using OCT. However, the initial OCT studies in albinism were performed using low-resolution TD-OCT and focused on the gross appearance of the macula. In 2002, Meyer et al. published a case report describing the OCT findings in the eye of a 10-year old female OCA patient and found the absence of a foveal pit.¹³⁷ Izquierdo et al. supported this finding in a more extensive study, which included 10 OCA patients. They reported that the foveal thickness in their patient cohort ranged between 200-299 μm (mean 245 μm) compared to values of 168-239 μm in the general population.¹³⁸ However, the wide range of values suggested that there was a spectrum of foveal development within the patients.

This spectrum of foveal development was also investigated by Harvey et al. who evaluated the macular architecture in 11 patients with albinism using a TD-OCT device with 10 μm axial resolution. They reported that foveal development within individuals affected by albinism varies from near normal level to being absent.¹³⁹

The development of SD-OCT has brought along the advantages of higher axial resolution and quicker scan acquisition time. This minimized potential interference

from motion artefacts due to nystagmus and allowed for better visualisation of the individual retinal layers.¹⁴⁰

Chong et al. (2009) used an SD-OCT device with 4.6µm resolution to examine the foveal morphology in 12 patients with albinism and they found that the nerve fibre layer, ganglion cell layer, inner plexiform layer, inner nuclear layer and outer plexiform layer all extend through the foveae of patients with albinism whereas in healthy controls, these layers discontinue.¹⁴¹

Seo et al. (2007) noted that typically, the fovea of albinism patients is hyporeflective. They speculated that this might perhaps be due to lack of melanin pigmentation within the retina affected by albinism.¹⁴² Meyer et al. also noticed a hyporeflectivity of the photoreceptors in the retina of their OCA patient.¹³⁷

However, this finding is disputed by Chong et al. who found no difference in reflectance between their patient and control groups. According to them, this finding could be due to the limited resolution of their TD-OCT machine or due to shadowing by the nerve fibre layer that persists across the fovea in albinism patients.¹⁴¹

Both Meyer et al and Seo et al. observed high reflectivity from the RPE and choroid of albinism patients. Seo et al. explained this by referring to the hyporeflectivity of the overlying photoreceptor layer. This meant that more of the signal could reach the RPE and choroid making them hyper-reflective. The group also described the appearance of a double hyper-reflective layer at the junction of the retina and the choroid that they termed the tram-track sign.¹⁴² Although Chong et al. did not comment on the reflectivity of the RPE amongst their patients. However, they did note the choroid to be hyperreflective. They explained this finding by referring to the lack of melanin present in the RPE, which means a more intense signal reaches, and hence is reflected back by, the choroid.¹⁴¹

OCT findings as a predictor of visual function albinism

Although various abnormalities have been documented in the retina of patients with albinism, there is still debate as to which of these features are most significant functionally. Harvey et al. found a weak inverse correlation ($r=-0.21$) between total retinal thickness and visual acuity indicating that size of the foveal pit plays some role in providing good vision.¹³⁹ However, Marmor et al. suggested that the foveal pit is visually insignificant, suggesting instead that photoreceptor specialization at the fovea, which can take place without the formation of a foveal pit, is the most important determinant of vision.¹⁴³ The same conclusion was reached by McAllister et al.¹⁴⁴

Seo et al. also correlated visual acuity with foveal hypoplasia. They developed a grading system based on the OCT findings of the fovea and compared its prognostic value with other clinical hallmarks of albinism such as the grade of iris transillumination and macular transparency. According to their results, this OCT based grading system had a better correlation with visual function compared to iris transillumination and macular transparency.¹⁴² However, the sample size ($n=13$) was too small to draw any statistically significant conclusions. In addition, Chong et al. have suggested that some of the features upon which Seo et al. have based their grading system such as the “tram-tract sign” and hyporeflectivity of the photoreceptor layers may have been due to the low resolution of images from the TD-OCT device they employed in their study. Apart from lower resolution, TD-OCT also has a slower scan acquisition time making it prone to motion artefacts in patients with eye-movement disorders. Chong et al. suggest an alternative grading system based on higher resolution OCT observations on twelve volunteers including the features (i) absence of central foveal depression, (ii) persistence of ganglion and plexiform retinal layers, (iii) persistence of the nerve fibre layer, and (iv) a very prominent image of the entire choroid.¹⁴¹

Advancement in the resolution provided by modern SD-OCT devices means that abnormalities within a particular group of retinal cells, such as the ganglion cell layer and photoreceptors, will be reflected by the appearance of that layer on OCT

morphology of the layer those cells belong to and therefore the impact of abnormalities within different cell populations can now be estimated.

A thorough review of the literature illustrates the need for a large study using high resolution OCT to explore the spectrum of retinal development in albinism and assess the impact of the foveal abnormalities on vision. This question is addressed in section 3.2 (page 120).

1.4.6 OPTIC NERVE ABNORMALITIES

1.4.6.1 NORMAL OPTIC NERVE

The optic nerve is the second of twelve paired cranial nerves. It is a unique part of the central nervous system as it lacks neuronal cell bodies and is isolated from the rest of the brain. It is derived from the optic stalk, an out-pouching of the diencephalon, during the seventh week of embryonic development and is responsible for transmitting visual information from the retinal photoreceptors to the brain.¹⁴⁵

The optic nerve is around 50mm long and may be divided into four parts based on its anatomy.

1. Intraocular portion (optic nerve head)
2. Orbital portion
3. Intracranial portion (situated within bony optic canal)
4. Intra-cranial portion

The optic nerve comprises of ganglion cell axons that travel in the nerve fibre layer before converging at the optic nerve head (ONH). The ONH is situated around 3-4mm nasal to the fovea and it extends from the optic disc (the clinically visible anterior surface of the ONH shown in Figure 1-14) to the posterior scleral surface where the optic nerve axons exit the globe.⁴⁰ As there are no photoreceptors overlying the optic disc, it corresponds to the physiological blind spot of the eye.¹⁴⁶ Within the disc, there is a depression known as the optic cup. The appearance of the optic disc is determined by the size of the scleral canal. The bigger the canal, the larger the optic disc.¹⁴⁷

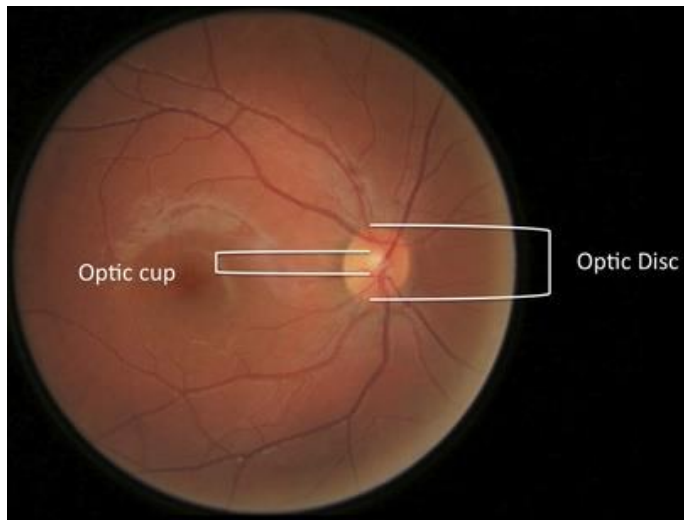


Figure 1-14: Fundus photograph of a healthy optic disc

Figure 1-15 demonstrates the anatomy of the optic nerve head. The anterior portion of the ONH consists of compact optic nerve fibres that are separated from the vitreous by a layer of astrocytes known as the inner limiting membrane of Elschnig. This is a continuation of the internal limiting membrane present at the vitreo-retinal interface.¹⁴⁸ In the central portion of the optic nerve head, this layer is known as the central meniscus of Kuhnt and its thickness is related to the size of the optic cup.¹⁴⁹ During embryological development, glial cells on the vitreal surface of the optic disc regress, and the degree of atrophy determines the optic cup size. Eyes with a small cup usually have a thick glial membrane while eyes with a large cup have a thinner membrane.¹⁵⁰ In some instances, a large amount of glial tissue can persist on the surface of the optic disc as a Bergmeister papilla.(Figure 1-16)

Figure removed from online version to avoid copyright infringement

Figure 1-15: Schematic diagram of the optic nerve head. Inner limiting membrane of the retina (1a) is continuous with internal limiting membrane of Elschnig (1b). In the centre of the optic nerve head, this is called the central meniscus of Kuhnt (2). The border tissue of Elschnig (3) separates the optic nerve from the stroma of the choroid (4) and anteriorly, it is continuous with intermediary tissue of Kuhnt (5), which lies at the termination of the retina. Astrocytes surround retinal nerve fibre axons and form fascicles (6) which traverse through the lamina cribrosa (7). The upper and lower extents of the lamina cribrosa are delineated with dotted lines on the diagram. Septal tissue (Sep) derived from pia mater continues to separate the nerve fibre bundles all the way to the chiasm. G.I.M depicts a mantle of astrocytes, which is continuous with the border tissue of Jacoby anteriorly. Post-orbital part of the optic nerve is covered by (Du) dura, (Ar) arachnoid, (Pia) pia mater.¹⁵¹

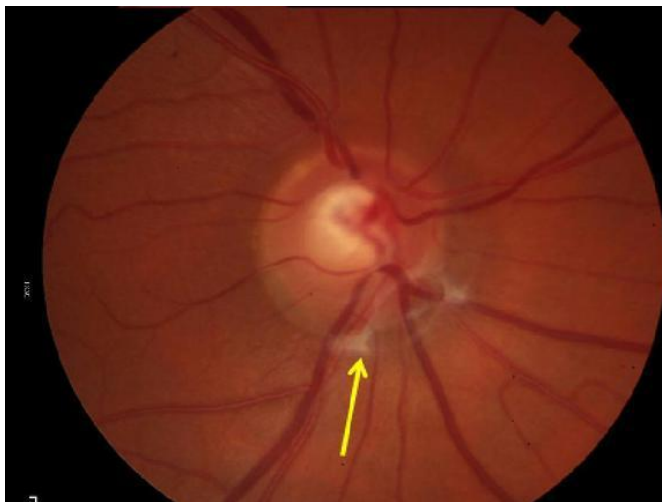


Figure 1-16: Fundus photograph showing an optic nerve head with Bergmeister papilla (yellow arrow)¹⁵²

Underneath its surface portion, lies the prelaminar part of the optic nerve head. In this region, the lateral margins of the optic nerve are separated from the adjacent retina by glial tissue known as the intermediary tissue of Kuhnt and from the choroid by the collagenous border tissue of Elschnig. A posterior extension of glia from the intermediary tissue of Kuhnt, the border tissue of Jacoby, is located internal to the border tissue of Elschnig.¹⁵³

At its posterior-most portion within the eye, the optic nerve axons traverse through a sieve like structure known as the lamina cribrosa. This is made of dense, compact collagenous sheets of scleral trabeculae alternating with glial sheets.^{154, 155}

Astrocytes lining the openings in the lamina cribrosa form a glial membrane that covers each nerve fibre bundle and separates it from the surrounding connective tissue.

The optic nerve leaves the orbit via the optic foramen, which is the anterior opening of the bony optic canal, carrying over a million axons, covered by all three meningeal layers. The optic canal is around 10mm in length and is formed by the union of the lesser wings of the sphenoid bone. Beyond the canal, the intracranial optic nerves travel posterior, superior and medially towards the chiasm.¹²⁸

The pattern of axon organisation within the optic nerve has been a matter of debate. Initial research suggested that the pattern of axons within the optic nerve is random.^{156, 157} However, subsequent larger studies have shown that there is retinotopic organisation of axons within the optic nerve.¹⁵⁸⁻¹⁶¹ Fibres from the macular region for example, occupy a wedge shape region in the temporal part of the optic nerve close to its origin in the globe but move more centrally towards as they move posteriorly.^{162, 163} However, it has been shown in some animals that near the chiasm, changes in glial organization mean that distribution of axons fibres becomes more widespread.¹⁶⁴⁻¹⁶⁶

1.4.6.2 OPTIC NERVE IN ALBINISM

Relatively little is known about the optic nerve morphology in albinism. Using fundus photography in 12 patients with albinism (i.e. 24 eyes), Spedick and Beauchamp reported typical optic nerve hypoplasia in six eyes of four patients. In an additional ten eyes of six patients, they observed subtle features that were suggestive of optic nerve hypoplasia.¹⁶⁷ Using magnetic resonance imaging Schmitz et al. found smaller post-orbital optic nerves compared to normal controls carried in 17 patients with albinism.¹⁶⁸ Tilted discs have also been described in albinism.¹⁶⁹

Tilted discs are a common occurrence with a prevalence of 0.5-3.5% and can be either a congenital or a non-congenital anomaly. Congenital tilted discs or tilted disc syndrome (TDS) is caused by delayed closure of the embryonic optic fissure causing the optic nerve to enter the globe at an extreme oblique angle.¹⁷⁰ The most common cause of non-congenital tilted disc is myopic tilted disc.¹⁷¹ This is due to the optic nerve being pulled in a temporal direction with elongation of the eye, which eventually leads the optic disc being elevated nasally and flattened temporally. These two forms of tilted disc have quite different appearance. TDS is characterized by inferior or infero-nasal tilting of the optic disc and an inferior or infero-nasal crescent of visible sclera. It is also associated with thinning of the ppRNFL in nasal and superior quadrants.¹⁷² Myopic tilted discs are usually elongated vertically with torsion of the disc usually being temporal (i.e. upper disc rotated temporally). A white, sharply defined area, the myopic temporal crescent, is usually visible lying on the temporal side of the optic disc where the inner surface of the sclera is visible.^{171, 173}

Only one group has so far described the optic nerve in albinism using spectral domain OCT (SD-OCT). Chong et al. observed an elevation of the optic nerve in four out of six patients with albinism using SD-OCT. However, as their study was focused on investigating foveal abnormalities, they did not assess the optic nerve head in detail.¹⁴¹

One of the aims of the present study was to use SD-OCT to characterise optic nerve head morphology in albinism using a sufficient sample size to represent the spectrum of abnormalities. This will be done via objective measurement of a number of

parameters within the optic nerve head such as of disc, rim and cup dimensions, peripapillary retinal nerve fibre layer (ppRNFL) thickness and assessment of disc tilt.

One of the greatest challenges in imaging the three dimensional structure of the optic nerve head using OCT is the problem of B-scan misalignment caused by nystagmus present in the vast majority of albinism patients. A suitable methodology needs to be devised overcome this limitation and unlock the potential of OCT to characterize the appearance of the optic nerve in albinism.

We have attempted to tackle this issue in section 3.3 by using retinal vasculature and the optic disc margins from fundus photography to realign B-scans and reconstruct the three dimensional appearance of the optic nerve head. This is possible since the nystagmus in albinism is almost exclusively along the horizontal axis.¹⁷⁴

1.4.7 CHIASMAL ABNORMALITIES

1.4.7.1 NORMAL OPTIC CHIASM

The optic chiasm is named after the Greek letter *Chi* due to its characteristic X shape. At this location, fibres from the nasal hemi-retina decussate to join axons from the contralateral temporal hemi-retina, which stay uncrossed. This arrangement allows the visual cortex to process information from both eyes, and provide stereoscopic vision.^{175, 176}

The chiasm is a flattened, band of axonal fibres formed by the confluence of the two converging optic nerve anteriorly and the two diverging optic tracts posteriorly.¹⁷⁷ Its dimensions vary between 4-13mm antero-posteriorly, 10-20mm transversely and 3-5mm in height.¹⁷⁸

Anatomically, the chiasm lies around 10mm above the diaphragma sellae, which is the dural covering of the sella turcica of the sphenoid bone. It is in direct contact with cerebrospinal fluid (CSF) of the subarachnoid space anteriorly, the supraoptic recess superiorly, the suprasellar cistern inferiorly and the anterior-inferior floor of the third ventricle posteriorly. The chiasm is flanked laterally by the supra-clinoid segments of the carotid arteries and inferolaterally by the cavernous sinuses.¹⁷⁹

During embryological development, the first retinal ganglion cell axons arrive at the chiasm around the fourth week of gestation. At the chiasm, the axons from the nasal hemi-retina decussate to the contralateral hemisphere while those from the temporal hemi-retina remain ipsilateral. Evolutionarily, the degree of decussation at the chiasm is dependent on the position of the eyes on the head. In small animals such as mice where the eyes are placed laterally to provide a wide field of view, majority of optic nerve axons decussate. Higher up in the food chain, as the eyes move to a more forward position and the visual fields overlap to provide binocular vision, the ratio of crossed fibres decreases.¹⁸⁰

The ratio of crossed to uncrossed fibres in the chiasm of humans is believed to be around 53:47.¹⁸¹ The naso-temporal line that segregates the contralaterally projecting

ganglion cells from the ipsilateral ones runs vertically through the centre of the fovea.^{175, 182}

The orientation of fibres within the chiasm varies between species. In the rodent optic chiasm, retinotopic orientation is quickly lost within the chiasm and fibres from the entire retina are distributed evenly throughout the chiasm.¹⁸³⁻¹⁸⁵

Studies on primate animal models have shown that decussating fibres from peripheral dorsal retinal cross in the caudal chiasm while axons from ventral locations cross more rostrally. After crossing, the fibres move laterally and ventrally forming a laminated configuration within the chiasm, with the crossed fibres from each region sandwiched between fibre groups from the other eye. Fibres from the central retina which make up the majority of the population are mostly concentrated centrally and dorsally but found throughout the chiasm.^{160, 165} Axons from the temporal hemi-retinae, which stay ipsilateral, are confined to the lateral peripheries of the chiasm.(see Figure 1-17)¹⁸⁰

Figure removed from online version to avoid copyright infringement

Figure 1-17: Schematic diagram showing the difference in the organisation of uncrossed fibres in normally pigmented rodents and primates¹⁸⁰

This arrangement within the chiasm within humans is corroborated by the fact the pituitary tumours affecting the central retina cause bi-temporal hemianopia hence impacting crossing fibres from the nasal hemi-retina. Compression of the lateral aspect

of the chiasm by internal carotid artery aneurysms on the other hand affects input from the uncrossed temporal fibres.^{180, 186}

Axons from the temporal hemi-retinae, which stay ipsilateral, are confined to the lateral peripheries of the chiasm.^{160, 165}

It was widely believed that the anteriorly placed crossing fibres loop forwards into the contralateral optic nerve before turning posteriorly, while posteriorly placed crossing fibres loop backwards into the origin of the ipsilateral optic tract before traversing the chiasm into the contralateral optic tract. This orientation is referred to as the “Wilbrand’s knee” after Hermann Wilbrand who first described it in the early 20th century while studying the chiasm of subjects where one eye had been lost several years prior to death.^{187, 188}

However, towards the end of the 20th century, Horton argued that Wilbrand's knee is an artefact of monocular enucleation that develops gradually and progressively over several years due to loss of myelin and atrophy of the remaining portion of the ON proximal to transaction.¹⁸⁹ This suggestion was supported by a further study by Lee et al.¹⁹⁰

The mechanisms, whereby an axon crosses or does not cross the chiasm are poorly understood. It has been strongly suggested that the time at which the axon reaches the chiasm determines the fate of decussation. In some mammals such as mice and ferrets, it has been shown that axons that reach the chiasm early during development are more likely to stay ipsilateral.¹⁸⁵

Cellular components at the chiasm also appear to play a role in directing axons.¹⁹¹ Regardless of whether they cross the midline or not, optic growth cones approach within several hundred microns of this region and intertwine with glial processes.¹⁹² At this point, axons from nasal retina cross the midline, but fibres from the temporal retina turn sharply towards the ipsilateral optic tract.¹⁹³⁻¹⁹⁵ This suggests that glial cells at the chiasmal midline respond differently to contact from axons originating in different retinal regions.¹⁹¹

Zinc finger transcription factor 2 (Zic2) appears to be an important genetic control factor in axonal guidance at the chiasm. It is expressed in the eye during early retinal development with highest degree of expression within the temporal retina. Zic2 regulates the expression of EphB1, which is a receptor tyrosine kinase important in divergence of axons at the chiasmal midline.¹⁹⁶ Lack of Zic2 leads to a downregulation in the number of ipsilateral fibres.¹⁹⁷

Guidance factors, which modulate midline crossing in other parts of the brain, have also been studied as candidates for axon guidance at the chiasm. These include Netrin-1, Sonic hedgehog as well as proteins from the Slit, Ephrin and Robos families.¹⁹⁸

At the chiasm, fibres from both optic nerves interact with each other and this contact also plays a role in chiasmal decussation. Removal of an eye in early development for example leads to an increased degree of crossing.^{164, 199, 200}

1.4.7.2 OPTIC CHIASM IN ALBINISM

Albinism is associated with an abnormal decussation of optic nerve fibres originating in the temporal hemi-retina.(Figure 1-18) This misrouting can be demonstrated using visually evoked potentials (VEP) and this is currently the gold-standard investigation for diagnosing albinism.²⁰¹

This technique uses a visual stimulus to evoke an electrical response within the brain that can be recorded using electroencephalography. As normally, almost equal numbers of nerve axons from the eye travel to each hemisphere, monocular stimulation results in a symmetrical response from both hemispheres of the brain. However, the misrouting of the optic nerve axons in albinism means that there is a dominant response from the contralateral hemisphere, which can be detected using VEP.

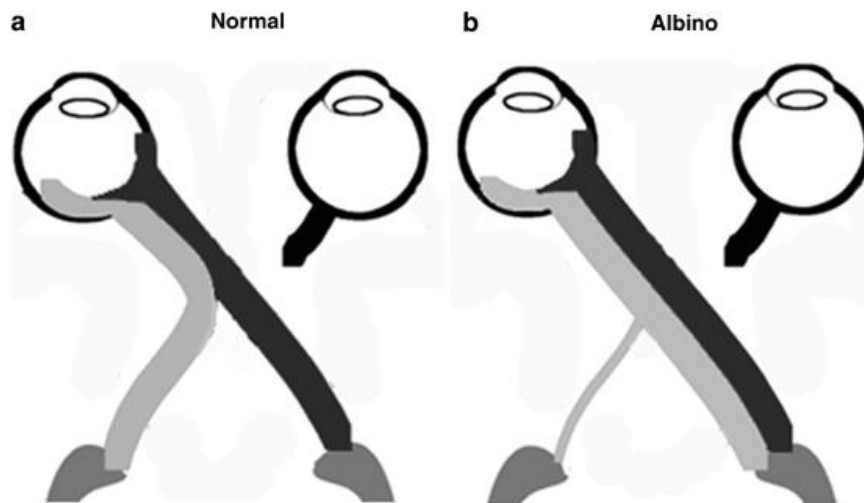


Figure 1-18: Schematic comparing (a) Normal visual pathways and (b) misrouting seen in albinism.²⁰²

It has been suggested that the cause for the chiasmal abnormalities in albinism originates in the retina.²⁰³ Absence of L-Dopa, a pre-cursor of melanin, in the retinal pigment epithelium delays the point at which cells in the developing albino retina exit the cell cycle.⁹⁴ As uncrossed retinal ganglion cells are generated earlier than those that project across the midline, a delay ganglion cell production means that axons from these cells reach the chiasm at a later point. This increases their probability of projecting to the contralateral hemisphere.

Study of albino mice has also demonstrated a reduced expression Zic2. As mentioned earlier, Zic2 appears to play an important role in guiding nerve fibres from the temporal retina to the ipsilateral optic tract and therefore its downregulation may help explain the increased decussation seen in albinism.¹⁹⁷

MRI studies of the optic chiasm in albinism

The abnormal decussation of the optic nerve in patients with albinism has led to interest in the morphology of their intracranial visual pathway. Magnetic resonance imaging has been employed to study the configuration of the post-orbital optic nerve and chiasm in albinism but the findings have been inconsistent. Brodsky et al. reported

them both to be of normal size and configuration.²⁰⁴ However, a larger study by Schmitz et al., 10 years later, found a reduction in optic nerve diameter with an increased angle between the two optic nerves compared to normally pigmented controls.¹⁶⁸ In addition, they also noted that the width of the optic chiasm was reduced in patients with albinism. (Figure 1-19)

Figure removed from online version to avoid copyright infringement

Figure 1-19: Comparison of MRI images of the optic chiasm in an individual with albinism (left) and healthy volunteer (right) shows narrow chiasm and increased angle between the optic nerves.¹⁶⁸

They suggested that this smaller size was due to a reduced number of axons carried into the chiasm by thinner optic nerves. This corresponds with histological studies of albino cats²⁰⁵ and primates²⁰⁶ that have shown reduced number of ganglion cells in the central retina. Schmitz et al. also reported smaller diameter of the optic tracts, again an indication of the reduced number of axons. Like the optic nerve, the angle between the two optic tracts was also increased.

So far, there is a lack of a comprehensive comparative study assessing the relationship between the chiasmal structure and retinal and optic nerve head abnormalities. Such a study would help shed light on whether misrouting seen in albinism originates at the retina.

It will be interesting to see out whether anatomical anomalies seen in the visual pathway reflect the degree of electrophysiological misrouting measured using VEP recordings. We address this question in section 3.4.

1.4.8 LATERAL GENICULATE NUCLEUS

1.4.8.1 NORMAL LATERAL GENICULATE NUCLEUS

After leaving the chiasm, axons from the ipsilateral temporal retina and the contralateral nasal retina travel in optic tracts towards the lateral geniculate nucleus (LGN). In the optic tract, the inferior retinal ganglion cell axons from each eye are positioned laterally and axons from the superior retinas are positioned medially.

At the LGN, there is an almost one-to-one synapse of retinal ganglion cell axons with the cells within the LGN.²⁰⁷ The input is organized in a retinotopic fashion, with macular vision processed in the central portion, the superior field in the lateral horn, and the inferior field in the medial horn.²⁰⁸ The cells within the LGN are arranged in six layers that each receive input from only one eye. Input from the ipsilateral temporal retina goes to layers 2, 3 and 5 while the contralateral nasal retina is represented in layers 1, 3 and 6.^{181, 209-211} Layers 1 and 2 are the magnocellular layers due to the presence of large neurons and receive input from the M-cells of the retina. Layers 3–6 contain small neurons (parvocellular) and receive input from the P-cells of the retina. The layers are separated by tiny “dust-like” koniocellular cells, which receive input from the bistratified cells of the retina.²¹²

1.4.8.2 LATERAL GENICULATE NUCLEUS IN ALBINISM

The LGN in albinism is fundamentally abnormal as it receives the majority of its input from just one eye.^{206, 213, 214} Development of the LGN in humans with albinism has been subject to a relatively small amount of research. Guillery et al. carried out a post-mortem examination of the LGN in a single subject and reported a smaller abnormally shaped LGN with fusion of the M and P layers.²¹³ McKetton et al. confirmed the finding of smaller LGN in a more recent MRI study, which looked at 12 patients with oculocutaneous albinism. The likely reason for this is thought to be the reduced number of retinal ganglion cells seen in albinism.²¹⁵

1.4.9 VISUAL CORTEX ABNORMALITIES

1.4.9.1 NORMAL VISUAL CORTEX

The geniculostriate neurons travel as optic radiations to the primary visual cortex (V1, Brodmann's area 17) located at the occipital pole, which is the posterior-most aspect of the brain. These neurons are grouped into two major bundles: the temporal radiations and the parietal radiations. The temporal radiations contain information from the upper quadrant of the contralateral visual field and take an anterior course through the temporal pole, termed the "Meyer's loop", before turning in a posterior direction to terminate in the lower bank of the calcarine sulcus. The parietal division contains input about the inferior quadrant of the contralateral visual field and projects to the upper bank of the calcarine sulcus.²¹⁶

V1 is the first cortical area to receive visual input, and is also known as the striate cortex due to the presence of the "line of Gennari", which is a distinctive stripe visible to the naked eye, formed by myelinated axons from the LGN.²¹⁷

The primary visual cortex is divided into six functionally distinct layers, with layer 1 being most superficial. This layer is composed mainly of dendritic and axonal connections. Layers 2 and 3 are labelled the supragranular layers and contain excitatory neurons that connect with upstream visual processing areas of the brain. Layer 4, the granular layer, is further sub-divided into four layers, labelled 4A, 4B, 4C α , and 4C β . The latter two are the major recipients of input from the lateral geniculate nucleus. Layers 5 and 6 are called the infragranular layers and contain neurons that provide feedback to the LGN.²¹⁸

Within the visual cortex, there is retinotopic mapping of the visual fields. The upper half of the visual cortex responds to the lower half of visual field while the reverse is true of the lower half. Over 50% of the striate cortex is devoted to the central 15° of the visual field. This central visual field is processed at the most posterior aspect of the visual cortex, while the peripheral retina is mapped more anteriorly.²¹⁹

Evidence of retinotopy was first put forward by neurologist Gordon Holmes and ophthalmologist Tatsuji Inouye who noticed that damage to the visual cortex from bullet and shrapnel wounds can reliably be localised to lesions in specific areas of the visual fields.^{220, 221} These maps have been further refined through functional magnetic resonance imaging (fMRI).²²²⁻²²⁴

The connection of layer 4 of the striate cortex with LGN axons forms the basis of the precise topographic maps discussed above. These connections form prior to eye opening and are driven by a combination of molecular signalling in the cortex²²⁵ and spontaneous neural activity.²²⁶

Retinotopy is not the only form of neuronal organisation in the visual cortex. As part of their Noble prize winning work, Hubel and Wiesel discovered that neurons within the visual cortex respond preferentially to stimulus from one eye.^{227, 228} In humans, these neurons are organised into bands around 2mm thick known as “ocular dominance columns”.²²⁹ Similarly, there is cortical organisation based on the features of the visual stimulus being presented such as orientation, spatial frequency, disparity, and direction.²³⁰

The visual cortex is a fine example of developmental plasticity demonstrated by the brain. The development of the brain is a protracted process that begins in the third week of gestation and continues well into the postnatal period. The cerebral hemispheres develop from walls of the telencephalon, which are bilateral evaginations from the most anterior part of the prosencephalon at around six weeks of gestation. The superior portions of these walls develop into the primordium of the cerebral cortex, the pallium. The visual cortex arises from the largest portion of the pallium called the neo-pallium.

During the eighth week of gestation, cells in the developing cortex migrate and organise into the six layers that form the final cortical architecture as described earlier. These then undergo further maturation and form synaptic connections with surrounding neurons as well as axons from subcortical areas.

During the intrauterine period of life, a great excess of neurons is produced, peaking at around 28 weeks of development. This number declines by around 70% around the time of birth.^{231, 232} Myelination of the visual pathways only begins at birth starting at the occipital poles and progressing anteriorly.^{128, 233, 234}

As mentioned earlier, the human visual cortex continues to develop in the post-natal period and only reaches maturity at around five years of age. During this period, the neurons and their synaptic connections undergo extensive re-modelling and pruning.^{235, 236} External stimulation plays an important role in its maturation. In their pioneering work, Hubel and Wiesel showed that monocular sensory deprivation disrupts the ocular dominance of V1 cells, with a loss of neurons driven by the deprived eye.²³⁷ Plasticity of the visual system during infancy means that reversible congenital abnormalities such as cataracts need to be treated early to minimize long-term impact.²³⁸

1.4.9.2 VISUAL CORTEX IN ALBINISM

Structural changes

Magnetic resonance imaging has shown that albinism is associated with subtle structural changes in the visual cortex. Using voxel based morphometry (VBM), Von dem Hagen et al. found that patients with albinism show a reduction in cortical volume at the occipital pole,²³⁹ while Neveu et al. found that the calcarine fissure is shorter. In addition, the latter study also reported a marked asymmetry in the calcarine sulcus between the left and right hemispheres of the majority of albinism patients. The authors noted that in the presence of a dominant eye, the calcarine sulcus in the contralateral hemisphere is displaced downwards.²⁴⁰

Using surface based analysis (SBA), a recent study by Bridge et al. showed reduced gyrification in the ventral occipital cortex of albinism patients that explains the reduced cortical volume reported by Von dem Hagen et al. In addition, they found cortical thickness to be increased at the occipital pole of patients with albinism. This

change was more profound in the left hemisphere and cortical thickness was negatively correlated to visual acuity. These findings were consistent with results from early blind²⁴¹ and anophthalmic subjects.²⁴² The authors suggested that these changes are due to a lack of post-natal neuronal pruning as a result of under-development of the fovea seen in albinism and a consequent absence of high-resolution input into V1.²⁴³

Bridge et al. suggested that the difference in results between the two previous studies were due to the two different analysis techniques being employed. VBM works by registering a T1-weighted image to a common stereotactic space to take into account differences in brain shape between different subjects. This leads to spatial alignment of voxels from different individuals. However, this process only corrects for global brain shape differences rather than matching each cortical feature exactly. This is because VBM tries to detect differences in the local concentration or volume of grey and white matter having discounted global shape differences. If the spatial normalisation was exact, all the segmented images would appear identical, and no significant differences would be detected at a local scale.

Subsequently, intensity from each voxel alongside prior knowledge of tissue class location allows segmentation of the image into grey matter, white matter and CSF. The value at each voxel represents the probability of the voxel belonging to one of these three classes on a scale of 0 to 1.

The grey matter voxel values can be scaled to take into account the deformation, which took place during the registration process. As spatial normalisation is not exact, the modulated and segmented images are then smoothed with an isotropic Gaussian kernel and voxel wise comparisons of grey matter volume between two or more experimental groups can be made.^{244, 245}

The estimation of local grey matter volume in the cortex depends on cortical thickness and surface area.²⁴⁶ As VBM tools transform and smooth MRI data from different individuals into common coordinate spaces based on voxel intensity without accounting for gyral or sulcal anatomic features of the cortex, it may miss subtle

differences in cortical morphology due to normal variation in gyrification patterns.²⁴⁷⁻
²⁴⁹ As a result, studies employing VBM have shown large heterogeneity in reporting structural changes.²⁵⁰

In our study, we use SBA, which provides an alternative methodology to assess cortical differences in the human brain by generating geometric models of the cortical surface.²⁵¹⁻²⁵³ The details of this methodology are described later in section 2.2.3.4 on page 103, with the main differences lying in the registration and smoothing steps. SBA applies smoothing at the cortical surface compared to VBM, which carries out three-dimensional smoothing.²⁴³

SBA uses non-rigid high-dimensional averaging to inflate cortical folding patterns and register them to a sphere. This leads to better inter-subject registration of homologous cortical regions and allows thickness and surface area components of the volume to be studied separately.²⁵⁴

Another advantage of using SBA over VBM is that while the latter technique can elucidate group differences in cortical morphology, due to individual variability in neuroanatomy, they do not allow inferences to be made at the level of the individual.²⁵⁵

Functional changes

In addition to anatomical changes, albinism is also associated with functional re-organisation of the visual cortex. Through animal studies of the retro-geniculate visual pathway in albinism, three distinct “Boston”, “Midwestern” and “True albino” models of cortical organisation have been recorded.

Hubel and Wiesel noted that in Siamese cats, input from the contralateral temporal hemi-retina is processed at a distinct and abnormal cortical location.²⁵⁶ The representation of the visual midline moves from the border of Brodmann areas 17/18 to well within area 17.²⁵⁷ These findings were termed the “Boston pattern” and were confirmed by subsequent studies.^{209, 258}

In the “Midwestern” pattern, geniculostriate pathways remain unchanged and project information from nasal and temporal hemi-retinae to the same part of the visual cortex. However, visual input from the abnormally routed temporal retina is suppressed to varying degrees. As a result, each hemisphere responds to stimuli presented on one aspect of the visual field.^{205, 209, 259}

Like the “Midwestern” pattern, geniculostriate patterns are anatomically unchanged in the “true-albino” pattern. However, instead of suppression of signal from the temporal retina, it is superimposed on top of the normal input from the nasal retina. At a cellular level, this is likely to be due to re-assignment of the usual ocular dominance columns.^{205, 206, 259}

Hoffmann and Dumoulin suggested that to describe the above cortical maps more descriptively, the “Boston” pattern should be renamed “contiguous representation”, while the “true-albino” and “Midwestern” patterns be referred to “interleaved” and “interleaved suppressed” representations respectively.²⁶⁰ In some studies, more than one pattern has been demonstrated at different locations within the visual cortex of the same animal.^{257, 258, 261}

In humans, fMRI studies have confirmed abnormal retinotopic representation in the striate cortex of patients with albinism.²⁶²⁻²⁶⁵ The usual arrangement of ocular dominance columns is replaced by hemifield dominance columns leading to a “true-albino” or “interleaved” representation of the visual field.²⁰⁶

In this arrangement, the nasal hemi-retina has a normal representation in the contralateral striate cortex, however, stimulation of the temporal retina at the corresponding eccentricity leads to activation of the same cortical regions as those activated by the stimulation of the nasal retina. Under normal circumstances, communication between successively arranged ocular dominance columns leads to stereoscopic vision. In albinism however, cortical plasticity leads to independent processing of input from the two hemi-fields. This avoids sensory conflict across the hemi-field columns and allows the abnormal retinal input to be processed for perception.²⁶⁶

Stimulation of the peripheral temporal hemi-retina, however, leads to activation of the anterior ipsilateral cortical hemisphere indicating normal uncrossed projection.²⁶⁷ This indicates that not all fibres originating in temporal retina project contralaterally and that there is a shift of the line of decussation from the vertical meridian through the centre of the fovea into the temporal retina²⁶⁸ that has been quantified as ranging between 2° and 15° of the visual angle.²⁶⁹ The degree of this shift is related to level of pigmentation, indicating that the extent of misrouting is a function of the severity of the albinism phenotype.²⁶⁷ The abnormal visual representation persists in the extra-striate visual areas.^{270, 271}

The range of abnormalities seen within the visual pathway of patients with albinism makes it difficult to determine whether the reported brain abnormalities are congenital or whether they develop because of abnormal visual input. In section 3.5 of this thesis, we attempt to bridge this gap in knowledge and compare ocular and cortical abnormalities in albinism, which have been imaged using OCT and MRI, respectively.

1.4.10 NYSTAGMUS

1.4.10.1 NORMAL EYE MOVEMENTS

Eye movements are controlled by six muscles that work synergistically to maintain fixation. Table 1-1 lists these alongside their innervations and actions.

<i>Muscle</i>	<i>Innervation</i>	<i>Primary action</i>	<i>Secondary action</i>	<i>Tertiary action</i>
<i>Inferior oblique</i>	Oculomotor nerve (CN III)	Extorsion	Elevation	Abduction
<i>Superior rectus</i>		Elevation	Intorsion	Adduction
<i>Inferior rectus</i>		Depression	Extorsion	Adduction
<i>Medial rectus</i>		Adduction	-	-
<i>Superior oblique</i>	Trochlear nerve (CN IV)	Intorsion	Depression	Abduction
<i>Lateral rectus</i>	Abducens nerve (CN VI)	Abduction	-	-

Table 1-1: Innervation and actions of the six extraocular muscles²⁷²

The primary function of eye movements is to maintain a steady fixation^{273, 274} as image resolution degrades rapidly with movement.²⁷⁵ The mechanisms employed to achieve this can be organized in to two groups:

1) **Gaze stabilization mechanisms** counteract the effect of self-motion by moving the eyes to stabilise the visual target on the retina.²⁷⁶

- a. Vestibulo-ocular reflex is driven by the vestibular apparatus that detects movements of the head and leads to compensatory eye movements.
- b. Optokinetic reflex relies on direction-selective retinal ganglion cells to detect movement of the visual world (retinal slip) and activates the oculomotor musculature to produce compensatory eye movements.^{277, 278}

The two gaze holding mechanisms work together with the vestibulo-ocular reflex being more efficient at higher frequencies, while the optokinetic system works best at lower frequencies of head movements.²⁷⁹

2) **Gaze shifting mechanisms** are used to fix gaze on a target.

- a. Saccadic movements are rapid movements of the eye that change the fixation point of the eyes.^{280, 281} Their amplitude ranges from small movements made while reading to much larger movements made while gazing around a room. They can be generated voluntarily or in response to a stimulus, which may be visual, auditory or somatosensory.²⁸²⁻²⁸⁵ Saccadic movements are controlled via a complex mechanism. The amplitude and direction of the eye movement (motor error) is determined by two principle structures, the superior colliculus and the frontal eye field.²⁸⁶ This motor error is then relayed to the paramedian pontine reticular formation where a group of “burst neurons” fire around 8-12ms before each saccade. These in turn are connected directly to the oculomotor nuclei.^{287, 288} At the end of the saccadic movement, the eye is kept in its new position by neural integrators in the medulla and midbrain^{289, 290} generating a tonic command to counteract the elastic forces which restore the eye back to the midline.^{291, 292}

- b. Smooth pursuit movements are slower tracking movements designed to keep a moving stimulus on the fovea.²⁹³ The eye movements respond to a stimulus within a small portion of the visual fields and are distinct from the optokinetic reflex, which responds to minimize the retinal slippage of the whole visual field.²⁹⁴

Functional brain imaging and neurophysiological research has demonstrated that the smooth pursuit is processed within the motion sensitive visual area V5,^{295, 296} frontal²⁹⁷ and supplementary eye fields.^{298, 299} In addition, a dense neural network facilitates the interaction of the smooth pursuit system with multiple other visual and non-visual sensorimotor systems for an optimal smooth pursuit response.³⁰⁰

- c. Vergence system leads to a disconjugate, convergent or divergent movement of the eyes to focus objects at different distances. The physiological rest position of eyes is known as “tonic vergence”.³⁰¹ There are three sources of information that determine the magnitude and direction of version movements.

- i. *Disparity/fusion vergence* occurs when the same stimulus appears on different locations on each retina.³⁰²
- ii. *Accommodation* state of both lenses is monitored by the brain and the information is used to calculate the distance to the target in focus.³⁰³
- iii. *Proximal vergence* uses monocular depth cues such as linear perspective to infer distance to the target.³⁰⁴

The neural control of vergence movements has been attributed neurons in both cerebellar and pontine nuclei as well as the frontal eye fields.³⁰⁵

Figure 1-20 summarizes how the interaction between the gaze systems mentioned above brings about stable fixation.

Figure removed from online version to avoid copyright infringement

Figure 1-20: Schematic diagram of the oculomotor command system. The saccadic system responds to target position (T) while the pursuit system is driven by target velocity (\dot{T}). The vestibular and optokinetic systems respond to head movements (\dot{H}) sensed by the semi-circular canals and retinal ganglion cells respectively. The vergence system is driven by the distance to the target (D). b_K = velocity signals from each subsystem (K), b = overall velocity signal from the OCS, n = position signal from the neural integrator, g = eye position.²⁷⁶

1.4.10.2 NYSTAGMUS

Nystagmus refers to a rhythmic involuntary to-and-fro oscillation of the eyes. The word nystagmus takes its origin from the Greek words “nystagmos” meaning drowsiness and “nystazein” which means to nod, as the downward head drift of a drowsy individual followed by an upward jerk, resembles the slow drift phase of the eyes followed by a quick phase seen in nystagmus.³⁰⁶

Nystagmus leads to reduced visual acuity because images rapidly move across the retina of the affected individual and they are not able to focus the image on their fovea.³⁰⁷ The constant movement of the eyes may also reduce motion sensitivity.³⁰⁸

1.4.10.2.1 CLASSIFICATION

Nystagmus can be broadly categorized into infantile and acquired forms based on age of onset. Infantile nystagmus (IN) usually appears in the first 6 months of life while acquired nystagmus appears later.³⁰⁹ Albinism is associated with IN. It is one of a number of subtypes of IN, which are subdivided based on the associated disorders. (Figure 1-21)

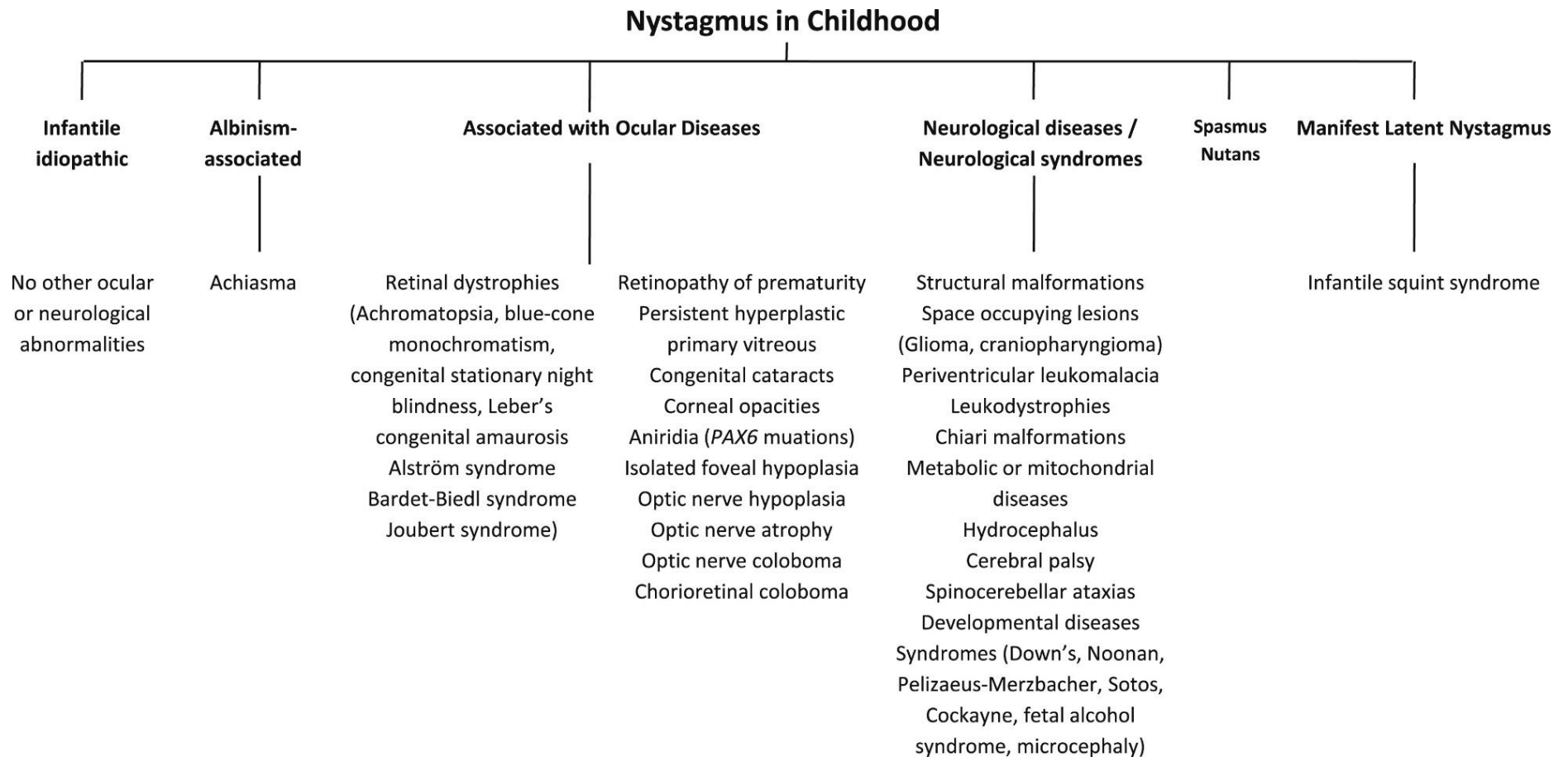


Figure 1-21: Classification of Infantile Nystagmus³¹⁰

1.4.10.2.2 NYSTAGMUS CHARACTERISTICS

The nature and severity of nystagmus type can vary between patients. The following terminology is used to describe nystagmus characteristics (Figure 1-22):

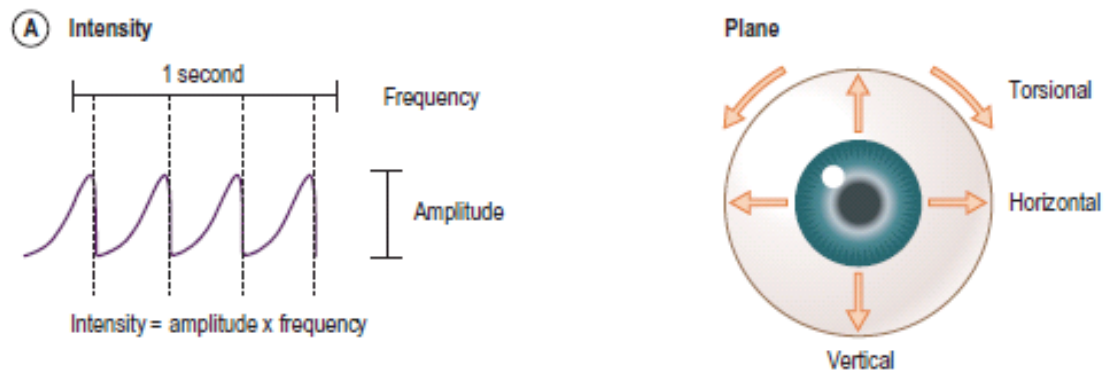


Figure 1-22: Nystagmus characteristics

- 1) **Intensity:** This is a measure of the speed of the eye movement. It is the product of the number of oscillations per second measured in Hz (frequency) and magnitude of the oscillation amplitude measured in degrees (amplitude), thus expressed in degrees/second.
- 2) **Direction:** This is determined based on the quick phase of the oscillation.
Nystagmus can occur in the vertical, horizontal and torsional planes.
- 3) **Conjugacy:** Describes whether both eyes are moving in the same direction.
- 4) **Waveform:** The above characteristics can be studied using eye movement recordings that have shown various waveforms of nystagmus. These were outlined by Dell'Osso and Daroff in 1975 and a summary of these different waveforms is depicted in Figure 1-23.

Figure removed from online version to avoid copyright infringement

Figure 1-23: Nystagmus waveforms as classified by Dell’Osso and Daroff³¹¹

- 5) **Foveation characteristics:** Figure 1-24 highlights the period during the nystagmus cycle where the eye velocity is at its lowest. This duration is known as the foveation period.³¹² The length of the foveation period can predict the degree of visual impairment caused by a patient's nystagmus. Dell'Osso and Jacobs have proposed an eXpanded Nystagmus Acuity Function (NAFX) that provides a measure of the amount of foveation based on a patient's nystagmus waveform. The authors have shown that this period can be used to predict a patient's best corrected visual acuity (BCVA) based on information on eye position and length of foveation periods.³¹³



Figure 1-24: Illustration of foveation periods

- 6) **Null region:** The waveform and intensity of nystagmus may change with head and eye position. The gaze position in which the intensity is lowest is known as the "null region". The foveation period and hence visual acuity is greatest in this null region and as a result, patients often turn their head to fixate at objects. This sign is known as "anomalous head posture".³¹⁴

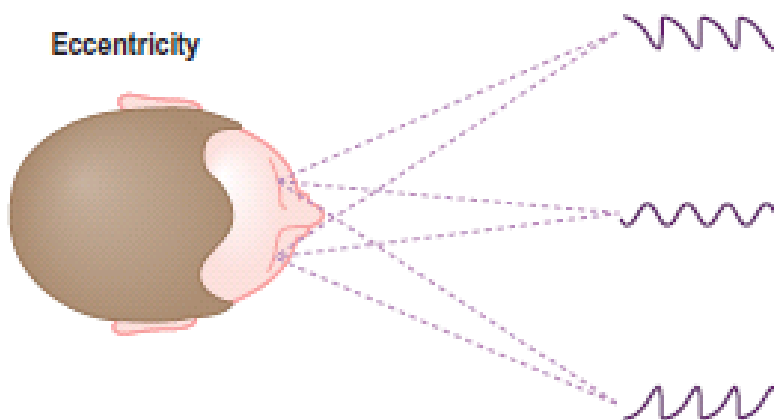


Figure 1-25: Change in nystagmus waveforms at various gaze positions

- 7) **Periodic alternating nystagmus:** A subset of patients display periodic alternating nystagmus, which is where the nystagmus direction changes periodically with an intervening quiet phase.^{315, 316}

Nystagmus characteristics in albinism

Nystagmus in albinism is primarily horizontal and conjugate.³¹⁷ In a detailed comparison of oculomotor characteristics of nystagmus associated with albinism and FRMD7 mutations, Kumar et al. observed that patients with albinism had a higher proportion of jerk nystagmus. They noted that nystagmus frequency is lower in albinism; they have better foveation characteristics and are more likely to possess a null-region. Around 30% of patients with albinism display periodic alternating nystagmus.¹⁷⁴

1.4.10.2.3 MECHANISMS BEHIND INFANTILE NYSTAGMUS

The mechanisms behind infantile nystagmus are poorly understood. There has been some debate concerning whether a direct cause of the nystagmus is common to these diverse subtypes. Multiple hypotheses have been devised to explain the waveforms seen in IN and the varied nature of mechanisms suggested in these models are testimony to the lack of agreement over this issue.

Efferent (motor) abnormalities: Initial models of IN focused on the neural integrator,^{318, 319} which is a neural network situated in the brainstem that converts eye-velocity signals into the eye-position commands that are essential for eye-movement control.^{320, 321} In addition, abnormalities in the saccadic system have also been blamed for the jerk nystagmus seen in IN.^{322, 323}

However, while the errors in the neural integrator and the saccadic systems can explain instability, they do not fully tackle the sinusoidal oscillations seen in IN.³²⁴

This has led some researchers to suggest that, rather than abnormal neural integrator feedback loops, oscillations in IN are due to abnormalities in the smooth pursuit

system with correcting saccades towards the centre explaining the jerk portions of the waveform.³¹⁹

Similarly, deficiencies in the optokinetic³²⁵ and vestibular systems³²⁶ have also been ruled in and out by various groups as the potential cause behind IN.³¹⁹

Afferent (sensory) abnormalities: While conventionally all forms of infantile nystagmus have been looked upon as having a common origin based on deficiencies within the ocular motor systems, as evidenced by the models above, this premise ignores the varied afferent abnormalities seen in the different conditions associated with IN. As our understanding of the sensory deficits associated with nystagmus enhances, various groups are proposing that the origins of nystagmus lie in the afferent defects. However, due to the variety of diseases associated IN, it is not yet clear what type of afferent deficit is culpable.

Two main sources of sensory abnormalities have been identified as potential culprits for causing nystagmus.

- 1) **Retinal deficits:** Harris and Berry have suggested that if the normal visual system is deprived of high-spatial frequency contrast stimulation during visual development, then the oculomotor system responds by developing oscillations that improve the contrast sensitivity to stimuli of lower spatial frequency.³²⁷ Brodsky and Dell'Osso have recently put forward an alternative hypothesis to explain the relationship between retinal deficits and nystagmus. They suggested that IN occurs due a failure of suppression of the subcortical accessory optic system (AOS).³²⁸ In lateral-eyed animals with no binocular vision, the AOS modulates visuovestibular reflexes. It receives input from direction specific retinal ganglion cells via the accessory optic tracts and processes information regarding retinal slip of the visual world to produce corrective movements and stabilise the retinal image.³²⁹⁻³³² In humans, this system is suppressed by the visual cortex. The authors suggest that abnormal or unequal input from the fovea means that this system remains active in patients with IN and leads to nystagmus.³²⁸

- 2) **Axonal misrouting:** Recent evidence from several experimental models, including zebrafish, mice and humans propose that abnormal crossed projections could lead to miswiring of motion sensors that directly generate erroneous sensory signals cause nystagmus.³³³⁻³³⁵

The above conflict in literature points to a need for a study that assesses the relationship of nystagmus with foveal and chiasmal abnormalities. In section 3.6 of this thesis, we attempt to resolve this by using infrared pupillography to record and analyse eye movements. This provides us with various objective measures of nystagmus severity such as frequency, amplitude, NAFX and null point characteristics. These can then be compared to objective measures of foveal and optic nerve abnormalities measured using OCT as well as chiasmal misrouting quantified via VEP and DTI. Any relationships between these abnormalities would enhance our understanding about an underlying mechanism behind nystagmus in albinism.

1.5 AIMS

1.5.1 OVERVIEW

As outlined above, the main deficits associated with albinism exist at the level of the retina and the optic chiasm. The focus of this research is to identify and quantify these abnormalities and explore the relationship between them. The study also attempts to ascertain the impact of these abnormalities on visual function.

Foveal and optic nerve structure will be assessed using high-resolution OCT while the chiasmal and the cortical anatomy will be imaged using MRI and compared to the OCT appearance of the fovea and optic nerve. In addition, we use diffusion tractography to evaluate chiasmal misrouting in albinism.

Finally, we will measure nystagmus characteristics using infrared eye tracking and compare these to structural abnormalities seen in albinism to see whether nystagmus generation is related to afferent abnormalities of the visual system.

Comparison of the OCT measures of the retinal, chiasmal and cortical deficits in albinism will allow us to find the association between (a) abnormal foveal development and chiasmal/cortical abnormalities; and (b) axonal loss and miswiring and chiasmal/cortical abnormalities and nystagmus.

Through this study, we hope to gain a better understanding of the visual dysfunction seen in albinism and use this information to enhance our knowledge about normal development and functioning of the visual system.

1.5.2 SPECIFIC AIMS

1.5.2.1 FOVEA

Section 3.2 (page 120) addresses the following aims:

1. Image the fovea of patients with albinism using high resolution OCT.
2. Assess the spectrum of foveal development in albinism.
3. Quantify the thickness of retinal layers at the fovea and compare this with healthy controls.
4. Assess the association between foveal abnormalities on vision in albinism.
5. Assess whether visual evoked potential asymmetry seen in albinism is related to foveal development

To achieve the above aims, we tested following hypotheses (H_0):

H_0 1.1: Foveal layers are thicker in patients with albinism compared to healthy controls.

H_0 1.2: The development of the photoreceptor and processing layers is related.

H_0 1.3: Visual acuity is related to foveal development

H_0 1.4: Chiasmal misrouting measured using VEP is related to foveal development.

1.5.2.2 OPTIC NERVE

Section 3.3 (page 136): addresses the following aims:

1. Using high resolution OCT, characterise optic nerve head (ONH) topography in albinism.
2. Investigate optic disc tilt that has been reported in albinism.¹⁶⁹
3. Analyse the arrangement of the peripapillary retinal nerve fibre layer (ppRNFL) around the optic nerve since miswiring of retinal projections is known to occur in albinism.²⁶⁴

4. Compare ONH and ppRNFL abnormalities in albinism with foveal abnormalities.
5. Compare ONH and ppRNFL abnormalities in albinism to other clinical measures such as refractive error, nystagmus, and best-corrected visual acuity.

The above aims will be addressed by testing the following hypotheses:

H₀ 2.1: OCT can be used to reliably measure the ONH and ppRNFL parameters in albinism.

H₀ 2.2: Patients with albinism have abnormally small optic discs, cup and rims.

H₀ 2.3: Patients with albinism have optic disc tilt and torsion.

H₀ 2.4: Patients with albinism have a smaller ppRNFL size

H₀ 2.5: Foveal and optic nerve development are related in patients with albinism.

H₀ 2.6: Optic nerve head abnormalities impact on visual acuity

H₀ 2.7: Optic nerve head abnormalities are related to chiasmal misrouting measured using VEP.

1.5.2.3 OPTIC CHIASM

Section 3.4 (page 157) addresses the following aims:

1. Quantify the size the intracranial optic nerve, chiasm and tracts in patients with albinism using MRI and compare them to healthy controls.
2. Investigate the relationship of the chiasm with the fovea and the optic nerve head.
3. Assess whether diffusion tensor tractography can be used to explore misrouting seen in albinism.

The above aims will be addressed by testing the following hypotheses:

H₀ 3.1: The optic nerve, chiasm and tract sizes are smaller in albinism compared to healthy controls.

H₀ 3.2: DTI can show increased decussation in patients with albinism.

H₀ 3.3: Chiasmal decussation measured using VEP and DTI are related.

H₀ 3.4: There connectivity at chiasm and foveal abnormalities are related.

H₀ 3.5: Connectivity at chiasm and ONH abnormalities are related.

H₀ 3.6: Chiasmal size impacts visual acuity.

1.5.2.4 VISUAL CORTEX

Section 3.5 (page 174) addresses the following aims:

1. Clarify the previous conflict in literature regarding the nature of cortical abnormality in albinism through high-resolution MR imaging and surface based analysis methodology in a sufficiently large group of patients.
2. Investigate the relationship of any cortical abnormalities with those seen within the fovea, optic nerve and chiasm.

The above aims will be addressed by testing the following hypotheses:

H₀ 4.1: Cortical thickness and volume at the occipital pole in is higher in patients with albinism compared to healthy controls.

H₀ 4.2: Occipital pole cortex size and foveal layer thickness are related in patients with albinism.

H₀ 4.3: Occipital pole cortex size and optic nerve head parameters are related in patients with albinism.

H₀ 4.4: Occipital pole cortex size and chiasm size are related in patients with albinism.

1.5.2.5 NYSTAGMUS

Section 3.6 (page185) addresses the following aims:

1. Compare efferent motor characteristics of the nystagmus in albinism with features of following three afferent deficits in albinism at different levels in the visual pathway:
 - the degree of foveal development quantified using macular OCT imaging,
 - the morphology of the peripapillary nerve fibre layer quantified using OCT imaging of the optic nerve region
 - the degree of chiasmal misrouting by measuring asymmetry of visual evoked potentials

The following hypotheses will be tested to address the above aims:

H₀ 5.1: Nystagmus intensity is related to foveal development.

H₀ 5.2: Nystagmus intensity is related to optic nerve abnormalities.

H₀ 5.3: Nystagmus intensity is related to chiasmal misrouting measured using VEP.

CHAPTER 2

METHODS

2.1 RECRUITMENT OF VOLUNTEERS

2.1.1 ALBINISM GROUP

Patients with albinism were recruited from neuro-ophthalmology clinic at the University Hospitals of Leicester NHS trust. In addition, the “Leicestershire Nystagmus Survey” database was used to invite additional patients with albinism residing in the Leicestershire area.³⁸

As part of their visit to the neuro-ophthalmology clinic, the patients underwent a detailed clinical examination that included assessment of visual acuity, colour vision, stereo acuity, visual fields, pupillary reactions, ocular movements, slit lamp examination and dilated fundus examination. Summers’ classification was used to grade the degree of iris transillumination. Fundi were examined clinically for tilted discs.^{170, 171} Best-corrected visual acuity (BCVA) was measured using a logMAR (logarithm of minimum angle of resolution) chart.

2.1.2 CONTROL GROUP

Control volunteers were recruited from amongst unaffected and genetically unrelated family members of the patient group and from within the staff members of the University of Leicester and the University Hospitals of Leicester NHS trust. Volunteers were only included in the study if they had no history of eye disease, had a BCVA of better than 0.0 logMAR and refraction errors between -3D and +3D.

In total, 60 healthy controls were recruited for the study (36 male and 24 female, mean age=39.2±14.7 years). Details regarding the demographics of the control group for individual experiments are stated in the relevant results sections.

2.1.3 INCLUSION AND EXCLUSION CRITERIA

The diagnosis of albinism was made by experienced ophthalmologists based on three key clinical features of albinism namely such and iris transillumination, macular hypopigmentation, foveal hypoplasia and nystagmus. The diagnosis was confirmed via the presence of an asymmetric VEP response and patients were only included in the study if they displayed interhemispheric VEP asymmetry of greater than 0.7 which has been stated as being diagnostic for albinism by Apkarian.²⁰¹ The method for calculating the interhemispheric is described on page 113.

As the OCT device could only correct for refractive errors up to +/-10D, three patients with refractive errors greater than this were excluded from the study. Children under the age of seven were excluded as their short attention span made it difficult to obtain reliable OCT and MRI scans.

Due to MRI safety considerations, a patient with a coronary stent in-situ and another in early pregnancy were not eligible for this part of the study. A copy of the safety questionnaire can be seen in the appendix (page 264).

2.1.4 ETHICAL APPROVAL AND CONSENT

The study was conducted in keeping with the declaration of Helsinki protocols and was approved by the Leicestershire, Northamptonshire & Rutland Research Ethics Committee (study reference number 6216). Prior to inclusion in the study, informed consent was sought from each participant after explaining nature and consequences of the study. For volunteers under 18, ascent from the parent/guardian was also obtained. Copies of the ethical approval, patient information letters and consent forms used for this study are included in the appendix (page 242 onwards).

2.2 OCT SCANNING

2.2.1 SCAN ACQUISITION

For our study, a high-resolution spectral domain OCT device (SOCT Copernicus HR, OPTOPOL Technology S.A., Zawiercie, Poland), with an axial resolution of $3\mu\text{m}$ and a transverse resolution of $12\mu\text{m}$ in tissue, was used to obtain 3-dimensional cross-sectional images of the macula and optic disc of both eyes in all the volunteers. At the time of the commencement of the study, this was one of the highest resolution commercially available devices. Due to small axial dimensions of the retinal layers, that can be as little as $10\mu\text{m}$ thick, high axial resolution is essential for their detailed assessment.³³⁶

Each 3-dimensional volumetric scan consisted of 75 B-scans with a distance of 0.09mm between successive B-scans. Each B-scan was 7mm wide, 2mm deep and contained 750 A-scans distance. Figure 2-1 outlines the dimensions of the volumetric scans that were used for this study.

As all the albinism patients displayed horizontal nystagmus, motion artefact was in the transverse direction. Therefore, this had minimal effect on the axial measurements of retinal layer thickness. Additionally, the rapid scan acquisition rate of 52,000 A scans per second meant that each B-scan took 14.4ms to acquire which helped to minimise motion induced artefact caused by the nystagmus (e.g. during the slow phase of a typical jerk nystagmus of 5° and 3.5Hz the average motion artefact is 1.25% of scan width). However, successive B-scans were misaligned which meant that multiple B-scans could not be averaged. The high signal to noise ratio provided by the Copernicus device allowed us to obtain measurements from single B-scans.

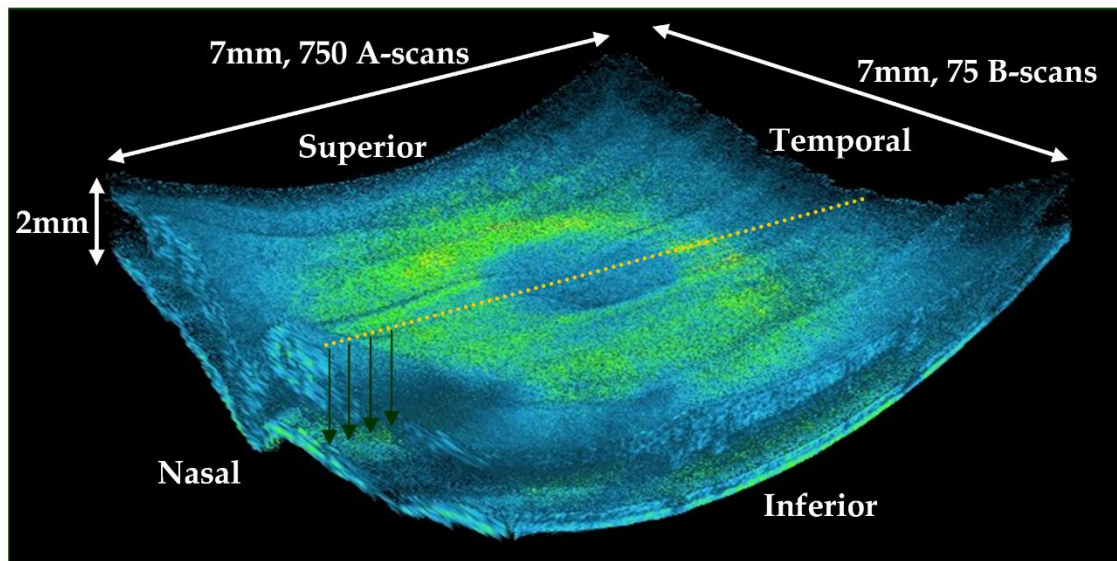


Figure 2-1: A 3-dimensional scan from a control volunteer outlining the dimensions of the OCT scan. The yellow dotted line indicates the orientation of the B-scan and the green arrows indicate the direction of the A-scans.

The scanning took place in a darkened room at the Leicester Royal Infirmary to achieve maximal pupillary dilation without the use of mydriatic drops. The patient's refractive error was input prior to scan acquisition as the OCT device provided compensation for refractive error up to ± 10 dioptres.

Volunteers were asked to sit on a chair and place their chin on the chinrest attached to the OCT device. Once their eyes were on the same level as the lens, the patients were asked to fixate upon a flashing target. A real-time preview generated by the OCT device was used to locate the macula prior to scanning. Some patients with albinism who had poor vision were unable to visualise and fixate upon the flashing light. In these patients, the macula was located by using the optic nerve head as a landmark. The relative positions of the optic nerve head and the fovea have been documented in previous studies.³³⁷⁻³³⁹

After the macular scan had been completed, the target was shifted in the nasal direction to image the optic disc. The volunteers were allowed to rest before scanning the other eye. Each eye was scanned three times and the best quality scan was used for analysis.

Each scan lasted around 30 seconds and the complete scanning session lasted around 10 minutes.

The scanning protocol was modified slightly for children. Instead of sitting on a chair, the children were asked to stand so they could reach the chinrest comfortably. A modified, taller chinrest was used to compensate for the small head size in children. They were also given extra rests between the scans to prevent fatigue.

The majority of scanning was done by the author with help from Mr Viral Sheth who also acquired scan of the anterior segment. These were used to analyse the iris morphology of patients with albinism.¹⁰⁰ Out of the 72 patients taking part in the study, foveal scans for 47 and optic nerve scans for 38 patients were acquired as part of an intercalated BSc project undertaken by the author.



Figure 2-2: SOCT Copernicus HR device that was used for this study

2.2.2 DATA ANALYSIS

2.2.2.1 MACULAR SCAN

Since foveal hypoplasia was evident on analysis of scans from albinism patients, analysis was performed unmasked.

The first step of the analysis was to identify the B-scan of the centre of the fovea. Although this was relatively straightforward in the control eyes, the foveal hypoplasia meant that it was difficult to differentiate the fovea from peripheral retina. To identify the fovea, the region of optic nerve had to be identified first. Once this was done, the B-scans in the macular area adjacent to this were rated for the presence of signs of foveal development based on the developmental processes that occur at the fovea. These include centrifugal displacement of cells of the inner retina toward the periphery forming a foveal pit that continues to deepen until 15 months postnatally and under normal circumstances leads to complete extrusion of the inner retinal layers. On the OCT scans, this is seen as thinning of the processing layers and presence of a foveal pit. It is accompanied by centripetal migration of cone photoreceptors toward the location of the incipient fovea, which on OCT is visible as thickening of the outer nuclear layer. At the same time, foveolar cone photoreceptors undergo specialisation that entails a reduction in diameter, allowing closer packing, and increase in length of the outer segments that can be identified on OCT images.³⁴⁰

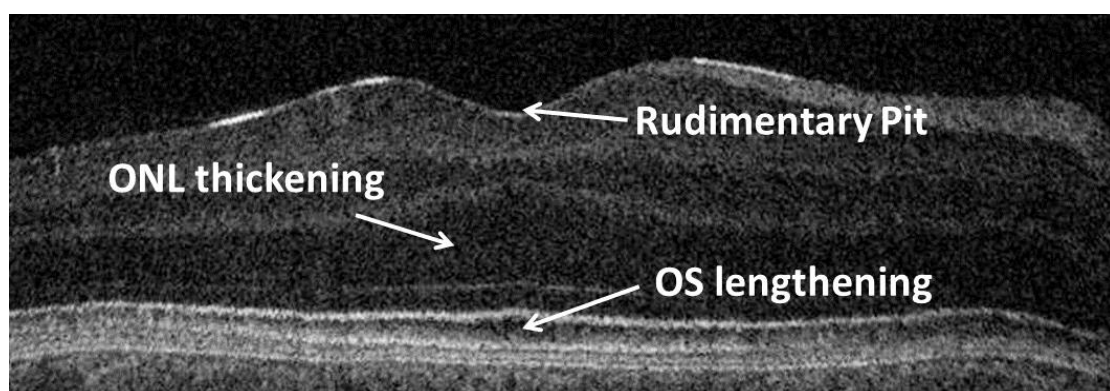


Figure 2-3: Development signs used to identify the fovea in the OCT scan of patients with albinism. These included outer nuclear layer (ONL) and photoreceptor outer segment (OS) layer thickening compared to the parafovea and presence of a foveal pit.

Presence of these three steps was used to determine the severity of foveal hypoplasia in each patients as per the grading system published by Thomas et al. The author of this thesis was part of the group, which developed this grading system and the paper is included in the appendix (page **Error! Bookmark not defined.**).³⁴⁰

According to this system, grade 1 foveal hypoplasia is associated with a shallow foveal pit, outer nuclear layer (ONL) widening, and outer segment (OS) lengthening relative to the parafoveal ONL and OS length, respectively. In Grade 2 foveal hypoplasia, all features of grade 1 are present except the presence of a foveal pit. Grade 3 foveal hypoplasia consists of all features of grade 2 foveal hypoplasia except the widening of the cone outer segment. Grade 4 foveal hypoplasia represents all the features seen in grade 3 except there is no widening of the ONL at the fovea. The group showed that the degree of foveal hypoplasia is related to visual acuity.

Thomas et al. also described an atypical form of foveal hypoplasia seen in patients with achromatopsia. Here, there is a shallower pit with disruption of the inner segment/outer segment (IS/OS) junction, possibly a sign of photoreceptor degeneration. This atypical form of foveal hypoplasia is not seen in patients with albinism.³⁴⁰ (Figure 2-4)

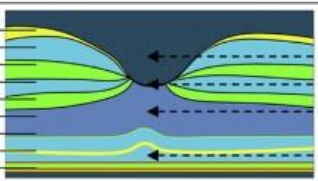
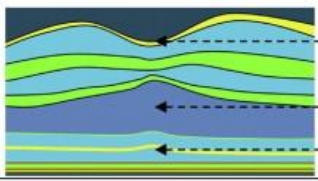
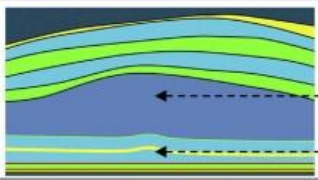
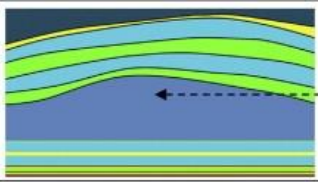
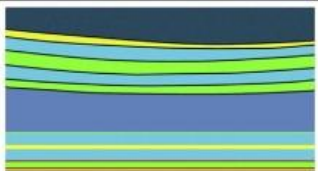
(A)		Normal foveal structural features detectable using optical coherence tomography		Illustration	
		(a) Extrusion of plexiform layers (b) Foveal pit (c) OS lengthening (d) ONL widening	RNFL GCL IPL INL OPL ONL ELM IS/OS RPE		(b) (a) (d) (c)
(B)		Grade of foveal hypoplasia	Structural features detected on optical coherence tomography	Present or absent	Illustration
		1	(a) Extrusion of plexiform layers (b) Foveal pit – Shallow (c) OS lengthening (d) ONL widening	(a) Absent (b) Present (c) Present (d) Present	
		2	(a) Extrusion of plexiform layers (b) Foveal pit (c) OS lengthening (d) ONL widening	(a) Absent (b) Absent (c) Present (d) Present	
		3	(a) Extrusion of plexiform layers (b) Foveal pit (c) OS lengthening (d) ONL widening	(a) Absent (b) Absent (c) Absent (d) Present	
		4	(a) Extrusion of plexiform layers (b) Foveal pit (c) OS lengthening (d) ONL widening	(a) Absent (b) Absent (c) Absent (d) Absent	

Figure 2-4: Grading system for assessment of foveal hypoplasia in albinism. (Adapted from Thomas et al.) A) Illustrates features of a normal fovea detectable on optical coherence tomography. B) Illustrates Grades 1-4 of foveal hypoplasia based on the degree of failure of normal development. ELM = external limiting membrane; GCL = ganglion cell layer; INL = inner nuclear layer; IPL = inner plexiform layer; OPL = outer plexiform layer; RNFL = retinal nerve fibre layer; RPE = retinal pigment epithelium.³⁴⁰

Once the correct B-scan was identified and graded, it was flattened along the choroid using SOCT Copernicus Software (version 4.2, OPTOPOL Technology S.A.). The flattening process aligns the scan along the retinal pigment epithelium through a pixel translation which allows retinal layer measurement close to the true axial plane hence minimising any inaccuracies which may be caused by taking measurements at varying angles through the retina. Figure 2-5 demonstrates an OCT scan from a patient with albinism before and after it was flattened.

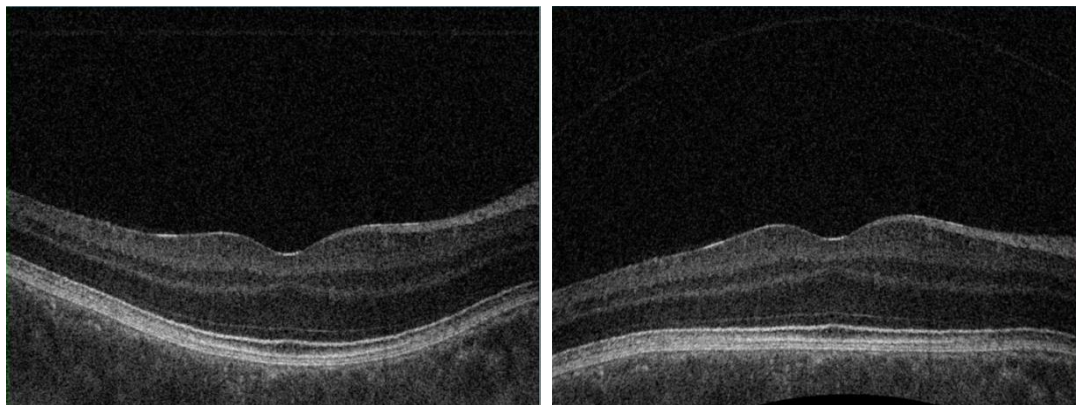


Figure 2-5: Foveal B-scan pre-flattening (left) and post-flattening (right)

The SOCT Copernicus software carries out automatic segmentation of RNFL, GCL, OS and RPE. However, to measure the thickness of all the retinal layers, ImageJ (National Institutes of Health, MD, USA) was used. This is a JAVA based image processing software that allows users to write customised programmes (macros) to aid their analyses. The author took advantage of this feature of ImageJ to write macros enabling partial automation of the analysis. The steps for this are detailed below. Figure 2-6 illustrates the boundaries used to differentiate between the layers.

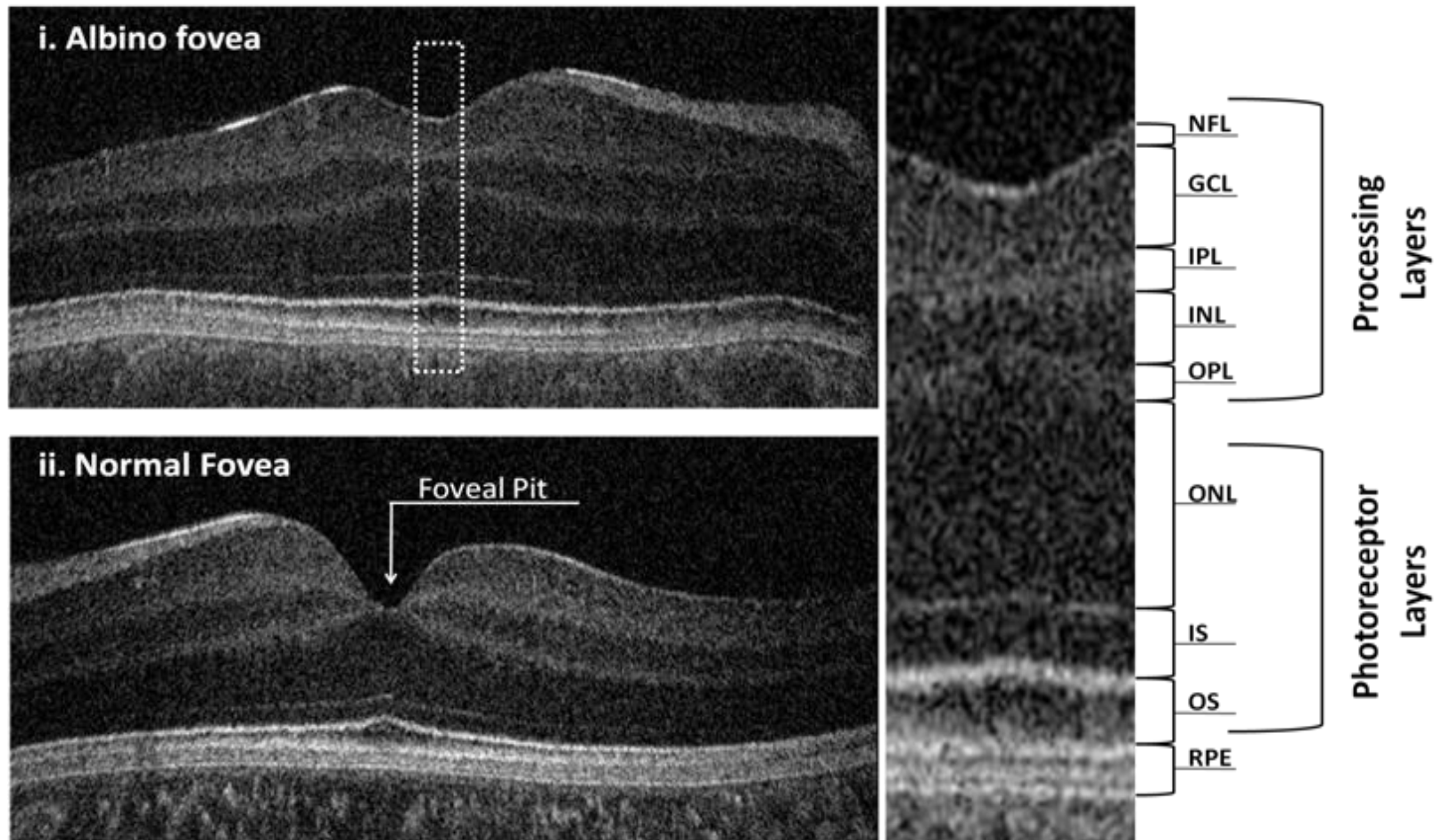
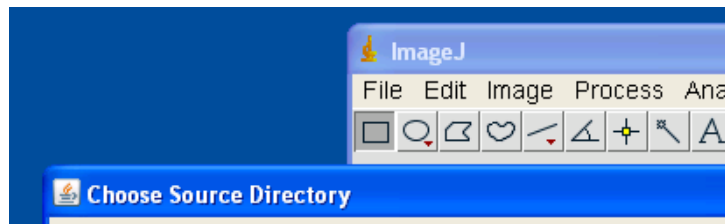


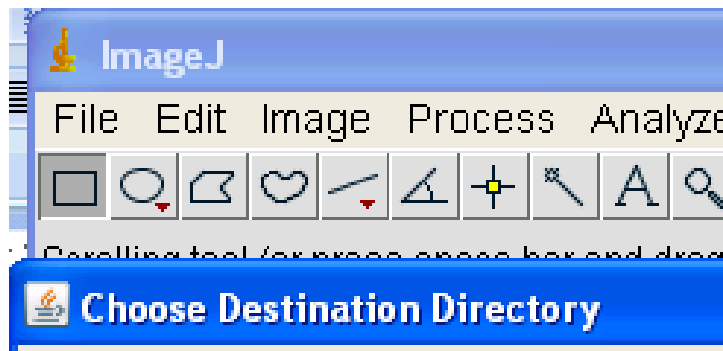
Figure 2-6: Figure illustrating the boundaries used to differentiate retinal layers while carrying out quantitative measurements in both albinism and control groups. NFL=Nerve fibre layer, GCL=ganglion cell layer, IPL=inner plexiform layer, INL=inner nuclear layer, OPL=outer plexiform layer, ONL=outer nuclear layer, IS=photoreceptor inner segment, OS=photoreceptor outer segment, RPE=retinal pigment epithelium.

Macro for Retinal Layer Segmentation

Step 1: Choose source directory where the flattened images are stored

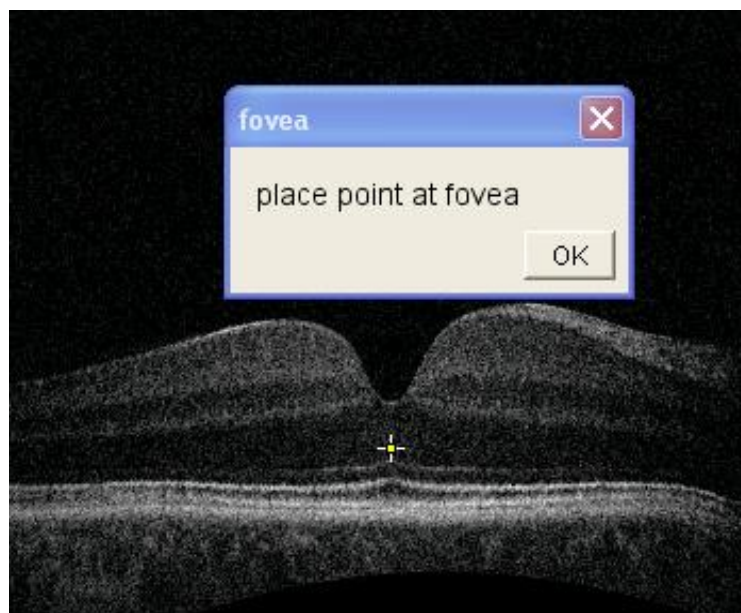


Step 2: Choose the destination directory in which results need to be stored



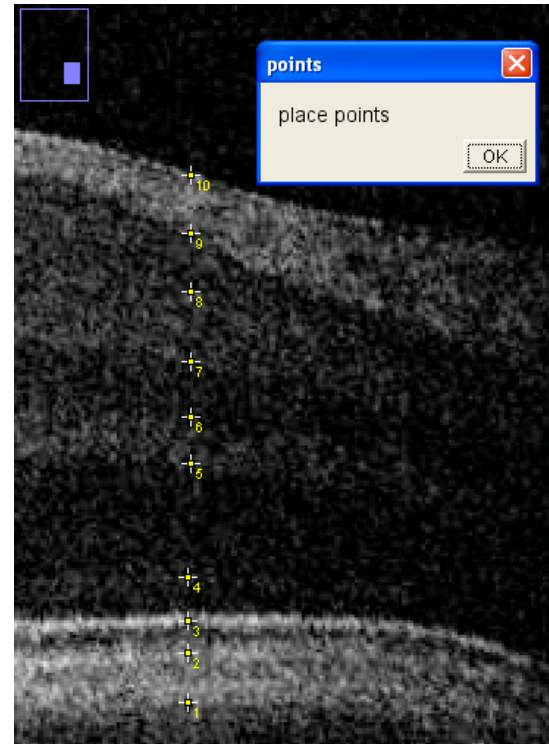
Step 3: The first image in the directory is opened by ImageJ

Step 4: Place a point at the fovea. The x, y co-ordinates from this point will be used as a reference point for the subsequent measurements



Step 5: The macro will now automatically generate 10 callipers at the fovea. These were manually placed at the boundaries of the different retinal layers. Once the points have been placed, the x, y co-ordinates of the points are saved on a text file.

Step 6: The next file in the directory is opened and the loop goes back to step four until all the images in the folder have been analysed.



The RPE complex consists of the RPE itself, Bruch's membrane and photoreceptor outer segment tips. However due to the presence of melanin in the RPE light from the OCT gets scattered making it difficult to differentiate between these layers. Therefore, this complex was treated as a single layer for measurement purposes. Figure 2-7 illustrates the comparison between the RPE complex from an albinism patient where different layers within the complex can be seen separately and a healthy control where the presence of melanin in the RPE obscures these.

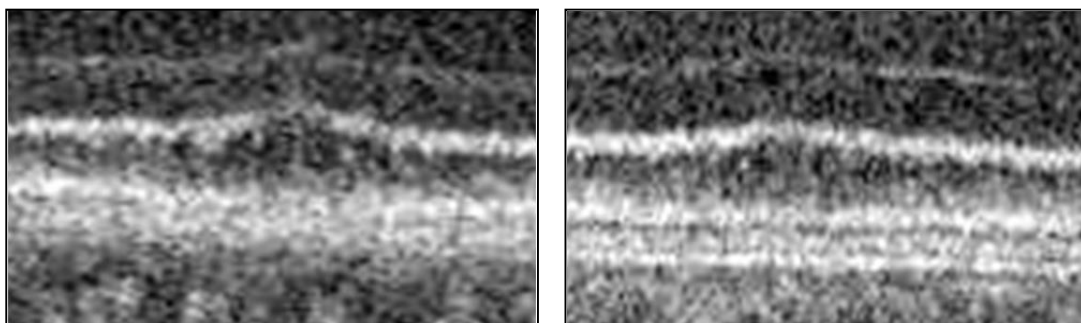


Figure 2-7: Comparison of foveal RPE complex in healthy control (left) and albinism (right)

B-Scan realignment

As mentioned above, nystagmus present in patients with albinism led to misalignment of successive B-scan slices that make up the volumetric scan. As the measurement of disc, rim and cup areas and volumes and ppRNFL sectors relies on multiple B-scans being analysed together, these had to be realigned by comparing the contours of the retinal vessels and disc margins en-face image from the SD-OCT scan to the fundus photograph from the same eye. (Figure 2-8)

This was a time-intensive and laborious process and had to be completed by the author using a custom macro in ImageJ written by Dr Frank Proudlock. Again, due to presence of nystagmus, the analysis had to be carried out unmasked.

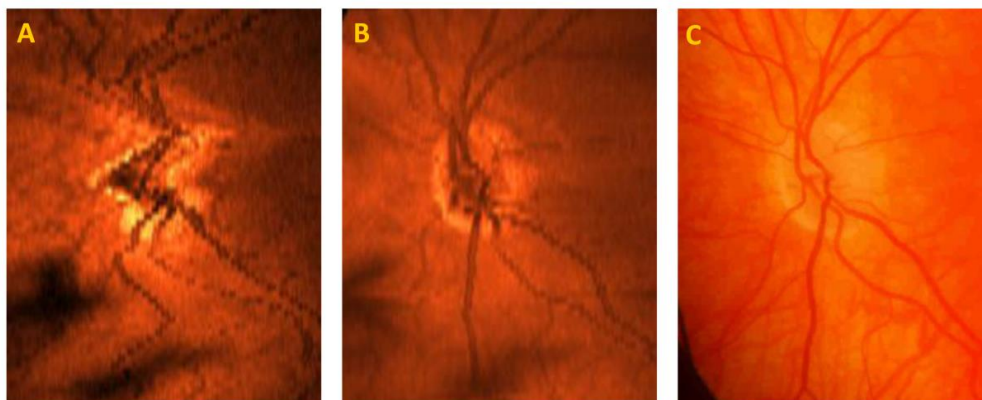


Figure 2-8: Re-alignment of B-scans to correct motion artefacts caused by nystagmus. Comparison of OCT B-scan alignment of the fundus picture of the right eye of a participant with albinism before motion correction (A), after motion correction (B) and a digital fundus photograph from the same eye (C).

Optic nerve head morphology (volumetric analysis)

Cup, disc and rim dimensions including diameters, areas and volumes were calculated from re-aligned SD-OCT scans using SOCT Copernicus Software (version 4.2, OPTOPOL Technology S.A.). The software automatically detects the internal limiting membrane and the edges of the RPE, which it uses as the margin for the

disc. These markers were manually checked and corrected where needed. The cup offset is determined using a line on each B-scan parallel to the plane of the disc for each B-scan with an anterior offset of 150µm. Within the disc margins, absence of tissue below the offset is designated as cup and presence of tissue above the offset as rim. Measurements in the retinal plane were adjusted using refractive error as per manufacturer's instructions (correction factor = $-0.0175 \times \text{spherical equivalent} + .965$ based on measurements with artificial eyes with extended or reduced axial lengths).

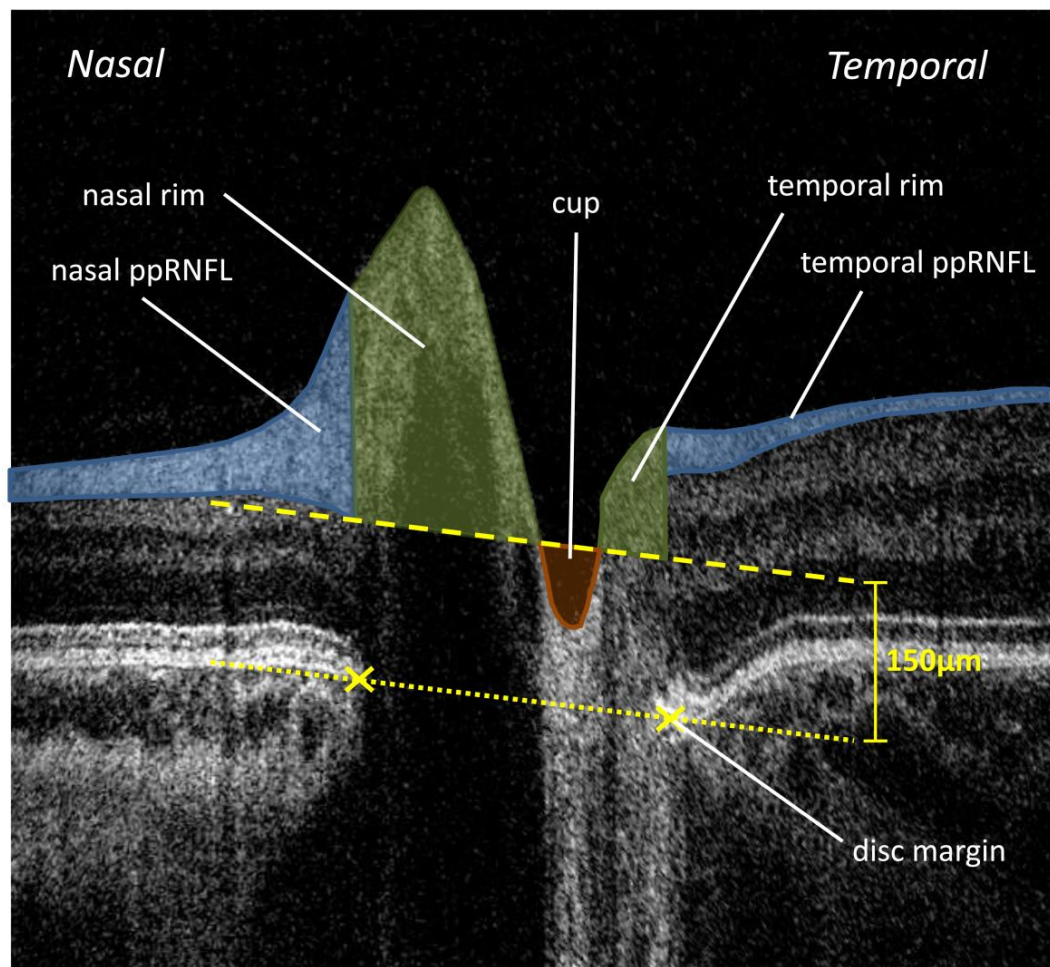


Figure 2-9: Method for estimating disc, rim and cup dimensions. The method is used by the automated volumetric analysis performed by the Copernicus software (SOCT Copernicus HR, OPTOPOL Technology S.A., Zawiercie, Poland). Within the disc margins, absence of tissue below the 150µm offset is designated as cup (shown in orange) and presence of tissue above the offset as rim (shown in green). Peripapillary retinal nerve fibre (ppRNFL) is shown in blue.

A similar manual cross-sectional analysis was also performed on a single B-scan (where the cup was deepest) to compare nasal and temporal rim areas using an ImageJ macro (not available on the automated Copernicus analysis) and to calculate disc tilt from the angle of tilt of the nasal and temporal disc margins.

Nasal and temporal rim (cross sectional analysis)

In order to accurately reconstruct the cross sectional profile of the ONH along the naso-temporal axis an ImageJ macro was written by the author to analyse the dimensions of the disc, rim and cup from a single horizontal B scan where the cup was at its deepest. This was based on an algorithm described by Hrynychak et al. whose study concluded that there is almost perfect agreement between cup to disc ratios measured stereoscopically and those measured using their OCT algorithm.¹¹

The macro incorporated the ABSnake plug-in

(http://imagejdocu.tudor.lu/doku.php?id=plugin:segmentation:active_contour:start,

date accessed: June 17, 2013) to detect the internal limiting membrane. The image was also flattened using a spline fitted to Bruch's membrane excluding the area immediately adjacent to the disc region. The macro estimates the temporal and nasal rim width, peak height, height at edge of the disc and rim area. (Figure 2-9)

Disc torsion and tilt

Disc torsion (i.e. rotation of the major axis of the disc with en-face view of the fundus) and horizontal disc tilt (i.e. through a cross sectional profile through the optic nerve head) were estimated using the definitions described by Witmer et al.³⁴¹ Disc torsion was measured using ImageJ software by fitting an ellipse to the disc edges, using either the fundus image, or occasionally the en-face view of disc edges marked on the SD-OCT scan where the disc edges were not clearly visible in the fundus image. Ovality was determined from the ratio of the major: minor axis length and angle of the axis calculated for discs with ovality > 1.1 (i.e. greater than a 10% difference between major and minor axes). Disc margins relative to the plane of the Bruch's membrane (on the flattened cross sectional image of the ONH described above) were used to estimate deformation of the disc edges in order to calculate horizontal disc tilt (Figure 2-9). Clinical examination of fundi and fundus images by experienced clinicians was used to subjectively identify tilted disc syndrome (with an inferior or infero-nasal crescent of visible sclera and infero-nasal disc tilt)¹⁷⁰ and

myopic tilted disc pattern (with temporal crescent of visible sclera, temporal disc torsion and significant myopia).¹⁷¹

Peripapillary retinal nerve fibre layer thickness

Thickness of the peripapillary nerve fibre layer (ppRNFL) was estimated using the automated algorithm in the Copernicus SD-OCT software, which detects the internal limiting membrane and the ppRNFL edges. To minimize measurement error, the disc margins, position of the internal limiting membrane and ppRNFL were manually checked and adjusted. The ppRNFL thickness was measured in two annuli: (i) 1.6 - 2.4mm diameter, and (ii) 2.4 - 3.2mm diameter each divided into 10 radial segments (using the GDx parameters).³⁴² Analysis of ppRNFL was not possible on four of the 56 participants mainly due to large nystagmus widening the extent of shadows caused by the iris.

Reliability of measures

Test-retest analysis of disc, cup and rim areas, cup:disc area ratios, cup and rim volumes and ppRNFL thickness in both inner and outer annuli was performed by repeating the analysis on two separate SD-OCT scans in a subset of participants in both groups. (albinism: n=37; controls n=27)

MRI SCANNING

2.2.3 SCAN ACQUISITION

Brain MR imaging was carried out by research radiographers at the Sir Peter Mansfield Magnetic Resonance Centre (SPMMRC), University of Nottingham. Patients were driven to Nottingham by the author once clinical assessment and OCT imaging had been completed at the Leicester Royal Infirmary. In some of the patients, it was not possible to complete both assessments on the same day therefore, they attended for MRI scanning at a later date.

A 3T Philips Achieva MRI scanner with a 32-channel SENSE head and neck coil was used to obtain 3D magnetization-prepared rapid acquisition gradient (3D-MPRAGE) sequences.³⁴³ Specifications for the 3D MPRAGE were as follows: (axial MPRAGE, TR=7.53 ms, TE=2.22 ms, flip angle=8°, matrix size 320 x 320, field of view=256 x 256, 0.8mm isotropic voxels, SENSE factor=1.7, 184 contiguous slices). The acquisition took 6.5minutes.

Prior to commencing the study, DTI protocols were optimized by Dr Paul Morgan, Dr Rob Dineen and Dr Chris Tench at the University of Nottingham. The chosen sequence represented the best compromise between the maximal resolution achievable (1.8mm isotropic voxel size) while maintaining an acceptable signal to noise ratio and appropriate scan duration.

Diffusion tensor imaging sequence lasting 9.5 minutes was carried out at the same visit. Protocol for this sequence are as follows: axial diffusion-weighted echo-planar imaging, a single b=0 volume and 61 directional diffusion weighted images with b=1000 s/mm², TE=67ms, TR=8270ms, sense factor 3, matrix size 240 x 240, 52 contiguous slices, 1.8 x 1.8 x 1.8 mm voxels interpolated to 0.9 x 0.9 x 1.8mm acquisitions.

In addition to the above two acquisition, resting state functional MR imaging was also carried out and used for collaborative work which is not part of this thesis.

Foam cushions were placed around the participants' heads by the radiographers to minimize head motion.



Figure 2-10: The 3T scanner at SPMMRC used for this study.

2.2.3.1 DATA ANALYSIS

The author was masked to the volunteer group during all the MRI analyses. The MPAGE data was exported from the scanner to an external hard drive in the Philips PAR/REC format. The PAR file is a text header describing the binary images stored in the REC file. These were converted to Analyze v7 of NIFTI-1 format using a Linux command line programme developed by Dr Paul Morgan at the University of Nottingham. (<http://www.nottingham.ac.uk/~msapm1>)

2.2.3.2 CHIASMAL ANALYSIS

The optic nerve, chiasm and tract dimensions were derived by manually on the MPAGE images by tracing ROIs around each structure. This was carried out using a custom written macro in ImageJ (available at: <http://rsbweb.nih.gov/ij/>; accessed December 11, 2014) by an assessor who was blinded to patient demographics and group membership.

As part of the analysis, the chiasm was identified in the axial plane. Optic nerve dimensions were taken from the first slice anterior to the chiasm where two distinct nerves could be identified and similarly posterior to the chiasm, the first slice where two distinct optic tracts could be visualised was used to take the measurements. For the chiasm measurements, ROIs were traced on each axial slice where the chiasm was identified and mean values for area and diameter were used.

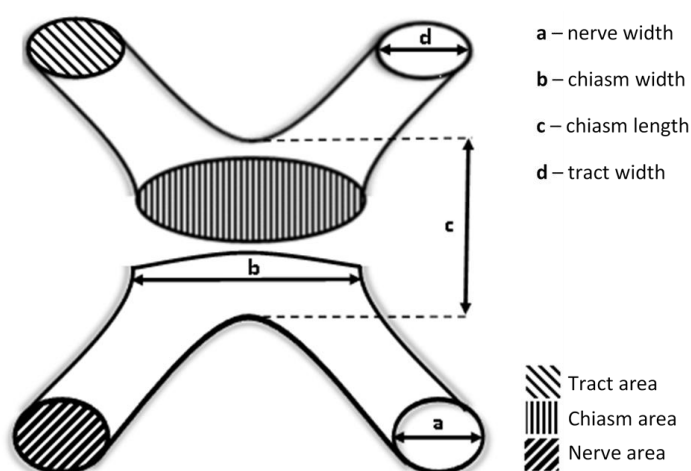


Figure 2-11: Schematic diagram showing how optic nerve, chiasm and tract dimensions were acquired

2.2.3.3 DTI ANALYSIS

The diffusion weighted images were exported from the scanner to an external hard drive as DICOM files. These were converted to Analyze format using dtoa which is a Linux command line software written by Dr Paul Morgan at the University of Nottingham. (<http://www.nottingham.ac.uk/~msapm1>)

The remaining analysis was completed using fMRIB's Diffusion Toolbox in FSL (v.4.1.8, <http://www.ndcn.ox.ac.uk/divisions/fmrib/>). First, artefacts induced by head motion and eddy currents were corrected by registering all image volumes to the first b0 image with an affine transformation. A binary mask of the brain was created and non-brain structures were removed with the Brain Extraction Tool. The DTIFit tool in FSL's Diffusion Toolkit, was used to fit tensors to the data and determine a variety of values including the fractional anisotropy, mean diffusivity and the three eigenvector and eigenvalues of each voxel. BEDPOSTX (Bayesian Estimation of Diffusion Parameters Obtained using Sampling Techniques) was used to build sampling distributions on the diffusion parameters at each voxel.

Probabilistic fibre tracking was performed using the streamline tractography algorithm, PROBTRACKX2. The algorithm propagates streamlines from each voxel in a given seed mask along the path with the largest principal axis of the diffusion tensor until some termination criteria are met (in this case, when the streamline reached the voxels in a termination mask). The number of streamlines generated allows estimation of the strength of connectivity between the seed and target voxels.

To avoid mis-registration artefacts, the seed and target ROIs were drawn on the FA maps rather than using the T1 MPAGE volume. As previously, optic nerve ROI was drawn on the first slice anterior to the chiasm where two distinct nerves could be identified and similarly posterior to the chiasm, the first slice where two distinct optic tracts could be visualised was used to draw the optic tract ROI.

To increase the signal to noise ratio, the algorithm was run initially with the optic nerve being the seed and the tract the target and then repeated with the seed and target masks reversed. Results from these two streamline counts were then averaged for subsequent analyses. A “streamline decussation index” was deduced by calculating the percentage of streamlines connecting with contralateral ROIs through the chiasm using the following formula:

$$SDI = \frac{RN_{LT} + LN_{RT}}{(RN_{LT} + RN_{RT} + LN_{LT} + LN_{RT})} \times 100$$

A_B = Number of streamlines between ROIs A and B

LN= left nerve, LT = left tract, RN = right nerve, RT = right tract.

A logarithmic transformation was performed on the DTI streamline count prior to comparison with with retinal measurements because of the large variation in number of streamlines generated between individuals in both albinism and control groups

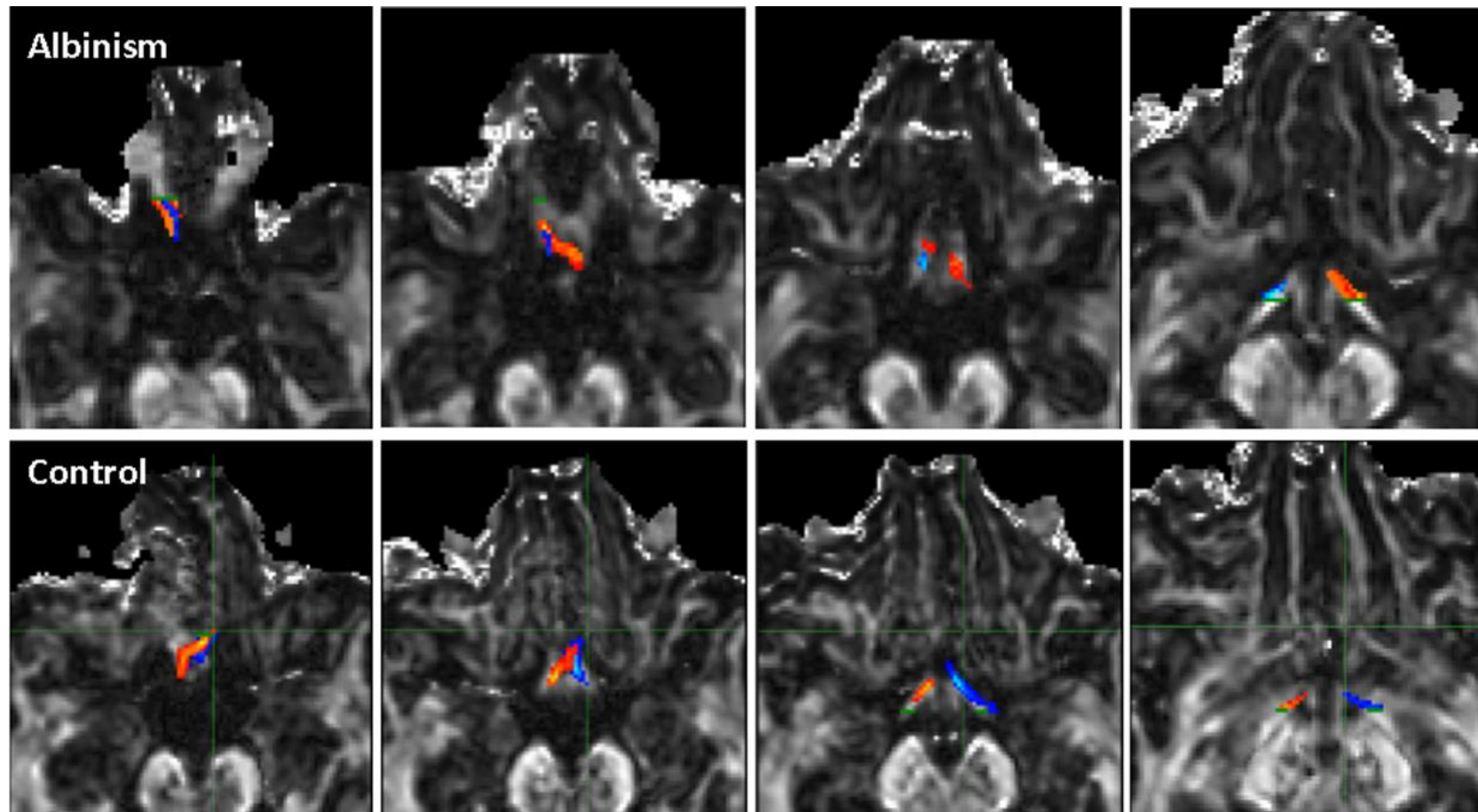


Figure 2-12: Example DTI data streamline data from albinism (top) and control (bottom) volunteers. The optic nerve (seed) and optic tract (target) masks are in green. Streamlines travelling from the optic nerve to the ipsilateral tract are in blue while streamlines travelling to the contralateral ROI are orange. The albinism subject shows predominantly orange coloured streamlines in keeping with increased decussation. The control volunteer displays around an equal number of contralateral and ipsilateral streamlines.

2.2.3.4 CORTICAL ANALYSIS

Cerebral cortical thickness was derived using Freesurfer software (<http://surfer.nmr.mgh.harvard.edu>).^{251, 252} The first step in the process is to reduce inter-subject variability by registering individual scans to a standardized 3-dimensional co-ordinate system based on an average volume of previously aligned scans.^{344, 345} Next, non-uniformities in intensity caused by radiofrequency field and magnetic susceptibility artefacts are corrected. Following this, non-cortical areas such as skull, neck and dura are removed from the image.³⁴⁶

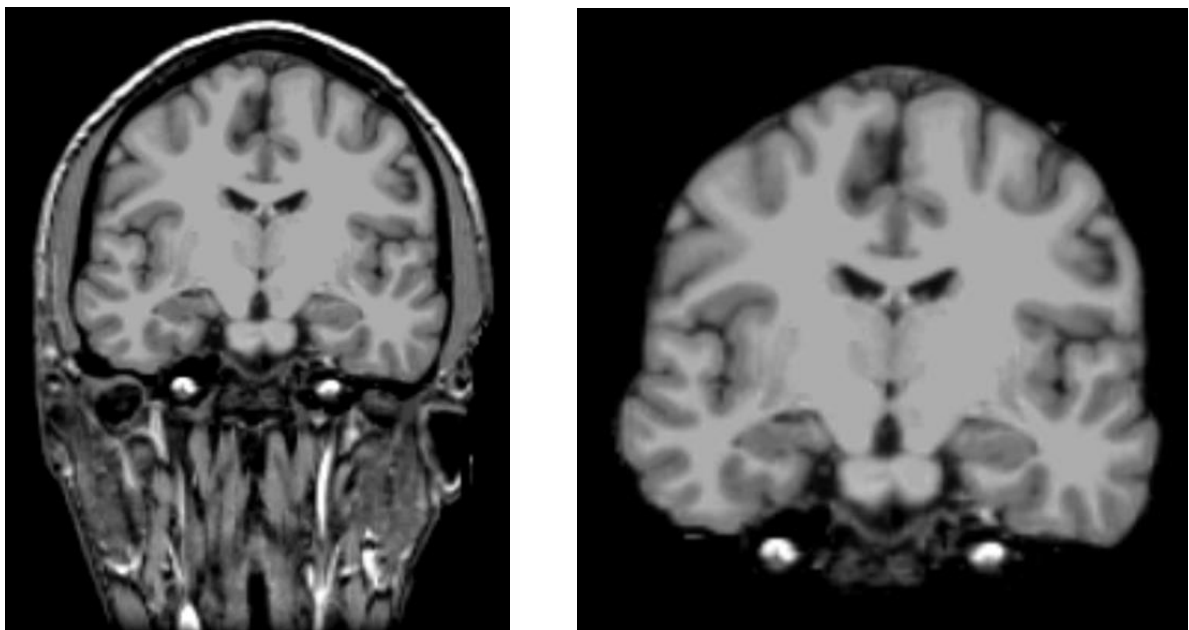


Figure 2-13: MRI image pre (left) and post (right) skull stripping

The skull stripped image then undergoes a segmentation procedure that identifies white/grey matter interface (white surface) and the grey matter/cerebrospinal fluid interface (pial surface). The distance between these two surfaces is used to calculate cortical thickness and volume. (Figure 2-14) Automatic parcellation of the cortex was performed based on the Destrieux atlas in Freesurfer.³⁴⁷

Figure removed from online version to avoid copyright infringement

Figure 2-14: Schematic showing how cortical thickness is measured using Freesurfer. White matter surface is delineated by the yellow line and pial surface by the red line. Distance between them (green arrows) represents cortical thickness.

Although the above process is automated, each scan was subject to meticulous manual inspection in axial, coronal and sagittal planes to check for errors in any of the above steps. Any inaccuracies were corrected and thickness measurements were recalculated.

2.3 EYE MOVEMENT RECORDING

2.3.1 DATA ACQUISITION

As part of their visit to the Leicester Royal Infirmary for clinical assessment, albinism patients underwent eye movement recordings that were performed mainly by Dr Rebecca McLean with help from the author and Mr Viral Sheth. The recordings were completed using a high-resolution infrared video system (EyeLink II eye tracker, SR Research, Ontario, Canada) that has a sampling rate of 500 Hz and a spatial resolution of 0.01° . The system comprises of three cameras mounted on a headband. The eye is illuminated using infrared light, the two eye cameras detect the pupillary position based on user set eye illumination threshold. The third camera detects four infrared markers on the display screen to determine head position. Figure 2-15 demonstrates the cameras and screens used for eye-movement recordings.

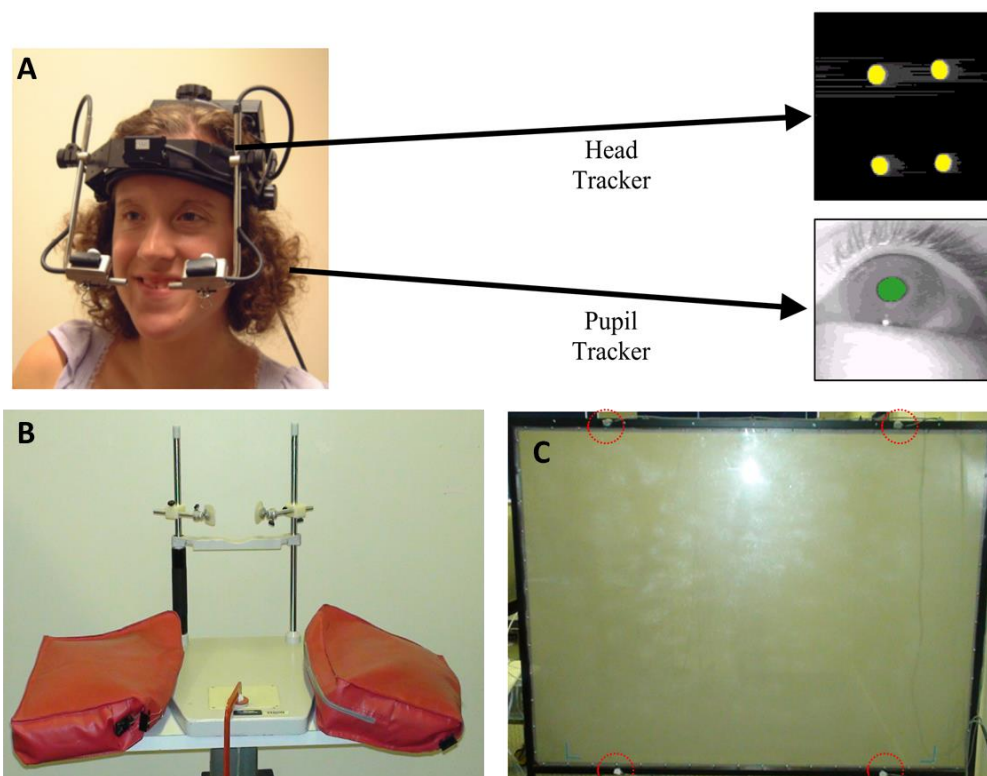


Figure 2-15: A) The eye movement headgear with a head tracking camera and two pupil tracking cameras. B) The chinrest with cheek support to minimize head motion during the eye movement recordings. Patients can place their arms on the red armrests for comfort. C) Projector screen with four infrared markers (red circles) which are detected by the head tracker (see yellow dots in A).

The patients were positioned at 1.2m from a rear projection screen and the eye trackers were placed away from the patient's visual field such that the whole of the screen was visible to the patients. This is diagrammatically illustrated in Figure 2-16.

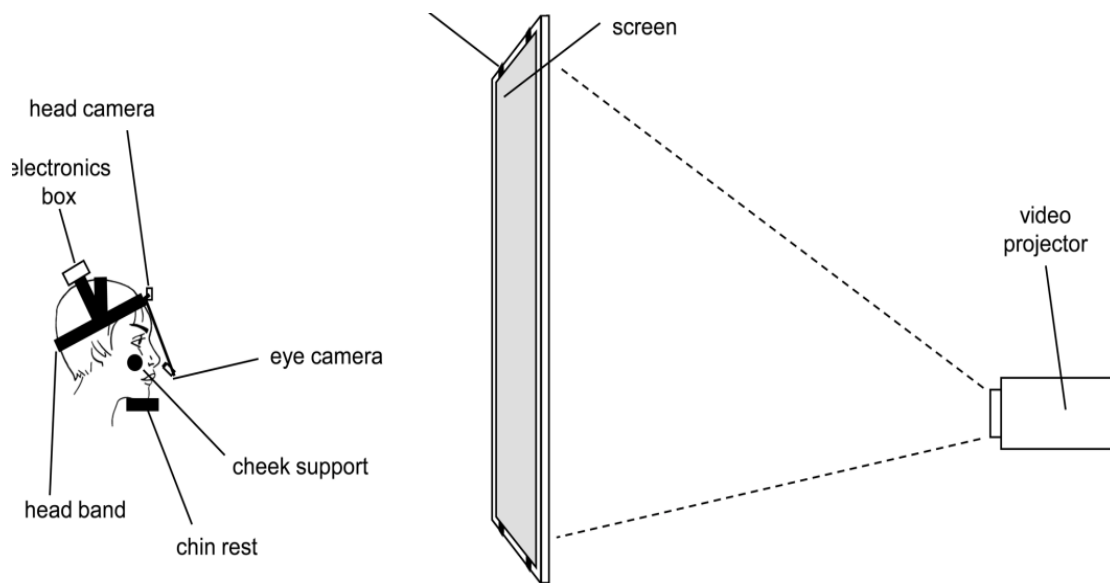


Figure 2-16: Diagram indicating the distance between the patients and the projector screen.

The participants are asked to follow a target, which moved from 30° to the left (-30°) to 30° to the right (+30°), every 7 seconds across the horizontal axis, with their head fixed to measure the null point characteristics.

The data from the EyeLink II apparatus is saved as an EDF file. This data is combined with a log file containing details of the stimuli used and converted into an SMR file which was analysed using Spike2 version 6.15(Cambridge Electronic Design, UK).

2.3.2 DATA ANALYSIS

An “offline” calibration of the eye movement data was carried out using Spike2. It was assumed that the gaze position corresponded with the position eyes during the foveation periods. These were defined using variable velocity and position thresholds (see extended Nystagmus Acuity Function (NAFX) routine mentioned later). Data with large numbers of blinks or excessive noise was excluded. (Figure 2-18)

The data from the calibration process was saved into a text file and was imported into an Excel template. This template creates a line of best fit using mean position of the eyes during foveation periods based on data from the previous step and known target positions. The equation for this best fit line is then used by Spike 2 to calibrate data along the horizontal axis.(Figure 2-17).

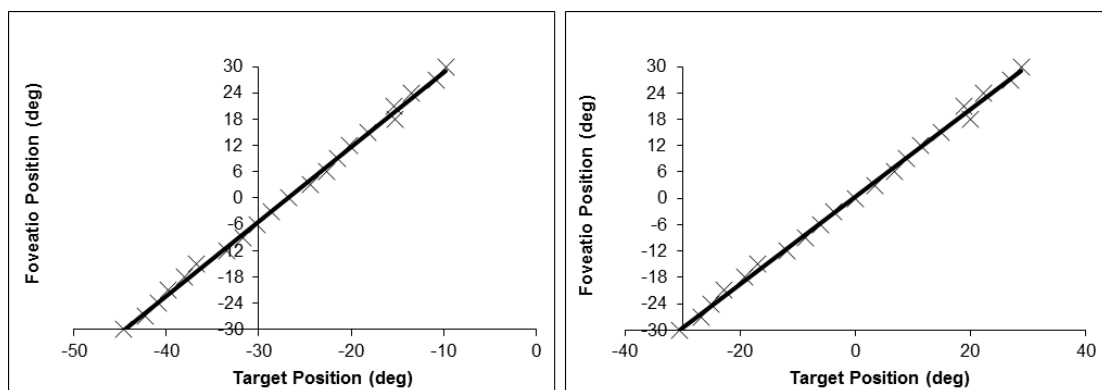


Figure 2-17: Foveation data pre-calibration (left) and post-calibration (right).

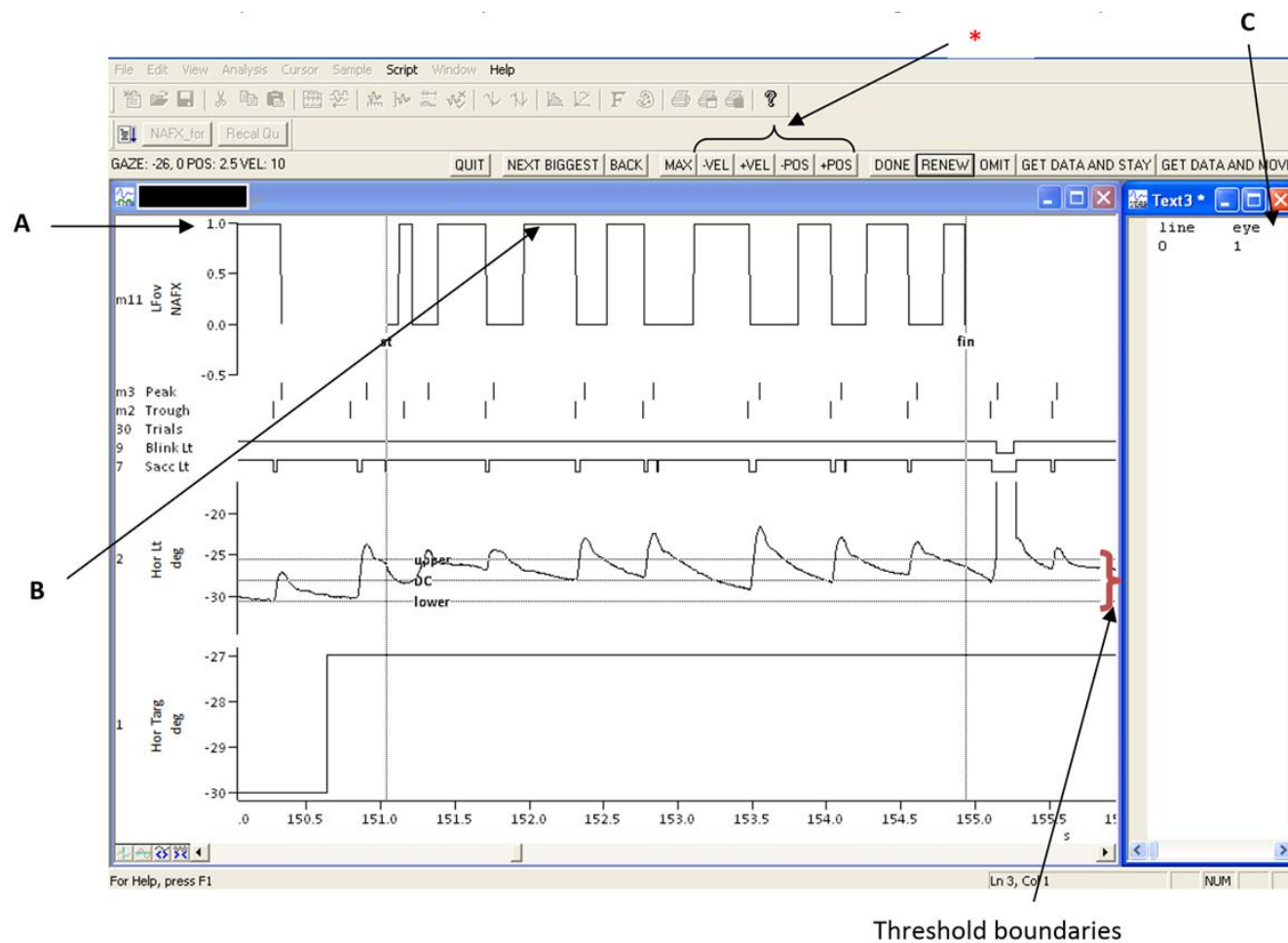


Figure 2-18: Calibration of data

The – and +VEL (velocity) and – and + POS (position) buttons (*) were used to alter thresholds until foveation zones were identified (line labelled 'DC').

The top trace indicates the foveations, which are when the values are at one (A). Altering the parameters mentioned above alter channel m1 representing foveations (B). The longer B is, the longer the foveation.

Once foveations were obtained, the next window of data was seen on pressing the 'get data and move' button of the far right of the screen.

On completion of the process, all the information was automatically printed into the text file on the right of the screen (C).

Once the data had been calibrated, nystagmus analysis is carried out in a similar manner to that described in Figure 2-18 where values for nystagmus amplitude, frequency, intensity and NAFX are calculated at each gaze position.

The amplitude and frequency measures (which in turn are used to calculate nystagmus intensity) are calculated by locating peaks and troughs in a copy of the nystagmus waveform that has been adaptively smoothed until only the fundamental frequency of the waveform is present. The program uses these points to locate maximum and minimum deviations in the original waveform.

NAFX is calculated by exporting sections of the waveform in each gaze position into the OMTools software (<http://omlab.org/software/software.html> accessed 23/2/2012) developed by Jacobs and Dell'Osso in a Matlab environment. The program requires manual setting of position (from 0.5 to 6°) and velocity (from four to 10°/s) thresholds until one foveation is visible on each nystagmus cycle. The final values at each gaze position are then be imported back into another Excel template.

Once the data had been imported into the Excel worksheet, the location of the null point was determined by finding the minimum point after the data had been smoothed with a five-point smooth to remove a small amount of point-to-point random fluctuation. The mean amplitude, frequency, intensity and NAFX were calculated for the null region and across the while curve (from 30° to the left to +30° to the right).

The patients were only considered to have a null region if the nystagmus intensity in the null region was less than 80% of the overall mean nystagmus intensity. Another qualification for having a null region was having a nystagmus intensity of greater than 6°/s.

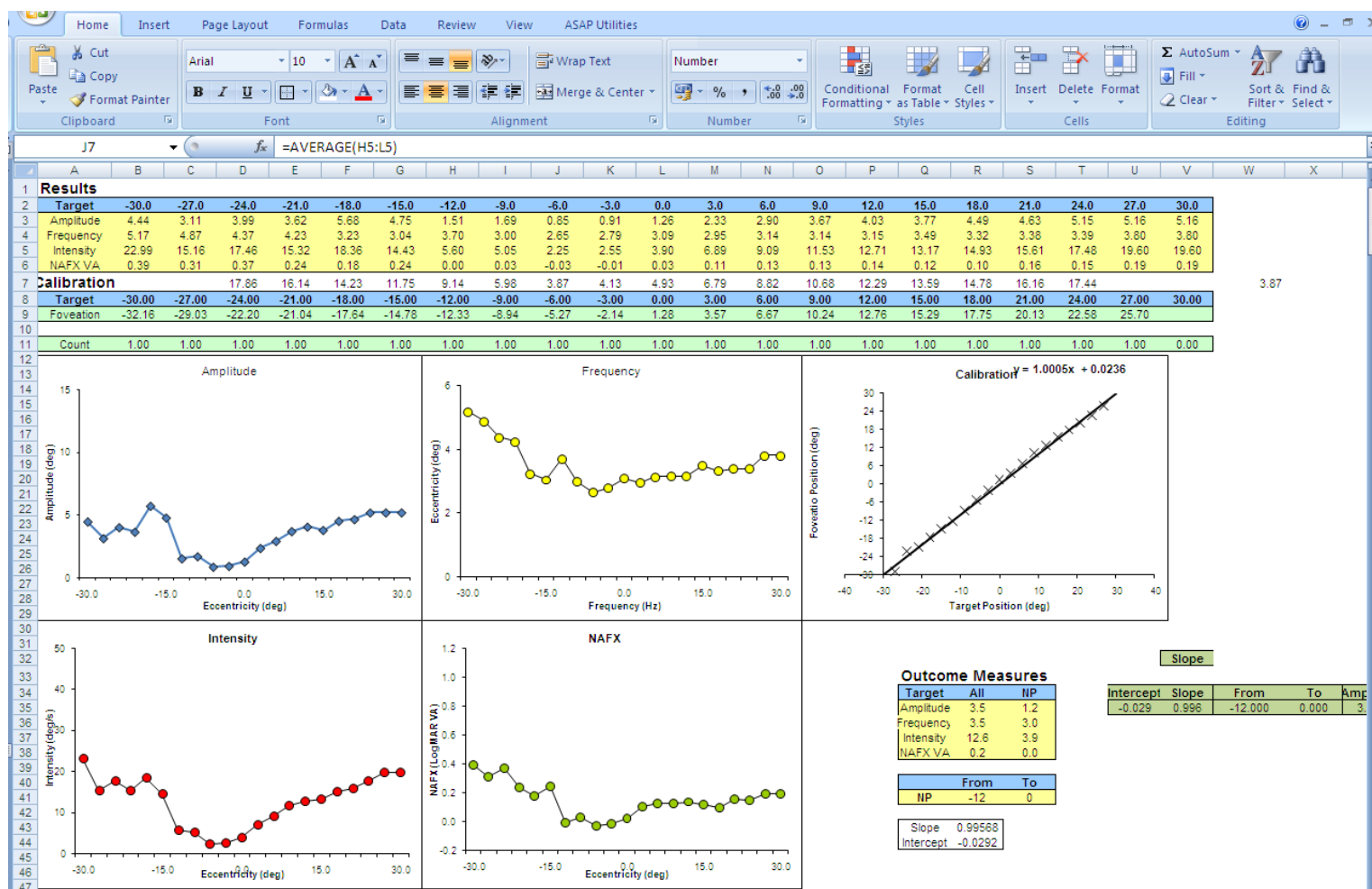


Figure 2-19: Screenshot of Microsoft Excel spreadsheet with values for nystagmus parameters and their graphical representation.

2.4 VISUAL EVOKED POTENTIALS

2.4.1 DATA ACQUISITION

This investigation was carried out in an electrically shielded room at the electrophysiology department of the Leicester Royal Infirmary by Dr Christopher Degg. The patients were seated comfortably and allowed to wear their full spectacle correction throughout the duration of the test. Five electrodes (1=PO₇, 2= O₁, 3= O_z, 4=O₂, 5=PO₈) were placed at 10% intervals in a horizontal chain across the posterior part of the scalp with O_z as the centre point. F_z was used as the reference for each electrode and C_z was used as ground. The positions of these electrodes are highlighted in Figure 2-20.

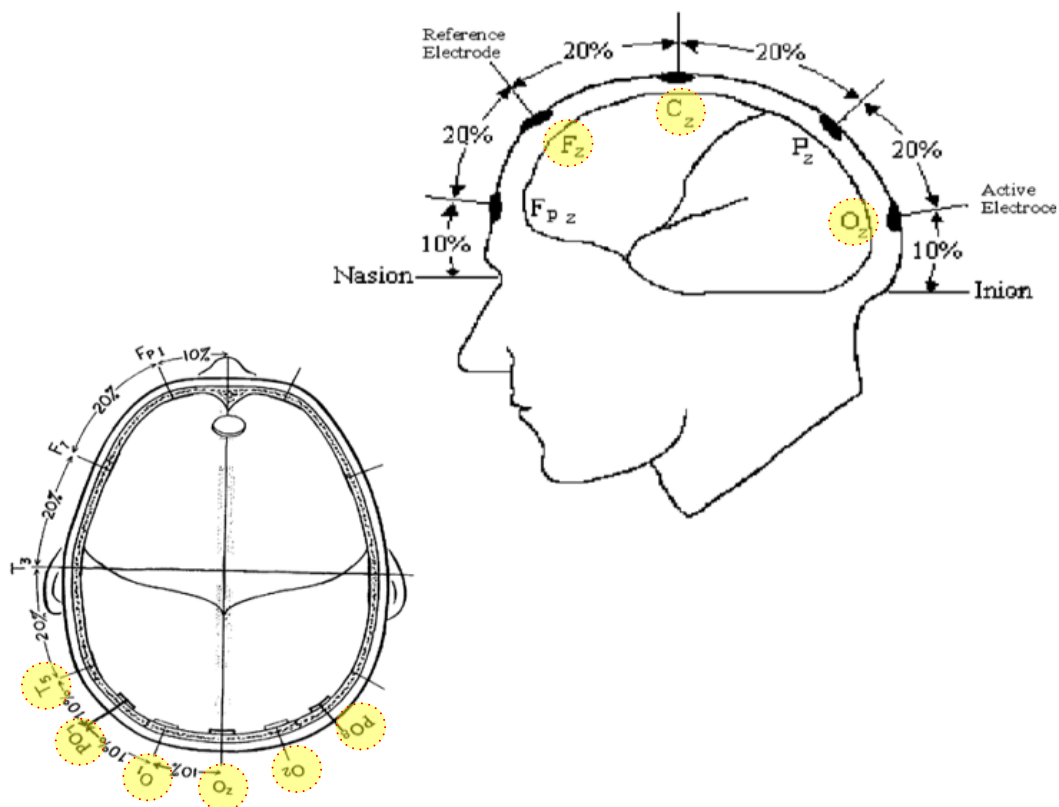


Figure 2-20: Electrodes positions used for VEP measurements. (Adapted from <http://www.iscev.org/standards/pdfs/vep-standard-2004.pdf>)

The stimulus was a black and white checkerboard pattern, with 100% contrast, a mean luminance of 96cd/m² and check size of 1° generated on a 17-inch CRT screen positioned at 46cm distance from the patient, which created a full-field size of 33°. The pattern appeared at a rate of 200ms onset, 400ms offset. Patients were asked to fixate a non-illuminated central spot. The responses for the left and right eyes were recorded separately with the other eye completely occluded. The test was performed twice on each eye an average of the two sets of results was used for analysis.



Figure 2-21: Patient undergoing Visual Evoked Response Testing

2.4.2 DATA ANALYSIS

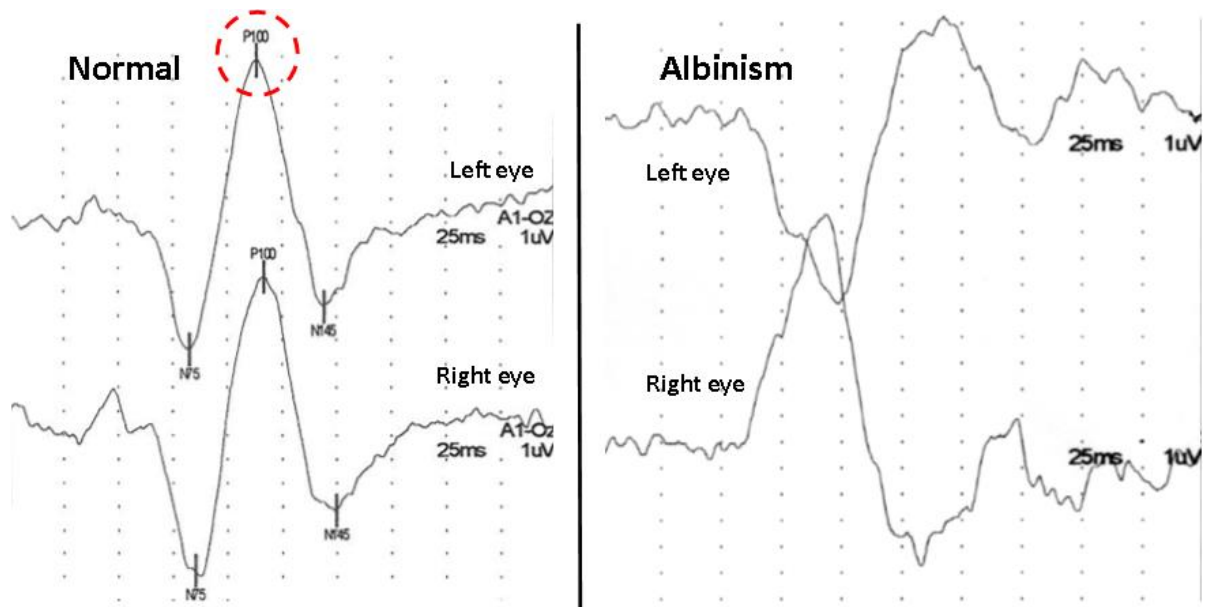


Figure 2-22: Example VEP traces from a normally pigmented adult (left) showing symmetrical VEP response in both eyes compared to a VEP trace from an adult with albinism (right) showing asymmetric response. Amplitude values of peak P100 (circled red) were used for calculating the interhemispheric asymmetry index³⁴⁸

VEP asymmetry was calculated by means of an interhemispheric asymmetry index (I_{asym}), based on a methodology described by Apkarian.²⁰¹ The first step for this is to calculate response lateralization (A.I.) for each eye separately. This involved quantifying the magnitude of response at the p100 peak (see Figure 2-22) for each electrode position following visual stimulation. The amplitude was then plotted against the function of electrode position and the graph was divided into left (electrode 1-3) and right (electrode 3-5) hemispheres. Area under the graph was calculated for each hemisphere (A_L and A_R) with baseline being determined by lowest response amplitude across the five electrodes.

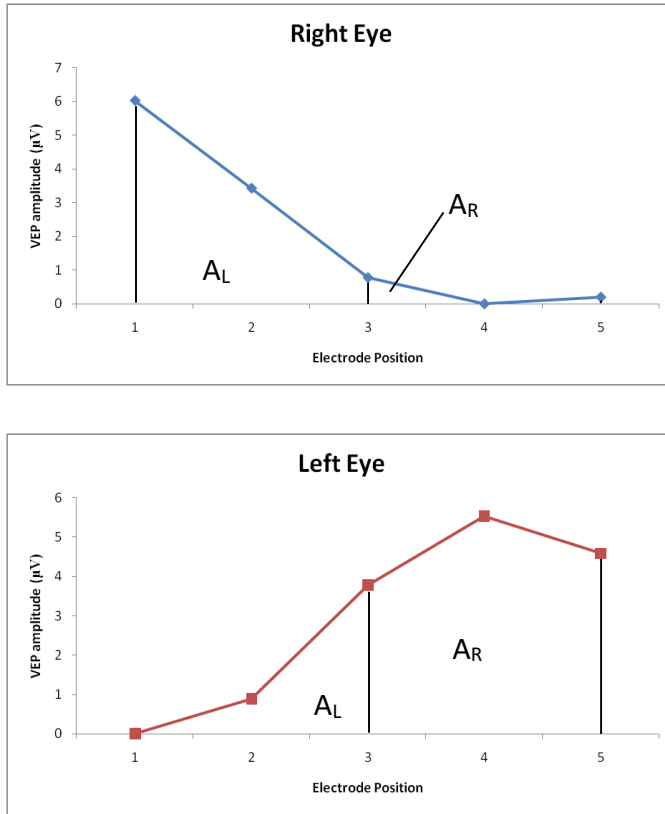


Figure 2-23: Quantification of VEP response lateralisation. Area under the curve joining electrodes 1-3 (A_L) is a measure of left hemisphere stimulation and area under the curve joining electrodes 3-5 (A_R) is a measure of right hemisphere stimulation.

The following formula was used to calculate the response lateralisation (A.I.) in each eye.

$$\text{for } A_L > A_R, \quad A.I. = \left(\frac{A_R}{A_L} \right)$$

$$\text{else } A.I. = 2 - \left(\frac{A_L}{A_R} \right)$$

The intra-ocular asymmetry index (I_{asym}) was calculated by subtracting response lateralization in the right eye from the response lateralization in the left eye.²⁰¹

2.5 STATISTICAL ANALYSES

Statistical analyses were based on advice provided by Professor Carol Jagger (Professor of Epidemiology, Department of Health Sciences, University of Leicester). SPSS software version 16.0 (SPSS, Inc., Chicago, IL) was used to carry out all statistical analyses while graphs were generated using Microsoft Excel 2013.

Normality testing

Shapiro-Wilk analysis and Q-Q plots were used to assess the distribution of data. In the majority of cases, our data was not normally distributed and therefore non-parametric testing was used for all statistical analyses to maintain consistency.

Left vs Right eye comparison

Wilcoxon matched pairs signed ranks test was used to compare left and right eyes of patient and control groups. Where there was no difference between the eyes, data from both eyes was averaged for further analyses. Details of these tests are presented in the relevant results section.

Group comparison

Comparisons of independent samples between albinism and control groups were carried out using Mann-Whitney U testing. All analyses were considered significant at a probability value of $p < 0.05$.

Correlations

Spearman's Rank Correlation Co-efficient were employed to assess relationship between foveal, optic nerve, chiasmal and cortical structures.

Multiple comparison correction

As the relationship between structures throughout the visual pathway is being assessed, one of the limitations of the study is the number of comparisons that needed to be carried out. This increases the risk of Type 1 error when testing our hypotheses. To counter this and ensure our results are biologically plausible, priori

hypotheses were devised based on previously published findings. In addition, where testing a hypothesis required multiple statistical comparisons, a Bonferroni-Holm correction is carried out to account for this. The corrected p-values have been labelled p' throughout the thesis.

CHAPTER 3

RESULTS & DISCUSSION

3.1 CLINICAL FEATURES

Table 3-1 lists the age, gender and best corrected visual acuity (BCVA) of our albinism patients group. It also indicates which sections of the study patients participated in. While not all patients were included in each study, there is considerable overlap amongst the cohorts.

Summary demographics of patients and healthy controls taking part in each study are provided in the relevant sections. Study 1 = fovea, Study 2 = Optic nerve, Study 3=Chiasm, Study 4=Cortex, Study 5=Eye movements

<i>ID</i>	<i>AGE</i>	<i>Gender</i>	<i>BCVA</i>	<i>Study 1</i>	<i>Study 2</i>	<i>Study 3</i>	<i>Study 4</i>	<i>Study 5</i>
1	21	Female	0.68	X	X			X
2	23	Female	0.48	X	X			X
3	28	Male	0.30	X	X			X
4	34	Male	0.78	X	X			
5	32	Male	0.60	X	X			X
6	20	Female	0.62	X	X			X
7	22	Male	0.54		X			X
8	38	Male	0.62	X	X	X	X	X
9	35	Male	0.60	X	X			X
10	42	Male	0.54		X	X	X	X
11	52	Female	0.60	X	X			X
12	23	Female	0.18	X	X	X	X	X
13	25	Female	0.28		X			X
14	42	Male	0.44		X	X	X	X
15	42	Female	0.48	X	X			X
16	51	Female	0.62	X	X			X
17	41	Male	0.60	X	X	X	X	
18	30	Male	0.48	X	X			
19	36	Female	0.48		X			
20	64	Male	0.48					X

21	69	Male	0.5		X	X	X	X
22	36	Female	0.78					X
23	24	Male	0.70	X	X	X	X	X
24	51	Male	0.18	X	X	X	X	X
25	33	Male	0.58	X	X			X
26	21	Male	0.2		X			
27	25	Male	0.26	X	X	X	X	X
28	48	Female	0.38		X			
29	59	Female	0.5		X			
30	50	Female	0.6		X			
31	24	Female	0.54	X	X	X	X	X
32	43	Male	0.44		X	X	X	X
33	60	Male	0.50	X	X	X	X	X
34	65	Male	0.44	X	X			X
35	52	Male	0.4	X	X			X
36	18	Male	0.78	X	X			
37	7	Male	0.725	X				
38	48	Female	0.6	X	X	X	X	X
39	39	Male	0.86	X				
40	25	Male	0.78		X			X
41	52	Male	0.28		X	X	X	X
42	7	Female	0.25	X				
43	37	Male	0.18		X	X	X	X
44	22	Male	1	X	X			
45	49	Female	0.30	X	X			X
46	26	Male	0.36		X	X	X	X
47	25	Female	0.2					X
48	27	Male	0.2	X	X			X
49	12	Male	0.52	X				
50	13	Male	0.62	X				
51	28	Male	0.60	X	X			X

52	53	Female	0.20	X	X	X	X	X
53	39	Male	0.38		X			X
54	24	Female	0.78	X	X			
55	29	Female	1	X	X	X	X	X
56	14	Male	0.50	X	X			
57	54	Male	0.60	X	X	X	X	X
58	22	Female	0.60	X	X	X	X	X
59	24	Male	0.48	X	X	X	X	X
60	48	Male	1		X			
61	37	Male	0.48	X	X			
62	36	Female	0.3					X
63	25	Male	0.60	X	X	X	X	X
64	38	Female	0.78	X	X			
65	14	Male	0.28					X
66	54	Male	1.04	X				X
67	22	Male	0.48		X			X
68	35	Female	0.32	X				X
69	44	Female	0.44		X			
70	30	Male	0.2			X	X	
71	9	Male	0.52	X				
72	44	Male	0.62	X	X			X

Table 3-1: Summary of age and gender breakdown of the albinism patients taking part in the study. Also included are their best-corrected visual acuity (BCVA) and which parts of the study they were involved in (marked with X). Study 1 = fovea, Study 2 = Optic nerve, Study 3=Chiasm, Study 4=Cortex, Study 5=Eye movements

3.2 FOVEA

3.2.1 BACKGROUND

As discussed in section 1.4.5, albinism is associated with abnormal foveal development.¹⁴¹ Recent advancements in OCT technology have allowed the study of retinal abnormalities in albinism but there is no comprehensive study that has carried out a quantitative analysis of the foveal abnormality seen in albinism. In addition, there has been recent debate on the impact of the foveal pit on visual acuity.¹⁴⁴

3.2.2 SUMMARY OF AIMS

- Image the fovea of patients with albinism using high resolution OCT.
- Assess the spectrum of foveal development in albinism.
- Quantify the thickness of retinal layers at the fovea and compare this with healthy controls.
- Assess the association between foveal abnormalities on vision in albinism.
- Assess whether visual evoked potential asymmetry seen in albinism is related to foveal development

3.2.3 FINDINGS

Forty-seven patients with albinism (28 male, 19 female, mean age = 26.8 ± 12.9 years) and 20 healthy control volunteers (12 male, 8 female, mean age = 36.7 ± 10.1 years), were imaged for this part of the study. In 44 patients, measurements from both eyes were available and these were averaged for statistical analyses. In two patients, macular area could only be imaged in one eye due to severity of nystagmus and one patient had a choroidal nevus in the right eye. In these three patients, data from just the one eye was used.

Qualitative analysis

Visual inspection of the OCT scans revealed that all patients with albinism had some degree of foveal hypoplasia and therefore the nerve fibre, ganglion cell, inner

plexiform, inner nuclear and outer plexiform layers continued through the fovea in all these patients.

Figure 3-1 illustrates the distribution of the severity of foveal hypoplasia in our albinism cohort while Figure 3-2 compares the OCT morphology of the fovea from a normal control with grades 1 to 3 of foveal hypoplasia.

Although none of the patients in the albinism group had a fully developed foveal pit, 17 patients did display a partial foveal depression and were therefore rated as having grade 1 foveal hypoplasia. 27 patients had grade 2 foveal hypoplasia and displayed lengthening of the outer segments. The remaining three patients were graded as 3 as they only displayed only widening of the ONL. No one in our study displayed Grade 4 foveal hypoplasia. In comparison, all the eyes in the control group had a fully developed foveal pit with a complete discontinuation of the nerve fibre, ganglion cell, inner plexiform and inner nuclear layers at the fovea. The OPL was the only processing layer found in the control group. All control eyes also displayed thickening of the outer nuclear layer and photoreceptor outer segments. On visual inspection, the left and right eyes displayed a similar appearance in both albinism and control groups.

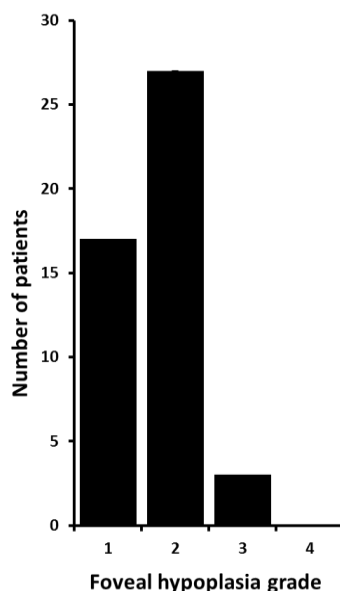


Figure 3-1: Degree of foveal hypoplasia seen in albinism patients. Based on grading system described by Thomas et al. Grade 1 = shallow foveal pit, outer nuclear layer (ONL) widening, and outer segment (OS) lengthening relative to the parafovea. Grade 2 = all features of grade 1 except presence of a foveal pit. Grade 3 = all features of grade 2 except lengthening of cone OS. Grade 4 = all features of grade 3 except widening of the ONL.

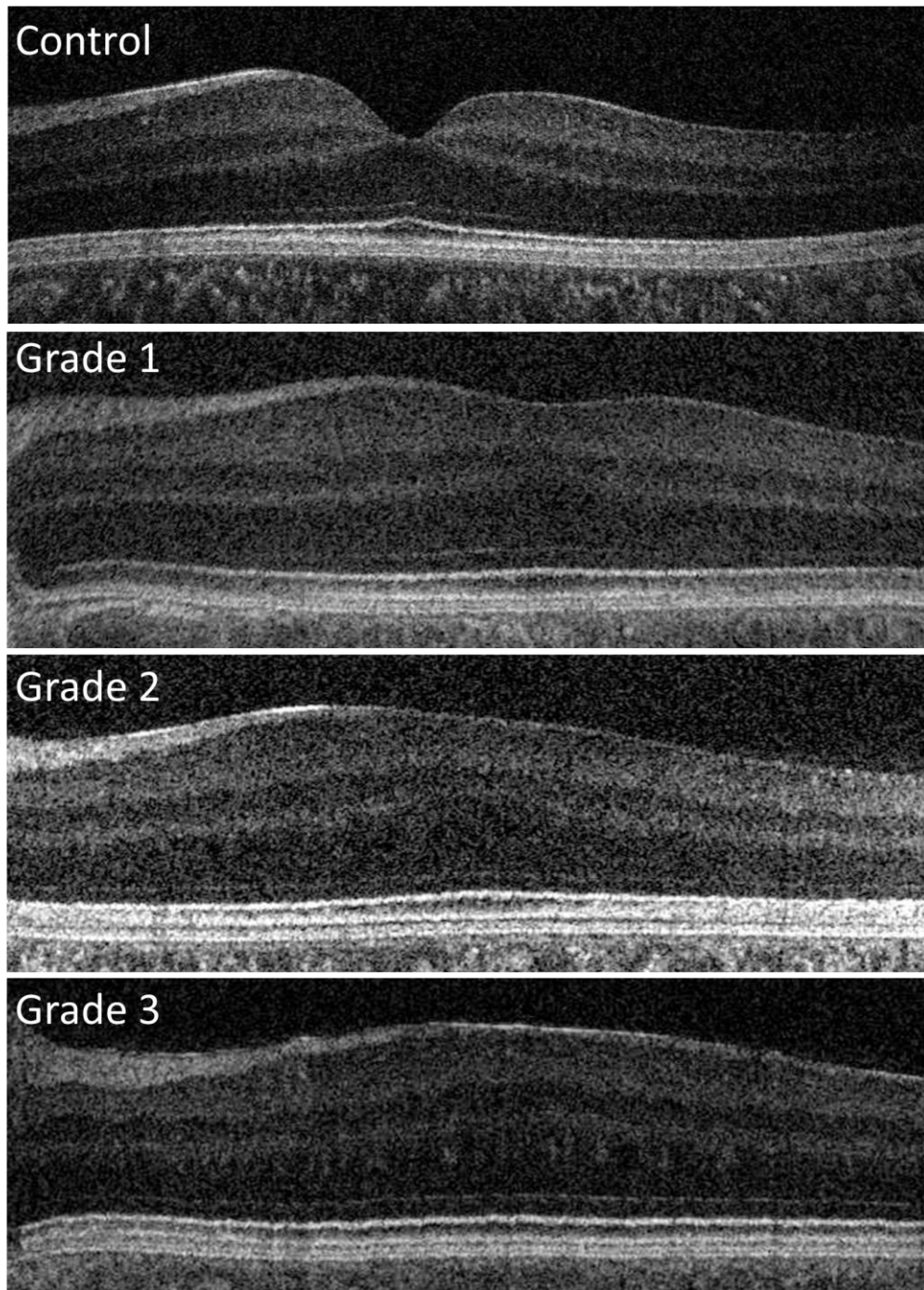


Figure 3-2: Comparison of OCT appearance of the fovea in a healthy control (top) with varying degrees of foveal hypoplasia in patients with albinism (bottom 3). Grade 1 has a rudimentary foveal pit, grade 2 shows thickening of the outer segment layer while the only sign of foveal specialisation in grade 3 is widening of the outer nuclear layer compared to the parafovea.

Shapiro-Wilk analysis showed that the thickness of retinal layers was not normally distributed; therefore, Mann-Whitney U test was used to compare the two groups. The total retinal thickness (sum of all photoreceptor, processing and RPE layers), foveal pit depth (reflecting the amount of foveal hypoplasia), the total thickness of the photoreceptor layers and the total thickness of the processing layers were correlated with visual acuity using Spearman's rank correlation.

Comparison of left and right eyes

Table 3-2 shows that there was no significant in the retinal layer size between the left and right eyes. Therefore, measurements from the two eyes were averaged for subsequent analyses.

		<i>NFL</i>	<i>GCL</i>	<i>IPL</i>	<i>INL</i>	<i>OPL</i>	<i>ONL</i>	<i>IS</i>	<i>OS</i>	<i>RPE</i>
Albinism	P	0.949	0.216	0.801	0.636	0.290	0.615	0.580	0.817	0.540
	Z	-0.064	-1.24	-0.252	-0.474	-1.06	-0.503	-0.554	-0.217	-0.612
Control	P	-	-	-	-	0.317	0.914	0.432	0.752	0.419
	Z	-	-	-	-	-1.00	-0.108	-0.787	-0.317	-0.809

Table 3-2: Comparison of retinal layer thickness between the left and right eyes of the albinism and control groups using Wilcoxon matched pairs signed ranks test

H₀ 1.1: Foveal layers are thicker in patients with albinism compared to healthy controls.

Figure 3-3 summarises the thickness of each of the retinal layers in the albinism and control groups. The total retinal thickness at the fovea was higher in the albinism group (total thickness=309±24.0µm) compared to the control group (total thickness=206±15.0µm; Z=-6.46, p=5.19x10⁻¹⁰).

Of the photoreceptor layers, the OS layer was the only significantly smaller layer in the patients with albinism ($Z=-6.18$, $p=3.12 \times 10^{-9}$). There were no significant differences in the thickness of the ONL, IS and RPE between the two groups ($p>0.05$).

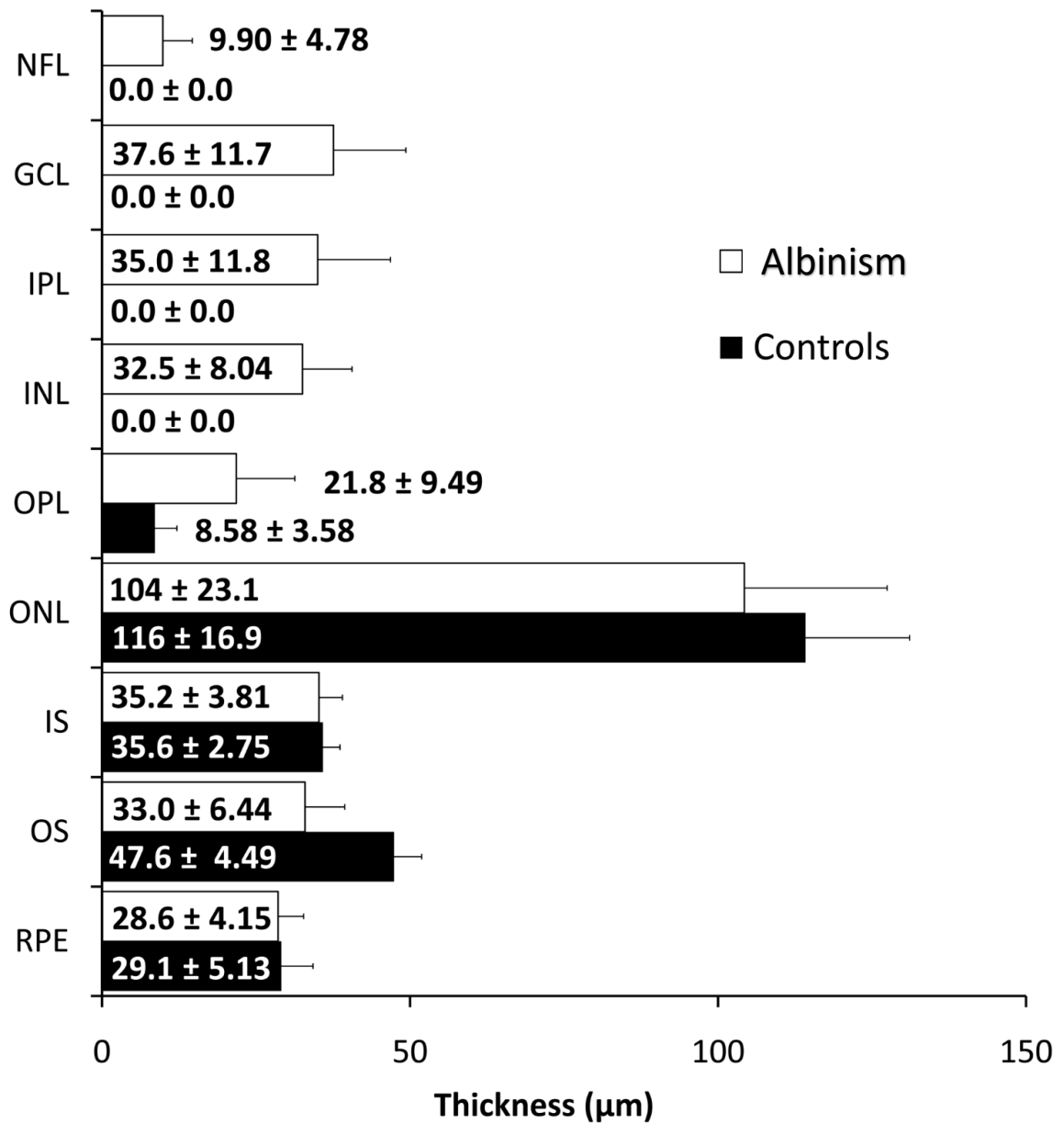


Figure 3-3: Bar chart illustrating the mean thickness of each retinal layer at the fovea in both albinism and control groups. The error bars indicate the standard deviation. Apart from the outer plexiform layer, no other processing layers were present in the control group. The outer segment length was significantly smaller in the albinism group.

H₀ 1.2: Photoreceptor and processing layer development is related in patients with albinism.

In the patients with albinism, there was strong inverse correlation between the total thickness of the photoreceptor and processing layers ($r=-0.690$, $p=4.03 \times 10^{-8}$). This comparison is illustrated in Figure 3-4.

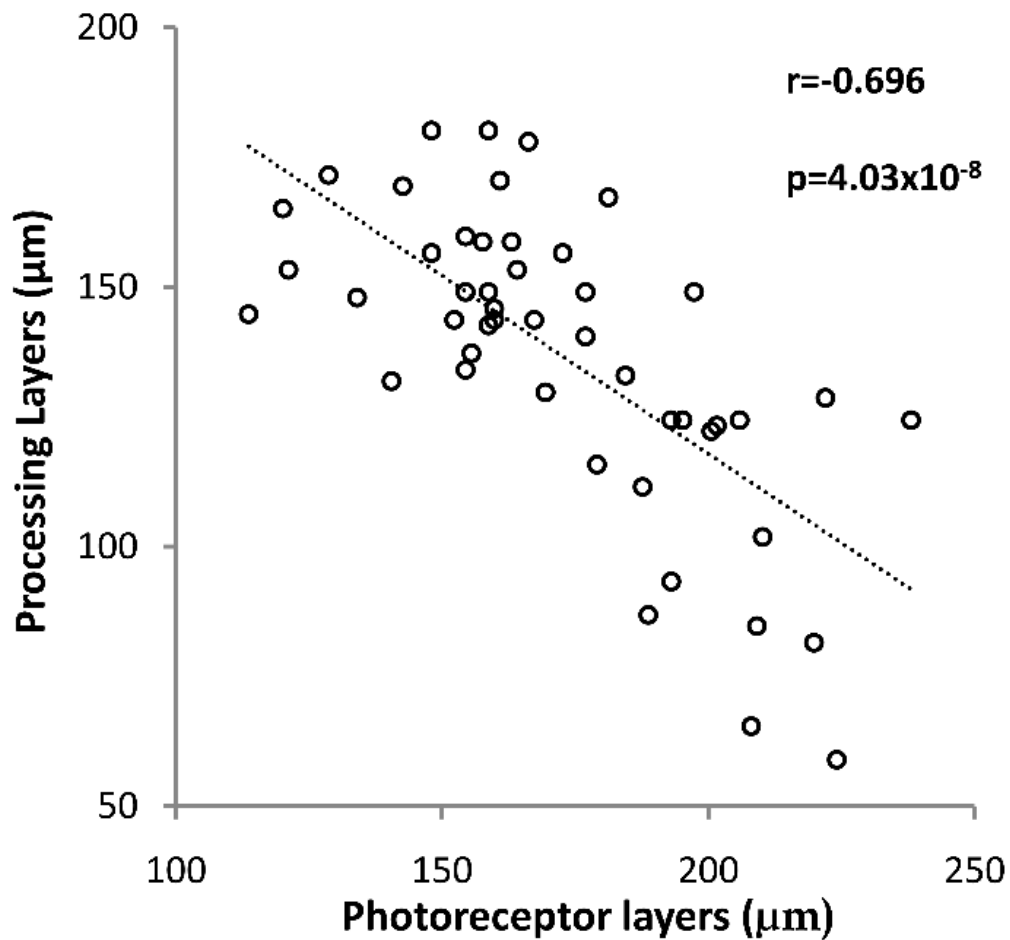


Figure 3-4: Plot of total photoreceptor layer thickness against processing layer thickness at the fovea for 47 patients with albinism. Data from both eyes was averaged where available.

Figure 3-5 displays the contribution of each of the retinal layers to the overall macular thickness with the volunteers organised in descending order according to the thickness of photoreceptor layer outer segment length. The albinism patients are on the left and

the control volunteers are on the right. The figure shows a clear distinction between the groups. In all the albinism patients, the processing layers persist at the fovea while in all the control volunteers, only OPL is present. It also clearly demonstrates that despite having a similar overall foveal thickness, patients with albinism may have a vastly different foveal morphology. Albinism patients on left of the figure show that despite having the highest overall retinal thickness, these individuals display retinal morphology that is closest to normal, with thicker photoreceptor layers and thinner processing

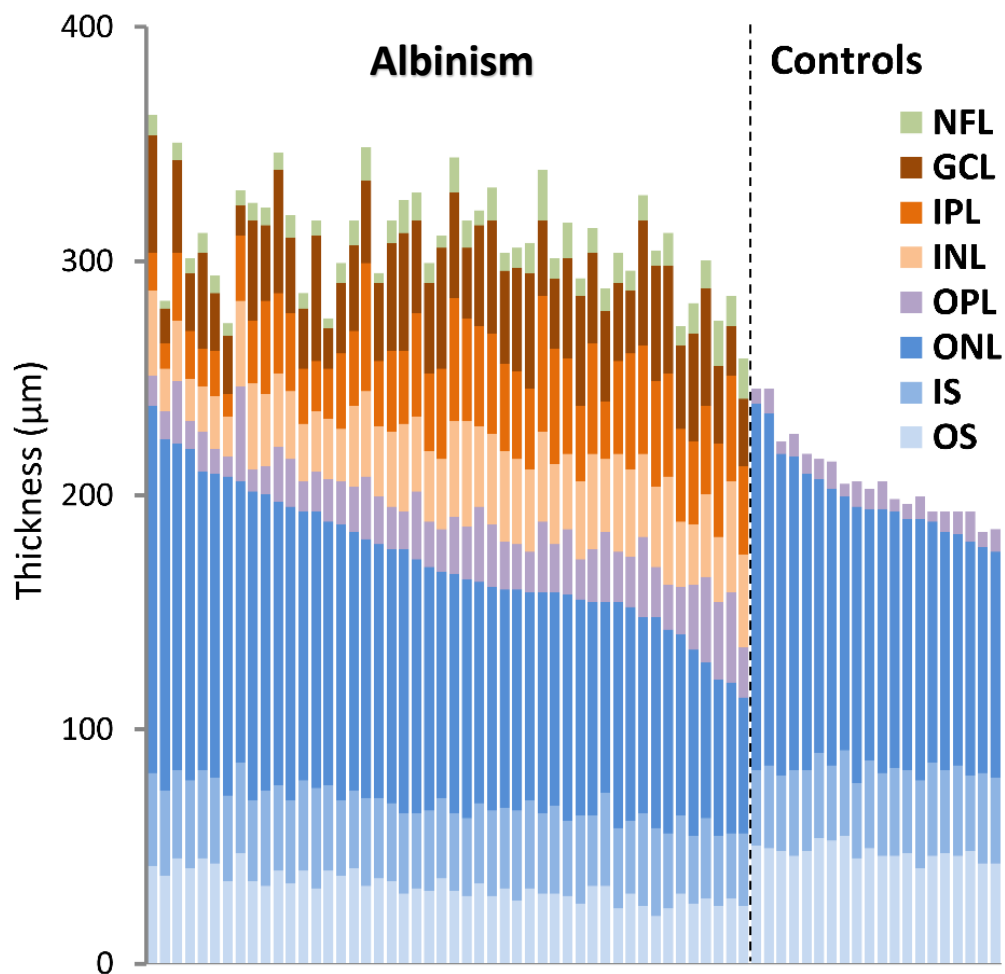


Figure 3-5: Bar chart illustrating the contribution of processing layers (red colours) and photoreceptor layers (blue colours) to overall retinal thickness. Each bar represents an individual patient. The data from both eyes was averaged except in three patients with albinism where data from only one eye was available. The patients are organised in descending order of photoreceptor layer thickness. The albinism patients are on the left and the controls are on the right. NFL=nerve fibre layer, GCL=ganglion cell layer, OPL=outer plexiform layer, ONL=outer nuclear layer, IPL=inner plexiform layer, INL=inner nuclear layer, IS=inner segment, OS=outer segment, RPE=retinal pigment epithelium.

H₀ 1.3: Visual acuity is related to foveal development in patients with albinism.

Figure 3-6 summarises results of Spearman's rank correlation co-efficient analysis which showed that neither total retinal thickness ($r=-0.232$, $p=0.144$) nor foveal pit depth ($r=-0.245$, $p=0.122$) were significantly correlated to best corrected visual acuity (BCVA). In contrast both total processing layer thickness ($r=0.364$, $p=0.019$) and total photoreceptor layer thickness ($r=-0.501$, 8.36×10^{-4}) were correlated to BCVA although this was much stronger for the total photoreceptor layer thickness. Correlation of the processing layer thickness was no longer significant once the Holm-Bonferroni correction had been applied ($p'=0.057$). When considering the photoreceptor layers individually both foveal OSL thickness ($r=-0.641$, 6.31×10^{-6}) and ONL thickness ($r=-0.504$, 7.84×10^{-4}) were significantly correlated with BCVA.

	<i>r-value</i>	<i>p-value</i>	<i>p'-value</i>
<i>Total retinal thickness</i>	-0.232	0.144	0.244
<i>Foveal pit depth</i>	-0.245	0.122	0.244
<i>Processing layer thickness</i>	0.364	0.019	0.057
<i>Photoreceptor layer thickness</i>	-0.501	8.36×10^{-4}	0.003
<i>Outer nuclear layer thickness</i>	-0.504	7.84×10^{-4}	0.004
<i>Outer segment thickness</i>	-0.641	6.31×10^{-6}	3.78×10^{-5}

Table 3-3: Comparison of best corrected visual acuity in patients with albinism with the total retinal thickness, foveal pit depth, photoreceptor, processing, outer nuclear layer and photoreceptor outer segment thickness at the fovea using Spearman's rank correlation co-efficient. Holm-Bonferroni corrected p' values are also included.

H₀ 1.4: Chiasmal misrouting measured using VEP is related to foveal development

Table 3-4 compares the degree of VEP asymmetry with retinal thickness, outer nuclear thickness and outer segment length. We found no significant relationship between the degree of VEP asymmetry and any of the retinal layers. Holm-Bonferroni correction was not deemed necessary as the uncorrected p-values were not significant.

<i>Total retinal thickness</i>	0.251	0.174	
<i>Outer nuclear layer</i>	-0.021	0.911	
<i>Outer segment</i>	0.081	0.667	

Table 3-4: Comparison of degree of visual evoked potential asymmetry in patients with albinism with the total retinal thickness, outer nuclear layer thickness and photoreceptor outer segment thickness at the fovea using Spearman's rank correlation co-efficient.

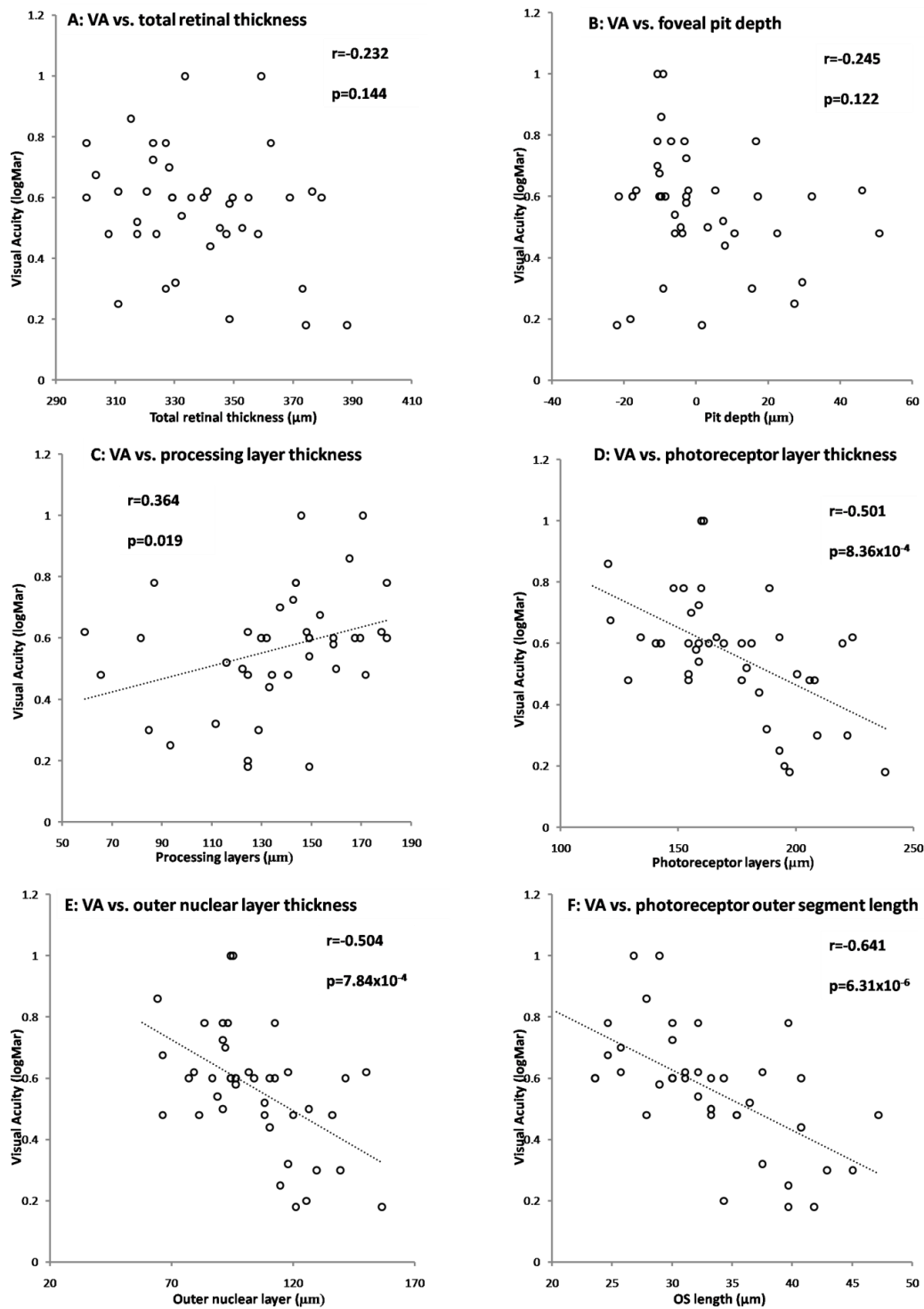


Figure 3-6: Comparison of binocular best corrected visual acuity (BCVA) with (A) the total thickness of the foveal retina, (B) foveal pit depth, (C) processing layer thickness, (D) photoreceptor layer thickness, (E) outer segment length, and (F) outer nuclear layer thickness at the fovea. In 43 patients with albinism where data from both eyes was available, this was averaged while in the remaining four data from one eye was used. The visual acuity is provided in logarithm of minimal angle of resolution (logMAR).

3.2.4 DISCUSSION

This is the first study using a large sample size to provide quantitative evidence for the functional significance of foveal photoreceptors in the retina of patients with albinism.

Foveal structure

Our results show that foveal thickness is higher in patients with albinism compared to controls. Macular thickness in patients with albinism has been previously quantified by five groups as 219 μ m (n=13),¹⁴² 233 μ m (n=11),¹³⁹ 240.4 μ m (n=10),¹³⁸ 247 μ m (n=13)³⁴⁹ and 300 μ m (n=1)¹³⁷. In our study, the albinism group had a mean retinal thickness of 309 μ m (\pm 24.0) which is at the higher end of the range quoted in previous studies.

Two important factors might be causing this variation in retinal thickness observed by various groups. Firstly, as demonstrated by our study, there is a wide spectrum of foveal development seen in patients with albinism. The range of foveal thickness in our study varied from a minimum of 258 μ m to a maximum of 362 μ m. As the previous studies either were single case studies, or involved a small number of patients, they are more prone to influence from extremes. This is especially true for the study by Harvey et al. who only measured foveal thickness in patients with a rudimentary foveal pit¹³⁹, which helps explain why their quoted value is the lowest out of four studies that have quantified retinal thickness. This illustrates the need for a large sample size when studying the retina in patients with albinism to reflect population diversity.

Secondly, all the previous studies had used the older generation time-domain OCT devices (TD-OCT). These have a longer acquisition time leading to greater movement artefact that would bias successful recordings from patients with less severe nystagmus. In addition, comparison of SD-OCT and TD-OCT in the past has shown that TD-OCT devices reported smaller measurements of retinal thickness compared to SD-OCT devices.³⁵⁰⁻³⁵³ The mean foveal thickness of 206 μ m (SD 15.8) in our control group is comparable to previous SD-OCT studies of the normal fovea indicating that our methodology is reliable.^{350, 354-356}

Several studies have reported the presence of significant percentage of albinism patients without nystagmus although the diagnosis is not confirmed in these studies using either VEP asymmetry or genetic testing. Possibly some of these studies may favour the inclusion of patients with minimal nystagmus to improve the quality of OCT recordings.^{143, 144} The use of eye movement recordings has confirmed the presence of nystagmus in all of our patients in accordance with the findings of Summers et al. who found 39 of 40 albinism patients to exhibit nystagmus.⁹⁹ We find that nystagmus oscillations in excess of 10° amplitude do not prevent successful capture of high quality OCT images due to the rapid acquisition of single B scans (14 ms).

Comparison to visual acuity

Visual acuities observed in our patient cohort ranged from 0.18 to 1 logMAR with a peak in the frequency of individuals with visual acuities between and 0.5 and 0.6 logMAR. This pattern is similar to the visual acuity distributions described in previous studies that contain a large cohort of individuals with albinism. The mean visual acuity of 0.57 logMAR also corresponds well with values quoted in previous studies.^{357, 358}

Development of OCT technology has allowed assessment of foveal morphology in-vivo and attempts have already been made to assess the relationship between foveal hypoplasia and visual acuity. Given that the most obvious abnormalities on a cursory viewing of OCT images from patients with albinism is the absent or diminished foveal pit and retinal thickening, it would be easy to assume that these features might be associated with poor visual function. One previous study suggests no relationship between foveal thickness and visual acuity.³⁴⁹ Harvey et al.¹³⁹ found a weak inverse relationship ($r=-0.21$) between foveal thickness and visual acuity in albinism. However, both of these studies used small numbers ($n=13$ and $n=11$, respectively).

Our findings agree with the correlation coefficient reported by Harvey et al where we also find a weak negative correlation ($r=-0.23$). Harvey et al. speculate that such weak correlation is possibly due to the difficulty they had in imaging the macula with a time domain OCT device.¹³⁹ However, we provide conclusive evidence that total macular

thickness is not a good predictor of visual acuity ($p=0.144$) using a higher resolution SD-OCT device with a faster scan acquisition time and a larger patient group.

Seo et al. also correlated visual acuity with foveal hypoplasia using a 10 μ m OCT device. Rather than attempting to correlate the BCVA directly with the size of the foveal pit, they developed a grading system that took many different OCT features into account.¹⁴² However, we could not visualise some of the features they describe such as the tram-track sign. This was also noted by Chong et al. who suggested that these signs were seen due to the low-resolution OCT device being used by Seo et al.¹⁴¹ and we agree with their conclusion that with the advent of higher resolution OCT devices, the grading system devised by Seo et al. has become obsolete. Chong et al. suggested that an alternative grading system should be devised based on high resolution OCT and recommended that this grading system should be based on the following cardinal signs of albinism:

- Absence of central foveal depression
- Persistence of ganglion and plexiform retinal layers
- Persistence of the nerve fibre layer
- A very prominent image of the entire choroid¹⁴¹

The first three of these suggestions have been incorporated by Thomas et al. in their grading system for foveal hypoplasia³⁴⁰ alongside specialisation of photoreceptor layers, which although not mentioned by Chong et al., plays a very important role in visual function as per our results.

We find photoreceptor outer segment length to be the strongest predictor of visual acuity. In contrast, there was no significant relationship between, either total retinal thickness or foveal pit depth, and visual acuity. This lack of correlation was due to the relationship between the total thickness of photoreceptor layers and the total thickness of processing layers, where increasing total thickness of photoreceptor layers was associated with decreasing thickness of processing layers. This meant that the degree of deviation away from normal foveal morphology was not related to overall retinal thickness.

Comparison to normal foveal development

Foveal pit formation

The above can be explained by the considering the sequence of events that occur in the developing fovea prior to reaching complete maturation. During embryonic development, the processing layers migrate centrifugally to form the foveal pit. The central retina develops in three distinct phases, which involve increase in thickness prenatally, transient thinning after birth and then resumption of thickening.³⁵⁹

Foveal development begins towards the end of the first trimester with the earliest marker of its future location being indicated by a region that contains cones exclusively and is identifiable at foetal week 11. When developing retina is encroached by vasculature at around gestational week 14, several anti-angiogenic factors form a molecular barrier at the fovea to prevent them from entering this region.³⁶⁰⁻³⁶² This leads to the formation of a “foveal avascular zone” (FAZ) that is surrounded by a ring of parafoveal vasculature. The FAZ is a critical requirement for the formation of the foveal pit.^{359, 363} The absence of blood vessels from the fovea give neural tissue in this area increased elasticity compared to the surrounding retina. Under the effect of intra-ocular pressure, this leads to the in-utero development of the foveal pit. The second phase of foveal pit formation occurs in the postpartum period and is dependent on active growth-induced stretch that remodels foveal morphology.³⁶⁴

Under normal circumstances, the GCL is the first layer to be displaced as it is at the vitreo-retinal interface and therefore is the first to be acted upon by intra-ocular pressure. It is followed by IPL, INL and OPL.³⁶⁵ This process may also be also driven by relative hypoxia of the inner retinal layers at the fovea due to the FAZ.³⁶⁶

In albinism, retinal vessels encroach the fovea and the FAZ fails to develop.^{129, 367} This leads to deficiency in the formation of the foveal pit and hence leads to the increased retinal thickness at the fovea.

The fovea continues to develop post-partum and does not reach full maturity until the age of five years.^{368, 369} The foveal pit continues to deepen and widen with the INL, IPL and GCL reducing to only 1 to 2 cells deep and eventually fusing into a single layer at the fovea.^{370, 371} This is evidenced in our study as the persistence of, what we have labelled as, the OPL through the fovea in our control group.

Another aspect of abnormal foveal development that we saw in our albinism group was persistence of the retinal nerve fibre layer through the fovea. In normal foveal development, the anti-angiogenic molecules such as pigment epithelium derived factor, ephrin A6 and semaphorin axon guidance gene families repel ganglion cell axons from the foveal area. Instead, these axons form the arcuate bundles around the fovea before congregating at the optic nerve head.³⁷² In albinism, it appears that there is a reduced functionality of these molecules leading to a deficiency in axon guidance and therefore persistence of the nerve fibre layer through the fovea.

Photoreceptor specialisation

There is a lack of consensus in previous literature regarding the relationship between foveal pit formation and photoreceptor specialization. Springer et al. proposed that foveolar cone density varies significantly at different stages of foveal pit development. When the pit depth increases from being non-existent to 88%, the cone approximately doubles. Subsequent decline in pit depth is associated with a three-fold increase in cone density. This suggestion is supported by studies in monkeys that have shown that the cone packing is not completed until the foveal pit reaches maximum depth.^{371, 373}

In contrast, Marmor et al. and McAllister et al. both found that even in the absence of foveal pit formation, other aspects of foveal specialization such as increased density of foveal cones, outer segment elongation and lengthening of Henle's fibres can still occur and individuals without a foveal pit can exhibit significant cone specialisation.^{143,}

We found a negative correlation between the size of the photoreceptor layers and the thickness of processing layers indicating that a relationship between the foveal specialisation of these two layers exists. However, it is difficult to infer whether this is a causal relationship or merely a reflection of severity of disease. In addition, we find that specialisation of the photoreceptor and processing layers can exist at the fovea without the formation of a pit.

In the initial embryonic period, the cone photoreceptors are cuboidal in shape and during foveal development, they undergo extensive morphogenesis³⁷⁴ to change into the thin, elongated shape seen in the adult eye.³⁷⁵ The development continues after birth and cone diameter changes from 7.5 μm at birth to 2 μm by 45 months.³⁷¹ This facilitates centripetal migration of peripheral cones and the density of cone cells at the fovea increases from 11,200/mm² at foetal week 11 to approximately 200,000/mm² in the adult eye.^{370, 376}

It appears that foveal pit remodelling influences early phases of cone packing but there are other factors, such as expression of fibroblast growth factor, that also play a role in this process.^{359, 377}

Summary

In summary, we for the first time, provide evidence of the functional significance of foveal OCT recordings in albinism. In particular, we find that the OSL is strongly correlated to visual acuity. Since nystagmus associated with albinism also leads to deterioration in vision due to motion blur, our findings indicate that OCT has a clinical use in recognizing patients who have potential for visual improvement because of treatments to reduce nystagmus intensity such as pharmacological interventions.³⁷⁸

3.3 OPTIC NERVE

3.3.1 BACKGROUND

Relatively little is known about the optic nerve morphology in albinism. Using fundus photography, Spedick and Beauchamp reported optic nerve hypoplasia¹⁶⁷ and tilted discs have also been described in albinism.¹⁶⁹ We attempt to characterize the optic nerve head in patients with albinism using high resolution SD-OCT and investigate whether optic nerve abnormalities seen in albinism are related to foveal and chiasmal abnormalities.

3.3.2 SUMMARY OF AIMS

- Characterize optic nerve head topography in albinism.
- Investigate optic disc tilt, which has been reported in albinism.
- Analyse the arrangement of the peripapillary retinal nerve fibre layer around the optic nerve in albinism since miswiring of retinal projections is known to occur in albinism.
- Compare optic nerve head and peripapillary retinal nerve fibre layer abnormalities in albinism with foveal abnormalities and other clinical measures such as refractive error, nystagmus and best-corrected visual acuity.

3.3.3 FINDINGS

Optic nerve scans were obtained and analysed from 56 patients with albinism (33 male and 23 female, mean age=36.1±11.9 years) and 60 healthy controls (36 male and 24 female, mean age=39.2±14.7 years).

As previously reported,^{103, 105} significant refractive errors existed in the albinism group with high levels of hyperopia (hyperopia: 22.2% ≥3D and 6.2% ≥5D spherical equivalent; myopia: 7.4% ≤ -3D and 2.5% ≤ -5D cylinder) and with-the-rule astigmatism (in the 23.4% of participants with significant astigmatism (cylinder ≥+3D or ≤-3D) 89.5% had with-the-rule astigmatism). Control volunteers were excluded if they had significant refractive error (spherical equivalent ≥+3D or ≤-3D).

Due to non-normality of the data, optic nerve and ppRNFL parameters were compared between albinism and controls using Mann-Whitney U test after averaging measures for right and left eyes. Linear regression analysis was used to determine the relationship between various optic nerve measures and the following measures:

1. Thickness of the photoreceptor and processing layers at the fovea
2. Best-corrected visual acuity (BCVA)
3. Refractive error
4. VEP asymmetry

H₀ 2.1: OCT can be used to reliably measure the ONH and ppRNFL parameters in albinism.

Table 3-5 shows results of test-retest analysis of the key optic nerve and ppRNFL parameters from two separate scans from the same patient. The intra-class correlation co-efficients were above 0.9 for all the parameters measured demonstrating high repeatability.

<i>Parameter</i>	<i>Albinism</i>	<i>Controls</i>
<i>Disc area</i>	<i>0.986</i>	<i>0.962</i>
<i>Cup area</i>	<i>0.973</i>	<i>0.993</i>
<i>Rim area</i>	<i>0.982</i>	<i>0.948</i>
<i>Cup:disc area ratio</i>	<i>0.978</i>	<i>0.984</i>
<i>Cup volume</i>	<i>0.987</i>	<i>0.989</i>
<i>Rim volume</i>	<i>0.978</i>	<i>0.946</i>
<i>RNFL (Inner annulus)</i>	<i>0.913</i>	<i>0.902</i>
<i>RNFL (Outer annulus)</i>	<i>0.912</i>	<i>0.962</i>

Table 3-5: Intra-class correlation coefficients from test-retest analysis of disc, cup and rim areas, cup:disc area ratios, cup and rim volumes and peripapillary nerve fibre layer (ppRNFL) thickness in both inner and outer annuli.

Left vs Right eyes

Using Wilcoxon matched pairs signed ranks test and we found no significant difference ($p>0.05$) between the 2 eyes in the disc, cup, rim or RNFL size.(Table 3-5).

		<i>Disc area</i>	<i>Cup area</i>	<i>Rim area</i>	<i>ppRNFL (inner)</i>	<i>ppRNFL (outer)</i>
Albinism	P	0.487	0.615	0.652	0.947	0.802
	Z	-0.694	-0.503	-0.452	-0.066	-0.251
Control	P	0.617	0.511	0.737	0.432	0.377
	Z	-0.500	-0.657	-0.366	-0.786	-0.883

Table 3-6: Disc, cup and rim areas and peripapillary nerve fibre layer (ppRNFL) thickness in both inner and outer annuli was compared between the two eyes.

Optic nerve head morphology

Figure 3-7 compares cross-sectional appearance of the optic nerve in albinism and controls at three locations. On visual inspection of OCT scans, the majority of individuals with albinism had very small or absent optic cups. Quantitative analysis of the ONH scans showed that 39.4% of eyes in the albinism group did not have a measurable optic cup (using 150µm offset from the disc) whereas all the control eyes displayed a cup.

Figure 3-8 shows B-scans from six different patients with albinism and demonstrates the spectrum of optic nerve abnormalities seen in this group. The degree of abnormality ranged from being gross (A) to resembling normal optic nerve head morphology (D). Apart from the small cups, main abnormal finding on cross-sectional slices appeared to be a sharp elevation of the nasal aspect of the rim, which was hyper-reflective at the vitreo-retinal margin. However, posterior to this, there was a hypo-reflective band of tissue that extended to the middle of the cup in the naso-

temporal axis and past the RPE in the antero-posterior axis. This band appeared to be more prominent in eyes where the cup is smaller and the nasal rim larger.

H₀ 2.2: Patients with albinism have abnormally small optic discs, cup and rims.

The findings from a quantitative analysis of the optic disc, cup and rim areas (en-face view) are illustrated schematically in Figure 3-9. Disc areas were similar in patients with albinism (Figure 3-9 A and B: median=1.65mm², range: 0.94-2.64mm²) and controls (Figure 3-9 F and G: median=1.71mm², range: 1.25-2.32mm², $p=0.128$) although disc areas were more narrowly distributed in the control group.

There was a highly significant difference in median cup area ($p=1.56 \times 10^{-5}$) that was 23.7% smaller in albinism (median=0.088mm², range: 0.00-1.22mm²) compared to controls (median=0.373mm², range: 0.095-1.03mm²). Although some cup areas in albinism were within normal ranges, overall the distribution was markedly skewed to the left compared to the control group.

Not surprisingly, cup: disc area ratios were much smaller in the albinism group compared to controls (albinism: median=0.059, range: 0.00-0.58; controls: median=0.267, range: 0.052-0.52; $p=1.54 \times 10^{-4}$). Rim areas (i.e. disc area–cup area) were slightly larger (114%) in albinism (median=1.42mm², range: 0.80-2.43mm²) compared to controls (median=1.25mm², range: 0.81-1.96mm²; $p=0.04$).

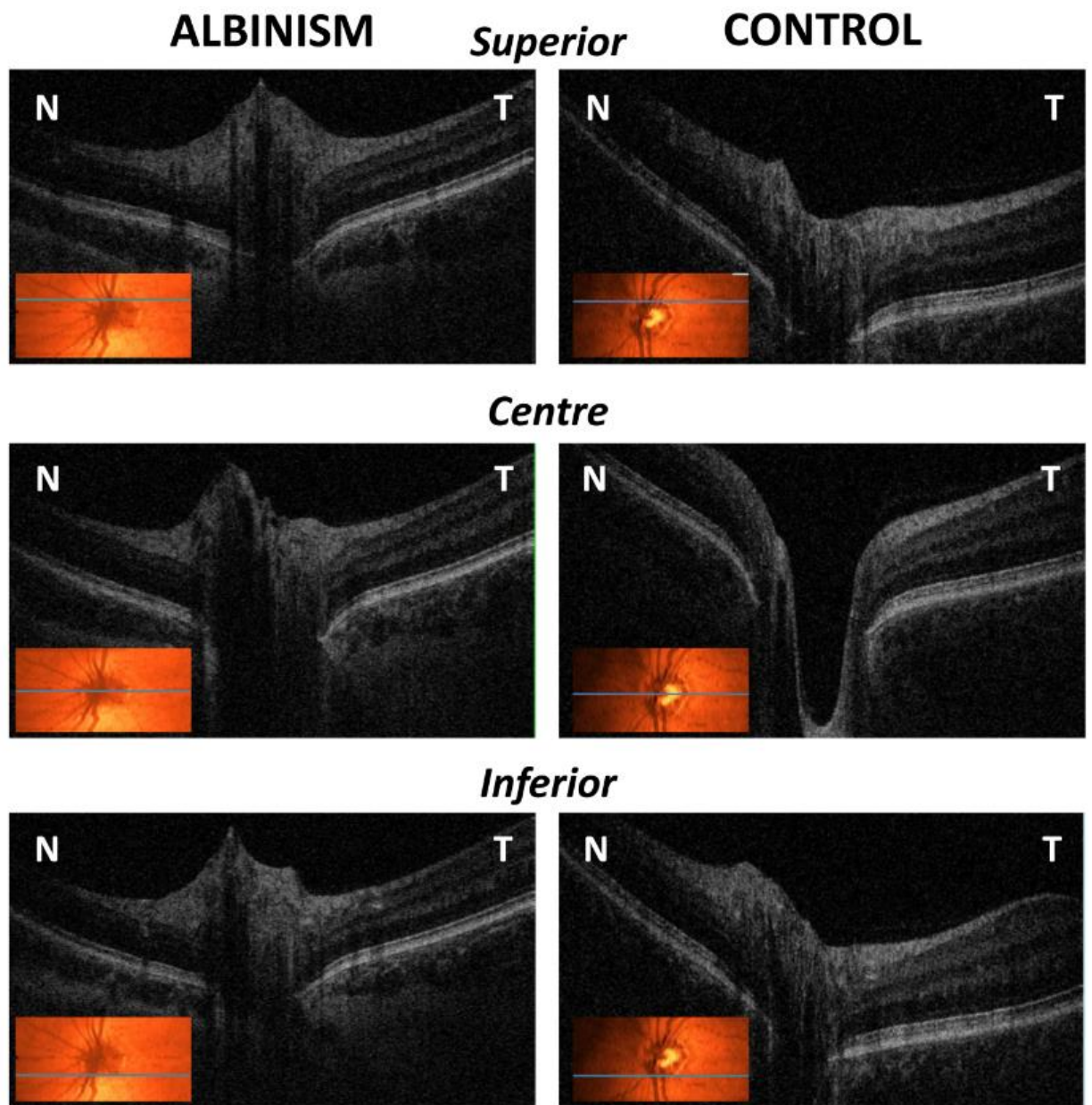


Figure 3-7: Comparison of optic nerve OCT scans of the right eyes from an albinism patient and a healthy volunteer. B-scans show the cross-sectional view of the superior edge of the optic nerve, the centre of the optic nerve and the inferior edge of the optic nerve of the two eyes. The location of the B scan on the en-face volume intensity projection of the retinal surface is shown in the insets. N is nasal and T is temporal.

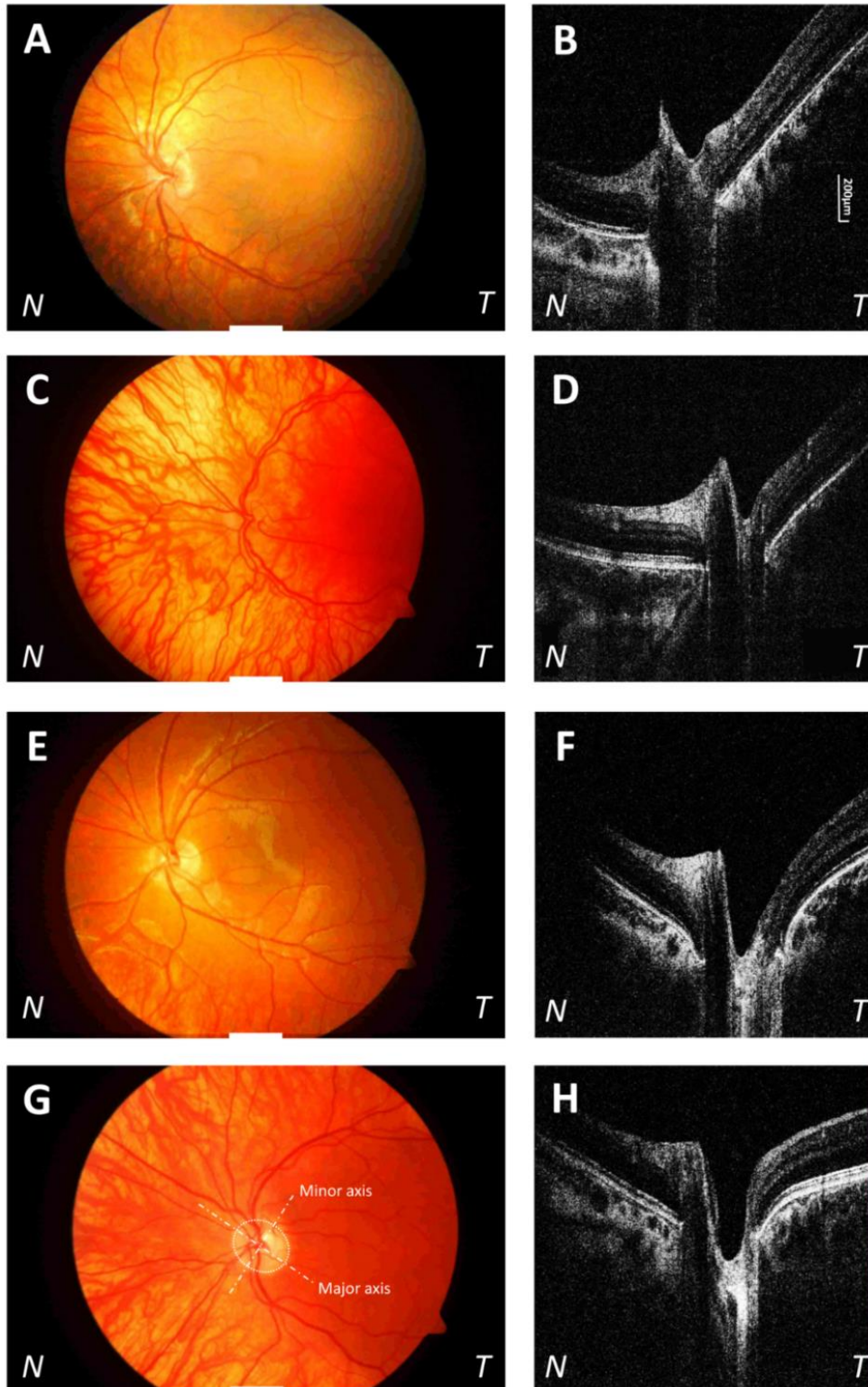


Figure 3-8: Comparison of fundus photographs and B scan cross-sectional images of left eyes through the deepest part of the cup for four patients with albinism showing the spectrum of abnormalities. An albinism patient with very small cup is shown in A and B. In contrast, an albinism patient with deep cups is shown in G and H. Panel G shows an example of the measurement of disc torsion with the major and minor axis of the ovality shown, although the direction of disc torsion appears to be abnormal. N is nasal and T is temporal.

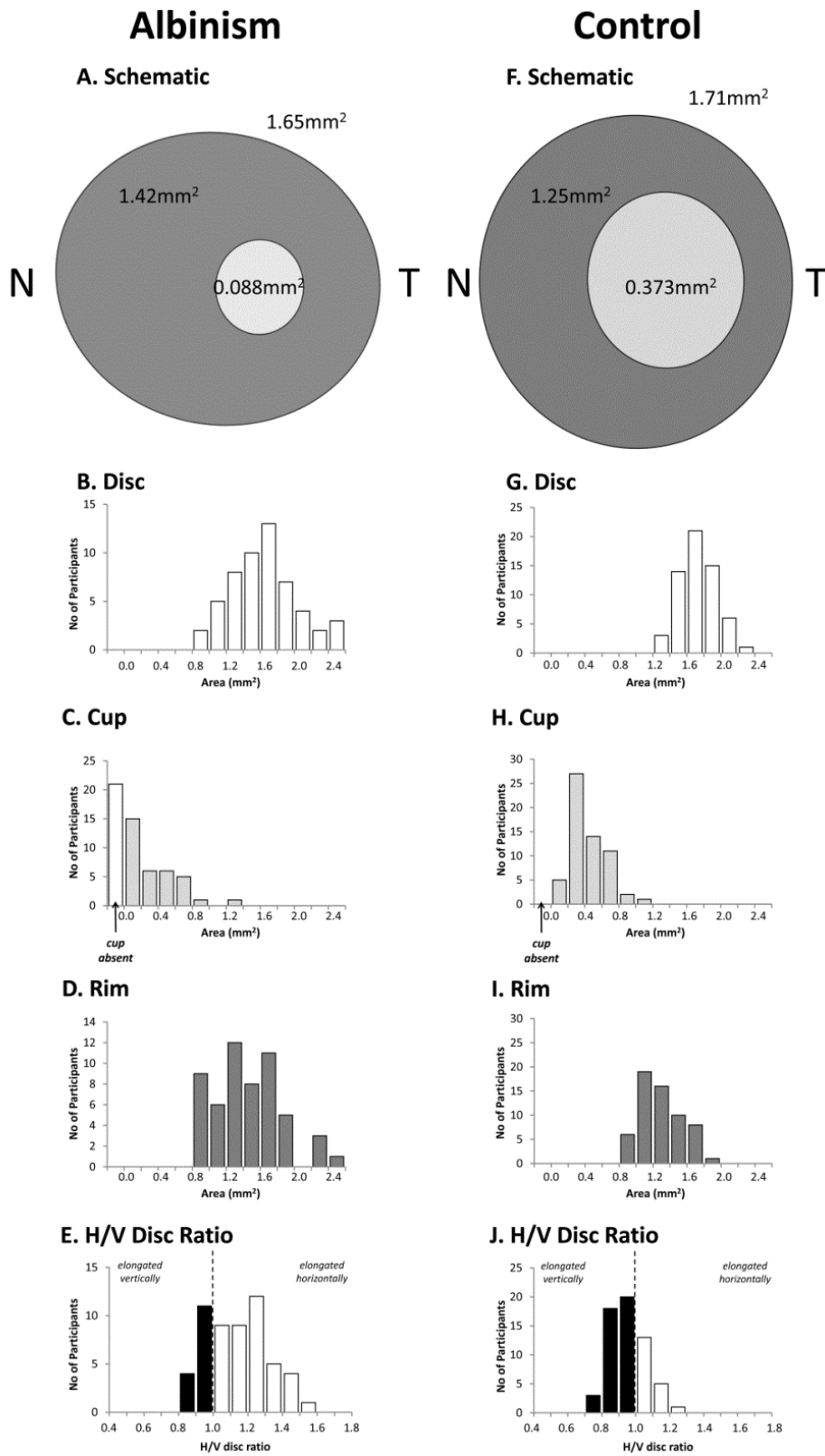


Figure 3-9: A and F are schematic diagrams comparing the median dimensions of albinism and control volunteers for disc, rim and cup in en-face view. The outer ellipse represents the disc area, the inner ellipse the cup area (light grey). The dark grey colour represents the rim area. Distributions of disc, cup and rim areas for each group are shown in B to D for albinism and G to I for controls, respectively. E and J show the ratio of disc diameter in the horizontal and vertical axes.

Cross Sectional View

Figure 3-10 shows a schematic cross-sectional view of the optic discs along the naso-temporal axis based on the analysis of single horizontal B-scans across the deepest portion of the optic cup. The cross-sectional analysis revealed that both nasal and temporal rim areas were significantly larger in the albinism group (nasal: median=0.176mm², range: 0.001-0.487mm²; temporal: median=0.038mm², range: 0.000-0.294mm²) compared to controls (nasal: median=0.101mm², range: 0.015-0.219mm²; temporal: median=0.015mm², range: 0.001-0.114mm²; $p=3.32 \times 10^{-6}$). The asymmetry of temporal and nasal rim areas (i.e. nasal rim area / nasal + temporal rim areas) was not significantly different between the two groups (median=0.83 in albinism, 0.86 in controls; $p=0.144$).

Rim volumes were estimated from all B-scans spanning the optic nerve head and found to be significantly larger in participants with albinism (136.6% of the volume in controls; median=0.273mm³, range: 0.048-0.635mm³) compared to controls (median=0.200mm³, range: 0.060-0.445mm³; $p=0.036$). Median cup volumes were much smaller in participants with albinism (median=0.009mm³) compared to controls (0.068mm³; $p=1.19 \times 10^{-6}$).

SCHEMATIC OF CROSS SECTIONAL VIEW

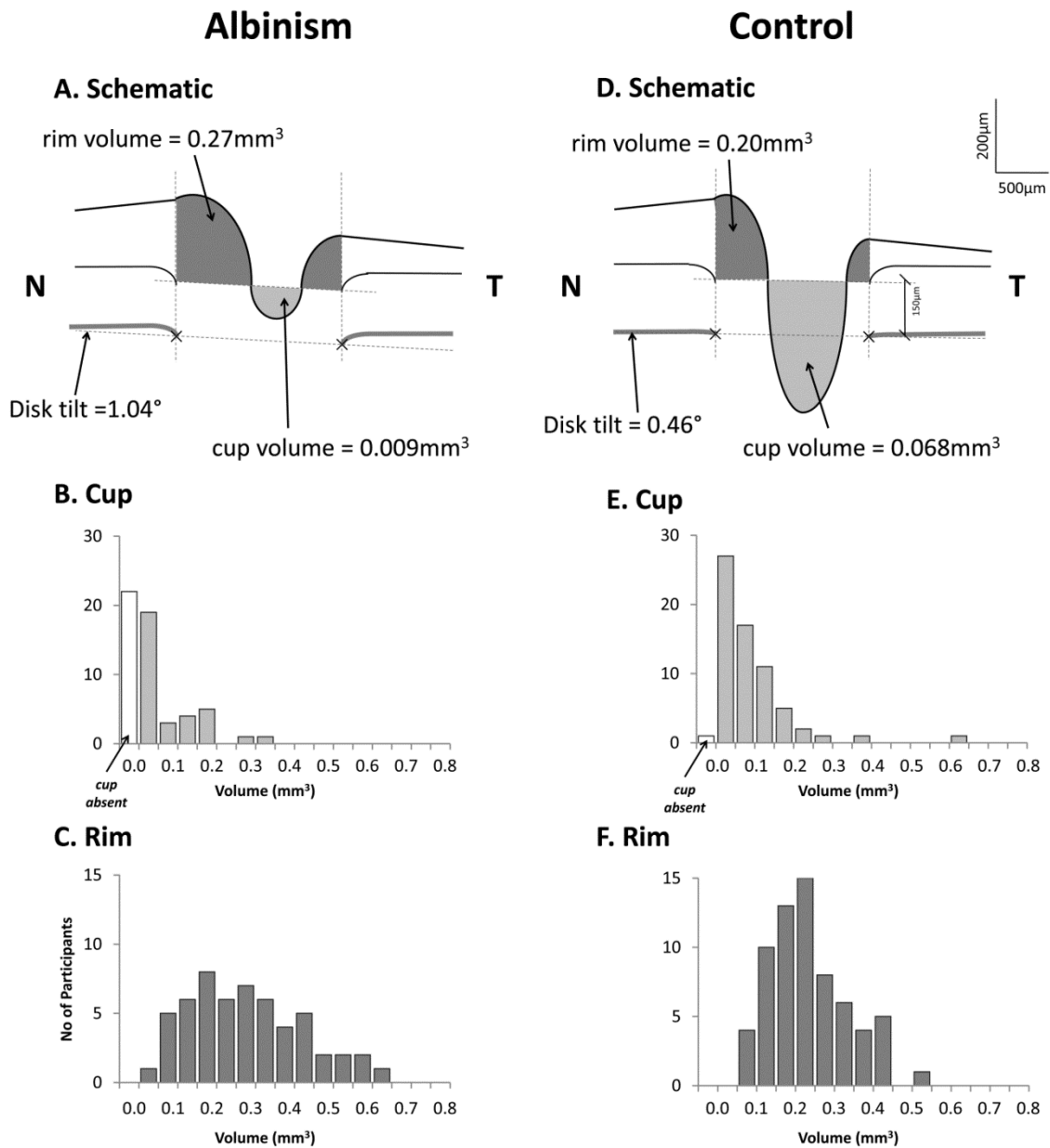


Figure 3-10: Cross sectional schematic diagram of optic nerve head through the naso-temporal axis. A. represents albinism and D. controls. Horizontal dotted lines represent the plane used for the measurement of the disc, rim and cup areas displayed in figure 5. This plane along with the disc edges (defined by the limits of the RPE indicated by the vertical dotted lines) and the internal limiting membrane was used to calculate cup and rim volumes the distributions of which are shown figures B and C for the albinism group and figures E and F for controls, respectively. N is nasal and T is temporal.

H₀ 2.3: Patients with albinism have optic disc tilt and torsion.

Disc Torsion: Ovality of the optic disc (>10%) was observed in 53.8% of albinism participants and 39.4% of controls ($p=0.22$). In albinism the most common orientation was close to the horizontal axis or rotated slightly with the nasal disc more superior with respect to the temporal disc

Figure 3-11 A) shows that 73.5% of albinism participants with ovality>10% demonstrated discs oriented between 10° anticlockwise (temporal disc more superior relative to nasal) and 30° clockwise (nasal disc more superior relative to temporal) from a horizontal orientation. In contrast, in the control group, discs were more commonly oriented along near the vertical axis with 76.9% of disc being oriented within $\pm 20^\circ$ of the vertical axis. The horizontal elongation of optic discs in albinism compared to control participants was also apparent from the distribution of the horizontal / vertical disc ratios which were more frequently >1 in albinism compared to controls (Figure 3-9 E and J) (albinism: median=1.12; range: 0.81-1.55; controls: median=0.93; range: 0.76-1.25; $p=6.45 \times 10^{-5}$). The median ovality and orientation of the disc is represented schematically in Figure 3-9 A and F.

Disc Tilt: Analysis of the positions of the disc margins relative to the plane of the Bruch's membrane in a cross-section of the ONH along the horizontal axis through the centre of the cup showed a small (median difference = 0.58°) but significantly greater horizontal tilt in albinism (median= -1.04° , range: -3.83 to 2.06° , where negative values indicate the nasal edge being more anterior relative to temporal edge) compared to controls ($p=0.001$; median= -0.46° , range: -3.18° to 1.96°). (

Figure 3-11 B)

On clinical examination of fundi and fundus images two participants with albinism had a clear pattern of tilted disc syndrome (with an inferior or infero-nasal crescent of visible sclera and infero-nasal disc tilt) and one participant a myopic tilted disc pattern (with temporal crescent of visible sclera, temporal disc torsion and significant myopia). 15.2% of patients with albinism displayed a marked temporal crescent of visible sclera but also had mainly horizontal elongation of the disc and no significant myopia (i.e.

spherical equivalent was <-3 dioptres). 12.1% of patients with albinism displayed a double ring sign. None of these features (obvious tilted disc syndrome, myopic tilted disc or marked temporal crescent of visible sclera) were seen in the control group.

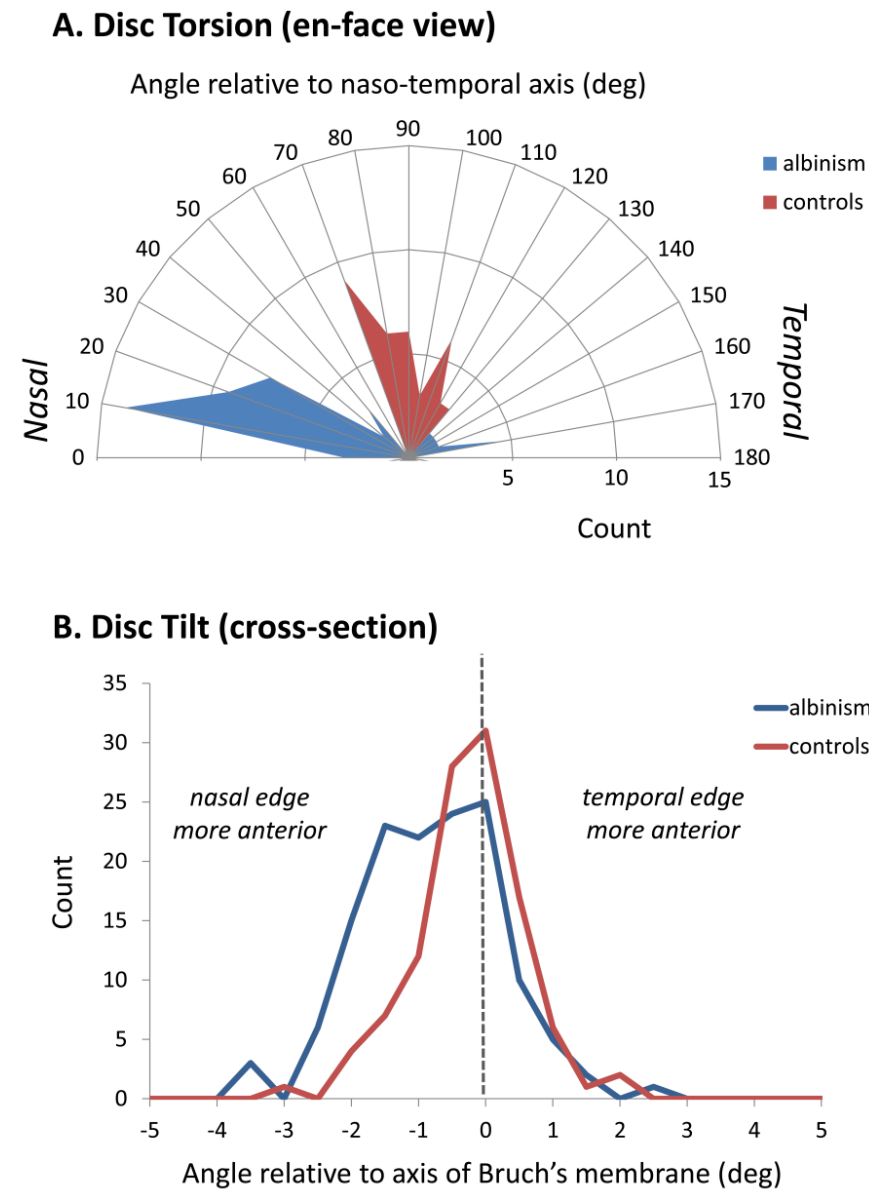


Figure 3-11: A. Optic disc torsion (calculated from the en-face view), B. optic disc tilt and disc edge distortion (calculated from the cross sectional view). In A. the major axis of the disc angle for individuals showing an ovality of $>10\%$ is displayed for albinism (in blue) and controls (in red). In B, optic disc tilt is estimated from the angle of the disc edges relative to the plane of the Bruch's membrane adjacent to the disc. The deformation of the disc edges is calculated from the mean displacement of the disc edges relative to the Bruch's membrane (where positive values indicate a posterior deformation of the disc edges).

H₀ 2.4: Patients with albinism have a thinner ppRNFL.

Figure 3-12 summarises the differences in ppRNFL between the albinism and control groups in 10 segments around the optic nerve head (using the GDx parameters) using 0.4mm annuli (1.6-2.4mm and 2.4-3.2mm diameter). Blue colours indicate that the overall ppRNFL thickness in the outer annulus was consistently smaller in albinism ($p=9.43 \times 10^{-10}$; 18.2% thinner than in controls). However, these differences were greater in the temporal retina, where mean differences were consistently between 20-30%, and highly significant statistically. Overall ppRNFL thickness in the inner annulus was much closer to control values (comparison of overall thickness was $p=0.89$). However, the nasal aspect was significantly thicker in albinism compared to controls and the temporal aspect significantly thinner ($p=0.012$).

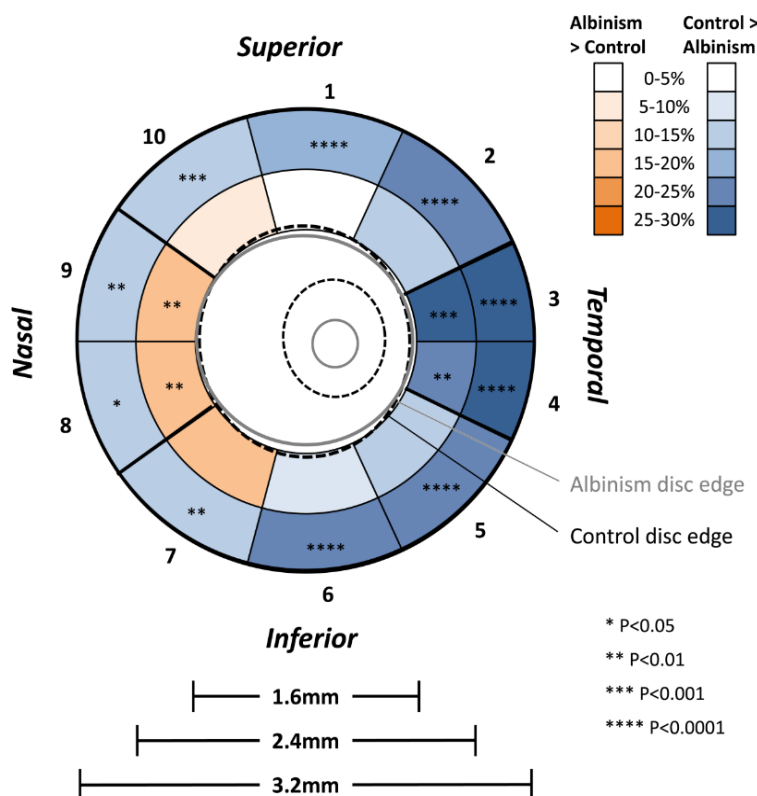


Figure 3-12: Percentage difference in mean peripapillary retinal nerve fibre layer (ppRNFL) thickness between participants with albinism and controls. The blue colours indicate NFL is thinner in albinism compared to controls and red colours indicate ppRNFL is thicker in albinism compared to controls. The grey ellipse indicates the median disc edge in albinism and the black dashed line in controls.

H₀ 2.5: Foveal and optic nerve abnormalities are related in patients with albinism

We found no significant correlation between ONH parameters and any of the central foveal layers analysed (Table 3-7). There was however, a strong correlation between ganglion cell (GCL) thickness at the central fovea and mean ppRNFL thickness in the outer annulus (2.4-3.2mm). Further analysis of nasal and temporal aspects of the ppRNFL (nasal ppRNFL: mean of segments 7-10; temporal ppRNFL: segments 2-5) showed a significant correlation between the central foveal GCL thickness and nasal ppRNFL in both inner ($r=0.374$, $p=0.016$) and outer annuli ($r=0.353$, $p=0.035$). There were no significant correlations, however, between temporal ppRNFL and foveal GCL thickness.

H₀ 2.6: Optic nerve head abnormalities impact visual acuity

Table 3-7 shows that refractive error was negatively correlated with disc ($r=-0.435$, $p=0.001$, $p'=0.009$), cup area ($r=-0.247$, $p=0.009$, $p'=0.072$), cup: disc ratio ($r=-0.213$, $p=0.014$, $p'=0.098$) and was positively correlated with inner ppRNFL ($r=-0.213$, $p=0.021$, $p'=0.126$). Only the correlation between refractive error and disc area was significant following Holm-Bonferroni correction.

Best-corrected visual acuity was also negatively correlated with disc size ($r=-0.383$, $p=0.006$, $p'=0.054$) but this correlation did not survive correction for multiple comparison.

H₀ 2.7: Optic nerve head abnormalities are related to chiasmal misrouting measured using VEP.

Table 3-7 also demonstrates that the VEP asymmetry was not significantly correlated with any ONH parameter ($p=0.503$ disc, $p=0.323$ cup, $p=0.970$ rim, $p=0.966$ ppRNFL)

parameter	statistic	areas			volumes		ratios		mean nerve fiber layer thickness	
		disc	cup	rim	cup	rim	cup: disc ratio	disc hor: ver dia. ratio	inner annulus	outer annulus
macular thickness	<i>r</i>	-0.138	-0.221	0.019	-0.272	0.282	-0.200	-0.169	0.098	0.174
	<i>p</i>	0.372	0.149	0.905	0.074	0.064	0.193	0.273	0.543	0.290
inner layers (ILM-OPL)	<i>r</i>	-0.153	-0.136	-0.055	-0.204	0.181	-0.086	-0.110	0.159	0.320
	<i>p</i>	0.322	0.377	0.724	0.184	0.239	0.577	0.479	0.322	0.047
outer layers (ONL-BM)	<i>r</i>	0.088	-0.015	0.096	0.018	0.031	-0.063	-0.027	-0.093	-0.211
	<i>p</i>	0.572	0.922	0.535	0.906	0.842	0.686	0.863	0.562	0.198
ganglion cell layer	<i>r</i>	-0.032	-0.091	0.032	-0.151	0.144	-0.090	-0.057	0.248	0.427
	<i>p</i>	0.838	0.559	0.837	0.328	0.352	0.561	0.711	0.118	0.007
refractive error (spherical equivalent)	<i>r</i>	-0.435	-0.247	-0.292	-0.205	0.019	-0.213	0.166	0.182	0.154
	<i>p</i>	0.001	0.009	0.129	0.051	0.458	0.014	0.150	0.021	0.455
best-corrected visual acuity	<i>r</i>	-0.383	-0.174	-0.251	-0.209	-0.095	-0.116	0.015	-0.009	0.057
	<i>p</i>	0.006	0.223	0.075	0.140	0.508	0.420	0.919	0.950	0.708
visual evoked potential asymmetry	<i>r</i>	-0.144	-0.211	0.008	-0.375	0.102	-0.219	-0.203	0.022	0.010
	<i>p</i>	0.503	0.323	0.970	0.071	0.636	0.303	0.340	0.924	0.966

Table 3-7: Linear regression analysis between optic nerve head (ONH) and peripapillary retinal nerve fibre layer (ppRNFL) parameters and central foveal measures and clinical measures. H:V disc ratio = horizontal:vertical diameter disc ratio.

Although previous studies have described the appearance of the optic nerve in albinism qualitatively, no previous investigation has quantified the degree and nature of these abnormalities.^{141, 167} In this study we have used high resolution SD-OCT to systematically characterize three-dimensional ONH topography in albinism for the first time. Similar to the fovea, patients with albinism show a spectrum of abnormalities that can vary from being minimal to gross.

The degree of abnormality observed in albinism patients is relatively consistent between the right and left eyes. This, alongside the repeatability measures we undertook, indicates that we were able to successfully overcome the problem of motion artefact caused by nystagmus in the analysis of optic nerve OCT images.

Optic nerve head morphology

Our results reveal that albinism is associated a small or absent (39.4% of patients) optic cup. Alongside this, there also appears to be an abnormal elevation of the nasal aspect of the optic rim that led to large rim volumes in our albinism cohort. This confirms the observation by Chong et al. that the ONH in albinism “appeared very prominently elevated”. Their observation was based on the study of the optic nerve head of six patients with albinism. However, as the focus of their investigation was the foveal morphology in albinism, they did not report detailed findings.¹⁴¹

Our results reveal that patients with albinism possess normal sized optic discs. This finding is in contrast with Spedick and Beauchamp’s finding of hypoplastic optic nerves seen on fundus photographs. It should be noted, however, that their study was based on subjective analysis of only 12 patients.¹⁶⁷

The shape and size of the optic nerve head can be explained by its embryological development. In the first 10 weeks of foetal development, there is a rapid rise in the number of retinal axons. Rakic and Riley reported that there were almost 2.85million

retinal axons present in the foetal rhesus monkey at this stage of development, which is over twice the number found in adults.³⁷⁹ This initial number of axons is believed to be the main determining factor in of the final size of the optic disc size. At this stage in development, the sclera is still flexible, as the extracellular matrix, which makes it rigid, has not been laid down yet.¹²⁸

Looking at our results, it appears that this first stage of development occurs normally in patients with albinism as we found no difference in the size of the optic disc between the albinism and control patients.

A striking observation we noted was that the ppRNFL in the outer annulus (i.e. 2.4–3.2mm diameter) is consistently and significantly thinner in the albinism group compared to controls, especially in temporal segments. The ppRNFL thickness provides an estimate of the number of nerve fibres entering the optic nerve. This indicates that the smaller cup size in albinism is not due to a failure of axonal apoptosis as axon numbers are in fact reduced at the optic nerve head. These findings are supported by previous studies, which reported a reduced numbers of ganglion cells and photoreceptors using histological methods and new adaptive optics imaging technology.^{132, 144} It is also corroborated by magnetic resonance imaging studies, which visualised smaller sized postorbital optic nerves in albinism.^{168, 380}

Rim size is also considered to be a measure of the number of axons entering the optic nerve,^{381, 382} and in contrast to the findings of thinner outer ppRNFL in albinism we observed a significantly larger rim volume in the albinism group compared to controls (162.1% larger, $p=3.23 \times 10^{-8}$).

Histological studies report that the pre-laminar aspect of the optic nerve head comprises mainly retinal ganglion cell axons and glial cells.³⁸³ After the first 10 weeks of foetal development, there is substantial cell death of retinal ganglion cells and their axons. Indirect evidence for this is provided by empty pores found in the lamina cribrosa. It is believed that in early stages of retinal development, all these pores are occupied by axons and the meshwork of lamina cribrosa formed around these axons. However, some of these axons fail to make appropriate synapses in the brain and subsequently undergo apoptosis leaving behind the empty pores seen at the lamina

cribrosa. It is thought that the optic cup and rim size is determined by the degree of regression in the number of axons and glial cells.^{128, 384} Consequently, the smaller optic cups and larger rim volumes observed could be an indication that this regression process is halted in albinism. Since there is a large body of evidence that ganglion cell numbers are reduced in albinism^{132, 385}, one simple explanation for the larger volumes in albinism could be that excess glial tissue has not been removed through the normal process of regression in embryological development.

The morphology of this excess glial tissue, which appears as an elevation that has a hyperreflective vitreal margin and a hyporefective band extending past the RPE in the anteroposterior axis, bears a striking resemblance to the OCT findings seen in the optic nerves with persistent hyaloid vasculature.^{386, 387}

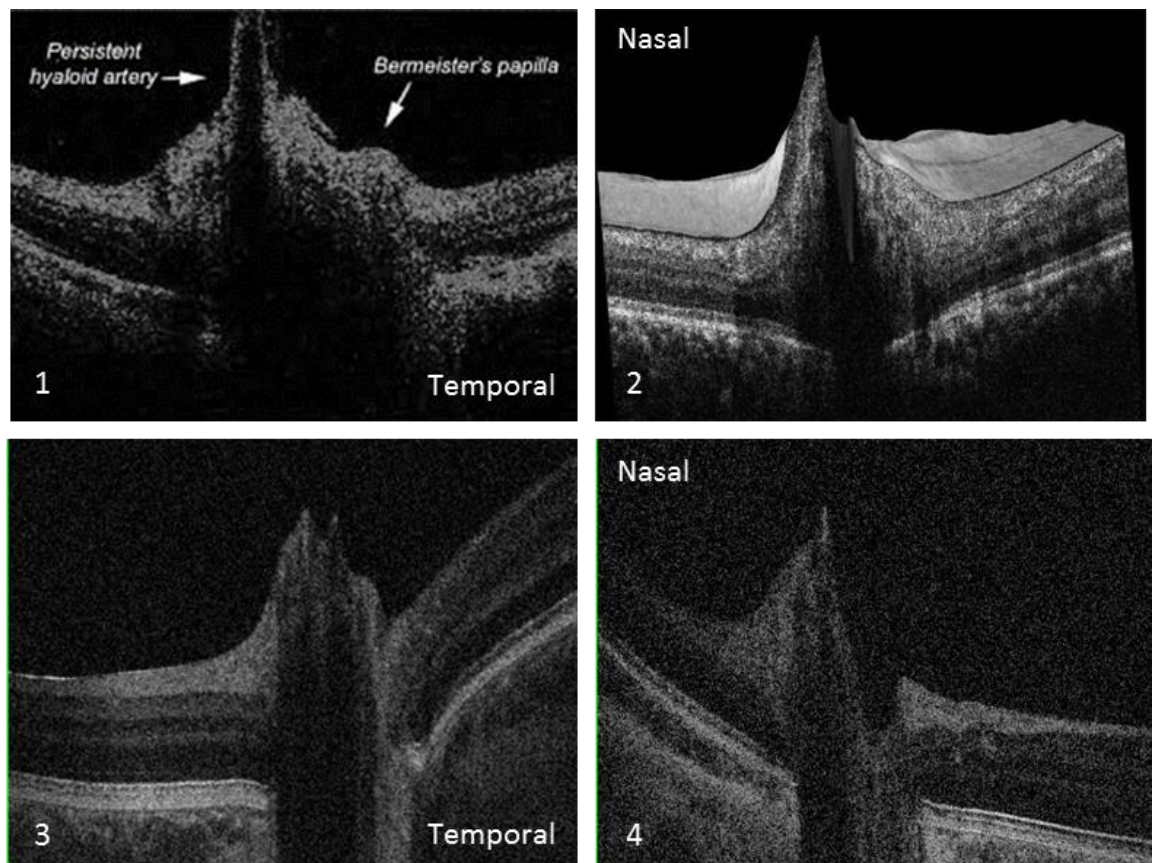


Figure 3-13: Comparison of left eye optic nerve head OCT scans from patients with persistent hyaloid artery (1 and 2) and our albinism cohort (3 and 4). All four show elevation of the nasal aspect of the optic rim with small or absent optic cups. 1 is adapted from Azrak et al. and retains labels from the authors indicating the placement of the persistent hyaloid artery and Bergmeister's papilla.³⁸⁷ 2 is adapted from Sheth et al.³⁸⁶ The differences in the quality of scans from the three studies are due to the different OCT devices used.

The hyaloid artery arises from the ophthalmic artery, which itself is a branch of the internal carotid artery. It is present within the optic stalk and extends from the optic disc to form a transient network of capillaries called the vasa hyaloidea propria that supply the primary vitreous humour and tunica vasculosa lentis that wrap around the developing lens.³⁸⁸⁻³⁹⁰ The hyaloid vascular system begins to form in the fourth to fifth week of gestation and becomes most prominent around ninth week of gestation. It starts regressing by the 12th gestational weeks during the formation of the avascular secondary vitreous that develops between the retina and the primary vitreous, and reaches completion in the third trimester.^{389, 391, 392} As the secondary vitreous develops, the posterior-most aspects of the vasa hyaloidea propria become the first elements of the hyaloid vasculature to undergo involution. Expansion of the secondary vitreous leads to obliteration of the more anteriorly placed tunica vasculosa lentis. The final step is regression of the main hyaloid trunk, which leaves behind a clear canal through the vitreous known as the hyaloid or Cloquet's canal.³⁸⁶ This regression coincides with development of the retinal vasculature.³⁹³

Occasionally, the hyaloid artery may not fully regress, leading to a condition known as persistent hyperplastic primary vitreous or persistent foetal vasculature (PFV).³⁹⁴ The disorder is one of the most common congenital malformation syndromes of the eye and is seen in 3% of full term infants and 95% of premature infants.^{395, 396} PFV may be isolated or seen in conjunction with other ocular abnormalities including neurofibromatosis, acute angle closure glaucoma, myopia, retinal tumours, retinopathy of prematurity, retinoschisis, morning glory disc syndrome and macular hypoplasia.^{395, 397} Many of these ocular syndromes have a genetic basis indicating that a PFV can be caused by a number of genetic mutations and it can be inherited as autosomal dominant or recessive trait.³⁹⁷

The degree of abnormality associated with PFV can vary from mild to severe. Mild cases may include persistence of the anterior vasculature as Mittendorf's dot that is usually located on the posterior lens capsule, infero-nasal to the posterior pole of the lens.

The posterior portion may persist in the form of glial tissue known as Bergmeister's papillae.³⁹⁸ More severe presentations may lead to tractional retinal detachments, cataracts, elevated intraocular pressure or rarely vitreous haemorrhage.³⁸⁷

The exact mechanism of hyaloid artery regression remains unknown, but various mechanisms have been put forward as playing a role in this process. These include programmed degradation of the hyaloid vascular system via macrophages, apoptosis factors, and anti-angiogenic molecules in the vitreous.³⁹²

In albinism, abnormalities in the retinal vasculature that lead to deficiency in the formation of the foveal avascular zone are already known.¹²⁹ Keeping this in mind, it appears entirely reasonable to infer that the molecular signalling which leads to regression of the hyaline artery under normal circumstances is also deficient in albinism. This leads to a mild form of PFV and remnants of glial tissue at the optic nerve head, which appears to be elevated on OCT imaging.

Optic Disc Torsion and Tilt

Nystagmus can pose difficulties in examination of the fundus clinically. Using SD-OCT and fundus photography, we only observed clear patterns of either TDS or myopic tilted discs in albinism in a small number of individuals. There were, however, features we observed which might suggest that optic discs in albinism could be on the spectrum of tilted disc abnormalities. For example, horizontal elongation of discs was commonly observed in albinism, a pattern consistent with TDS. Also similar to myopic tilted discs, a temporal crescent of sclera was seen in 15% of patients with albinism, although there was no significant myopia in these individuals. Several disc parameters such as cup and disc area were also negatively correlated to refractive error (see discussion below).

However, several observations we made challenge this view. Analysis of horizontal disc tilt by measuring RPE edges in a cross-sectional SD-OCT B-scan images suggests that median approach angles for the optic nerves are not extreme in albinism (median tilt = -1.04° in albinism compared to -0.46° in controls). Also thinning of the ppRNFL was

greater in temporal quadrant, which does not match the pattern of nasal and superior quadrant thinning observed in TDS. Finally, hyperopia was more common in our study sample compared to myopia (hyperopia: 22.2% $\geq 3D$ and 6.2% $\geq 5D$ spherical equivalent; myopia: 7.4% $\leq 3D$ and 2.5% $\leq 5D$ spherical equivalent).

Relationship between disc/ppRNFL abnormalities and foveal abnormalities

We observed a strong positive correlation between outer ppRNFL and ganglion cell layer (GCL) thickness at the central fovea ($p=0.007$). In the normal retina, the GCL is very thin due to centrifugal migration of inner retinal layers during development. One might expect an inverse correlation between outer ppRNFL and GCL thickness, so that significant foveal hypoplasia (indicated by thickened GCL) is associated with ppRNFL thinning. However, as the centrifugal migration fails to occur in albinism, the thickness of GCL at the fovea likely indicates the overall number of ganglion cell population. It is the axons of these ganglion cells that give rise to the ppRNFL therefore a positive correlation is not surprising.

Relationship between disc/ppRNFL abnormalities and clinical measures

Several ONH abnormalities in albinism were negatively correlated with refractive errors such as disc and cup areas. These could be due to the ONH changing in scale with eye elongation. For example, myopia (negative refractive error) is associated with longer eyes (i.e. increased axial length of the eye) which could lead to larger disc and cup areas. One of the most consistent features of the ONH in albinism was horizontal elongation of the disc (e.g. see figure 5E compared to 5J). Interestingly, however, H/V disc ratio was not significantly correlated with refractive error, which suggests that this feature is not related to changes in the overall shape of the eye. It is well known that the zone of transition of fibres projecting ipsilaterally and contralaterally is temporally displaced away from the midline of the retina in albinism.²⁶⁷ One possibility is that reorganization of retinal nerve fibres approaching the ONH in albinism lead to abnormally shaped discs. Differences we observed in the reorganization of the inner

ppRNFL in albinism (i.e. thicker nasally and thinner temporally) also support this supposition.

Summary

Our study provides novel findings about the topography of the ONH in albinism and explains its appearance in the light of normal development patterns and their disturbance in albinism. Although treatment options for this disorder are currently limited, progress is underway to formulate suitable pharmacological and gene therapies to improve visual function in these patients.^{399, 400} Our study provides a reference point for clinicians to assess the structural abnormalities in the optic nerves of patients with albinism using in-vivo OCT imaging.

3.4 OPTIC CHIASM

3.4.1 BACKGROUND

Albinism is associated with an abnormal chiasmal decussation of optic nerve fibres originating in the temporal hemi-retina.²⁰¹ Previous MRI studies looking at the configuration of the post-orbital optic nerve and chiasm have reported inconsistent findings. Brodsky et al. reported them both to be of normal size and configuration.²⁰⁴ However, a larger study by Schmitz et al., 10 years later, found a reduction in optic nerve diameter.¹⁶⁸ We aim to clarify this discrepancy in previous literature by quantifying the size of the optic nerve, tract and chiasm in patients with albinism and comparing to healthy controls. In addition, we employ DTI tractography to study the chiasmal misrouting seen in albinism for the first time.

We also attempt to investigate, for the first time, whether the chiasmal anomalies seen in albinism are related to retinal and optic nerve abnormalities outlined in the previous sections. This relationship has been poorly understood due to a lack of suitable animal models as the commonly used models such as mice and zebrafish are afoveate. Therefore, our approach that employs *in-vivo* imaging approach is perhaps the most suitable method to answer this query.

3.4.2 SUMMARY OF AIMS

1. Quantify the size of the intracranial optic nerve, chiasm and tract in patients with albinism using MRI and compare it to healthy controls.
2. Investigate the relationship of the intracranial optic nerves, optic chiasm and tracts with the fovea and the optic nerve head.
3. Assess whether diffusion tensor tractography can be used to explore misrouting seen in albinism.

3.4.3 FINDINGS

3D-MPRAGE and DTI scans were obtained from 23 patients with albinism (17 male, 6 female, mean age 35.0 ± 13.6 years) and 20 healthy volunteers (14 male, 6 female, mean age 31.9 ± 10.6 years). Shapiro-Wilk analysis showed that the data was not normally distributed and therefore non-parametric testing was used for statistical analyses.

H₀ 3.1: The optic nerve, chiasm and tract sizes are smaller in albinism compared to healthy controls.

Table 3-6 summarises the optic nerve, tract and chiasm dimensions in both albinism and control groups. Comparison of the groups showed that the nerve ($Z=-3.26$, $p=0.001$) and tract ($Z=-2.53$, $p=0.010$) width measurements were smaller in the albinism group. The same was true for the nerve area ($Z=-2.23$, $p=0.026$). However, the difference in tract area did not reach statistical significance. ($Z=-1.631$, $p=0.103$)

The width ($Z=-4.91$, $p=1.23 \times 10^{-4}$), area ($Z=-2.76$, $p=0.006$) and volume ($Z=-2.79$, $p=0.005$) of the chiasm were significantly larger in the control group.

		Optic nerve		Optic tract		Optic chiasm		
		<i>Width (mm)</i>	<i>Area (mm²)</i>	<i>Width (mm)</i>	<i>Area (mm²)</i>	<i>Width (mm)</i>	<i>Area (mm²)</i>	<i>Volume (mm³)</i>
Albinism	<i>Mean</i>	6.22	16.0	5.54	16.5	11.7	30.7	261
	<i>St. Dev</i>	0.782	2.87	0.993	4.61	1.30	4.97	64.4
Control	<i>Mean</i>	6.86	17.5	6.28	18.3	14.4	36.3	319
	<i>St. Dev</i>	0.781	2.81	1.34	5.21	1.14	5.59	66.33
Mann-Whitney U	<i>p</i>	0.001	0.026	0.010	0.103	<0.001	0.006	0.005
	<i>Z</i>	-3.26	-2.23	-2.53	-1.631	-4.91	-2.76	-2.79

Table 3-8: Comparison of optic nerve and tract width and areas and optic chiasm width, area and volume between the albinism and control groups. Significant p-values are in bold.

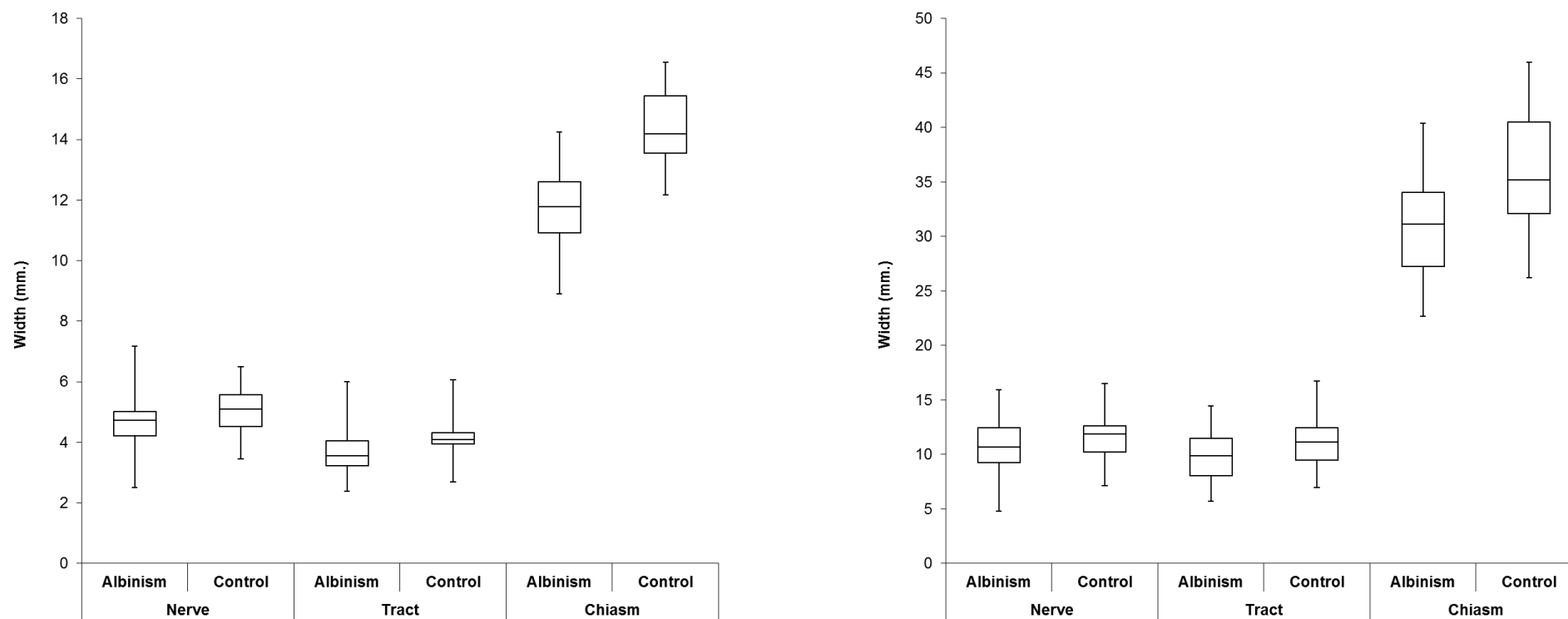


Figure 3-14 : Comparison of the optic nerve, tract and chiasm width (left) and area (right) differences between albinism and control groups. Significant differences are highlighted in Table 3-8

Diffusion Tractography

H₀ 3.2: DTI can show increased decussation in patients with albinism.

Figure 3-15 summarizes the mean number of streamlines connecting the nerve and tract regions of interest (ROIs) of both albinism and control groups. Mann-Whitney U comparison showed no significant difference ($Z=-1.01$, $p=0.433$) in the total number of streamlines generated between the two groups.

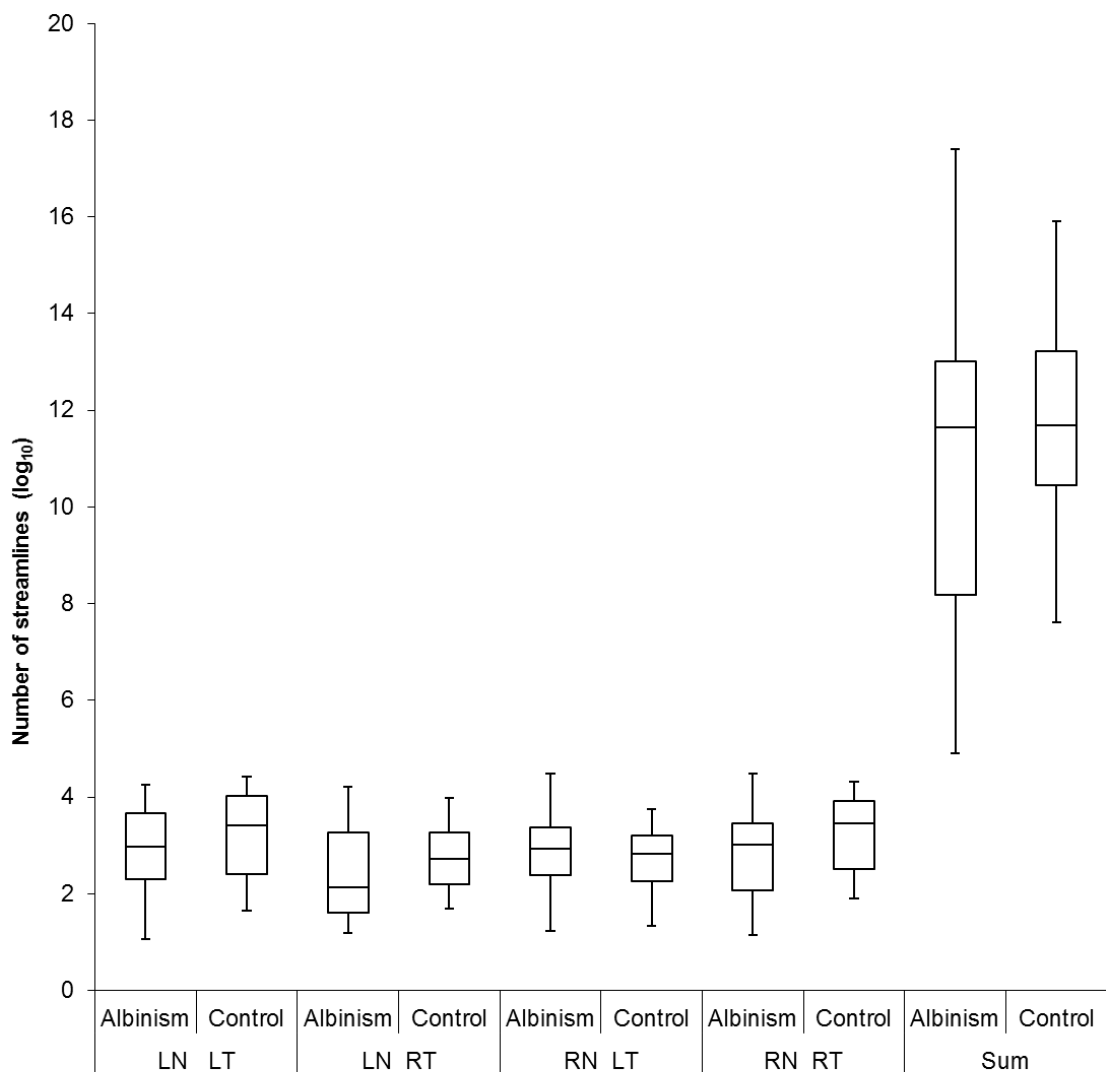


Figure 3-15: Comparison of total number of streamline (log₁₀) between optic nerve and optic tract ROIs. The box represents the upper, median and lower quartiles while the whiskers represent the range. LN= left nerve, LT = left tract, RN = right nerve, RT = right tract

Figure 3-16 shows that patients with albinism had a higher percentage of decussating streamlines at the chiasm compared to the controls ($Z=-2.24$, $p=0.025$).

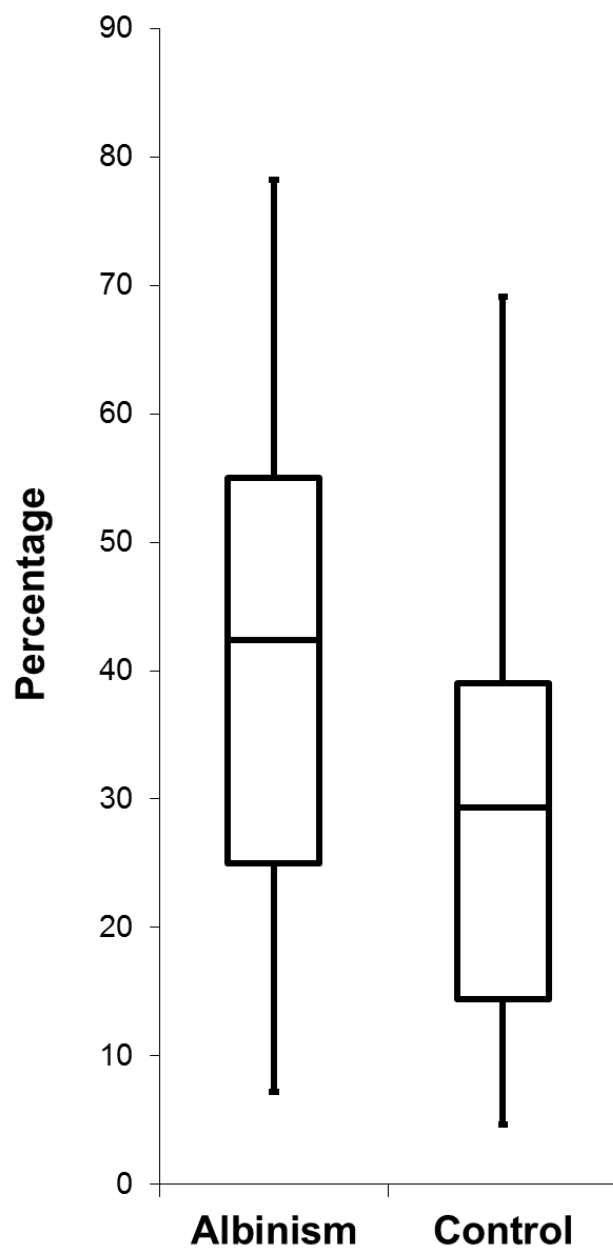


Figure 3-16 : Comparison of the streamline decussation index (percentage of streamlines connecting with the contralateral hemisphere) between albinism (n=23) and control (n=20) groups.

H₀ 3.3: Chiasmal decussation measured using VEP and DTI are related.

Using Spearman's Rank Correlation Co-efficient, we find that within the albinism group, the streamline decussation index (percentage of total streamlines connecting with contralateral hemisphere) correlated significantly with inter-hemispheric asymmetry measured using VEP ($r=0.484$, $p=0.042$). (Figure 3-17)

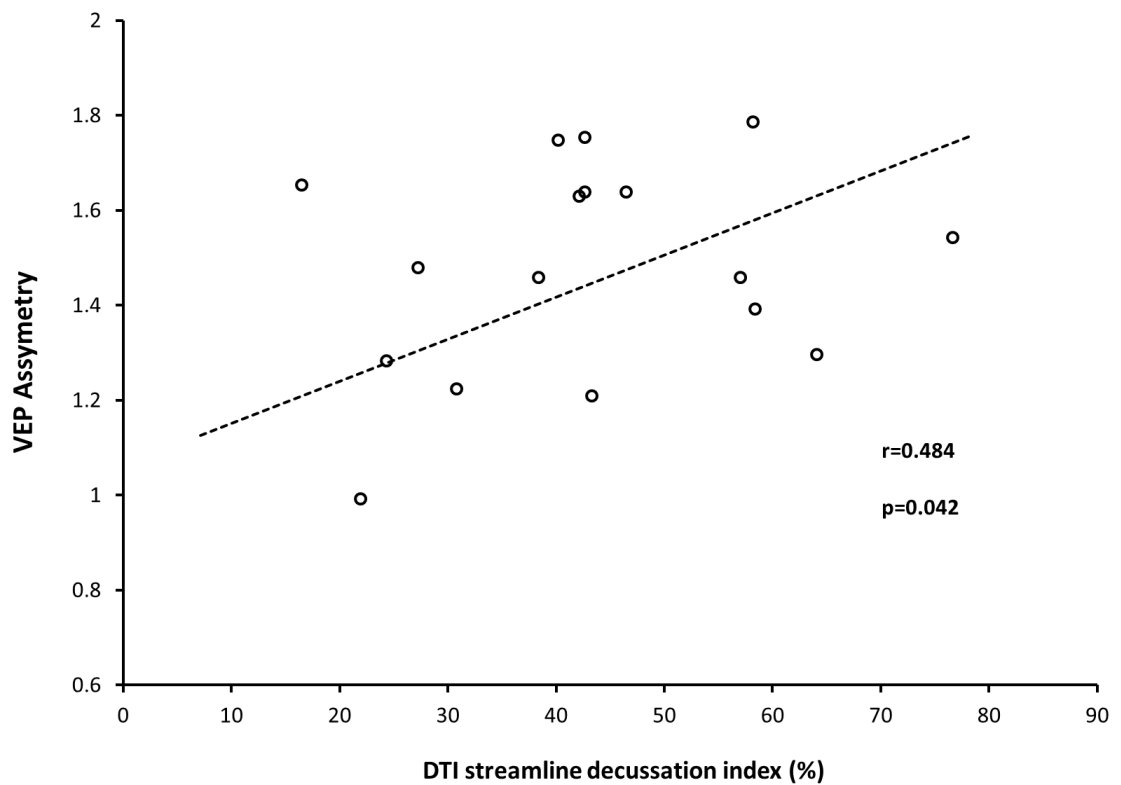


Figure 3-17 Comparison of cross-hemispheric connectivity at the chiasm measured using DTI and VEP asymmetry seen in patients with albinism.

H₀ 3.4: There connectivity at chiasm and foveal abnormalities are related

Table 3-9 shows that we did not find any significant relationship of the optic nerve, chiasm or tract size measured using MRI with foveal layer size or foveal development index. However, comparison of the DTI data with OCT parameters showed a strong relationship between the degree of foveal development and the total number of streamlines. The total number of streamlines were found to be related to both photoreceptor ($r=0.506$, $p=0.020$, $p'=0.020$) and processing layer thicknesses ($r=-0.676$, $p=0.001$, $p'=0.003$) and consequently with the foveal development index. ($r=0.662$, $p=0.001$, $p'=0.003$). Figure 3-18 shows the comparison between the foveal development index and total number of streamlines.

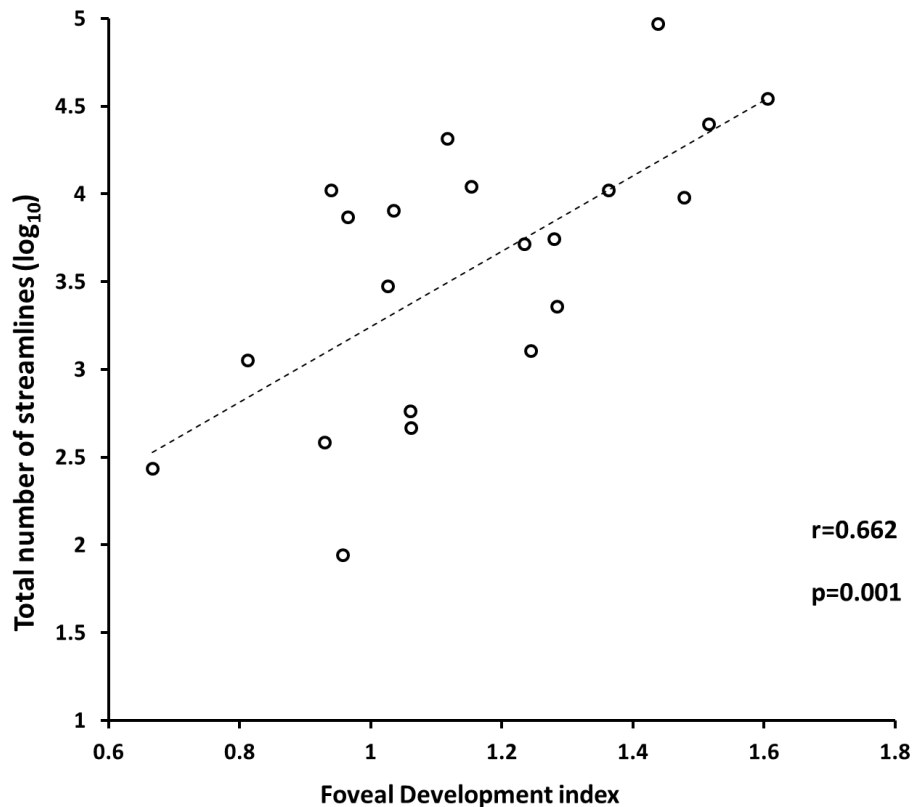


Figure 3-18: Comparison of total connectivity at the chiasm estimated using DTI with foveal development index in albinism.

The relationship between streamline decussation and foveal development indices, however did not reach statistical significance. ($r=0.411$, $p=0.064$, $p'=0.192$)

		<i>Area</i>			<i>Tractography</i>	
		<i>Nerve</i>	<i>Tract</i>	<i>Chiasm</i>	<i>Total number of streamlines</i>	<i>Streamline decussation index</i>
Photoreceptor layers	<i>r</i>	0.045	-0.016	-0.047	0.506	0.390
	<i>p</i>	0.767	0.919	0.759	0.019	0.082
	<i>p'</i>	1.00	1.00	1.00	0.019	0.192
Processing Layers	<i>r</i>	-0.0067	-0.029	0.006	-0.676	0.390
	<i>p</i>	0.661	0.849	0.970	0.001	0.082
	<i>p'</i>	1.00	1.00	1.00	0.003	0.192
Foveal Development Index	<i>r</i>	-0.303	0.255	0.367	0.662	0.411
	<i>p</i>	0.160	0.241	0.085	0.001	0.064
	<i>p'</i>	0.320	0.320	0.255	0.003	0.192

Table 3-9: Comparison of foveal development with optic nerve, chiasm and tract areas measured via MRI, DTI measures of connectivity at the chiasm (total number of streamlines) and chiasm crossing (streamline decussation index). Holm-Bonferroni corrected p' values are also included.

H₀ 3.5: Connectivity at chiasm and optic nerve head abnormalities are related.

To test the relationship, the optic nerve head and ppRNFL parameters from each eye were used separately to compare with the ipsilateral optic nerve and contralateral optic tract measurements obtained from the T1 MRI volumes. This approach was chosen due to the abnormal decussation seen in albinism which means that the optic nerve axons from the entire retina cross-over at the chiasm and make up the

contralateral optic tract. For comparison with the chiasm, the average measurements from both eyes were used. Table 3-10 shows significant positive correlations between temporal ppRNFL thickness measured using OCT and both optic nerve area ($r=0.608$, $p=5.61 \times 10^{-5}$, $p'=2.81 \times 10^{-4}$) and optic tract area ($r=0.483$, $p=0.001$, $p'=0.004$). These comparisons are also illustrated in figure 3-18. There was no significant correlation of the nerve or tract area with any other ppRNFL sectors.

The optic nerve area measured using MRI was also related to optic cup ($r=0.367$, $p=0.018$, $p'=0.090$) and rim ($r=-0.325$, $p=0.038$, $p'=0.190$) areas measured using OCT, however these comparisons were not significant following Holm-Bonferroni correction. The tract and chiasm areas were not related to the optic nerve head measurements.

We did not observe any significant relationship between the total number of streamlines or the degree of decussation and ppRNFL or optic nerve head measurements.

		<i>ppRNFL</i>				<i>Optic nerve head</i>		
		<i>Superior</i>	<i>Nasal</i>	<i>Inferior</i>	<i>Temporal</i>	<i>Disc area</i>	<i>Cup area</i>	<i>Rim area</i>
<i>Ipsilateral optic nerve area</i>	<i>r</i>	0.245	-0.036	0.270	0.608	0.014	0.367	-0.325
	<i>p</i>	0.127	0.825	0.092	5.61x10⁻⁵	0.931	0.018	0.038
	<i>p'</i>	0.635	1.00	0.460	2.81x10⁻⁴	1.00	0.090	0.190
<i>Contralateral optic tract area</i>	<i>R</i>	0.363	-0.042	0.442	0.483	0.062	-0.194	0.156
	<i>p</i>	0.127	0.825	0.092	0.001	0.699	0.225	0.331
	<i>p'</i>	0.635	1.00	0.460	0.004	1.00	0.450	0.993
<i>Optic chiasm area</i>	<i>r</i>	-0.057	-0.211	0.109	0.096	-0.002	-0.181	0.107
	<i>p</i>	0.795	0.334	0.620	0.662	0.992	0.257	0.505
	<i>p'</i>	1.00	1.00	1.00	1.00	1.00	0.450	1.00
<i>Total number of streamlines</i>	<i>r</i>	0.133	0.142	0.133	0.094	-0.122	0.422	-0.444
	<i>p</i>	0.556	0.529	0.556	0.676	0.641	0.091	0.074
	<i>p'</i>	1.00	1.00	1.00	1.00	1.00	0.364	0.296
<i>Streamline decussation index</i>	<i>r</i>	0.205	-0.161	-0.082	0.202	-0.387	-0.367	-0.013
	<i>p</i>	0.360	0.474	0.717	0.367	0.125	0.147	0.961
	<i>p'</i>	1.00	1.0	1.00	1.00	0.625	0.441	1.00

Table 3-10: Comparison of MRI measurements of optic nerve, tract and chiasm areas, DTI streamline count, and streamline decussation index with ppRNFL sector thickness and optic disc, cup and rim areas derived from OCT imaging. Significant values are in bold. Holm-Bonferroni corrected *p'* values are also included.

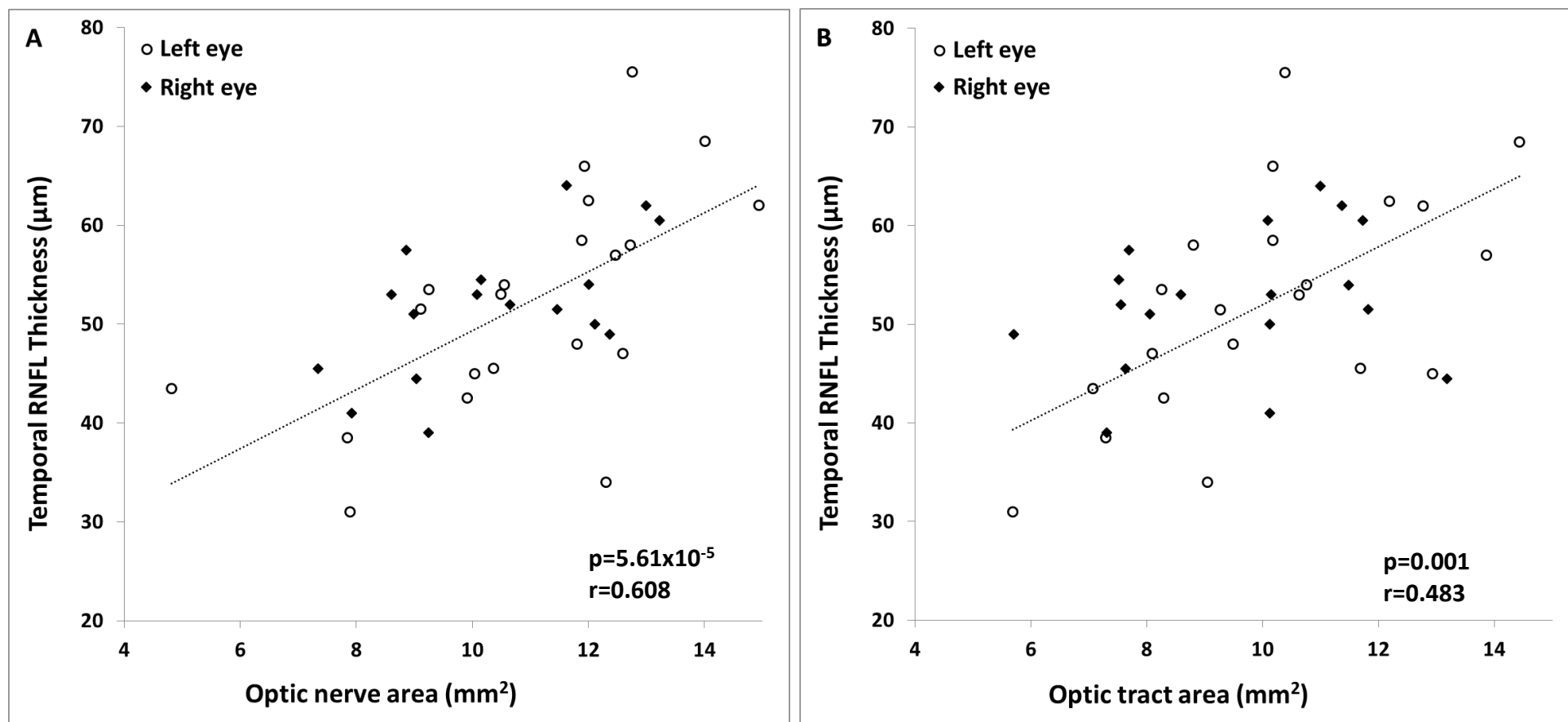


Figure 3-19: Comparison of temporal ppRNFL thickness measured using OCT with the ipsilateral optic nerve (A) and contralateral optic tract (B) area measured using MRI

H₀ 3.6: Chiasmal size impacts visual acuity

Our results show that best-corrected visual acuity was not related to optic nerve ($r=0.205$, $p=0.360$), tract ($r=-0.016$, $p=0.919$) or chiasm ($r=-0.045$, $p=0.848$) areas. The relationship between BCVA and streamline decussation index did not reach statistical significance. ($p=0.051$, $r=0.432$). The total number of streamlines were not related to BCVA.

		<i>Area</i>			<i>Tractography</i>	
		<i>Nerve</i>	<i>Tract</i>	<i>Chiasm</i>	<i>Total number of streamlines</i>	<i>Streamline decussation index</i>
BCVA	<i>r</i>	0.205	-0.016	-0.045	0.099	0.432
	<i>p</i>	0.360	0.919	0.848	0.673	0.051

Table 3-11: Comparison of best-corrected visual acuity (BCVA) with optic nerve, tract and chiasm areas measured using MRI and diffusion tractography data.

This study represents the only attempt thus far to investigate the relationship between ocular and chiasmal abnormalities associated with human albinism. To achieve this, the visual pathway was imaged using OCT, structural MRI and DTI. In addition, the anatomical data was compared to clinical measurements such as visual acuity and VEP asymmetry.

We show for the first time that DTI tractography can be used to demonstrate chiasmal misrouting in albinism. We found that the connectivity to the contralateral hemisphere (i.e. the streamline decussation index) was significantly higher in patients with albinism compared to healthy controls. These findings are validated by the positive correlation between the chiasmal streamline decussation index and VEP asymmetry, which is a functional measure of chiasmal misrouting.

Our results agreed with the findings of previous studies regarding smaller optic nerve, tract, and chiasm sizes in albinism.^{168, 215, 239} It had been hypothesized by the authors of these earlier studies that one of the reason for these findings could be the underdevelopment of the fovea seen in albinism.^{215, 239} Schmitz et al also reported that the patients with albinism show an increased angle between the two optic nerves as they approach the chiasm and the two optic tracts as they leave the chiasm. We did not measure these angles as the chiasm lies in an oblique plane with the anterior edge of the chiasm placed more inferiorly than the posterior edge. The degree of tilt can vary greatly between subjects and hence angle measurements can prove to be unreliable.

Although we did not see any relationship between foveal development and the physical size of the chiasm, our DTI data shows significant relationship between foveal development and strength of connectivity at the chiasm.

The size of the chiasm and streamline count should both reflect the number of axons, therefore, the fact that only one of these relate to foveal development appears puzzling. An explanation for this apparent contradiction may lie in a previous study looking at the optic nerves of albino ferrets. The authors reported that a delay in the

axonal outgrowth from the retina means that there is a disruption in the distribution of large and small diameter axons within the optic nerve. The myelin sheath of the optic nerve axons was also found to be abnormally thickened⁴⁰¹ Consequently a gross measurement of the optic nerve and chiasm on MRI might not accurately reflect the number of axons within it.

We found that the optic nerve size measured using MRI is correlated with the temporal quadrant of the ppRNFL thickness in the ipsilateral eye. Using *ex-vivo* axon tracing studies and through mapping of the visual field to the optic nerve in glaucoma patients, previous studies have indicated that axons from the foveal retinal ganglion cells aggregate in the temporal region of the optic nerve head.^{342, 402, 403} Therefore, any variation in the numbers of central ganglion cells would influence the size of the temporal ppRNFL and hence the optic nerve size. Previous animal studies have shown a reduced number of central retinal ganglion cells in albino animals.^{205, 206, 404-406}

The degree of chiasmal decussation estimated using DTI tractography did not relate to any foveal or optic nerve head abnormalities. Foveal hypoplasia and misrouting of the optic nerve are two cardinal features of albinism. Aberrations in the melanin synthesis pathway are believed to be the cause of both these abnormalities.⁴⁰⁷ However, our findings suggest that there is no direct relationship between these two features. These findings agree with previous suggestion by Neveu et al. who compared the retinal findings in patients with albinism and aniridia. Both these conditions are characterized by foveal hypoplasia but patients with aniridia have normal retino-fugal projections. The authors therefore concluded that optic chiasm formation is independent from foveal development.⁴⁰⁸

It is more likely that the misrouting in albinism is a function of delayed cell mitosis in albinism, which is a process regulated by L-dopa, a precursor of melanin.⁹⁴ The factor determining whether an axon will decussate is thought to be dependent on the timing at which it reaches the chiasm during the development of the optic nerve. In animal models it has been shown that axons originating in the temporal retina, which develop earlier than those originating in the nasal retina, remain ipsilateral as they grow backwards past the chiasm, while the later developing retinally derived axons

decussate through the chiasm.⁴⁰⁹ It is proposed that in albinism, a lack of melanin in the retinal pigment epithelium leads to a delay in the development of the temporal retina and hence a delay in these axons reaching the chiasm leading to increased decussation.^{94, 407, 410}

Finally, it is important to point out the inherent limitations in our methodology. While diffusion tractography is currently the only tool that allows *in-vivo* quantification of white matter connectivity, many factors including anatomical characteristics of the structure being studied, image acquisition parameters and choice of tract reconstruction algorithm can significantly alter the results. This is demonstrated by the large spread of streamline data in our study.

The anterior optic pathways are particularly challenging to study with DTI due to the complex convergence, divergence and crossing of axons as they pass through the chiasm. Within each voxel, there may be multiple fibre orientations of axons making it difficult to distinguish between axons that are kissing, crossing, converging or diverging as they all capable of generating a similar diffusion signal. This means the tractography algorithm may jump between two fibre pathways. There is also potential for partial volume effects of CSF contamination affecting the tractography algorithm in voxels along the surface of the cisternal segments, and the effect of susceptibility distortions due to the adjacent skull base and paranasal sinuses.

Prior to commencing the study, we undertook optimisation of the DTI protocol by selecting the maximal resolution achievable (1.8mm isotropic voxel size) while maintaining an acceptable signal to noise ratio and appropriate scan duration. We remain cautious regarding the interpretation of absolute streamline counts in our data but feel that expressing the streamline decussation as a percentage of the total streamline count provides a plausible measure of fibre crossing at the chiasm given the positive correlation that we found with VEP asymmetry.

In addition to the limitations of the DTI methodology, the VEP measurements are also prone to inaccuracies due to inter-individual differences in brain shape, electrical impedance of the scalp and visual acuity of the patients. We attempted to increase our signal to noise ratio by repeating the measurements twice and averaging the results.

The Apkarian method that we utilised to measure VEP response lateralisation is commonly used. However, when it's accuracy was evaluated by Soong et al. they found that the method generated 71% sensitivity and 86% specificity. The authors propose an alternative method for evaluating response lateralisation which involves looking at the Pearson's correlation between the VEP responses generated with monocular stimulation of left and right eyes. Here a correlation of +1.0 shows a completely symmetrical response while a Pearson's r value of -1.0 indicates a completely asymmetrical response. The authors found that this methodology demonstrated 86% sensitivity and 83% specificity. Therefore, using this methodology may improve the correlation we see between VEP and DTI asymmetry in albinism.⁴¹¹

In conclusion, our study provides novel insights in to the relationship between retinal and chiasmal abnormalities in albinism. In addition, we demonstrate the ability of diffusion tractography to exhibit abnormal chiasmal crossing seen in albinism. Study of the connectome is currently a hot topic of research and there is a great focus in improving methodology in this area. Hence, in the future, DTI is likely to prove to be a useful tool in the assessment of patients with albinism.

3.5 CORTEX

3.5.1 BACKGROUND

Reports on the visual cortex abnormalities seen in albinism have been inconsistent. Using voxel based morphometry (VBM), Von dem Hagen et al. found that patients with albinism show a reduction in cortical volume at the occipital pole,²³⁹ while using surface based analysis (SBA), a recent study by Bridge et al. showed reduced increased occipital pole volume and thickness. Bridge et al. suggested that the difference in results between the two previous studies were due to the two different analysis techniques being employed.²⁴³ We attempt to resolve this conflict in previous literature by assessing the cortical size in patients with albinism using surface based analysis.

The reason behind these cortical changes in albinism is also unclear. Bridge et al. suggested that these changes are due to a lack of post-natal neuronal pruning as a result of under-development of the fovea seen in albinism and a consequent absence of high-resolution input into V1.²⁴³ By comparing cortical structure assessed using MRI with foveal, optic nerve and chiasmal abnormalities, we investigate for the first time whether the cortical abnormalities seen in albinism are related to anomalies in the afferent visual pathway.

3.5.2 SUMMARY OF AIMS

- Clarify the previous conflict in literature regarding the nature of cortical abnormality in albinism through high-resolution MR imaging and latest structural analysis methodology in a sufficiently large group of patients.
- Investigate the relationship of any cortical abnormalities with those seen within the fovea, optic nerve head and chiasm.

3.5.3 FINDINGS

T1 weighted 3D-MPRAGE scans were obtained from 23 patients with albinism (17 male, 6 female, mean age 35.0 ± 13.6 years) and 20 healthy volunteers (14 male, 6 female, mean age 31.9 ± 10.6 years). Automatic parcellation of the cortex was performed based on the Destrieux atlas in freesurfer.³⁴⁷ Measurements for the occipital pole region were used for comparison with the foveal and optic nerve head OCT parameters. Shapiro-Wilk analysis showed that the data was not normally distributed and therefore non-parametric testing was used to for statistical analyses.

H₀ 4.1: Cortical thickness and volume at the occipital pole in is higher in patients with albinism compared to healthy controls.

Our results showed that on average, cortical thickness at the occipital pole was 6.88% higher in our albinism group compared to healthy controls. ($Z=-4.10$, $p=0.002$) The cortical volume at the occipital pole was 16.2% higher ($Z=-2.42$, $p=0.016$) in patients with albinism. (Figure 3-20)

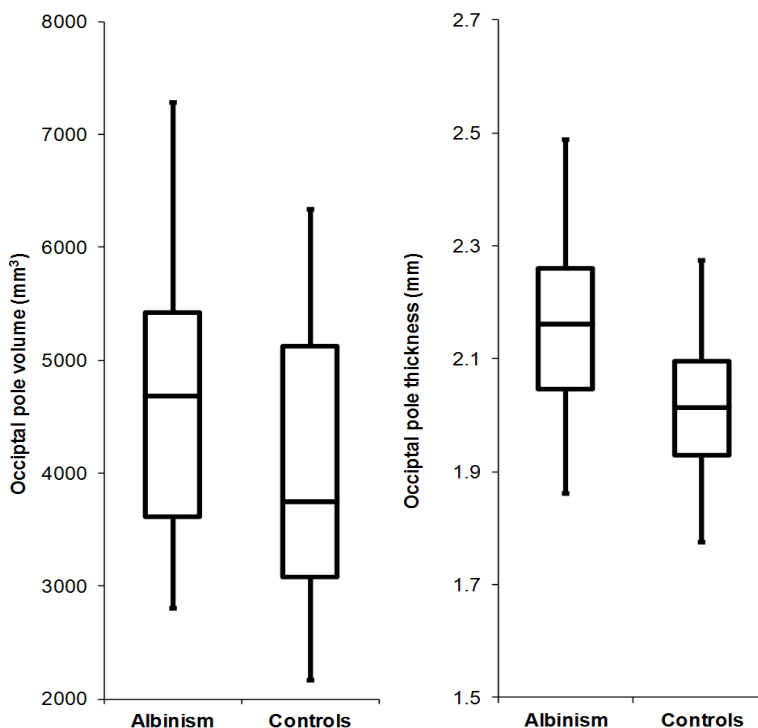


Figure 3-20: Comparison of occipital pole thickness and volume averaged across both hemispheres between the albinism and control groups

H₀ 4.2: Occipital pole cortex size and foveal layer thickness are related in patients with albinism

While comparing the cortex with the fovea, we found that the mean cortical thickness at the occipital pole was inversely correlated with the size of the mean thickness of the foveal RPE. (Figure 3-21) However, there was no relationship of cortical thickness or volume with the outer photoreceptor or inner processing layers at the fovea. (Table 3-12)

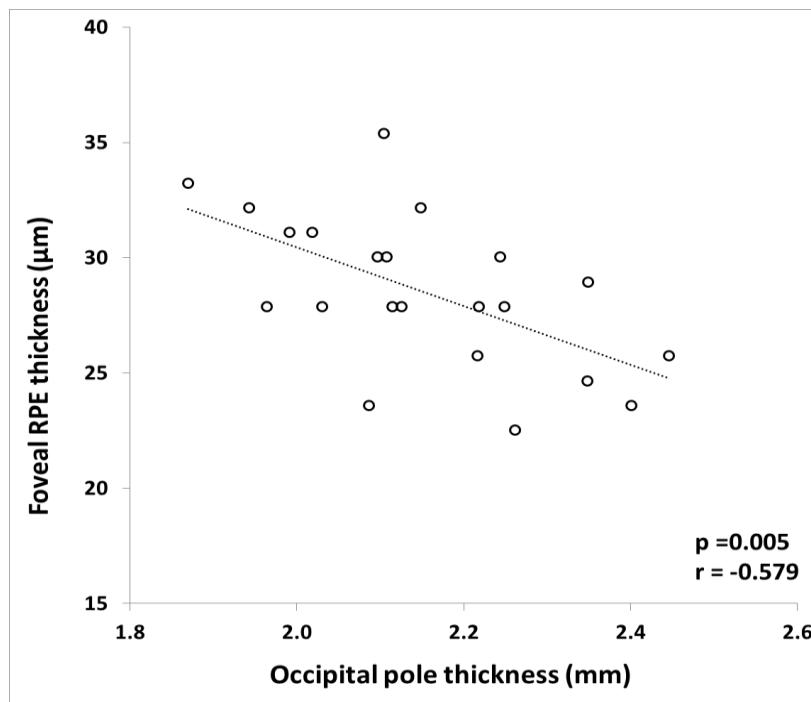


Figure 3-21: Comparison of foveal retinal pigment epithelium (RPE) thickness measured using OCT with the cortical thickness in the contralateral (left) and ipsilateral (right) occipital pole.

		<i>Photoreceptor</i>	<i>Processing</i>	<i>FDI</i>
<i>Occipital pole thickness</i>	<i>r</i>	-0.029	0.071	-0.016
	<i>p</i>	0.896	0.748	0.941
<i>Occipital pole volume</i>	<i>r</i>	0.099	0.193	-0.047
	<i>p</i>	0.652	0.377	0.830

Table 3-12: Comparison of photoreceptor layer thickness, processing layer thickness and foveal development index (FDI) with cortical thickness and volume at the occipital pole.

H₀ 4.3: Occipital pole cortex size and optic nerve head parameters are related in patients with albinism

Figure 3-22 shows that within optic nerve head, the disc and rim areas correlated with the cortical thickness at the occipital pole. Cortical volume was not related to optic nerve head parameters. (Table 3-13)

		<i>Optic nerve head</i>		
		<i>Disc area</i>	<i>Cup area</i>	<i>Rim area</i>
Thickness	<i>r</i>	0.478	-0.143	0.597
	<i>p</i>	0.021	0.515	0.003
	<i>p'</i>	0.042	0.515	0.009
Volume	<i>r</i>	0.161	0.026	0.150
	<i>p</i>	0.463	0.907	0.495
	<i>p'</i>	1.00	1.00	1.00

Table 3-13: Comparison of optic disc, cup and rim areas measured using OCT with cortical thickness and volume. Significant correlations are in bold. Holm-Bonferroni corrected *p'* values are also included.

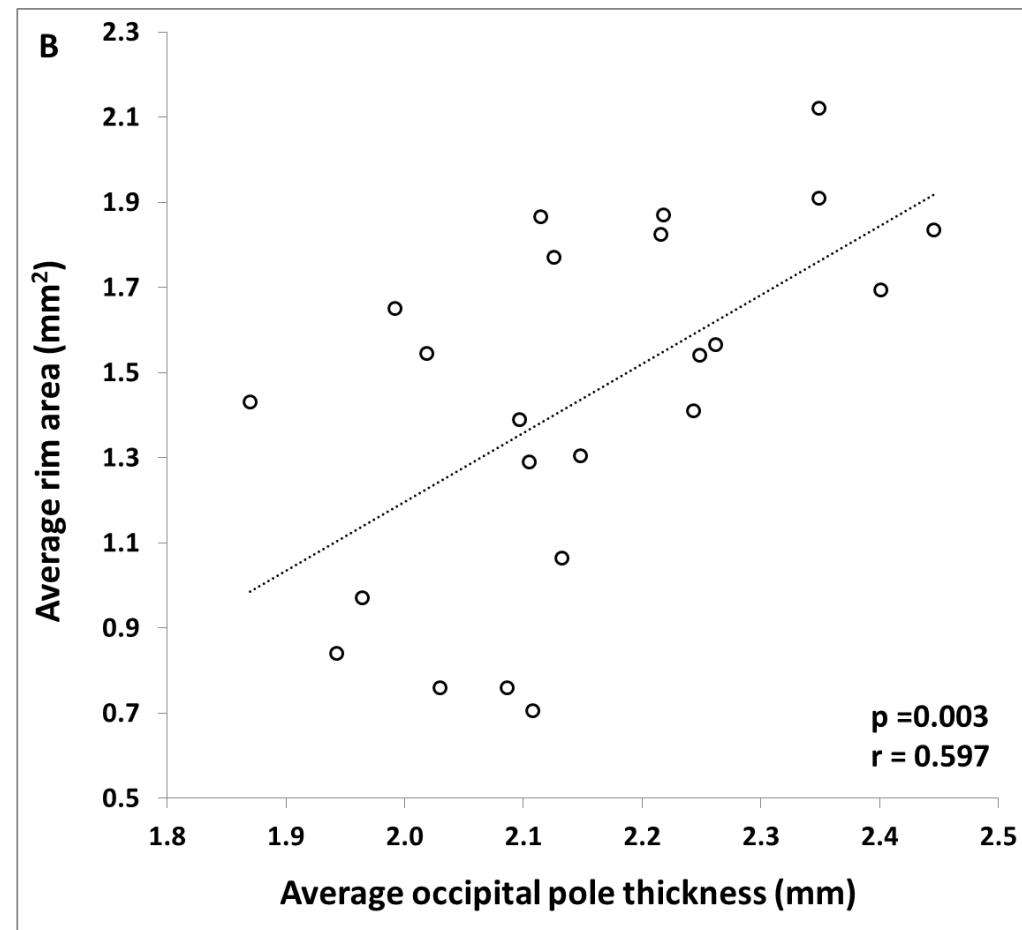
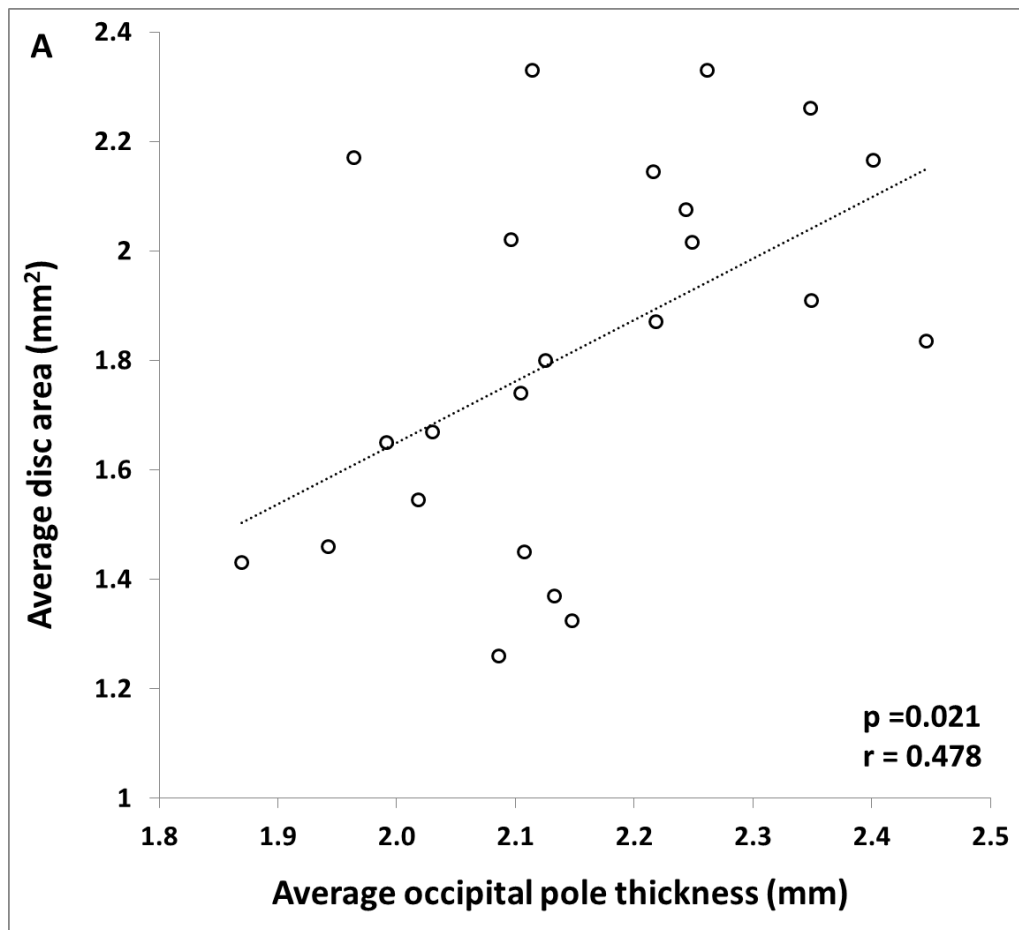


Figure 3-22: Comparison of cortical thickness at the occipital pole with optic disc (A) and rim (B) areas averaged across both eyes of patients with albinism

Table 3-13 shows comparison of the ppRNFL with the visual cortex. This comparison demonstrated that the superior ($r=0.369$, $p=0.018$, $p'=0.072$) and nasal ($r=0.340$, $p=0.030$, $p'=0.090$) aspects of the ppRNFL were positively correlated with cortical thickness of the contralateral hemisphere however these did not remain significant following correction for multiple comparisons.(Figure 3-23) There was no correlation of the cortex with the ppRNFL of the ipsilateral eye ($p>0.05$). Cortical volume was not related to any ipsilateral or contralateral ppRNFL sectors.

Cortex		ppRNFL			
		Superior	Nasal	Inferior	Temporal
Ipsilateral thickness	<i>r</i>	0.237	0.232	0.173	-0.057
	<i>p</i>	0.137	0.145	0.279	0.722
Ipsilateral volume	<i>r</i>	-0.106	-0.050	0.050	-0.105
	<i>p</i>	0.509	0.758	0.755	0.515
Contralateral thickness	<i>r</i>	0.369	0.340	0.251	-0.125
	<i>p</i>	0.018	0.030	0.115	0.435
Contralateral volume	<i>r</i>	-0.020	0.168	-0.110	-0.252
	<i>p</i>	0.903	0.293	0.494	0.112

Table 3-14: Comparison of cortical thickness and volume with peripapillary nerve fibre layer thickness (ppRNFL)

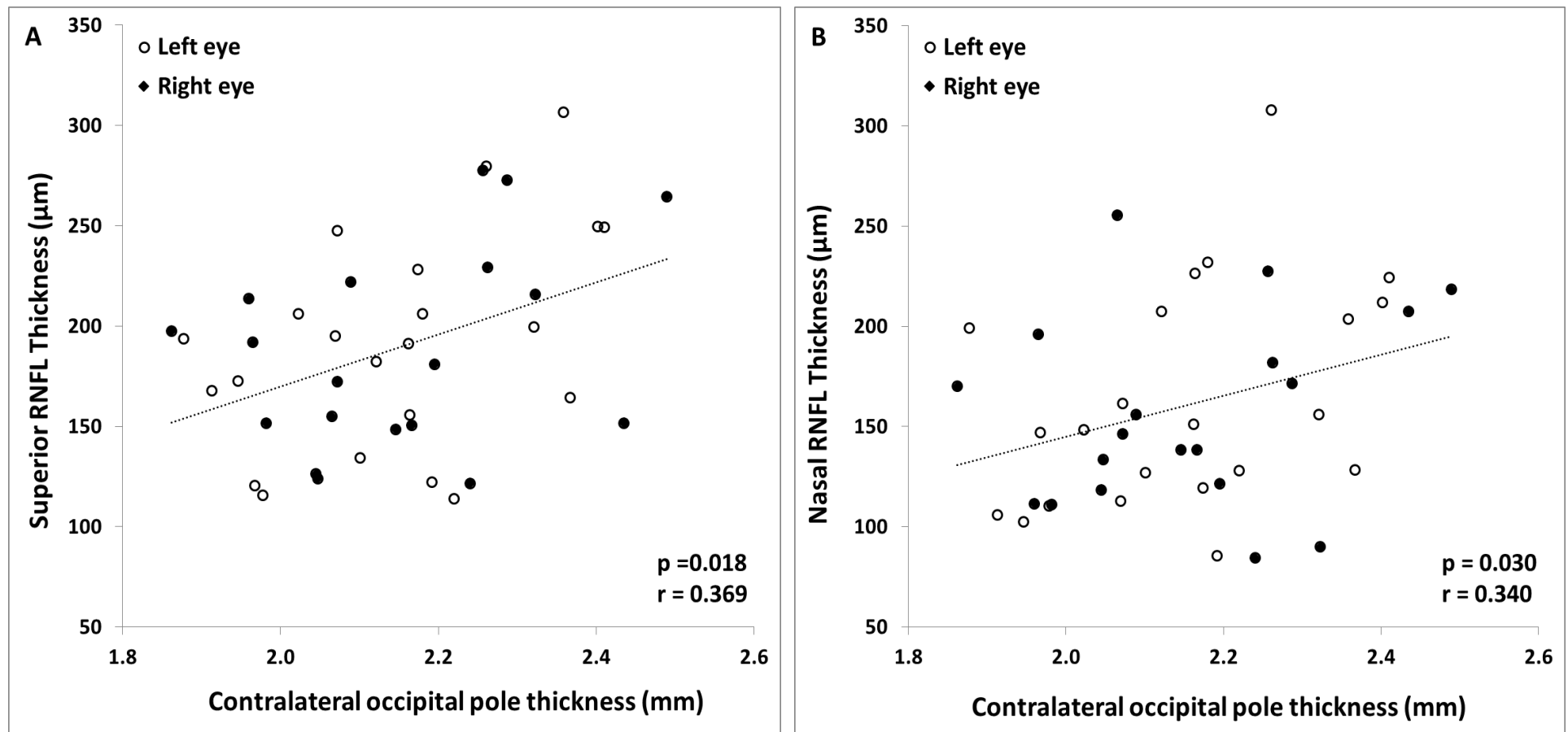


Figure 3-23: Comparison of superior (A) and nasal (B) ppRNFL thickness of each eye in the albinism group with cortical thickness at the occipital pole of the contralateral hemisphere.

H₀ 4.4: Occipital pole cortex size and chiasm size are related in patients with albinism

The optic chiasm area was negatively correlated with cortical thickness at the occipital pole averaged across both hemispheres. (Figure 3-24) We did not find any significant relationship between cortical thickness and chiasmal streamline decussation index or VEP asymmetry ($p > 0.05$).

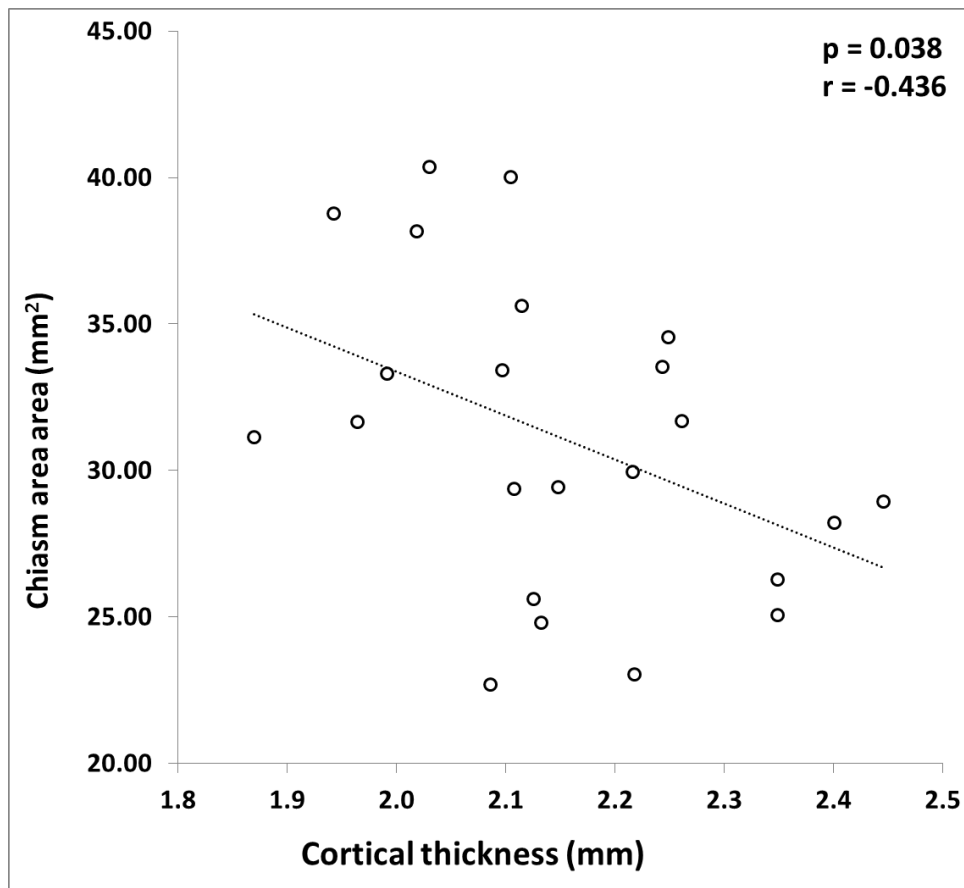


Figure 3-24: Comparison of mean cortical thickness at the occipital pole, with chiasm area in albinism patients

Comparison of visual cortex size with BCVA

We found no significant correlation between best corrected visual acuity and occipital pole thickness ($r = 0.116$, $p = 0.606$) or volume ($r = 0.224$, $p = 0.317$)

Using surface based analysis (SBA), we have been able to shed light on a conflict in previous literature regarding the nature of structural changes within the visual cortex of patients with albinism. Using voxel based morphometry (VBM), von dem Hagen et al. found that patients with albinism have a reduction in grey matter volume in the occipital cortex. A more recent study by Bridge et al. used SBA to conclude that visual cortex thickness is increased in patients with albinism.²⁴³

Bridge et al. suggested that the difference in results between the two previous studies were due to the two different analysis techniques being employed. Differences between the two techniques are explained earlier in section 1.4.9.2.

Using a similar technique to Bridge et al., we have found that patients with albinism do indeed have increased cortical thickness at the occipital pole. Bridge et al. found decreased gyrification in patients with albinism, which might explain why the earlier VBM study may have reported reduced cortical volume in albinism.^{239, 243}

OCT data regarding foveal and optic nerve abnormalities has allowed us to explore the possible causes behind cortical changes seen in albinism. We noted a number of significant relationships of cortical thickness with the fovea, optic nerve and chiasm.

Comparison of the visual cortex with the fovea showed that cortical thickness was inversely related to the size of the RPE in patients with albinism. The thickness of the RPE measured on OCT is impacted by the amount of melanin present within the RPE cells. This is due to the optical properties of melanin⁴¹², which mean that the light from the OCT device is scattered when it passes through melanin leading to the thick band like appearance of the RPE seen in OCT images.⁴¹³ This indicates that the amount of melanin within the RPE of patients with albinism affects the specialisation of the visual cortex. Von dem Hagen et al. have previously found that level of skin pigmentation is related to the degree of functional reorganisation of the visual cortex.²⁶⁷ Our results suggest that in addition to functional changes, pigmentation defects in albinism also lead to structural changes of the visual cortex.

While comparing the occipital pole to optic nerve head, we found that the disc and rim areas were positively correlated with cortical thickness at the occipital pole. Within the ppRNFL, the superior and nasal sectors also correlated positively with cortical thickness of the contralateral eye.

Bridge et al. noted that the thicker visual cortex in albinism is consistent with findings from early blind²⁴¹ and anophthalmic²⁴² individuals and suggested that this is due to a lack of pruning during development. In addition, increased chiasmal decussation means that there is a reduction in binocular competition at V1, which may be another factor in driving axonal pruning. The visual cortex undergoes rapid expansion during foetal and first four months of post-natal life and reaches peak levels (~150% of adult) by 7 months' gestation.⁴¹⁴ This early post-natal time corresponds with a critical period of visual development.^{415, 416}

The rapid growth phase is followed by synaptic revision with loss of the excess 40% of synapses between ages 8 months and 11 years. Subsequently, these synapse numbers remain stable into adulthood.⁴¹⁷ The synaptic elimination has shown to be dependent on visual experience.⁴¹⁸ In albinism reduced foveal cone density results in a lack of high-resolution input to V1. However, our results showed no relationship between cortical thickness at the occipital pole and foveal development

As mentioned in section 3.3 (page 136) where we characterized the optic nerve head structure in albinism. We found that rim size is increased in patients with albinism possibly due to arrest in normal embryological development of the optic nerve. The nasal aspect of the ppRNFL in particular appears to be composed of glial tissue, which is remnant of the hyaloid vascular system that has failed to fully regress. This would support the theory that a lack of pruning is responsible for increased thickness of the visual cortex seen in albinism and that it is a phenomenon that affects more than one location in the visual pathway.

We find that the area measurements of the optic chiasm showed an inverse relationship with V1 thickness. This indicates that white matter connectivity also has a role to play in maturation of the visual cortex.

During post-natal development, white matter tracts undergo structural changes such as increase in axonal diameter and progressive myelination.⁴¹⁹ These changes have a role to play in the structural and functional maturation of the visual cortex.⁴²⁰ Albino animal models have shown that melanin deficiency is associated with abnormal myelination and axonal distribution in the optic tract.⁴⁰¹ Functionally, this manifests as abnormal latency seen on VEP stimulation.^{421, 422} Our results indicate that altered input due to abnormal white matter tract morphology of the visual pathway disturbs normal development of the visual cortex.

Conclusion

Over recent years, advances in MR imaging protocols and analysis techniques have allowed characterization of structural and functional abnormalities in the visual cortex of patients with albinism. Using a combination of OCT and MRI imaging, we have been able to resolve conflict in previous literature regarding the nature of cortical abnormalities associated with albinism. Our results suggest that much like abnormalities in the anterior visual pathway, the cortical abnormalities also represent abnormal embryological and early post-natal development.

Moreover, we show for the first time that cortical abnormalities are related to pigmentation levels of the RPE and axonal disorganisation of the optic nerve head. However, we found no relationship between foveal hypoplasia and cortical abnormalities in albinism.

3.6 NYSTAGMUS

3.6.1 BACKGROUND

As discussed in section 1.4.10, the mechanism behind nystagmus in albinism is poorly understood. Traditionally, nystagmus was considered to be a result of an aberration in the motor mechanisms that control eye movements. More recently, there has been a shift in thinking which implicates sensory abnormalities in the visual pathway such as retinal deficits³²⁸ and axonal misrouting as the source for the nystagmus.³³³⁻³³⁵ By comparing nystagmus characteristics obtained through eye movement recordings with retinal defects assessed via OCT and chiasmal misrouting quantified via VEP, we aim to investigate whether sensory deficits are the cause behind nystagmus generation in albinism. Summary of aims

Compare motor characteristics of the nystagmus in albinism with the degree of foveal development and morphology of the peripapillary nerve fibre layer quantified using OCT imaging. The degree of chiasmal misrouting estimated by VEP.

3.6.2 FINDINGS

Forty-nine patients with albinism (31 male, 18 female) with a mean age of 35.6 ± 11.2 years were recruited for this part of the study. Each participant underwent eye movement recordings as described in section 2.3 (page 105). This provided us with information regarding nystagmus severity and foveation in the null region as well as across all gaze positions (whole curve).

Using Spearman's rank correlation co-efficient, the eye movement data was compared to the structural abnormalities in the fovea and optic nerve measured using OCT and chiasmal misrouting quantified via VEP. Thickness measurements of photoreceptor and processing layers were used to calculate the foveal development index using the following formula:

$$\text{Foveal Development Index} = 1 - \frac{\text{Processing layer thickness}}{\text{Photoreceptor layer thickness}}$$

H₀ 5.1: Nystagmus intensity is related to foveal development

Table 3-15 shows that nystagmus amplitude ($r=0.508$, $p=2.67 \times 10^{-4}$, $p'=0.001$), intensity ($r=0.441$, $p=0.002$, $p'=0.009$) and NAFX ($r=0.425$, $p=0.003$, $p'=0.009$) are strongly related to foveal development. Photoreceptor layers ($r=-0.495$, $p=4.06 \times 10^{-4}$, $p'=0.002$) provided a bigger contribution to this relationship compared to the processing layers ($r=0.422$, $p=0.003$, $p'=0.023$) (see Table 3-15)

Figure 3-25 compares the relationship between foveal development and nystagmus amplitude. This correlation was more powerful in the null region ($r=0.524$, $p=1.50 \times 10^{-5}$, $p'=0.001$) compared to the average of all gaze positions ($r=0.508$, $p=2.67 \times 10^{-4}$, $p'=0.001$).

Interestingly, nystagmus frequency was not related to foveal development ($r=-0.462$, $p>0.05$).

			PRL	ProL	FDI
Whole Curve	Amplitude	<i>r</i>	<i>-0.495</i>	<i>0.422</i>	<i>0.508</i>
		<i>p</i>	<i>4.06×10^{-4}</i>	<i>0.003</i>	<i>2.67×10^{-4}</i>
		<i>p'</i>	<i>0.002</i>	<i>0.023</i>	<i>0.001</i>
	Frequency	<i>r</i>	<i>-0.065</i>	<i>0.079</i>	<i>0.054</i>
		<i>p</i>	<i>0.666</i>	<i>0.599</i>	<i>0.720</i>

		<i>p'</i>	1.00	1.00	1.00
	Intensity	<i>r</i>	-0.462	0.353	0.441
		<i>p</i>	0.001	0.015	0.002
		<i>p'</i>	0.005	0.075	0.009
	NAFX	<i>r</i>	-0.348	0.426	0.425
		<i>p</i>	0.016	0.003	0.003
		<i>p'</i>	0.049	0.023	0.009
Null region	Amplitude	<i>r</i>	-0.529	0.402	0.524
		<i>p</i>	1.32x10 ⁻⁴	0.005	1.50x10 ⁻⁵
		<i>p'</i>	0.001	0.031	0.001
	Frequency	<i>r</i>	-0.088	-0.0202	0.025
		<i>p</i>	0.556	0.893	0.866
		<i>p'</i>	1.00	1.00	1.00
	Intensity	<i>r</i>	-0.466	0.332	0.445
		<i>p</i>	9.59x10 ⁻⁴	0.023	0.002
		<i>p'</i>	0.006	0.091	0.009
	NAFX	<i>r</i>	-0.465	0.328	0.450
		<i>p</i>	9.88x10 ⁻⁴	0.025	0.002
		<i>p'</i>	0.006	0.091	0.009

Table 3-15: Comparison of nystagmus severity and NAFX in the null region and across all gaze positions (whole curve) with foveal photoreceptor layer thickness (PRL), processing layer thickness (ProL) and foveal development index (FDI). Holm-Bonferroni corrected *p'* values are also included.

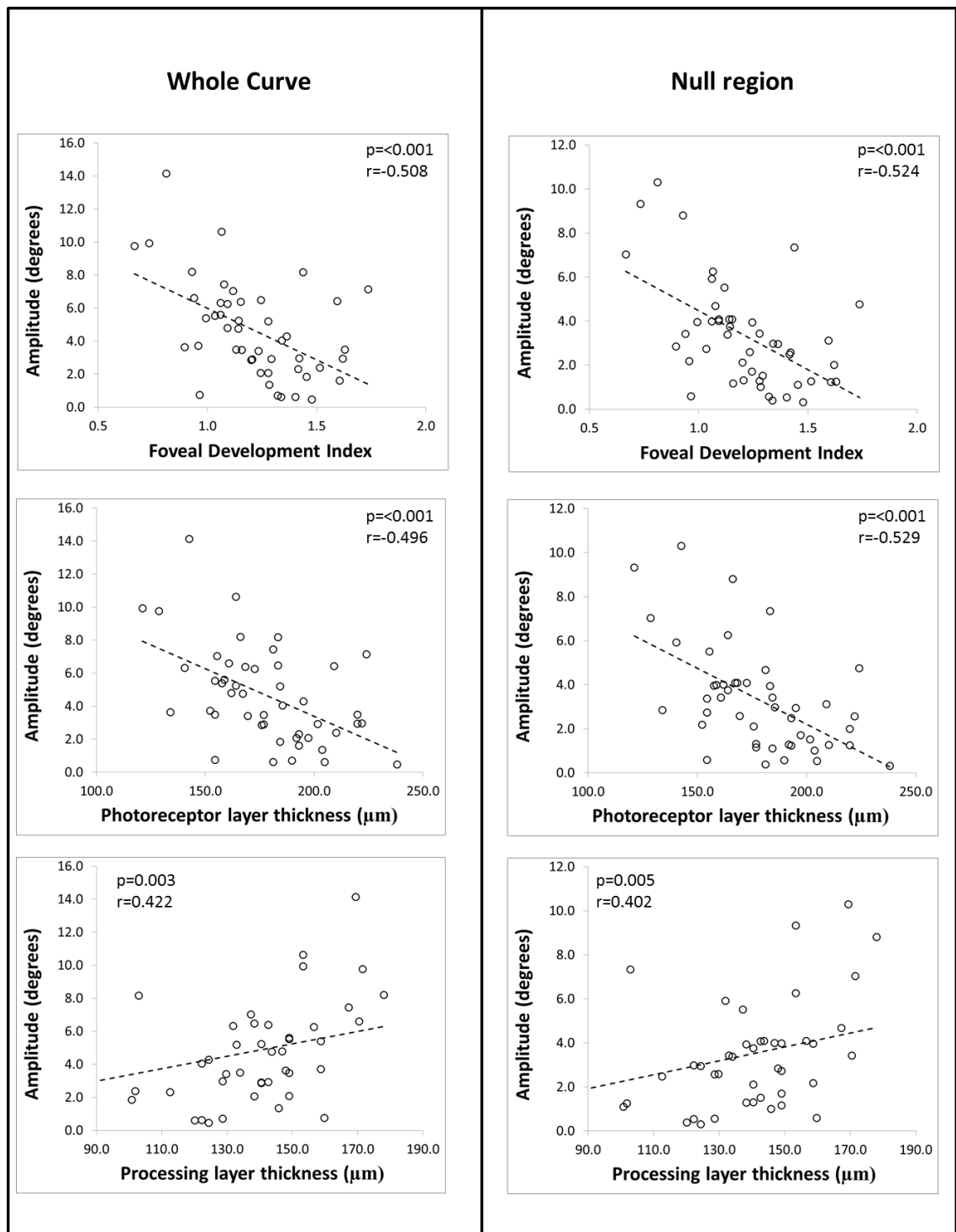


Figure 3-25: Comparison of nystagmus amplitude with foveal development, photoreceptor and processing layers

H₀ 5.2: Nystagmus intensity is related to optic nerve abnormalities

Table 3-16 shows comparison of nystagmus characteristics with optic disc, cup and rim areas and ppRNFL sector thickness did not reveal any significant correlations ($p>0.05$). As the uncorrected p-values were not significant, a Holm-Bonferroni correction was not carried out.

			<i>Superior</i>	<i>Nasal</i>	<i>Inferior</i>	<i>Temporal</i>	<i>Disc area</i>	<i>Rim area</i>	<i>Cup area</i>
Whole Curve	Amplitude	<i>r</i>	-0.128	0.027	-0.085	-0.076	-0.202	-0.146	-0.142
		<i>p</i>	0.479	0.880	0.637	0.675	0.237	0.396	0.408
	Frequency	<i>r</i>	-0.030	-0.137	-0.146	-0.016	0.021	0.232	-0.176
		<i>p</i>	0.867	0.447	0.417	0.932	0.904	0.173	0.304
	Intensity	<i>r</i>	-0.117	0.034	-0.123	-0.017	-0.165	-0.074	-0.155
		<i>p</i>	0.518	0.853	0.494	0.923	0.336	0.666	0.366
	NAFX	<i>r</i>	-0.037	-0.021	0.145	0.069	0.083	0.001	0.021
		<i>p</i>	0.837	0.912	0.422	0.699	0.627	0.991	0.902
Null region	Amplitude	<i>r</i>	-0.165	-0.008	-0.122	-0.020	-0.200	-0.130	-0.169
		<i>p</i>	0.358	0.965	0.501	0.914	0.242	0.448	0.323
	Frequency	<i>r</i>	-0.196	-0.131	-0.294	-0.136	-0.014	0.224	-0.217
		<i>p</i>	0.275	0.466	0.097	0.449	0.938	0.189	0.205
	Intensity	<i>r</i>	-0.220	-0.029	-0.173	-0.058	-0.135	-0.018	-0.207
		<i>p</i>	0.218	0.873	0.337	0.751	0.432	0.916	0.225
	NAFX	<i>r</i>	-0.337	-0.104	-0.116	-0.107	-0.044	0.020	-0.143
		<i>P</i>	0.055	0.565	0.519	0.552	0.797	0.906	0.407

Table 3-16: Comparison of nystagmus severity and NAFX in the null region and across all gaze positions (whole curve) with optic disc, rim and cup areas as well as peripapillary retinal nerve fibre layer (ppRNFL) thickness in the superior, nasal, inferior and temporal sectors.

H₀ 5.3: Nystagmus intensity is related to chiasmal misrouting measured using VEP.

Table 3-17 shows that in contrast to the foveal development, which was most strongly related to nystagmus amplitude, VEP asymmetry had a moderate negative association with nystagmus frequency. Again this association was greater in the null region ($r=-0.358$, $p=0.038$) compared to the whole curve ($r=-0.339$, $p=0.037$). None of these relationships survived correction for multiple comparisons.

		<i>Amplitude</i>	<i>Frequency</i>	<i>Intensity</i>	<i>NAFX</i>
Whole Curve	r	-0.286	-0.155	-0.339	-0.118
	p	0.081	0.353	0.037	0.481
	p'	0.243	0.706	0.148	0.706
Null region	r	-0.237	-0.364	-0.358	-0.353
	p	0.153	0.025	0.028	0.038
	p'	0.153	0.100	0.100	0.100

Table 3-17: Comparison of nystagmus severity and NAFX in the null region and across all gaze positions (whole curve) with visual evoked potential (VEP asymmetry). Holm-Bonferroni corrected p' values are also included.

Figure 3-26 compares the relationship of foveal development index and VEP asymmetry with nystagmus characteristics in the null region.

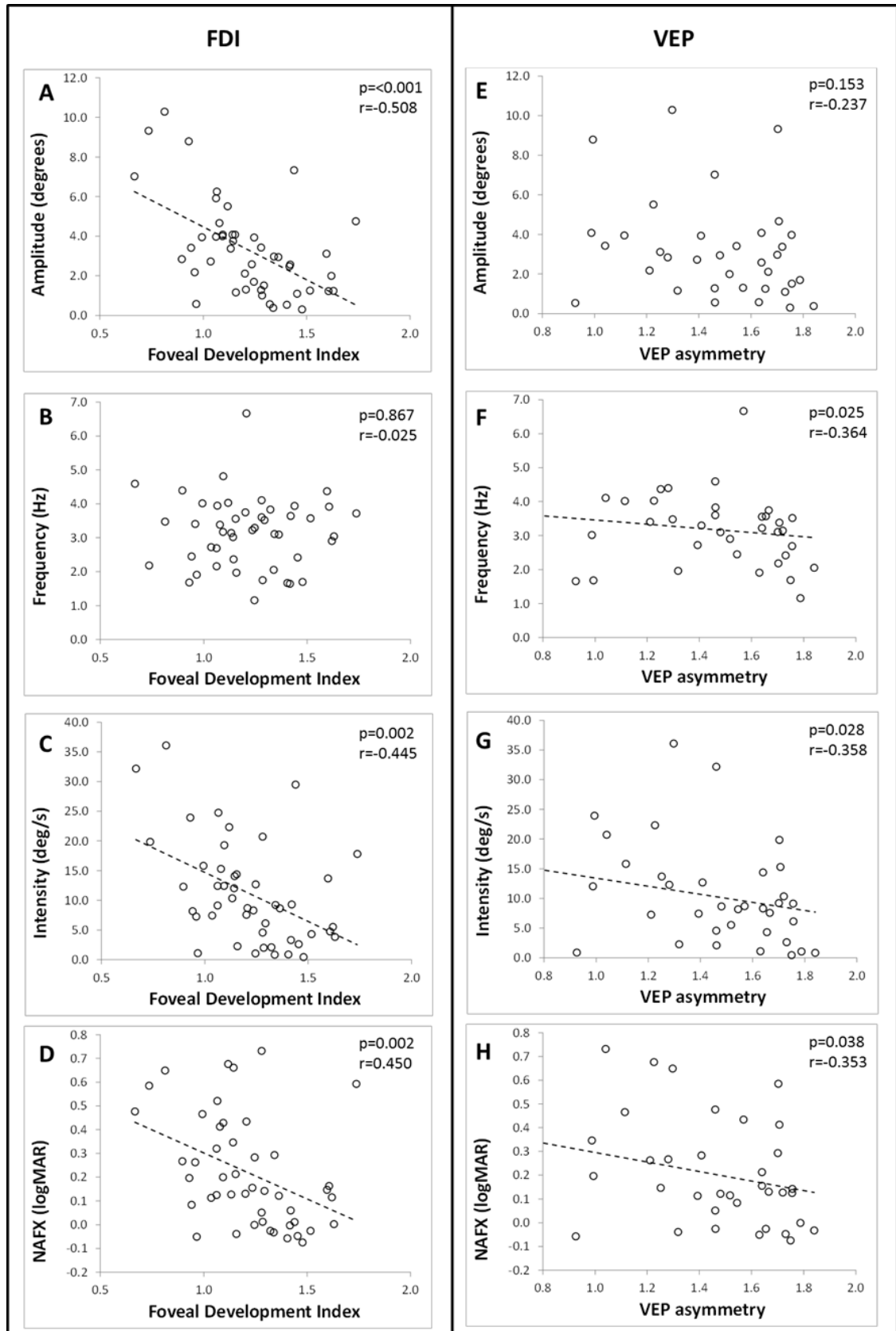


Figure 3-26: Comparison of nystagmus characteristics of amplitude, frequency, intensity and NAFX, within the null region, with foveal development index (FDI) (A-D) and visual evoked potential (VEP) asymmetry (E-H).

In this study we demonstrate that a highly significant positive correlation exists between the level of foveal development (FDI) measured using OCT and the degree of nystagmus, and in particular between FDI and the amplitude of the nystagmus. Meanwhile, we find a significant negative association between the amount of crossed fibres, estimated using VEP and the degree of nystagmus. In contrast to FDI however, VEP asymmetry is related to frequency rather than the amplitude of nystagmus. No significant correlations were noted between peripapillary retinal nerve fibre layer (ppRNFL) thickness or optic disc, cup and rim areas and nystagmus parameters.

Foveal Development and Infantile Nystagmus

Many subtypes of infantile nystagmus demonstrate clear evidence of foveal hypoplasia including albinism, PAX6 mutations, achromatopsia and isolated foveal hypoplasia.^{174, 423-425} High-resolution imaging with OCT has recently been used to describe and quantify foveal deficits in these subtypes with a greater clarity and precision than before. In fact, OCT has also recently been used to describe foveal deficits in so-called “idiopathic IN” using OCT, a subtype that has previously been defined as idiopathic because retinal deficits were thought to be absent from this group.⁴²⁶ New technology that permits OCT imaging in infants and children now makes it possible to describe these foveal deficits as they develop from birth.⁴²⁷⁻⁴³⁰

The strong correlation we observe between degree of foveal development and amount of nystagmus supports the theory that disrupted foveal development is the underlying cause behind most subtypes of IN. This positive correlation stands in contrast to the absent correlation between peripapillary RNFL (a measure of ganglion cell number) and nystagmus and the negative correlation between VEP asymmetry (a measure of the amount of crossed fibres) and nystagmus. The importance of disrupted foveal development to nystagmus generation is also substantiated by the observation that whenever fovea is disrupted during visual development, usually nystagmus develops as a result.⁴³¹ The exact link between erroneous afferent inputs caused by foveal

hypoplasia, and how the ocular motor system generates nystagmus however is not clear.⁴³²

Harris and Berry suggested that nystagmus caused by foveal maldevelopment in IN is an adaptive response in early visual development to reduced contrast sensitivity to high-spatial frequencies. Since contrast sensitivity to low spatial frequencies is enhanced by motion, they propose that nystagmus is generated in order to improve vision.³²⁷ A recent hypothesis has also recently been suggested by Brodsky and Dell'Osso in which nystagmus in IN is generated due to abnormal interaction between two normally complementary systems. In the healthy human adult visual system, a cortical foveal pursuit system acts to suppress the perception of full-field optokinetic motion during active pursuit, a subcortical system predominantly driven by monocular contralateral inputs that have a bias for nasal-ward motion. They suggest that abnormal development of the cortical foveal system leads to inappropriate expression of this sub-cortical system, which facilitates the development of the unstable oscillatory activity of the eyes.³²⁸

It is interesting to note that in our cohort, the foveal development correlated with amplitude but not frequency of nystagmus. This indicates that as foveal development improves, the mechanisms that control eye movements exert a bigger influence to keep the visual world on the fovea. This is also evident by previous studies of IN in infants and children have shown an age-dependent evolution of waveforms during infancy from pendular to jerk. This change in waveform is thought to represent modulation of nystagmus by the developing afferent visual system to maximise foveation.⁴³³

Post-natal visual development involves increased aggregation of cones at the fovea. However, this fails to occur in albinism.¹⁴⁴ Therefore, it is possible that lack of foveal specialisation means that there is no motivation to focus the image on a tight area within the central retina hence the larger amplitude of nystagmus. This is also backed up by the strong correlation we see between NAFX (a measure of foveation) and FDI (i.e. foveation is more likely if the fovea is better developed). However, a previous

report of increased proportion of the jerk waveform compared to pendular nystagmus in patients with albinism negates this hypothesis.¹⁷⁴

Having said all of this, there are some arguments against the importance of interrupted foveal development for nystagmus generation. These include the observation that nystagmus exists in some conditions where the fovea appears relatively normal. This includes a sub-group of individuals with “idiopathic” IN associated with FRMD7 mutations who do not appear to show structural abnormalities, although it is possible that functional foveal deficits may exist which may not be apparent from observing foveal morphology.⁴²⁶ Congenital cataract also leads to nystagmus without any direct effect on foveal development, although the cataract will mean that only information with low spatial resolution will reach the cortex, which bears a similarity to the functional consequences of reduced foveal inputs.^{434, 435}

Nystagmus is also observed in afoveate animals with albinism. This has been beautifully demonstrated recently by Traber et al. in albino mice where the degree of hypopigmentation is associated with the amount of nystagmus.⁴³⁶ Other examples of afoveate animals displaying nystagmus include zebrafish⁴³⁷ and canines.⁴³⁸⁻⁴⁴⁰

Crossing Abnormalities and Nystagmus Generation

A surprising finding from this study was the observation that the degree of decussation abnormality was negatively correlated with amount of nystagmus. Recently, zebrafish with miswired crossed projections have been shown to have similar waveforms to those observed in humans with IN, including pendular, jerk and bidirectional waveforms.⁴³⁷ Similar “nystagmus-like” waveforms have been observed in healthy adult humans using gaze-contingent feedback in which motion viewed on a monitor is inverted to normal. These experiments suggest that inappropriately crossed projections and hence miswired motion detectors have the potential to generate nystagmus. However, the moderate negative correlation we observed between the

amount of abnormally crossed fibres and degree of nystagmus implies that misrouting of fibres of the optic is not the underlying cause of nystagmus in albinism.

Interestingly we observed an inverse correlation between VEP asymmetry and frequency of nystagmus but not the amplitude of nystagmus. In a previous study it has been observed that nystagmus in albinism shares many similar features compared to those seen in idiopathic IN caused by *FRMD7* mutations. However, one difference we have observed is that the frequency of nystagmus is significantly lower in albinism (mean = 3.3 Hz) compared with idiopathic IN (caused by *FRMD7* mutation, mean = 4.3 Hz).¹⁷⁴ Why more foveal hypoplasia should lead to lower frequencies of nystagmus is not clear.

Summary

There has been a lack of consensus in previous literature regarding whether infantile nystagmus is caused by abnormalities in the efferent ocular-motor control or whether it originates from disruption of the afferent sensory input. In our albinism cohort, we have been able to compare nystagmus characteristics with two such sensory abnormalities, namely foveal hypoplasia and chiasmal misrouting. Both have been under recent scrutiny as candidates for nystagmus generation.^{327, 328, 333} However, our results show that nystagmus severity is strongly related to foveal maldevelopment. On the other hand, we found VEP asymmetry was inversely correlated with nystagmus severity.

In conclusion, this study provides a significant breakthrough in advancing the understanding of the mechanism behind generation of nystagmus associated with albinism. Our findings lay credence towards the recent recognition of the role sensory abnormalities play in causing nystagmus.⁴³²

CHAPTER 4

CONCLUSION

4.1 SUMMARY OF FINDINGS

Albinism refers to a group of genetic abnormalities in the melanin synthesis pathway that are associated with profound visual abnormalities. These include foveal hypoplasia, optic nerve anomalies, chiasmal misrouting, visual cortex reorganisation, and nystagmus.⁹⁹

The focus of this research was to characterise the structural defects found in albinism using high-resolution optical coherence tomography (OCT) and magnetic resonance imaging (MRI) and explore the relationship between them.

Anatomical characterization

Table 4-1 summarises the key anatomical abnormalities found in albinism at the level of the fovea, optic nerve head, optic chiasm and visual cortex.

<i>Fovea</i> <ul style="list-style-type: none"> • <i>Abnormal development of foveal pit</i> • <i>Continuation of inner layers (GCL through to OPL)</i> • <i>Reduced thickness of outer layers (i.e. ONL and OS)</i>
<i>Optic Nerve</i> <ul style="list-style-type: none"> • <i>ppRNFL thinning (especially temporally)</i> • <i>Change in ppRNFL distribution around ON</i> • <i>Enlarged rims and smaller cups</i> • <i>Horizontally elongated discs</i>
<i>Optic Chiasm</i> <ul style="list-style-type: none"> • <i>Reduced size cross sectional areas/widths of optic nerves, tracts and chiasm</i> • <i>Increased DTI streamline decussation</i>
<i>Visual Cortex</i> <ul style="list-style-type: none"> • <i>Higher occipital pole thickness and volume in albinism</i>

Table 4-1 Summary of key anatomical abnormalities found in albinism at the level of the fovea, optic nerve head, optic chiasm and visual cortex.

Fovea

In section 3.2, we found that patients in patients with albinism, there is disruption of foveal development that results in increased macular thickness due to the intrusion of inner retinal layers through the foveal region. This was accompanied by a failure of photoreceptor cells to specialise.

Optic nerve

Section 3.3 represents the first attempt at a comprehensive structural analysis of the optic nerve head structure in albinism. Using a novel motion correction algorithm, we were able to overcome the issue of misalignment of successive B-scans due to motion artefact created by nystagmus. This methodology withstood robust test-retest analysis confirming its validity.

We found that albinism is associated with small or absent optic cup and enlarged optic rim. This is likely due to failure of the embryonic hyaloid vasculature to regress fully, which results in an excess of remnant glial tissue at the vitreal surface of the optic nerve head.¹²⁸ We compared OCT images from our albinism patients, with previously published findings in patients with a persistent hyaloid artery, and found striking similarities that support this suggestion.^{386, 387}

Another prominent abnormality we noted was thinner peripapillary retinal nerve fibre layer(ppRNFL) in the albinism group. The size of the ppRNFL was related to ganglion cell layer thickness at the fovea. This corresponds with previous reports of reduced ganglion cell population in the retinae of albino animals and human post-mortem histology reports.^{132, 385, 404, 405, 441}

Through assessment of OCT scans in conjunction with fundus photographs, we were able to reject previous suggestions that albinism is associated with optic nerve hypoplasia and tilted disc syndrome.^{167, 169}

Optic chiasm

In section 3.4, we confirmed previous reports of smaller optic nerve, chiasm and tracts in albinism.^{168, 215, 239} The size of the intracranial optic nerves was related to ppRNFL thickness at the optic nerve head indicating that the ppRNFL size provides an estimation of the number of retinal ganglion cell axons which form the optic nerve.

We utilised DTI tractography to study the optic chiasm in albinism for the first time. Chiasmatal misrouting estimated through DTI tractography correlated with VEP asymmetry indicating that this technique is a valid tool for assessing axonal decussation at the chiasm.

Visual cortex

In section 3.5, we demonstrated that the disagreement in previous literature regarding the nature of cortical abnormalities in albinism stems from the difference in the analysis techniques used by the two studies (voxel based morphometry vs surface based analysis).^{239, 243} We used surface based analysis to replicate the findings of Bridge et al. who stated that visual cortical thickness is increased in albinism. This feature is consistent with cortical changes seen in the early blind and anophthalmic patients^{241, 242} and is likely to be a result of reduction in post-natal synaptic pruning that which is driven by visual experience.⁴¹⁸

4.1.1 COMPARISON OF OCULAR AND POST-ORBITAL STRUCTURES

The use of multiple imaging modalities in the same group of patients permitted us to assess the relationship of ocular abnormalities measured via OCT with those seen in the post-orbital visual pathway using MRI. These comparisons are summarised in Table 4-2.

			<i>Fovea</i>	<i>Optic Nerve</i>
<i>Chiasm</i>	<i>Area</i>	<i>Post-orbital Optic nerve</i>	<i>No association</i>	<i>Strong +ve correlation with temporal ppRNFL thickness</i>
		<i>Chiasm</i>	<i>No association</i>	<i>Strong +ve correlation with temporal ppRNFL thickness</i>
		<i>Optic tract</i>	<i>No association</i>	<i>No association</i>
	<i>DTI</i>	<i>Total streamlines</i>	<i>Strong -ve correlation foveal hypoplasia</i>	<i>No association</i>
		<i>Decussation index</i>	<i>No association</i>	<i>No association</i>
<i>Visual cortex</i>	<i>Thickness</i>		<i>Strong -ve correlation with RPE thickness</i>	<i>-Contralateral occipital pole moderate +ve correlation with superior and nasal ppRNFL</i>
	<i>Volume</i>		<i>No association</i>	<i>-Strong +ve correlation with rim and disc areas</i>

Table 4-2: Summary of key findings while comparing foveal and optic nerve head abnormalities with post-orbital optic nerves, optic chiasm, optic tracts and the visual cortex.

In chapter 3.4 we found that although strength of connectivity at the chiasm was related to foveal development, the degree of decussation did not show significant relationship with any foveal or optic nerve measures, indicating that retinal and chiasmal abnormalities in albinism are independent features confirming previous suggestion to this effect by Neveu et al.⁴⁰⁸ It is more likely that chiasmal misrouting is a feature of delayed axonal outgrowth due to melanin deficiency within the RPE.^{94, 407, 410}

Cortical thickness was related to a number of anterograde structures of the visual pathway including foveal RPE complex thickness, optic disc and rim areas, superior and nasal ppRNFL thickness as well as optic chiasm area. These relationships provide a number of clues as to the reasoning behind the structural changes seen in visual cortex of patients with albinism.

Using functional MRI, von dem Hagen et al. have already shown that cutaneous pigmentation levels predict the extent of temporal shift in chiasmal decussation and therefore relate to the level of functional adaptation of the visual cortex.²⁶⁷ Our finding about the relationship between RPE and visual cortex thickness suggests that in addition to functional changes, pigmentation defects in albinism also leads to structural reorganisation of the visual cortex.

The RPE cells also have a role to play in determining the timing of axonal outgrowth from retinal ganglion cells.^{94, 407, 410} Lack of melanin in albinism leads to a delay in this process and results in abnormal axonal distribution and myelination within the optic tract.⁴⁰¹ These changes affect the structural and functional maturation of the visual cortex.⁴²⁰ Our results indicate that altered input due to abnormal white matter tract morphology of the visual pathway disturbs normal development of the visual cortex. This is consistent with the suggestion by Bridge et al. regarding disrupted synaptic regression as the cause of increased cortical thickening in albinism.²⁴²

As mentioned earlier, we found that failure of hyaloid vasculature to fully regress leaves behind glial tissue on the nasal aspect of the optic rim. The relationship of cortical thickness with optic rim area and supero-nasal ppRNFL sector thickness indicates that failure of structural maturity in these two structures is related and is likely to be caused by reduced melanin within the RPE.

4.1.2 COMPARISON OF ANATOMICAL AND FUNCTIONAL MEASUREMENTS

We compared anatomical data to functional measurements such as best-corrected visual acuity, visual evoked potentials and eye-movement recordings. This enabled us to assess the impact of structural abnormalities on visual function. These comparisons are summarised in Table 4-3.

In section 3.2, we clarified conflict in previous literature regarding the role played by foveal pit formation on visual function.^{139, 143} We provide quantitative evidence that photoreceptor outer segment specialisation is the strongest predictor of visual acuity in albinism. Since nystagmus associated with albinism also leads to deterioration in vision due to motion blur, our findings indicate that OCT has a clinical use in recognizing patients who have potential for visual improvement

In section 3.6, we provide evidence for the importance of foveal development on the severity of nystagmus. There has been debate in previous literature regarding the aetiology of nystagmus associated with albinism.⁴³² Our findings indicate that a lack of high-resolution sensory input due to an abnormal fovea is the reason behind nystagmus in albinism. However, it is difficult to ascertain whether the nystagmus is an adaptation to improve contrast sensitivity³²⁷ or whether it is due to inappropriate expression of the subcortical accessory optic pathway.³²⁸

The negative relationship between nystagmus amplitude and foveal specialisation indicates that as the fovea develops, there is modulation of nystagmus by the visual system, which leads to a decrease in nystagmus amplitude to keep the image close to the foveal region.

A surprising finding from this study was the observation that the degree of VEP asymmetry was negatively correlated with the intensity of nystagmus indicating that chiasmal misrouting does not cause nystagmus in albinism.

	<i>Fovea</i>	<i>Optic nerve</i>	<i>Chiasm</i>	<i>Visual Cortex</i>
<i>Nystagmus</i>	Strong +ve correlation between nystagmus amplitude and degree of foveal hypoplasia	No association	No association	No association
<i>LogMAR best-corrected visual acuity (BCVA)</i>	Strong +ve correlation with degree of foveal hypoplasia	No association	No association	No association
<i>VEP asymmetry</i>	No association	No association	Strong +ve correlation between DTI and VEP asymmetry	No association

Table 4-3: Comparison of anatomical abnormalities at the fovea, optic nerve head, optic chiasm and visual cortex with nystagmus, best corrected visual acuity and VEP asymmetry.

4.2 SCIENTIFIC IMPACT

The study represents a big step forward in our understanding about the influence of albinism on the visual pathway. Using high-resolution imaging, we have been able to characterize structural abnormalities throughout the visual pathway and their impact on visual function.

As summarised in the previous section, our research uncovers a number of novel findings and sheds light on several of disagreements in previous literature regarding the nature and consequences of visual dysfunction associated with albinism. These include clarifying the respective impact of foveal pit formation, macular thickness and photoreceptor specialisation on visual acuity,^{139, 143} rejecting the suggestion that albinism is associated with optic nerve hypoplasia and tilted disc syndrome,¹⁶⁷ confirming the more recent findings of smaller optic nerve, chiasm and tracts in albinism^{168, 215, 239} while rejecting the earlier study by Brodsky et al. which found no difference²⁰⁴ and reproducing the findings by Bridge et al. that indicated increased visual cortical thickness in albinism in contrast with previous suggestions of reduced cortical volume.^{239, 243} In addition we also validated the recent shift in thinking towards a sensory model of nystagmus generation rather than considering it as a purely ocular motor disorder.⁴³²

The research also provides a number of advances in methodology. Retinal segmentation algorithm developed by the author has since been used to measure the retinal thickness in further studies.^{100, 442} Motion correction algorithm used to study the optic nerve here can easily be applied to study the optic nerve in other disorders associated with nystagmus. By comparing it to VEP asymmetry, we have also been able to provide cautious endorsement for the use of diffusion tractography in studying chiasmal decussation.

Finally, the work carried out by the author as part of this research has led to a number of collaborative projects that have already been published. These include assessment of the iris in albinism using OCT,¹⁰⁰ developing a grading system for the assessment of foveal hypoplasia,³⁴⁰ assessment of the parafovea in patients with foveal hypoplasia⁴⁴³ and assessment of difference in normal macular structure across ethnicities.⁴⁴²

In addition, there is further work ongoing to evaluate the impact of retinal and optic nerve abnormalities on visual fields in patients with albinism. Another study, which employed resting-state fMRI and DTI data collected by the author to assess the whole-brain adaptations to abnormal visual input in albinism, is also soon to be published.

4.3 CLINICAL IMPLICATIONS

The clinical implications of this work are multi-fold. Our findings have the potential to positively influence, both the diagnosis, and management of patients with albinism. As OCT devices are available in most ophthalmology clinics, this impact can be immediate.

From a diagnostic point of view, the morphological abnormalities we have characterized can form the basis of diagnostic criteria to help differentiate between albinism and other eye movement disorders such as idiopathic infantile nystagmus that may present in a similar manner.⁴⁴⁴ Currently, the gold-standard investigation for the diagnosis of albinism is 5-channel VEP testing. However, this time consuming investigation requires a specialist electrophysiology setup. OCT on the other hand is now an integral part of most ophthalmology clinics due to its application in the assessment of a wide variety of ophthalmic diseases. Therefore, it has the potential make the diagnosis of albinism easier and faster.

The degradation of vision in albinism is multifactorial. Currently, structural deficits of the visual pathway such as foveal hypoplasia, optic nerve abnormalities, and cortical changes are not modifiable. However, clinical trials have shown the efficacy of various pharmacological⁴⁴⁵⁻⁴⁴⁸ and surgical treatments^{358, 378, 449-451} to treat nystagmus. Our findings about the relationship between photoreceptor specialisation and visual acuity as well as the foveal hypoplasia grading system developed by the author in collaboration with other members of the research group will allow better clinical judgement regarding which patients will benefit most from intensive treatment.

Over the last few years, gene therapy has been shown to be a viable option in delivering treatment to the retina and optic nerve in a number of animal models of disease.⁴⁵²⁻⁴⁵⁷ Gargiulo et al. have demonstrated that adeno-associated virus based

vector can be used to deliver gene transfer therapy in the mouse model of OCA1. This treatment resulted in melanogenesis in the RPE and improvement in photoreceptor function.³⁹⁹ Similar results were achieved by Surace et al. in the mouse model of OA1.⁴⁵⁸ Recent clinical trials in Leber's congenital amaurosis have demonstrated the efficacy and safety of gene therapy in humans.^{459, 460}

These advances herald the beginning of an exciting era where treatment of hitherto untreatable abnormalities seems achievable. Our findings provide important baseline information regarding visual dysfunction in albinism and paint a picture of arrested development throughout the visual pathway. This indicates that any potential therapy needs to be applied in early childhood to be achieve maximum results, as the first five years of life represent a critical period in visual development.^{375, 461} Introduction of hand-held OCT allows monitoring of foveal development from birth onwards and will be a key tool to monitor the efficacy of any such treatments.^{368, 427, 429, 430}

4.4 LIMITATIONS AND FUTURE WORK

A major limitation of this study was a lack of genetic analysis available in the volunteers. As a result, we are unable to provide a definitive mutation based diagnosis and therefore subdivide them accordingly. As discussed in section 1.3.1, albinism is associated with a variety of genetic mutations, not all of which have yet been characterized.³³⁶ This leads a heterogeneity in phenotypical manifestations.⁴²

While conducting the current study, the author also collected saliva samples from the albinism patients that will be used in future genetic analysis. Such a genotype-phenotype correlation study would shed light on the precise impact of these mutations on patients with albinism. As the mutations impact at different levels in the melanin synthesis pathway, this will also enhance our understanding regarding what products of this pathway lead to the clinical picture we see in albinism and aid the development of any future treatments.

The use of a table-top OCT device meant that we were unable to image the retina in young children. This means that we cannot be sure about the time at which retinal development comes to a halt in albinism. This is exacerbated by the fact that this was a cross-sectional study based on a single visit, which meant that we are not able to say whether the abnormalities we find are static or dynamic. However, our group has recently shown the efficacy of hand-held OCT in monitoring normal foveal development⁴²⁷ and is in the process of applying the same methodology to carry out a prospective study of retinal development in young children with albinism.⁴²⁸

Another important future study would be to develop a prediction model for visual acuity that incorporates the various different affecting vision in albinism. Preliminary work in this regard by our group has been the subject of a previous conference presentation.⁴⁶² This will allow more accurate identification and monitoring of patients undergoing treatment for nystagmus or any other future therapies.

The comparative nature of this study meant that we have carried out multiple correlations to elucidate the relationships between various functional and anatomical abnormalities seen in albinism. This raises the possibility of type I error in our results.

To counter this, we used a hypothesis driven approach based on previous literature to carry out these comparisons. In addition, for each hypothesis where multiple comparisons were carried out using the same data, a Holm-Bonferroni correction has been applied. In the majority of cases, the relationships remained significant following the correction and are therefore unlikely to be caused by statistical anomalies. However, in cases where significance was marginal, such as comparison of DTI with VEP ($p=0.42$) we have been cautious with our interpretation of results.

4.5 FINAL CONCLUSION

In conclusion, this work enhances our understanding of visual deficits associated with albinism. Using multiple imagining modalities, we have described a number of known and novel structural abnormalities in our patient group and assessed the relationship of ocular abnormalities with those seen in the post-orbital visual pathway and to visual function.

We find that in albinism, normal development of the visual pathways appears to have halted prior to reaching completion. Patients with albinism show a range of defects that can range from resembling normality to being grossly atypical. This spectrum closely resembles stages in normal visual development.

The work has major immediate and future implications in the diagnosis and treatment of patients with albinism and improves our scientific knowledge about this complex yet fascinating condition.

REFERENCES

1. Huang D, Swanson EA, Lin CP, et al. Optical coherence tomography. *Science* 1991;254(5035):1178-81.
2. Fercher AF, Hitzenberger CK, Drexler W, et al. In vivo optical coherence tomography. *Am J Ophthalmol* 1993;116(1):113-4.
3. Coxson HO, Quiney B, Sin DD, et al. Airway wall thickness assessed using computed tomography and optical coherence tomography. *Am J Respir Crit Care Med* 2008;177(11):1201-6.
4. Gerckens U, Buellesfeld L, McNamara E, et al. Optical coherence tomography (OCT). potential of a new high-resolution intracoronary imaging technique. *Herz* 2003;28(6):496-500.
5. Evans CL, Rizvi I, Hasan T, et al. In vitro ovarian tumor growth and treatment response dynamics visualized with time-lapse OCT imaging. *Opt Express* 2009;17(11):8892-906.
6. Testoni PA, Mariani A, Mangiavillano B, et al. Intraductal optical coherence tomography for investigating main pancreatic duct strictures. *Am J Gastroenterol* 2007;102(2):269-74.
7. Drexler W, Fujimoto JG. State-of-the-art retinal optical coherence tomography. *Prog Retin Eye Res* 2008;27(1):45-88.
8. Sakata LM, Deleon-Ortega J, Sakata V, et al. Optical coherence tomography of the retina and optic nerve - a review. *Clin Experiment Ophthalmol* 2009;37(1):90-9.
9. van Velthoven ME, Faber DJ, Verbraak FD, et al. Recent developments in optical coherence tomography for imaging the retina. *Prog Retin Eye Res* 2007;26(1):57-77.
10. Costa RA, Skaf M, Melo LA, Jr, et al. Retinal assessment using optical coherence tomography. *Prog Retin Eye Res* 2006;25(3):325-53.
11. Hrynchak P, Simpson T. Optical coherence tomography: An introduction to the technique and its use. *Optom Vis Sci* 2000;77(7):347-56.
12. Schmitt JM. Optical coherence tomography (OCT): A review. *Selected Topics in Quantum Electronics, IEEE Journal of* 1999;5(4):1205-15.
13. Wojtkowski M, Srinivasan V, Fujimoto JG, et al. Three-dimensional retinal imaging with high-speed ultrahigh-resolution optical coherence tomography. *Ophthalmology* 2005;112(10):1734-46.

14. Hammer DX, Ferguson RD, Magill JC, et al. Active retinal tracker for clinical optical coherence tomography systems. *J Biomed Opt* 2005;10(2):024038.
15. Hammer D, Ferguson RD, Iftimia N, et al. Advanced scanning methods with tracking optical coherence tomography. *Opt Express* 2005;13(20):7937-47.
16. Thomas MG, Kumar A, Thompson JR, et al. Is high-resolution spectral domain optical coherence tomography reliable in nystagmus? *Br J Ophthalmol* 2013;97(4):534-6.
17. Hagmann P, Jonasson L, Deffieux T, et al. Fibertract segmentation in position orientation space from high angular resolution diffusion MRI. *Neuroimage* 2006;32(2):665-75.
18. Scherzinger AL, Hendee WR. Basic principles of magnetic resonance imaging--an update. *West J Med* 1985;143(6):782-92.
19. Habib J. Development & Optimization of Diffusion Tensor Imaging at High Field Strengths in Translational Research. Nottingham, UK: University of Nottingham; 2010.
20. MRI from Picture to Proton. 2nd ed. Cambridge: Cambridge University Press; 2007.
21. Brown MA. MRI : Basic Principles and Applications. 3rd ed. Hoboken, N.J. ; Chichester: Wiley-Liss; 2003.
22. Basser PJ, Mattiello J, LeBihan D. MR diffusion tensor spectroscopy and imaging. *Biophys J* 1994;66(1):259-67.
23. Pierpaoli C, Basser PJ. Toward a quantitative assessment of diffusion anisotropy. *Magn Reson Med* 1996;36(6):893-906.
24. Zhou D. Statistical Analysis of Diffusion Tensor Imaging. Nottingham, UK: University of Nottingham; 2010.
25. Jellison BJ, Field AS, Medow J, et al. Diffusion tensor imaging of cerebral white matter: A pictorial review of physics, fiber tract anatomy, and tumor imaging patterns. *AJNR Am J Neuroradiol* 2004;25(3):356-69.
26. Catani M, Howard RJ, Pajevic S, et al. Virtual in vivo interactive dissection of white matter fasciculi in the human brain. *Neuroimage* 2002;17(1):77-94.
27. Lazar M, Alexander AL. An error analysis of white matter tractography methods: Synthetic diffusion tensor field simulations. *Neuroimage* 2003;20(2):1140-53.
28. Hagler DJ, Jr, Ahmadi ME, Kuperman J, et al. Automated white-matter tractography using a probabilistic diffusion tensor atlas: Application to temporal lobe epilepsy. *Hum Brain Mapp* 2009;30(5):1535-47.

29. Istoc A, Habas C, Iba-Zizen MT, et al. Value of the functional neural tractography in the reconstruction of the visual pathways in DTMRI. *J Fr Ophtalmol* 2010;33(9):670-9.
30. Hofer S, Karaus A, Frahm J. Reconstruction and dissection of the entire human visual pathway using diffusion tensor MRI. *Front Neuroanat* 2010;415.
31. Ge M, Li S, Wang L, et al. The role of diffusion tensor tractography in the surgical treatment of pediatric optic chiasmatic gliomas. *J Neurooncol* 2015;122(2):357-66.
32. Zhang Y, Wan SH, Wu GJ, et al. Magnetic resonance diffusion tensor imaging and diffusion tensor tractography of human visual pathway. *Int J Ophthalmol* 2012;5(4):452-8.
33. Roebroek A, Galuske R, Formisano E, et al. High-resolution diffusion tensor imaging and tractography of the human optic chiasm at 9.4 T. *Neuroimage* 2008;39(1):157-68.
34. Kamali A, Hasan KM, Adapa P, et al. Distinguishing and quantification of the human visual pathways using high-spatial-resolution diffusion tensor tractography. *Magn Reson Imaging* 2014;32(7):796-803.
35. Cruz-Inigo AE, Ladizinski B, Sethi A. Albinism in africa: Stigma, slaughter and awareness campaigns. *Dermatol Clin* 2011;29(1):79-87.
36. Kinnear PE, Jay B, Witkop CJ, Jr. Albinism. *Surv Ophthalmol* 1985;30(2):75-101.
37. Levin AV, Stroh E. Albinism for the busy clinician. *J AAPOS* 2011;15(1):59-66.
38. Sarvananthan N, Surendran M, Roberts EO, et al. The prevalence of nystagmus: The leicestershire nystagmus survey. *Invest Ophthalmol Vis Sci* 2009;50(11):5201-6.
39. Hong ES, Zeeb H, Repacholi MH. Albinism in africa as a public health issue. *BMC Public Health* 2006;6212.
40. Duane TD, Tasman W, Jaeger EA, et al. *Duane's Ophthalmology*. Philadelphia, Pa.: Lippincott, Williams & Wilkins; 2006.
41. Orlow SJ. Albinism: An update. *Semin Cutan Med Surg* 1997;16(1):24-9.
42. King RA, Summers CG. Albinism. *Dermatol Clin* 1988;6(2):217-28.
43. Cooksey CJ, Garratt PJ, Land EJ, et al. Evidence of the indirect formation of the catecholic intermediate substrate responsible for the autoactivation kinetics of tyrosinase. *J Biol Chem* 1997;272(42):26226-35.
44. Montoliu L, Gronskov K, Wei AH, et al. Increasing the complexity: New genes and new types of albinism. *Pigment Cell Melanoma Res* 2014;27(1):11-8.

45. Elshatory YM. Albinism .
46. Tomita Y, Takeda A, Okinaga S, et al. Human oculocutaneous albinism caused by single base insertion in the tyrosinase gene. *Biochem Biophys Res Commun* 1989;164(3):990-6.
47. Rinchik EM, Bultman SJ, Horsthemke B, et al. A gene for the mouse pink-eyed dilution locus and for human type II oculocutaneous albinism. *Nature* 1993;361(6407):72-6.
48. Brilliant MH. The mouse p (pink-eyed dilution) and human P genes, oculocutaneous albinism type 2 (OCA2), and melanosomal pH. *Pigment Cell Res* 2001;14(2):86-93.
49. Chen K, Manga P, Orlow SJ. Pink-eyed dilution protein controls the processing of tyrosinase. *Mol Biol Cell* 2002;13(6):1953-64.
50. Manga P, Boissy RE, Pifko-Hirst S, et al. Mislocalization of melanosomal proteins in melanocytes from mice with oculocutaneous albinism type 2. *Exp Eye Res* 2001;72(6):695-710.
51. Toyofuku K, Valencia JC, Kushimoto T, et al. The etiology of oculocutaneous albinism (OCA) type II: The pink protein modulates the processing and transport of tyrosinase. *Pigment Cell Res* 2002;15(3):217-24.
52. Durham-Pierre D, Gardner JM, Nakatsu Y, et al. African origin of an intragenic deletion of the human P gene in tyrosinase positive oculocutaneous albinism. *Nat Genet* 1994;7(2):176-9.
53. Kato A, Fukai K, Oiso N, et al. A novel P gene missense mutation in a japanese patient with oculocutaneous albinism type II (OCA2). *J Dermatol Sci* 2003;31(3):189-192.
54. King RA, Lewis RA, Townsend D, et al. Brown oculocutaneous albinism. clinical, ophthalmological, and biochemical characterization. *Ophthalmology* 1985;92(11):1496-505.
55. Manga P, Kromberg JG, Box NF, et al. Rufous oculocutaneous albinism in southern african blacks is caused by mutations in the TYRP1 gene. *Am J Hum Genet* 1997;61(5):1095-101.
56. Boissy RE, Zhao H, Oetting WS, et al. Mutation in and lack of expression of tyrosinase-related protein-1 (TRP-1) in melanocytes from an individual with brown oculocutaneous albinism: A new subtype of albinism classified as "OCA3". *Am J Hum Genet* 1996;58(6):1145-56.

57. Gronskov K, Ek J, Brondum-Nielsen K. Oculocutaneous albinism. *Orphanet J Rare Dis* 2007;243.
58. Newton JM, Cohen-Barak O, Hagiwara N, et al. Mutations in the human orthologue of the mouse underwhite gene (*uw*) underlie a new form of oculocutaneous albinism, OCA4. *Am J Hum Genet* 2001;69(5):981-8.
59. Inagaki K, Suzuki T, Shimizu H, et al. Oculocutaneous albinism type 4 is one of the most common types of albinism in japan. *Am J Hum Genet* 2004;74(3):466-71.
60. Kausar, Bhatti, Ali, et al. OCA5, a novel locus for non-syndromic oculocutaneous albinism, maps to chromosome 4q24. *Clinical Genetics, Clin Genet* 2013;84(1):91-3.
61. Wei AH, Zang DJ, Zhang Z, et al. Exome sequencing identifies SLC24A5 as a candidate gene for nonsyndromic oculocutaneous albinism. *J Invest Dermatol* 2013;133(7):1834-40.
62. Ginger RS, Askew SE, Ogborne RM, et al. SLC24A5 encodes a trans-golgi network protein with potassium-dependent sodium-calcium exchange activity that regulates human epidermal melanogenesis. *J Biol Chem* 2008;283(9):5486-95.
63. Lamason RL, Mohideen MA, Mest JR, et al. SLC24A5, a putative cation exchanger, affects pigmentation in zebrafish and humans. *Science* 2005;310(5755):1782-6.
64. Gronskov K, Dooley CM, Ostergaard E, et al. Mutations in *c10orf11*, a melanocyte-differentiation gene, cause autosomal-recessive albinism. *Am J Hum Genet* 2013;92(3):415-21.
65. Montoliu L, Gronskov K, Wei AH, et al. Increasing the complexity: New genes and new types of albinism. *Pigment Cell Melanoma Res* 2014;27(1):11-8.
66. Bassi MT, Bergen AA, Bitoun P, et al. Diverse prevalence of large deletions within the OA1 gene in ocular albinism type 1 patients from europe and north america. *Hum Genet* 2001;108(1):51-4.
67. Bassi MT, Schiaffino MV, Renieri A, et al. Cloning of the gene for ocular albinism type 1 from the distal short arm of the X chromosome. *Nat Genet* 1995;10(1):13-9.
68. Fang S, Guo X, Jia X, et al. Novel GPR143 mutations and clinical characteristics in six chinese families with X-linked ocular albinism. *Mol Vis* 2008;14:1974-82.
69. Micale L, Augello B, Fusco C, et al. GPR143 mutational analysis in two italian families with X-linked ocular albinism. *Genet Test Mol Biomarkers* 2009;13(4):527-31.

70. Palmisano I, Bagnato P, Palmigiano A, et al. The ocular albinism type 1 protein, an intracellular G protein-coupled receptor, regulates melanosome transport in pigment cells. *Hum Mol Genet* 2008;17(22):3487-501.
71. d'Addio M, Pizzigoni A, Bassi MT, et al. Defective intracellular transport and processing of OA1 is a major cause of ocular albinism type 1. *Hum Mol Genet* 2000;9(20):3011-8.
72. Oetting WS. New insights into ocular albinism type 1 (OA1): Mutations and polymorphisms of the OA1 gene. *Hum Mutat* 2002;19(2):85-92.
73. Lam BL, Fingert JH, Shutt BC, et al. Clinical and molecular characterization of a family affected with X-linked ocular albinism (OA1). *Ophthalmic Genet* 1997;18(4):175-84.
74. Lang GE, Rott HD, Pfeiffer RA. X-linked ocular albinism. characteristic pattern of affection in female carriers. *Ophthalmic Paediatr Genet* 1990;11(4):265-71.
75. Schnur RE, Gao M, Wick PA, et al. OA1 mutations and deletions in X-linked ocular albinism. *Am J Hum Genet* 1998;62(4):800-9.
76. Scheinfeld NS. Syndromic albinism: A review of genetics and phenotypes. *Dermatol Online J* 2003;9(5):5.
77. Schneier AJ, Fulton AB. The hermansky-pudlak syndrome: Clinical features and imperatives from an ophthalmic perspective. *Semin Ophthalmol* 2013;28(5-6):387-91.
78. Wei AH, Li W. Hermansky-pudlak syndrome: Pigmentary and non-pigmentary defects and their pathogenesis. *Pigment Cell Melanoma Res* 2013;26(2):176-92.
79. Barbosa MD, Barrat FJ, Tchernev VT, et al. Identification of mutations in two major mRNA isoforms of the chediak-higashi syndrome gene in human and mouse. *Hum Mol Genet* 1997;6(7):1091-8.
80. Kaplan J, De Domenico I, Ward DM. Chediak-higashi syndrome. *Curr Opin Hematol* 2008;15(1):22-9.
81. Lozano ML, Rivera J, Sanchez-Guiu I, et al. Towards the targeted management of chediak-higashi syndrome. *Orphanet J Rare Dis* 2014;9:132,014-0132-6.
82. Griscelli C, Durandy A, Guy-Grand D, et al. A syndrome associating partial albinism and immunodeficiency. *Am J Med* 1978;65(4):691-702.
83. Kumar M, Sackey K, Schmalstieg F, et al. Griscelli syndrome: Rare neonatal syndrome of recurrent hemophagocytosis. *J Pediatr Hematol Oncol* 2001;23(7):464-8.

84. Pastural E, Barrat FJ, Dufourcq-Lagelouse R, et al. Griscelli disease maps to chromosome 15q21 and is associated with mutations in the myosin-va gene. *Nat Genet* 1997;16(3):289-92.
85. Kurugol Z, Ozkinay F, Vardar F, et al. Griscelli syndrome: Report of a case and review of the literature. *Pediatr Int* 2001;43(3):298-301.
86. Menasche G, Pastural E, Feldmann J, et al. Mutations in RAB27A cause griscelli syndrome associated with haemophagocytic syndrome. *Nat Genet* 2000;25(2):173-6.
87. Westbroek W, Klar A, Cullinane AR, et al. Cellular and clinical report of new griscelli syndrome type III cases. *Pigment Cell Melanoma Res* 2012;25(1):47-56.
88. Azuma N, Yamaguchi Y, Handa H, et al. Mutations of the PAX6 gene detected in patients with a variety of optic-nerve malformations. *Am J Hum Genet* 2003;72(6):1565-70.
89. Ihnatko R, Eden U, Fagerholm P, et al. Congenital aniridia and the ocular surface. *Ocul Surf* 2016;14(2):196-206.
90. Poulter JA, Al-Araimi M, Conte I, et al. Recessive mutations in SLC38A8 cause foveal hypoplasia and optic nerve misrouting without albinism. *Am J Hum Genet* 2013;93(6):1143-50.
91. Al-Araimi M, Pal B, Poulter JA, et al. A new recessively inherited disorder composed of foveal hypoplasia, optic nerve decussation defects and anterior segment dysgenesis maps to chromosome 16q23.3-24.1. *Mol Vis* 2013;19:2165-72.
92. Hu DN, Simon JD, Sarna T. Role of ocular melanin in ophthalmic physiology and pathology. *Photochem Photobiol* 2008;84(3):639-44.
93. Tibber MS, Whitmore AV, Jeffery G. Cell division and cleavage orientation in the developing retina are regulated by L-DOPA. *J Comp Neurol* 2006;496(3):369-81.
94. Ilia M, Jeffery G. Retinal mitosis is regulated by dopa, a melanin precursor that may influence the time at which cells exit the cell cycle: Analysis of patterns of cell production in pigmented and albino retinæ. *J Comp Neurol* 1999;405(3):394-405.
95. Summers CG. Albinism: Classification, clinical characteristics, and recent findings. *Optom Vis Sci* 2009;86(6):659-62.
96. Boston University.
97. Eagle RC, Jr. Iris pigmentation and pigmented lesions: An ultrastructural study. *Trans Am Ophthalmol Soc* 1988;86:581-687.

98. Sturm RA, Larsson M. Genetics of human iris colour and patterns. *Pigment Cell Melanoma Res* 2009;22(5):544-62.
99. Summers CG. Vision in albinism. *Trans Am Ophthalmol Soc* 1996;94:1095-155.
100. Sheth V, Gottlob I, Mohammad S, et al. Diagnostic potential of iris cross-sectional imaging in albinism using optical coherence tomography. *Ophthalmology* 2013;120(10):2082-90.
101. COURTNEY GR. Refractive problems of albinos. *Am J Optom Arch Am Acad Optom* 1965;42:88-93.
102. Wildsoet CF, Oswald PJ, Clark S. Albinism: Its implications for refractive development. *Invest Ophthalmol Vis Sci* 2000;41(1):1-7.
103. Sampath V, Bedell HE. Distribution of refractive errors in albinos and persons with idiopathic congenital nystagmus. *Optom Vis Sci* 2002;79(5):292-9.
104. Weiss AH, Kelly JP. Acuity development in infantile nystagmus. *Invest Ophthalmol Vis Sci* 2007;48(9):4093-9.
105. Wang J, Wyatt LM, Felius J, et al. Onset and progression of with-the-rule astigmatism in children with infantile nystagmus syndrome. *Invest Ophthalmol Vis Sci* 2010;51(1):594-601. Accessed 15/08/2011.
106. Gronskov K, Ek J, Sand A, et al. Birth prevalence and mutation spectrum in danish patients with autosomal recessive albinism. *Invest Ophthalmol Vis Sci* 2009;50(3):1058-64.
107. Perez-Carpinell J, Capilla P, Illueca C, et al. Vision defects in albinism. *Optom Vis Sci* 1992;69(8):623-8.
108. Grosvenor T. What causes astigmatism? *J Am Optom Assoc* 1976;47(7):926-32.
109. Grosvenor T. Etiology of astigmatism. *Am J Optom Physiol Opt* 1978;55(3):214-8.
110. Loshin DS, Browning RA. Contrast sensitivity in albinotic patients. *Am J Optom Physiol Opt* 1983;60(3):158-66.
111. Lennerstrand G. Strabismus and eye muscle function. *Acta Ophthalmol Scand* 2007;85(7):711-23.
112. Brodsky MC, Fray KJ. Positive angle kappa: A sign of albinism in patients with congenital nystagmus. *Am J Ophthalmol* 2004;137(4):625-9.
113. Tabernero J, Benito A, Nourrit V, et al. Instrument for measuring the misalignments of ocular surfaces. *Opt Express* 2006;14(22):10945-56.

114. Summers CG, Knobloch WH, Witkop CJ, Jr, et al. Hermansky-pudlak syndrome. ophthalmic findings. *Ophthalmology* 1988;95(4):545-54.
115. Putnam CM, Bland PJ. Macular pigment optical density spatial distribution measured in a subject with oculocutaneous albinism. *J Optom* 2014;7(4):241-5.
116. Bernstein PS, Khachik F, Carvalho LS, et al. Identification and quantitation of carotenoids and their metabolites in the tissues of the human eye. *Exp Eye Res* 2001;72(3):215-23.
117. Abadi RV, Cox MJ. The distribution of macular pigment in human albinos. *Invest Ophthalmol Vis Sci* 1992;33(3):494-7.
118. Whitehead AJ, Mares JA, Danis RP. Macular pigment: A review of current knowledge. *Arch Ophthalmol* 2006;124(7):1038-45.
119. Saidha S, Eckstein C, Ratchford JN. Optical coherence tomography as a marker of axonal damage in multiple sclerosis. *Int J Clin Rev* 2010;1001.
120. Davson H. *Physiology of the Eye*. New York: Academic Press; 1980.
121. Dowling JE. Organization of vertebrate retinas. *Invest Ophthalmol* 1970;9(9):655-80.
122. Livingstone M. Segregation of form, color, movement, and depth processing in the visual system: Anatomy, physiology, art, and illusion. *Res Publ Assoc Res Nerv Ment Dis* 1990;67:119-38.
123. Livingstone M, Hubel D. Segregation of form, color, movement, and depth: Anatomy, physiology, and perception. *Science* 1988;240(4853):740-9.
124. Croner LJ, Kaplan E. Receptive fields of P and M ganglion cells across the primate retina. *Vision Res* 1995;35(1):7-24.
125. Hendry SH, Yoshioka T. A neurochemically distinct third channel in the macaque dorsal lateral geniculate nucleus. *Science* 1994;264(5158):575-7.
126. Hendry SH, Reid RC. The koniocellular pathway in primate vision. *Annu Rev Neurosci* 2000;23:127-53.
127. Kandel EJ. *Principles of Neural Science*. 4th ed. East Norwalk, Conn.; Hemel Hempstead: Appleton & Lange; Prentice Hall; 1999.
128. Miller N, Walsh F, Hoyt WG. *Walsh and Hoyt's Clinical Neuro-Ophthalmology*. Philadelphia: Lippincott Williams & Wilkins; 2005.

129. Dubis AM, Hansen BR, Cooper RF, et al. Relationship between the foveal avascular zone and foveal pit morphology. *Invest Ophthalmol Vis Sci* 2012;53(3):1628-36.
130. Hendrickson AE, Yuodelis C. The morphological development of the human fovea. *Ophthalmology* 1984;91(6):603-12.
131. Tombran-Tink J, Barnstable CJ. *Visual Transduction and Non-Visual Light Perception (Ophthalmology Research)*. Humana Press.
132. Akeo K, Shirai S, Okisaka S, et al. Histology of fetal eyes with oculocutaneous albinism. *Arch Ophthalmol* 1996;114(5):613-6.
133. Usher CH. Histological examination of an adult human albino's eyeball, with a note on mesoblastic pigmentation in foetal eyes. *Biometrika* 1920;13(1):46-56. Available at <http://www.jstor.org/stable/2331723>.
134. Elschmig A. *Zur Anatomie Des Menschlichen Albinoauges*. - Springer-Verlag; 1913.
135. Naumann GO, Lerche W, Schroeder W. Foveolar aplasia in tyrosinase-positive oculocutaneous albinism (author's transl). *Albrecht Von Graefes Arch Klin Exp Ophthalmol* 1976;200(1):39-50.
136. Fulton AB, Albert DM, Craft JL. Human albinism. light and electron microscopy study. *Arch Ophthalmol* 1978;96(2):305-10.
137. Meyer CH, Lapolice DJ, Freedman SF. Foveal hypoplasia in oculocutaneous albinism demonstrated by optical coherence tomography. *Am J Ophthalmol* 2002;133(3):409-10.
138. Izquierdo NJ, Emanuelli A, Izquierdo JC, et al. Foveal thickness and macular volume in patients with oculocutaneous albinism. *Retina* 2007;27(9):1227-30.
139. Harvey PS, King RA, Summers CG. Spectrum of foveal development in albinism detected with optical coherence tomography. *J AAPOS* 2006;10(3):237-42.
140. Yaqoob Z, Wu J, Yang C. Spectral domain optical coherence tomography: A better OCT imaging strategy. *BioTechniques* 2005;39(6 Suppl):S6-13.
141. Chong GT, Farsiu S, Freedman SF, et al. Abnormal foveal morphology in ocular albinism imaged with spectral-domain optical coherence tomography. *Arch Ophthalmol* 2009;127(1):37-44.
142. Seo JH, Yu YS, Kim JH, et al. Correlation of visual acuity with foveal hypoplasia grading by optical coherence tomography in albinism. *Ophthalmology* 2007;114(8):1547-51.

143. Marmor MF, Choi SS, Zawadzki RJ, et al. Visual insignificance of the foveal pit: Reassessment of foveal hypoplasia as fovea plana. *Arch Ophthalmol* 2008;126(7):907-13.
144. McAllister JT, Dubis AM, Tait DM, et al. Arrested development: High-resolution imaging of foveal morphology in albinism. *Vision Res* 2010;50(8):810-7.
145. Mann I. *The Development of the Human Eye*. 3rd ed. British Medical Association; 1964.
146. Sing NM, Anderson SF, Townsend JC. The normal optic nerve head. *Optom Vis Sci* 2000;77(6):293-301.
147. Miller NR, Newman NJ. *Walsh and Hoyt's Clinical Neuro-Ophthalmology*. 5th ed. USA: Williams & Wilkins; 1998.
148. Heegaard S, Jensen OA, Prause JU. Structure of the vitread face of the monkey optic disc (macaca mulatta). SEM on frozen resin-cracked optic nerveheads supplemented by TEM and immunohistochemistry. *Graefes Arch Clin Exp Ophthalmol* 1988;226(4):377-83.
149. Sebag J. Anatomy and pathology of the vitreo-retinal interface. *Eye (Lond)* 1992;6 (Pt 6)(Pt 6):541-52.
150. Fine BS. *Ocular Histology : A Text and Atlas*. 2nd ed. Hagerstown ; London: Harper and Row; 1979.
151. Anderson DR, Hoyt WF. Ultrastructure of intraorbital portion of human and monkey optic nerve. *Arch Ophthalmol* 1969;82(4):506-30.
152. Anonymous Bergmeister's papilla - the retina reference . Accessed 6/14/2016.
153. Hayreh SS. Anatomy and physiology of the optic nerve head. *Trans Am Acad Ophthalmol Otolaryngol* 1974;78(2):OP240-54.
154. Hernandez MR, Luo XX, Igoe F, et al. Extracellular matrix of the human lamina cribrosa. *Am J Ophthalmol* 1987;104(6):567-76.
155. Hernandez MR, Igoe F, Neufeld AH. Extracellular matrix of the human optic nerve head. *Am J Ophthalmol* 1986;102(2):139-48.
156. Horton JC, Greenwood MM, Hubel DH. Non-retinotopic arrangement of fibres in cat optic nerve. *Nature* 1979;282(5740):720-2.
157. HUBEL DH, WIESEL TN. Receptive fields of optic nerve fibres in the spider monkey. *J Physiol* 1960;154:572-80.

158. Jeffery G. Distribution of uncrossed and crossed retinofugal axons in the cat optic nerve and their relationship to patterns of fasciculation. *Vis Neurosci* 1990;5(1):99-104.
159. Baker GE, Jeffery G. Distribution of uncrossed axons along the course of the optic nerve and chiasm of rodents. *J Comp Neurol* 1989;289(3):455-61.
160. Naito J. Retinogeniculate projection fibers in the monkey optic chiasm: A demonstration of the fiber arrangement by means of wheat germ agglutinin conjugated to horseradish peroxidase. *J Comp Neurol* 1994;346(4):559-71.
161. Naito J. Retinogeniculate projection fibers in the monkey optic nerve: A demonstration of the fiber pathways by retrograde axonal transport of WGA-HRP. *J Comp Neurol* 1989;284(2):174-86.
162. DEAN G, USHER CH. EXPERIMENTAL RESEARCH ON THE COURSE OF THE OPTIC FIBRES. *Brain* 1903;26(4):524-42.
163. BROUWER B, ZEEMAN WPC. THE PROJECTION OF THE RETINA IN THE PRIMARY OPTIC NEURON IN MONKEYS. *Brain* 1926;49(1):1-35.
164. Drager UC, Olsen JF. Origins of crossed and uncrossed retinal projections in pigmented and albino mice. *J Comp Neurol* 1980;191(3):383-412.
165. HOYT WF, LUIS O. Visual fiber anatomy in the infrageniculate pathway of the primate. *Arch Ophthalmol* 1962;68:94-106.
166. Guillery RW, Walsh C. Changing glial organization relates to changing fiber order in the developing optic nerve of ferrets. *J Comp Neurol* 1987;265(2):203-17.
167. Spedick MJ, Beauchamp GR. Retinal vascular and optic nerve abnormalities in albinism. *J Pediatr Ophthalmol Strabismus* 1986;23(2):58-63.
168. Schmitz B, Schaefer T, Krick CM, et al. Configuration of the optic chiasm in humans with albinism as revealed by magnetic resonance imaging. *Invest Ophthalmol Vis Sci* 2003;44(1):16-21.
169. Kaimbo DK. Tilted disc syndrome in congolese patients. *J Fr Ophtalmol* 2010;33(3):174-7.
170. Shinohara K, Moriyama M, Shimada N, et al. Analyses of shape of eyes and structure of optic nerves in eyes with tilted disc syndrome by swept-source optical coherence tomography and three-dimensional magnetic resonance imaging. *Eye (Lond)* 2013;27(11):1233,41; quiz 1242.

171. Park KA, Park SE, Oh SY. Long-term changes in refractive error in children with myopic tilted optic disc compared to children without tilted optic disc. *Invest Ophthalmol Vis Sci* 2013;54(13):7865-70.
172. Lee SY, Kim TW, Hwang JM, et al. Peripapillary retinal nerve fibre thickness profile with optical coherence tomography in congenital tilted disc syndrome. *Acta Ophthalmol* 2012;90(5):e412-3.
173. Kim TW, Kim M, Weinreb RN, et al. Optic disc change with incipient myopia of childhood. *Ophthalmology* 2012;119(1):21,6.e1-3.
174. Kumar A, Gottlob I, McLean RJ, et al. Clinical and oculomotor characteristics of albinism compared to FRMD7 associated infantile nystagmus. *Invest Ophthalmol Vis Sci* 2011;52(5):2306-13.
175. Fukuda Y, Sawai H, Watanabe M, et al. Nasotemporal overlap of crossed and uncrossed retinal ganglion cell projections in the japanese monkey (*macaca fuscata*). *J Neurosci* 1989;9(7):2353-73.
176. Hubel DH, Wiesel TN. Receptive fields and functional architecture of monkey striate cortex. *J Physiol* 1968;195(1):215-43.
177. O'Connell JE. The anatomy of the optic chiasma and heteronymous hemianopia. *J Neurol Neurosurg Psychiatry* 1973;36(5):710-23.
178. Whitnall SE. *The Anatomy of the Human Orbit*. Second Edition. ed. ; 1932.
179. Schaeffer JP. Some points in the regional anatomy of the optic pathway, with especial reference to tumors of the hypophysis cerebri and resulting ocular changes. *Anat Rec* 1924;28(4):243-79.
180. Jeffery G, Erskine L. Variations in the architecture and development of the vertebrate optic chiasm. *Prog Retin Eye Res* 2005;24(6):721-53.
181. Kupfer C, Chumbley L, Downer JC. Quantitative histology of optic nerve, optic tract and lateral geniculate nucleus of man. *J Anat* 1967;101(Pt 3):393-401.
182. Chalupa LM, Lia B. The nasotemporal division of retinal ganglion cells with crossed and uncrossed projections in the fetal rhesus monkey. *J Neurosci* 1991;11(1):191-202.
183. Baker GE, Jeffery G. Distribution of uncrossed axons along the course of the optic nerve and chiasm of rodents. *J Comp Neurol* 1989;289(3):455-61.
184. Baker GE. Prechiasmatic reordering of fibre diameter classes in the retinofugal pathway of ferrets. *Eur J Neurosci* 1990;2(1):24-33.

185. Baker GE, Reese BE. Chiasmatic course of temporal retinal axons in the developing ferret. *J Comp Neurol* 1993;330(1):95-104.
186. Day AL. Aneurysms of the ophthalmic segment. A clinical and anatomical analysis. *J Neurosurg* 1990;72(5):677-91.
187. Wilbrand I. Schema Des Verlaufs Der Sehnervenfasern Durch Das Chiasma. ; 1926.
188. Polyak S, Klüver H. The Vertebrate Visual System. University of Chicago Press; 1968.
189. Horton JC. Wilbrand's knee of the primate optic chiasm is an artefact of monocular enucleation. *Trans Am Ophthalmol Soc* 1997;95:579-609.
190. Lee JH, Tobias S, Kwon JT, et al. Wilbrand's knee: Does it exist? *Surg Neurol* 2006;66(1):11,7; discussion 17.
191. Wang LC, Dani J, Godement P, et al. Crossed and uncrossed retinal axons respond differently to cells of the optic chiasm midline in vitro. *Neuron* 1995;15(6):1349-64.
192. Marcus RC, Blazeski R, Godement P, et al. Retinal axon divergence in the optic chiasm: Uncrossed axons diverge from crossed axons within a midline glial specialization. *J Neurosci* 1995;15(5 Pt 2):3716-29.
193. Godement P, Salaun J, Mason CA. Retinal axon pathfinding in the optic chiasm: Divergence of crossed and uncrossed fibers. *Neuron* 1990;5(2):173-86.
194. Sretavan DW, Reichardt LF. Time-lapse video analysis of retinal ganglion cell axon pathfinding at the mammalian optic chiasm: Growth cone guidance using intrinsic chiasm cues. *Neuron* 1993;10(4):761-77.
195. Godement P, Wang LC, Mason CA. Retinal axon divergence in the optic chiasm: Dynamics of growth cone behavior at the midline. *J Neurosci* 1994;14(11 Pt 2):7024-39.
196. Garcia-Frigola C, Carreres MI, Vegar C, et al. Zic2 promotes axonal divergence at the optic chiasm midline by EphB1-dependent and -independent mechanisms. *Development* 2008;135(10):1833-41.
197. Herrera E, Brown L, Aruga J, et al. Zic2 patterns binocular vision by specifying the uncrossed retinal projection. *Cell* 2003;114(5):545-57.
198. Petros TJ, Rebsam A, Mason CA. Retinal axon growth at the optic chiasm: To cross or not to cross. *Annu Rev Neurosci* 2008;31:295-315.
199. Jeffery G. Retinal ganglion cell death and terminal field retraction in the developing rodent visual system. *Brain Res* 1984;315(1):81-96.

200. Godement P, Salaun J, Metin C. Fate of uncrossed retinal projections following early or late prenatal monocular enucleation in the mouse. *J Comp Neurol* 1987;255(1):97-109.
201. Apkarian P, Reits D, Spekrijse H, et al. A decisive electrophysiological test for human albinism. *Electroencephalogr Clin Neurophysiol* 1983;55(5):513-31.
202. Neveu MM, Jeffery G. Chiasm formation in man is fundamentally different from that in the mouse. *Eye (Lond)* 2007;21(10):1264-70.
203. Jeffery G. Architecture of the optic chiasm and the mechanisms that sculpt its development. *Physiol Rev* 2001;81(4):1393-414.
204. Brodsky MC, Glasier CM, Creel DJ. Magnetic resonance imaging of the visual pathways in human albinos. *J Pediatr Ophthalmol Strabismus* 1993;30(6):382-5.
205. Leventhal AG, Creel DJ. Retinal projections and functional architecture of cortical areas 17 and 18 in the tyrosinase-negative albino cat. *J Neurosci* 1985;5(3):795-807.
206. Guillery RW, Hickey TL, Kaas JH, et al. Abnormal central visual pathways in the brain of an albino green monkey (*cercopithecus aethiops*). *J Comp Neurol* 1984;226(2):165-83.
207. Spear PD, Kim CB, Ahmad A, et al. Relationship between numbers of retinal ganglion cells and lateral geniculate neurons in the rhesus monkey. *Vis Neurosci* 1996;13(1):199-203.
208. KUPPER C. The projection of the macula in the lateral geniculate nucleus of man. *Am J Ophthalmol* 1962;54:597-609.
209. Kaas JH, Guillery RW. The transfer of abnormal visual field representations from the dorsal lateral geniculate nucleus to the visual cortex in siamese cats. *Brain Res* 1973;59:61-95.
210. Kaas JH, Huerta MF, Weber JT, et al. Patterns of retinal terminations and laminar organization of the lateral geniculate nucleus of primates. *J Comp Neurol* 1978;182(3):517-53.
211. Kupfer C. The laminar pattern and distribution of cell size in the lateral geniculate nucleus of man. *J Neuropathol Exp Neurol* 1965;24(4):645-52.
212. Leventhal AG, Rodieck RW, Dreher B. Retinal ganglion cell classes in the old world monkey: Morphology and central projections. *Science* 1981;213(4512):1139-42.
213. Guillery RW, Okoro AN, Witkop CJ, Jr. Abnormal visual pathways in the brain of a human albino. *Brain Res* 1975;96(2):373-7.

214. Guillery RW, Casagrande VA, Oberdorfer MD. Congenitally abnormal vision in siamese cats. *Nature* 1974;252(5480):195-9.
215. Mcketton L, Kelly KR, Schneider KA. Abnormal lateral geniculate nucleus and optic chiasm in human albinism. *J Comp Neurol* 2014;522(11):2680-7.
216. Yamamoto A, Miki Y, Urayama S, et al. Diffusion tensor fiber tractography of the optic radiation: Analysis with 6-, 12-, 40-, and 81-directional motion-probing gradients, a preliminary study. *AJNR Am J Neuroradiol* 2007;28(1):92-6.
217. Funkhouser EB. The visual cortex, its localization, histological structure, and physiological function. *J Exp Med* 1915;21(6):617-28.
218. De Moraes CG. Anatomy of the visual pathways. *J Glaucoma* 2013;22 Suppl 5S2-7.
219. Sereno MI, Dale AM, Reppas JB, et al. Borders of multiple visual areas in humans revealed by functional magnetic resonance imaging. *Science* 1995;268(5212):889-93.
220. Inouye T. Die Sehstörungen Bei Schussverletzungen Der Kortikalen Sehsphäre, Nach Beobachtungen an Verwundeten Der Letzten Japanischen Kriege, Von Dr. Tatsuji Inouye... Leipzig: W. Engelmann; 1909.
221. HOLMES G, LISTER WT. DISTURBANCES OF VISION FROM CEREBRAL LESIONS, WITH SPECIAL REFERENCE TO THE CORTICAL REPRESENTATION OF THE MACULA. *Brain* 1916;39(1-2):34-73.
222. Engel SA, Rumelhart DE, Wandell BA, et al. fMRI of human visual cortex. *Nature* 1994;369(6481):525.
223. Engel SA, Glover GH, Wandell BA. Retinotopic organization in human visual cortex and the spatial precision of functional MRI. *Cereb Cortex* 1997;7(2):181-92.
224. DeYoe EA, Carman GJ, Bandettini P, et al. Mapping striate and extrastriate visual areas in human cerebral cortex. *Proc Natl Acad Sci U S A* 1996;93(6):2382-6.
225. Feldheim DA, O'Leary DD. Visual map development: Bidirectional signaling, bifunctional guidance molecules, and competition. *Cold Spring Harb Perspect Biol* 2010;2(11):a001768.
226. Wong RO, Meister M, Shatz CJ. Transient period of correlated bursting activity during development of the mammalian retina. *Neuron* 1993;11(5):923-38.
227. Hubel DH, Wiesel TN. Anatomical demonstration of columns in the monkey striate cortex. *Nature* 1969;221(5182):747-50.
228. HUBEL DH, WIESEL TN. Receptive fields, binocular interaction and functional architecture in the cat's visual cortex. *J Physiol* 1962;160:106-54.

229. Adams DL, Sincich LC, Horton JC. Complete pattern of ocular dominance columns in human primary visual cortex. *J Neurosci* 2007;27(39):10391-403.
230. Nauhaus I, Nielsen KJ. Building maps from maps in primary visual cortex. *Curr Opin Neurobiol* 2014;24(1):1-6.
231. Rabinowicz T, de Courten-Myers GM, Petetot JM, et al. Human cortex development: Estimates of neuronal numbers indicate major loss late during gestation. *J Neuropathol Exp Neurol* 1996;55(3):320-8.
232. Burek MJ, Oppenheim RW. Programmed cell death in the developing nervous system. *Brain Pathol* 1996;6(4):427-46.
233. Brody BA, Kinney HC, Kloman AS, et al. Sequence of central nervous system myelination in human infancy. I. an autopsy study of myelination. *J Neuropathol Exp Neurol* 1987;46(3):283-301.
234. Kinney HC, Brody BA, Kloman AS, et al. Sequence of central nervous system myelination in human infancy. II. patterns of myelination in autopsied infants. *J Neuropathol Exp Neurol* 1988;47(3):217-34.
235. Bourne JA. Unravelling the development of the visual cortex: Implications for plasticity and repair. *J Anat* 2010;217(4):449-68.
236. Boothe RG, Dobson V, Teller DY. Postnatal development of vision in human and nonhuman primates. *Annu Rev Neurosci* 1985;8:495-545.
237. WIESEL TN, HUBEL DH. Single-cell responses in striate cortex of kittens deprived of vision in one eye. *J Neurophysiol* 1963;26:1003-17.
238. Levin N, Dumoulin SO, Winawer J, et al. Cortical maps and white matter tracts following long period of visual deprivation and retinal image restoration. *Neuron* 2010;65(1):21-31.
239. von dem Hagen EA, Houston GC, Hoffmann MB, et al. Retinal abnormalities in human albinism translate into a reduction of grey matter in the occipital cortex. *Eur J Neurosci* 2005;22(10):2475-80.
240. Neveu MM, von dem Hagen E, Morland AB, et al. The fovea regulates symmetrical development of the visual cortex. *J Comp Neurol* 2008;506(5):791-800.
241. Jiang J, Zhu W, Shi F, et al. Thick visual cortex in the early blind. *J Neurosci* 2009;29(7):2205-11.

242. Bridge H, Cowey A, Ragge N, et al. Imaging studies in congenital anophthalmia reveal preservation of brain architecture in 'visual' cortex. *Brain* 2009;132(Pt 12):3467-80.
243. Bridge H, von dem Hagen EA, Davies G, et al. Changes in brain morphology in albinism reflect reduced visual acuity. *Cortex* 2014;56:64-72.
244. Ashburner J, Friston KJ. Voxel-based morphometry--the methods. *Neuroimage* 2000;11(6 Pt 1):805-21.
245. Whitwell JL. Voxel-based morphometry: An automated technique for assessing structural changes in the brain. *J Neurosci* 2009;29(31):9661-4.
246. Hutton C, Draganski B, Ashburner J, et al. A comparison between voxel-based cortical thickness and voxel-based morphometry in normal aging. *Neuroimage* 2009;48(2):371-80.
247. Bookstein FL. "Voxel-based morphometry" should not be used with imperfectly registered images. *Neuroimage* 2001;14(6):1454-62.
248. Jones DK, Symms MR, Cercignani M, et al. The effect of filter size on VBM analyses of DT-MRI data. *Neuroimage* 2005;26(2):546-54.
249. Voets NL, Hough MG, Douaud G, et al. Evidence for abnormalities of cortical development in adolescent-onset schizophrenia. *Neuroimage* 2008;43(4):665-75.
250. Honea R, Crow TJ, Passingham D, et al. Regional deficits in brain volume in schizophrenia: A meta-analysis of voxel-based morphometry studies. *Am J Psychiatry* 2005;162(12):2233-45.
251. Dale AM, Fischl B, Sereno MI. Cortical surface-based analysis. I. segmentation and surface reconstruction. *Neuroimage* 1999;9(2):179-94.
252. Fischl B, Sereno MI, Dale AM. Cortical surface-based analysis. II: Inflation, flattening, and a surface-based coordinate system. *Neuroimage* 1999;9(2):195-207.
253. Fischl B, Dale AM. Measuring the thickness of the human cerebral cortex from magnetic resonance images. *Proc Natl Acad Sci U S A* 2000;97(20):11050-5.
254. Dickerson BC, Fenstermacher E, Salat DH, et al. Detection of cortical thickness correlates of cognitive performance: Reliability across MRI scan sessions, scanners, and field strengths. *Neuroimage* 2008;39(1):10-8.
255. Scarpazza C, Sartori G, De Simone MS, et al. When the single matters more than the group: Very high false positive rates in single case voxel based morphometry. *Neuroimage* 2013;70:175-88.

256. Hubel DH, Wiesel TN. Aberrant visual projections in the siamese cat. *J Physiol* 1971;218(1):33-62.
257. Akerman CJ, Tolhurst DJ, Morgan JE, et al. Relay of visual information to the lateral geniculate nucleus and the visual cortex in albino ferrets. *J Comp Neurol* 2003;461(2):217-35.
258. Cooper ML, Blasdel GG. Regional variation in the representation of the visual field in the visual cortex of the siamese cat. *J Comp Neurol* 1980;193(1):237-53.
259. Schmolesky MT, Wang Y, Creel DJ, et al. Abnormal retinotopic organization of the dorsal lateral geniculate nucleus of the tyrosinase-negative albino cat. *J Comp Neurol* 2000;427(2):209-19.
260. Hoffmann MB, Dumoulin SO. Congenital visual pathway abnormalities: A window onto cortical stability and plasticity. *Trends Neurosci* 2015;38(1):55-65.
261. Berman NE, Payne BR. An exuberant retinocollicular pathway in siamese kittens: Effects of competition and abnormal activity on its maturation. *Brain Res* 1985;354(2):197-209.
262. Morland AB, Baseler HA, Hoffmann MB, et al. Abnormal retinotopic representations in human visual cortex revealed by fMRI. *Acta Psychol (Amst)* 2001;107(1-3):229-47.
263. Morland AB, Hoffmann MB, Neveu M, et al. Abnormal visual projection in a human albino studied with functional magnetic resonance imaging and visual evoked potentials. *J Neurol Neurosurg Psychiatry* 2002;72(4):523-6.
264. von dem Hagen EA, Hoffmann MB, Morland AB. Identifying human albinism: A comparison of VEP and fMRI. *Invest Ophthalmol Vis Sci* 2008;49(1):238-49.
265. Hoffmann MB, Tolhurst DJ, Moore AT, et al. Organization of the visual cortex in human albinism. *J Neurosci* 2003;23(26):8921-30.
266. Klemen J, Hoffmann MB, Chambers CD. Cortical plasticity in the face of congenitally altered input into V1. *Cortex* 2012;48(10):1362-5.
267. von dem Hagen EA, Houston GC, Hoffmann MB, et al. Pigmentation predicts the shift in the line of decussation in humans with albinism. *Eur J Neurosci* 2007;25(2):503-11.
268. Morgan JE, Henderson Z, Thompson ID. Retinal decussation patterns in pigmented and albino ferrets. *Neuroscience* 1987;20(2):519-35.

269. Hoffmann MB, Lorenz B, Morland AB, et al. Misrouting of the optic nerves in albinism: Estimation of the extent with visual evoked potentials. *Invest Ophthalmol Vis Sci* 2005;46(10):3892-8.
270. Wolynski B, Kanowski M, Meltendorf S, et al. Self-organisation in the human visual system--visuo-motor processing with congenitally abnormal V1 input. *Neuropsychologia* 2010;48(13):3834-45.
271. Kaule FR, Wolynski B, Gottlob I, et al. Impact of chiasma opticum malformations on the organization of the human ventral visual cortex. *Hum Brain Mapp* 2014;35(10):5093-105.
272. Neuroscience. 2nd ed. Sunderland, Mass. ; Great Britain: Sinauer Associates; 2001.
273. Walls GL. The evolutionary history of eye movements. *Vision Res* 1962;2(1-4):69-80.
274. Ditchburn RW. *Eye-Movements and Visual Perception*. Oxford: Clarendon Press; 1973.
275. Westheimer G, McKee SP. Visual acuity in the presence of retinal-image motion. *J Opt Soc Am* 1975;65(7):847-50.
276. Carpenter RHS. *Movements of the Eyes*. 2nd ed. Pion; 1988.
277. Mustari MJ, Ono S. Optokinetic eye movements. In: Squire LR, ed. *Encyclopedia of Neuroscience*. Oxford: Academic Press; 2009:285-93.
278. Delgado-García JM. Why move the eyes if we can move the head? *Brain Res Bull* 2000;52(6):475-82.
279. Baarsma E, Collewyn H. Vestibulo-ocular and optokinetic reactions to rotation and their interaction in the rabbit. *J Physiol* 1974;238(3):603-25.
280. Cassin B. *Dictionary of Eye Terminology*. 3rd ed. Gainesville, Fla.: Triad; 1997.
281. Luschei ES, Fuchs AF. Activity of brain stem neurons during eye movements of alert monkeys. *J Neurophysiol* 1972;35(4):445-61.
282. Jay MF, Sparks DL. Sensorimotor integration in the primate superior colliculus. II. coordinates of auditory signals. *J Neurophysiol* 1987;57(1):35-55.
283. Jay MF, Sparks DL. Auditory receptive fields in primate superior colliculus shift with changes in eye position. *Nature* 1984;309(5966):345-7.

284. Goldberg ME, Wurtz RH. Activity of superior colliculus in behaving monkey. II. effect of attention on neuronal responses. *J Neurophysiol* 1972;35(4):560-74.
285. Goldberg ME, Wurtz RH. Activity of superior colliculus in behaving monkey. I. visual receptive fields of single neurons. *J Neurophysiol* 1972;35(4):542-59.
286. Schiller PH, True SD, Conway JL. Deficits in eye movements following frontal eye-field and superior colliculus ablations. *J Neurophysiol* 1980;44(6):1175-89.
287. Keller EL. Participation of medial pontine reticular formation in eye movement generation in monkey. *J Neurophysiol* 1974;37(2):316-32.
288. Strassman A, Highstein SM, McCrea RA. Anatomy and physiology of saccadic burst neurons in the alert squirrel monkey. I. excitatory burst neurons. *J Comp Neurol* 1986;249(3):337-57.
289. Crawford J, Cadera W, Vilis T. Generation of torsional and vertical eye position signals by the interstitial nucleus of cajal. *Science* 1991;252(5012):1551 <last_page> 1553.
290. FUKUSHIMA K. The interstitial nucleus of cajal and its role in the control of movements of head and eyes. *Prog Neurobiol* 1987;29(2):107 <last_page> 192.
291. Robinson DA. Eye movement control in primates. *Science* 1968;161(3847):1219 <last_page> 1224.
292. Robinson DA. The use of control systems analysis in the neurophysiology of eye movements. *Annu Rev Neurosci* 1981;4:463-503.
293. Glasauer S. Neuro-ophthalmology; current models of the ocular motor system. 2007;158 <last_page> 174.
294. Yee RD, Daniels SA, Jones OW, et al. Effects of an optokinetic background on pursuit eye movements. *Invest Ophthalmol Vis Sci* 1983;24(8):1115-22.
295. Chawla D, Buechel C, Edwards R, et al. Speed-dependent responses in V5: A replication study. *Neuroimage* 1999;9(5):508-15.
296. Barton JJ, Simpson T, Kiriakopoulos E, et al. Functional MRI of lateral occipitotemporal cortex during pursuit and motion perception. *Ann Neurol* 1996;40(3):387-98.
297. Rosano C, Krisky CM, Welling JS, et al. Pursuit and saccadic eye movement subregions in human frontal eye field: A high-resolution fMRI investigation. *Cerebral Cortex* 2002;12(2):107 <last_page> 115.

298. Burke JP, O'Keefe M, Bowell R. Optic nerve hypoplasia, encephalopathy, and neurodevelopmental handicap. *Br J Ophthalmol* 1991;75(4):236-9.
299. Burke MR, Barnes GR. Sequence learning in two-dimensional smooth pursuit eye movements in humans. *J Vis* 2007;7(1):5.
300. Lencer R, Trillenber P. Neurophysiology and neuroanatomy of smooth pursuit in humans. *Brain Cogn* 2008;68(3):219-28.
301. Fisher SK, Ciuffreda KJ, Tannen B, et al. Stability of tonic vergence. *Invest Ophthalmol Vis Sci* 1988;29(10):1577-81.
302. Stark L, Kenyon RV, Krishnan VV, et al. Disparity vergence: A proposed name for a dominant component of binocular vergence eye movements. *Am J Optom Physiol Opt* 1980;57(9):606-9.
303. FINCHAM EF, WALTON J. The reciprocal actions of accommodation and convergence. *J Physiol* 1957;137(3):488-508.
304. Wick B, Bedell HE. Magnitude and velocity of proximal vergence. *Invest Ophthalmol Vis Sci* 1989;30(4):755-60.
305. Gamlin PD. Neural mechanisms for the control of vergence eye movements. *Ann N Y Acad Sci* 2002;956:264-72.
306. Fox JC. Nystagmus. *Yale J Biol Med* 1929;1(4):224-36.
307. Chung ST, Bedell HE. Velocity criteria for "foveation periods" determined from image motions simulating congenital nystagmus. *Optom Vis Sci* 1996;73(2):92-103.
308. Bedell HE. Sensitivity to oscillatory target motion in congenital nystagmus. *Invest Ophthalmol Vis Sci* 1992;33(5):1811-21.
309. Papageorgiou E, McLean RJ, Gottlob I. Nystagmus in childhood. *Pediatr Neonatol* 2014;.
310. McLean R, Gottlob I, Proudlock F. What we know about the generation of nystagmus and other ocular oscillations: Are we closer to identifying therapeutic targets? *Current Neurology and Neuroscience Reports* 2012;12(3):325-33. Available at <http://dx.doi.org/10.1007/s11910-012-0259-6>.
311. Dell'Osso LF, Daroff RB. Congenital nystagmus waveforms and foveation strategy. *Doc Ophthalmol* 1975;39(1):.
312. Dell'Osso LF, van der Steen J, Steinman RM, et al. Foveation dynamics in congenital nystagmus. I: Fixation. *Doc Ophthalmol* 1992;79(1):1-23.

313. Dell'Osso LF, Jacobs JB. An expanded nystagmus acuity function: Intra- and intersubject prediction of best-corrected visual acuity. *Doc Ophthalmol* 2002;104(3):249-76.
314. Abadi RV, Whittle J. The nature of head postures in congenital nystagmus. *Arch Ophthalmol* 1991;109(2):216-20.
315. Abadi RV, Pascal E. Periodic alternating nystagmus in humans with albinism. *Invest Ophthalmol Vis Sci* 1994;35(12):4080-6.
316. Baloh RW, Honrubia V, Konrad HR. Periodic alternating nystagmus. *Brain* 1976;99(1):11-26.
317. Abadi RV, Bjerre A. Motor and sensory characteristics of infantile nystagmus. *Br J Ophthalmol* 2002;86(10):1152-60.
318. Optican LM, Zee DS. A hypothetical explanation of congenital nystagmus. *Biol Cybern* 1984;50(2):119-34.
319. Jacobs JB, Dell'Osso LF. Congenital nystagmus: Hypotheses for its genesis and complex waveforms within a behavioral ocular motor system model. *J Vis* 2004;4(7):604-25.
320. Robinson DA. Integrating with neurons. *Annu Rev Neurosci* 1989;12:33-45.
321. Cannon SC, Robinson DA, Shamma S. A proposed neural network for the integrator of the oculomotor system. *Biol Cybern* 1983;49(2):127-36.
322. Akman OE, Broomhead DS, Clement RA, et al. Nonlinear time series analysis of jerk congenital nystagmus. *J Comput Neurosci* 2006;21(2):153-70. Available at <http://dx.doi.org/10.1007/s10827-006-7816-4>.
323. Broomhead DS, Clement RA, Muldoon MR, et al. Modelling of congenital nystagmus waveforms produced by saccadic system abnormalities. *Biol Cybern* 2000;82(5):391-9.
324. Barreiro AK, Bronski JC, Anastasio TJ. Bifurcation theory explains waveform variability in a congenital eye movement disorder. *J Comput Neurosci* 2009;26(2):321-9.
325. Yee RD, Baloh RW, Honrubia V. Study of congenital nystagmus: Optokinetic nystagmus. *Br J Ophthalmol* 1980;64(12):926-32.
326. Yamazaki A. Abnormalities of smooth pursuit and vestibular eye movements in congenital jerk nystagmus. *Ophthalmology*. Amsterdam: Excerpta Medica 1979;1162-5.

327. Harris C, Berry D. A developmental model of infantile nystagmus. *Semin Ophthalmol* 2006;21(2):63-9. Available at <http://dx.doi.org/10.1080/08820530600613746>.
328. Brodsky MC, Dell'Osso LF. A unifying neurologic mechanism for infantile nystagmus. *JAMA Ophthalmol* 2014;132(6):761-8.
329. Simpson JJ, Soodak RE, Hess R. The accessory optic system and its relation to the vestibulocerebellum. *Prog Brain Res* 1979;50:715-24.
330. Oyster CW, Simpson JJ, Takahashi ES, et al. Retinal ganglion cells projecting to the rabbit accessory optic system. *J Comp Neurol* 1980;190(1):49-61.
331. Simpson JJ, Leonard CS, Soodak RE. The accessory optic system. analyzer of self-motion. *Ann N Y Acad Sci* 1988;545:170-9.
332. Simpson JJ. The accessory optic system. *Annu Rev Neurosci* 1984;7:13-41.
333. Huang YY, Rinner O, Hedinger P, et al. Oculomotor instabilities in zebrafish mutant *belladonna*: A behavioral model for congenital nystagmus caused by axonal misrouting. *J Neurosci* 2006;26(39):9873-80.
334. Huber-Roggi SP, Chen CC, Grimm L, et al. Severity of infantile nystagmus syndrome-like ocular motor phenotype is linked to the extent of the underlying optic nerve projection defect in zebrafish *belladonna* mutant. *J Neurosci* 2012;32(50):18079-86.
335. Chen CC, Bockisch CJ, Olasagasti I, et al. Positive or negative feedback of optokinetic signals: Degree of the misrouted optic flow determines system dynamics of human ocular motor behavior. *Invest Ophthalmol Vis Sci* 2014;55(4):2297-306.
336. Hutton SM, Spritz RA. A comprehensive genetic study of autosomal recessive ocular albinism in caucasian patients. *Invest Ophthalmol Vis Sci* 2008;49(3):868-72.
337. Rohrschneider K. Determination of the location of the fovea on the fundus. *Invest Ophthalmol Vis Sci* 2004;45(9):3257-8.
338. Rohrschneider K, Gluck R, Kruse FE, et al. Location of the fovea at the fundus in relation to the optic nerve head. *Ophthalmologe* 1998;95(10):706-9.
339. Williams TD, Wilkinson JM. Position of the fovea centralis with respect to the optic nerve head. *Optom Vis Sci* 1992;69(5):369-77.
340. Thomas MG, Kumar A, Mohammad S, et al. Structural grading of foveal hypoplasia using spectral-domain optical coherence tomography: A predictor of visual acuity? *Ophthalmology* 2011;118(8):1653-60.

341. Witmer MT, Margo CE, Drucker M. Tilted optic disks. *Surv Ophthalmol* 2010;55(5):403-28.
342. Zangwill LM, Bowd C, Weinreb RN. Evaluating the optic disc and retinal nerve fiber layer in glaucoma. II: Optical image analysis. *Semin Ophthalmol* 2000;15(4):206-20.
343. Brant-Zawadzki M, Gillan GD, Nitz WR. MP RAGE: A three-dimensional, T1-weighted, gradient-echo sequence--initial experience in the brain. *Radiology* 1992;182(3):769-75.
344. Talairach J. Co-Planar Stereotaxic Atlas of the Human Brain : 3-Dimensional Proportional System : An Approach to Cerebral Imaging. Stuttgart: Thieme; 1988.
345. Fischl B, Sereno MI, Tootell RB, et al. High-resolution intersubject averaging and a coordinate system for the cortical surface. *Hum Brain Mapp* 1999;8(4):272-84.
346. Segonne F, Dale AM, Busa E, et al. A hybrid approach to the skull stripping problem in MRI. *Neuroimage* 2004;22(3):1060-75.
347. Destrieux C, Fischl B, Dale A, et al. Automatic parcellation of human cortical gyri and sulci using standard anatomical nomenclature. *Neuroimage* 2010;53(1):1-15.
348. Anonymous Visually evoked potentials by donnell J. creel – webvision . Accessed 6/22/2016.
349. Holmstrom G, Eriksson U, Hellgren K, et al. Optical coherence tomography is helpful in the diagnosis of foveal hypoplasia. *Acta Ophthalmol* 2009;.
350. Leung CK, Cheung CY, Weinreb RN, et al. Comparison of macular thickness measurements between time domain and spectral domain optical coherence tomography. *Invest Ophthalmol Vis Sci* 2008;49(11):4893-7.
351. Knight OJ, Chang RT, Feuer WJ, et al. Comparison of retinal nerve fiber layer measurements using time domain and spectral domain optical coherent tomography. *Ophthalmology* 2009;116(7):1271-7.
352. Carpineto P, Nubile M, Toto L, et al. Correlation in foveal thickness measurements between spectral-domain and time-domain optical coherence tomography in normal individuals. *Eye (Lond)* 2010;24(2):251-8.
353. Forooghian F, Cukras C, Meyerle CB, et al. Evaluation of time domain and spectral domain optical coherence tomography in the measurement of diabetic macular edema. *Invest Ophthalmol Vis Sci* 2008;49(10):4290-6.

354. Paunescu LA. Reproducibility of nerve fiber thickness, macular thickness, and optic nerve head measurements using StratusOCT. *Invest Ophthalmol Vis Sci* 2004;45(6):1716 <last_page> 1724.
355. Eriksson U, Holmstrom G, Alm A, et al. A population-based study of macular thickness in full-term children assessed with stratus OCT: Normative data and repeatability. *Acta Ophthalmol* 2008;.
356. Anonymous Comparison of macular thickness measurements between time domain and spectral domain optical coherence tomography -- leung et al. 49 (11): 4893 -- *investigative ophthalmology & visual science* . Accessed 5/23/2010.
357. Wolf AB, Rubin SE, Kodsi SR. Comparison of clinical findings in pediatric patients with albinism and different amplitudes of nystagmus. *J AAPOS* 2005;9(4):363-8. Accessed 26/11/2010.
358. Bagheri A, Aletaha M, Abrishami M. The effect of horizontal rectus muscle surgery on clinical and eye movement recording indices in infantile nystagmus syndrome. *Strabismus* 2010;18(2):58-64.
359. Springer AD. New role for the primate fovea: A retinal excavation determines photoreceptor deployment and shape. *Vis Neurosci* 1999;16(4):629-36.
360. Provis JM. Development of the primate retinal vasculature. *Prog Retin Eye Res* 2001;20(6):799-821.
361. Provis JM, Hendrickson AE. The foveal avascular region of developing human retina. *Arch Ophthalmol* 2008;126(4):507-11.
362. Provis JM, Sandercoe T, Hendrickson AE. Astrocytes and blood vessels define the foveal rim during primate retinal development. *Invest Ophthalmol Vis Sci* 2000;41(10):2827-36.
363. Springer AD, Hendrickson AE. Development of the primate area of high acuity, 3: Temporal relationships between pit formation, retinal elongation and cone packing. *Vis Neurosci* 2005;22(2):171-85.
364. Wu W, Peters WH,3rd, Hammer ME. Basic mechanical properties of retina in simple elongation. *J Biomech Eng* 1987;109(1):65-7.
365. Krebs IP, Krebs W. Discontinuities of the external limiting membrane in the fovea centralis of the primate retina. *Exp Eye Res* 1989;48(2):295-301.
366. Sandercoe TM, Geller SF, Hendrickson AE, et al. VEGF expression by ganglion cells in central retina before formation of the foveal depression in monkey retina: Evidence of developmental hypoxia. *J Comp Neurol* 2003;462(1):42-54.

367. Chui TY, Zhong Z, Song H, et al. Foveal avascular zone and its relationship to foveal pit shape. *Optom Vis Sci* 2012;89(5):602-10.
368. Dubis AM, Costakos DM, Subramaniam CD, et al. Evaluation of normal human foveal development using optical coherence tomography and histologic examination. *Arch Ophthalmol* 2012;130(10):1291-300.
369. Abramov I, Gordon J, Hendrickson A, et al. The retina of the newborn human infant. *Science* 1982;217(4556):265-7.
370. Diaz-Araya C, Provis JM. Evidence of photoreceptor migration during early foveal development: A quantitative analysis of human fetal retinae. *Vis Neurosci* 1992;8(6):505-14.
371. Yuodelis C, Hendrickson A. A qualitative and quantitative analysis of the human fovea during development. *Vision Res* 1986;26(6):847-55.
372. Gelfand MV, Hong S, Gu C. Guidance from above: Common cues direct distinct signaling outcomes in vascular and neural patterning. *Trends Cell Biol* 2009;19(3):99-110.
373. Hendrickson A. A morphological comparison of foveal development in man and monkey. *Eye (Lond)* 1992;6 (Pt 2)(Pt 2):136-44.
374. Bumsted K, Hendrickson A. Distribution and development of short-wavelength cones differ between macaca monkey and human fovea. *J Comp Neurol* 1999;403(4):502-16.
375. Hendrickson AE. Primate foveal development: A microcosm of current questions in neurobiology. *Invest Ophthalmol Vis Sci* 1994;35(8):3129-33.
376. Curcio CA, Allen KA, Sloan KR, et al. Distribution and morphology of human cone photoreceptors stained with anti-blue opsin. *J Comp Neurol* 1991;312(4):610-24.
377. Cornish EE, Natoli RC, Hendrickson A, et al. Differential distribution of fibroblast growth factor receptors (FGFRs) on foveal cones: FGFR-4 is an early marker of cone photoreceptors. *Mol Vis* 2004;101-14.
378. Thurtell MJ. Treatment of nystagmus. *Semin Neurol* 2015;35(5):522-6.
379. Rakic P, Riley KP. Overproduction and elimination of retinal axons in the fetal rhesus monkey. *Science* 1983;219(4591):1441-4.
380. Kasmann-Kellner B, Schafer T, Krick CM, et al. Anatomical differences in optic nerve, chiasma and tractus opticus in human albinism as demonstrated by standardised clinical and MRI evaluation. *Klin Monbl Augenheilkd* 2003;220(5):334-44.

381. Caprioli J, Miller JM. Optic disc rim area is related to disc size in normal subjects. *Arch Ophthalmol* 1987;105(12):1683-5.
382. Radius RL, Pederson JE. Laser-induced primate glaucoma. II. histopathology. *Arch Ophthalmol* 1984;102(11):1693-8.
383. Trivino A, Ramirez JM, Salazar JJ, et al. Immunohistochemical study of human optic nerve head astroglia. *Vision Res* 1996;36(14):2015-28.
384. Tasman WS, Jaeger EA. *The Wills Eye Hospital Atlas of Clinical Ophthalmology*. Philadelphia: Lippincott Williams & Wilkins; 2001.
385. Jeffery G, Kinsella B. Translaminar deficits in the retinae of albinos. *J Comp Neurol* 1992;326(4):637-44.
386. Sheth JU, Sharma A, Chakraborty S. Persistent hyaloid artery with an aberrant peripheral retinal attachment: A unique presentation. *Oman J Ophthalmol* 2013;6(1):58-60.
387. Azrak C, Campos-Mollo E, Lledo-Riquelme M, et al. Vitreous haemorrhage associated with persistent hyaloid artery. *Arch Soc Esp Oftalmol* 2011;86(10):331-4.
388. Lambert SR, Buckley EG, Lenhart PD, et al. Congenital fibrovascular pupillary membranes: Clinical and histopathologic findings. *Ophthalmology* 2012;119(3):634-41.
389. Pollard ZF. Treatment of persistent hyperplastic primary vitreous. *J Ophthalmic Nurs Technol* 1991;10(4):155-9.
390. Pollard ZF. Results of treatment of persistent hyperplastic primary vitreous. *Ophthalmic Surg* 1991;22(1):48-52.
391. Albe E, Escalona E, Rajagopal R, et al. Proteomic identification of activin receptor-like kinase-1 as a differentially expressed protein during hyaloid vascular system regression. *FEBS Lett* 2005;579(25):5481-6.
392. Albe E, Chang JH, Azar NF, et al. Proteomic analysis of the hyaloid vascular system regression during ocular development. *J Proteome Res* 2008;7(11):4904-13.
393. Saint-Geniez M, D'Amore PA. Development and pathology of the hyaloid, choroidal and retinal vasculature. *Int J Dev Biol* 2004;48(8-9):1045-58.
394. Gulati N, Eagle RC, Jr, Tasman W. Unoperated eyes with persistent fetal vasculature. *Trans Am Ophthalmol Soc* 2003;101:59,64; discussion 64-5.
395. Goldberg MF. Persistent fetal vasculature (PFV): An integrated interpretation of signs and symptoms associated with persistent hyperplastic primary vitreous (PHPV). LIV edward jackson memorial lecture. *Am J Ophthalmol* 1997;124(5):587-626.

396. JONES HE. Hyaloid remnants in the eyes of premature babies. *Br J Ophthalmol* 1963;47:39-44.
397. Shastri BS. Persistent hyperplastic primary vitreous: Congenital malformation of the eye. *Clin Experiment Ophthalmol* 2009;37(9):884-90.
398. Cockburn DM, Dwyer PS. Posterior persistent hyperplastic primary vitreous. *Am J Optom Physiol Opt* 1988;65(4):316-7.
399. Gargiulo A, Bonetti C, Montefusco S, et al. AAV-mediated tyrosinase gene transfer restores melanogenesis and retinal function in a model of oculo-cutaneous albinism type I (OCA1). *Mol Ther* 2009;17(8):1347-54.
400. Onojafe IF, Adams DR, Simeonov DR, et al. Nitisinone improves eye and skin pigmentation defects in a mouse model of oculocutaneous albinism. *J Clin Invest* 2011;121(10):3914-23.
401. Guibal C, Baker GE. Abnormal axons in the albino optic tract. *Invest Ophthalmol Vis Sci* 2009;50(12):5516-21.
402. Yucel YH, Gupta N, Kalichman MW, et al. Relationship of optic disc topography to optic nerve fiber number in glaucoma. *Arch Ophthalmol* 1998;116(4):493-7.
403. Sihota R, Sony P, Gupta V, et al. Diagnostic capability of optical coherence tomography in evaluating the degree of glaucomatous retinal nerve fiber damage. *Invest Ophthalmol Vis Sci* 2006;47(5):2006-10.
404. Robinson SR, Horsburgh GM, Dreher B, et al. Changes in the numbers of retinal ganglion cells and optic nerve axons in the developing albino rabbit. *Dev Brain Res* 1987;35(2):161-74.
405. Donatien P, Aigner B, Jeffery G. Variations in cell density in the ganglion cell layer of the retina as a function of ocular pigmentation. *Eur J Neurosci* 2002;15(10):1597-1602.
406. Stone J, Rowe MH, Campion JE. Retinal abnormalities in the siamese cat. *J Comp Neurol* 1978;180(4):773-82.
407. Jeffery G. The albino retina: An abnormality that provides insight into normal retinal development. *Trends Neurosci* 1997;20(4):165-9.
408. Neveu MM, Holder GE, Sloper JJ, et al. Optic chiasm formation in humans is independent of foveal development. *Eur J Neurosci* 2005;22(7):1825-9.

409. Drager UC. Birth dates of retinal ganglion cells giving rise to the crossed and uncrossed optic projections in the mouse. *Proc R Soc Lond B Biol Sci* 1985;224(1234):57-77.
410. Jeffery G. The retinal pigment epithelium as a developmental regulator of the neural retina. *Eye (Lond)* 1998;12 (Pt 3b)(Pt 3b):499-503.
411. Soong F, Levin AV, Westall CA. Comparison of techniques for detecting visually evoked potential asymmetry in albinism. *J AAPOS* 2000;4(5):302-10.
412. Wolbarsht ML, Walsh AW, George G. Melanin, a unique biological absorber. *Appl Opt* 1981;20(13):2184-6.
413. Chauhan DS, Marshall J. The interpretation of optical coherence tomography images of the retina. *Invest Ophthalmol Vis Sci* 1999;40(10):2332-42.
414. Goswami U. Neuroscience and education. *Br J Educ Psychol* 2004;74(Pt 1):1-14.
415. Huttenlocher PR, de Courten C. The development of synapses in striate cortex of man. *Hum Neurobiol* 1987;6(1):1-9.
416. Leuba G, Garey LJ. Evolution of neuronal numerical density in the developing and aging human visual cortex. *Hum Neurobiol* 1987;6(1):11-8.
417. Garey LJ. Structural development of the visual system of man. *Hum Neurobiol* 1984;3(2):75-80.
418. Bourgeois JP, Jastreboff PJ, Rakic P. Synaptogenesis in visual cortex of normal and preterm monkeys: Evidence for intrinsic regulation of synaptic overproduction. *Proc Natl Acad Sci U S A* 1989;86(11):4297-301.
419. Paus T. Growth of white matter in the adolescent brain: Myelin or axon? *Brain Cogn* 2010;72(1):26-35.
420. Fornari E, Knyazeva MG, Meuli R, et al. Myelination shapes functional activity in the developing brain. *Neuroimage* 2007;38(3):511-8.
421. Dorey SE, Neveu MM, Burton LC, et al. The clinical features of albinism and their correlation with visual evoked potentials. *Br J Ophthalmol* 2003;87(6):767-72.
422. Neveu MM, Jeffery G, Burton LC, et al. Age-related changes in the dynamics of human albino visual pathways. *Eur J Neurosci* 2003;18(7):1939-49.
423. Azuma N, Nishina S, Yanagisawa H, et al. PAX6 missense mutation in isolated foveal hypoplasia. *Nat Genet* 1996;13(2):141-2.

424. Holmström G, Bondeson M, Eriksson U, et al. ?Congenital? nystagmus may hide various ophthalmic diagnoses. *Acta Ophthalmol* 2013;n/a,n/a.
425. Thomas MG, Kumar A, Kohl S, et al. High-resolution in vivo imaging in achromatopsia. *Ophthalmology* 2011;118(5):882-7.
426. Thomas MG, Crosier M, Lindsay S, et al. Abnormal retinal development associated with FRMD7 mutations. *Hum Mol Genet* 2014;.
427. Lee H, Purohit R, Patel A, et al. In vivo foveal development using optical coherence tomography. *Invest Ophthalmol Vis Sci* 2015;56(8):4537-45.
428. Lee H, Purohit R, Sheth V, et al. Retinal development in albinism: A prospective study using optical coherence tomography in infants and young children. *Lancet* 2015;385 Suppl 1S14,6736(15)60329-4.
429. Lee H, Proudlock F, Gottlob I. Is handheld optical coherence tomography reliable in infants and young children with and without nystagmus? *Invest Ophthalmol Vis Sci* 2013;54(13):8152-9.
430. Lee H, Sheth V, Bibi M, et al. Potential of handheld optical coherence tomography to determine cause of infantile nystagmus in children by using foveal morphology. *Ophthalmology* 2013;120(12):2714-24.
431. Weiss AH, Biersdorf WR. Visual sensory disorders in congenital nystagmus. *Ophthalmology* 1989;96(4):517-23.
432. Gottlob I, Proudlock FA. Aetiology of infantile nystagmus. *Curr Opin Neurol* 2014;27(1):83-91.
433. Hertle RW. Nystagmus in infancy and childhood. *Semin Ophthalmol* 2008;23(5):307-17.
434. Chan WH, Biswas S, Ashworth JL, et al. Congenital and infantile cataract: Aetiology and management. *Eur J Pediatr* 2012;171(4):625-30.
435. Young MP, Heidary G, VanderVeen DK. Relationship between the timing of cataract surgery and development of nystagmus in patients with bilateral infantile cataracts. *J AAPOS* 2012;16(6):554-7.
436. Traber GL, Chen CC, Huang YY, et al. Albino mice as an animal model for infantile nystagmus syndrome. *Invest Ophthalmol Vis Sci* 2012;53(9):5737-47.
437. Huber-Reggi SP, Mueller KP, Straumann D, et al. Individual larvae of the zebrafish mutant belladonna display multiple infantile nystagmus-like waveforms that are influenced by viewing conditions. *Invest Ophthalmol Vis Sci* 2014;55(6):3971-8.

438. Dell'Osso LF, Williams RW, Jacobs JB, et al. The congenital and see-saw nystagmus in the prototypical achiasma of canines: Comparison to the human achiasmatic prototype. *Vision Res* 1998;38(11):1629-41.
439. Dell'Osso LF, Williams RW. Ocular motor abnormalities in achiasmatic mutant belgian sheepdogs: Unyoked eye movements in a mammal. *Vision Res* 1995;35(1):109-16.
440. Jacobs JB, Dell'Osso LF, Wang ZI, et al. Using the NAFX to measure the effectiveness over time of gene therapy in canine LCA. *Invest Ophthalmol Vis Sci* 2009;50(10):4685-92.
441. Leventhal AG. Evidence that retinal ganglion cell density affects foveal development. *Perspect Dev Neurobiol* 1996;3(3):203-11.
442. Pilat AV, Proudlock FA, Mohammad S, et al. Normal macular structure measured with optical coherence tomography across ethnicity. *Br J Ophthalmol* 2014;98(7):941-5.
443. Thomas MG. Genotype-Phenotype Studies in Infantile Nystagmus with Emphasis on the Novel FRMD7 Gene. Leicester, United Kingdom: University of Leicester; 2011.
444. Holmstrom G, Bondeson ML, Eriksson U, et al. 'Congenital' nystagmus may hide various ophthalmic diagnoses. *Acta Ophthalmol* 2014;92(5):412-6.
445. Hertle RW, Yang D, Adkinson T, et al. Topical brinzolamide (azopt) versus placebo in the treatment of infantile nystagmus syndrome (INS). *Br J Ophthalmol* 2015;99(4):471-6.
446. McLean RJ, Gottlob I. The pharmacological treatment of nystagmus: A review. *Expert Opin Pharmacother* 2009;10(11):1805-16.
447. McLean R, Proudlock F, Thomas S, et al. Congenital nystagmus: Randomized, controlled, double-masked trial of memantine/gabapentin. *Ann Neurol* 2007;61(2):130-8.
448. Shery T, Proudlock FA, Sarvananthan N, et al. The effects of gabapentin and memantine in acquired and congenital nystagmus: A retrospective study. *Br J Ophthalmol* 2006;90(7):839-43.
449. Hertle RW, Yang D, Adams K, et al. Surgery for the treatment of vertical head posturing associated with infantile nystagmus syndrome: Results in 24 patients. *Clin Experiment Ophthalmol* 2011;39(1):37-46.
450. Atilla H, Demir HD, Isikcelik Y. Long-term results of four horizontal rectus muscle recession in nystagmus treatment. *Strabismus* 2014;22(2):81-5.

451. Atilla H, Erkam N, Isikcelik Y. Surgical treatment in nystagmus. *Eye (Lond)* 1999;13 (Pt 1)(Pt 1):11-5.
452. Vandenberghe LH, Bell P, Maguire AM, et al. AAV9 targets cone photoreceptors in the nonhuman primate retina. *PLoS One* 2013;8(1):e53463.
453. Stieger K, Lheriteau E, Moullier P, et al. AAV-mediated gene therapy for retinal disorders in large animal models. *ILAR J* 2009;50(2):206-24.
454. Cideciyan AV, Rachel RA, Aleman TS, et al. Cone photoreceptors are the main targets for gene therapy of NPHP5 (IQCB1) or NPHP6 (CEP290) blindness: Generation of an all-cone Nphp6 hypomorph mouse that mimics the human retinal ciliopathy. *Hum Mol Genet* 2011;20(7):1411-23.
455. Lechauve C, Augustin S, Cwerman-Thibault H, et al. Neuroglobin gene therapy prevents optic atrophy and preserves durably visual function in harlequin mice. *Mol Ther* 2014;22(6):1096-109.
456. Murata T, Hoffmann S, Ishibashi T, et al. Retrovirus-mediated gene transfer targeted to retinal photocoagulation sites. *Diabetologia* 1998;41(5):500-6.
457. Du W, Tao Y, Deng WT, et al. Vitreal delivery of AAV vectored Cnga3 restores cone function in CNGA3-/-/nrl/- mice, an all-cone model of CNGA3 achromatopsia. *Hum Mol Genet* 2015;24(13):3699-707.
458. Surace EM, Domenici L, Cortese K, et al. Amelioration of both functional and morphological abnormalities in the retina of a mouse model of ocular albinism following AAV-mediated gene transfer. *Mol Ther* 2005;12(4):652-8.
459. Cideciyan AV, Aguirre GK, Jacobson SG, et al. Pseudo-fovea formation after gene therapy for RPE65-LCA. *Invest Ophthalmol Vis Sci* 2014;56(1):526-37.
460. Jacobson SG, Cideciyan AV, Ratnakaram R, et al. Gene therapy for leber congenital amaurosis caused by RPE65 mutations: Safety and efficacy in 15 children and adults followed up to 3 years. *Arch Ophthalmol* 2012;130(1):9-24.
461. Hendrickson A. A morphological comparison of foveal development in man and monkey. *Eye (Lond)* 1992;6 (Pt 2)(Pt 2):136-44.
462. Frank A. Proudlock, Sarim Mohammad, Viral Sheth, Anil Kumar, Rebecca J. McLean, Mervyn G. Thomas, Christopher Degg, Irene Gottlob. **Prediction of Visual Acuity in Albinism Based on Objective Measurements of Sensory and Motor Function.** ; 2011.

CHAPTER 5

APPENDICES

CONTENTS

A.	PATIENT INVITATION LETTER.....	244
B.	ADULT INFORMATION LEAFLET.....	245
C.	ADULT CONSENT FORM.....	249
D.	CHILDREN'S INFORMATION LEAFLET.....	252
E.	PARENT INFORMATION LEAFLET.....	253
F.	CHILDREN'S CONSENT FORM.....	257
G.	MRI INFORMATION LEAFLET.....	259
H.	GP LETTER	262
I.	MRI SAFETY QUESTIONNAIRE	264

A. PATIENT INVITATION LETTER

University Hospitals of Leicester



NHS Trust

Leicester Royal Infirmary

Leicester
LE1 5WW

Tel: 0116 2541414
Fax: 0116 2585631
Minicom: 0116 2586878

Clinical and Genetic Assessment of Nystagmus

LETTER OF INVITATION TO PARTICIPATE IN THE STUDY

Date

Dear member of the Nystagmus Network,

We would like to invite you to participate in a study in which we aim to identify genes in hereditary nystagmus forms. This may help in the future to allow genetic counseling and to better understand the mechanisms of nystagmus.


It would be of great help to us if as many as possible large and small families participate.

If you are interested in participating please answer the questions below and send this letter back in the enclosed self-addressed envelope. No stamp is necessary. We will then send you further information.

Yours sincerely,

Irene Gottlob
Professor of Ophthalmology

B. ADULT INFORMATION LEAFLET

University Hospitals of Leicester 
NHS Trust

Leicester Royal Infirmary
Leicester
LE1 5WW

Tel: 0116 2541414
Fax: 0116 2585631
Minicom: 0116 2586878

Clinical and Genetic Assessment of Nystagmus ADULT INFORMATION LEAFLET

Principal Investigator: Professor Irene Gottlob, Ophthalmology

We invite you to consider taking part in a research project. Before you decide it is important for you to understand why the research is being done and what it will involve. Please take time to read the following information carefully and discuss it with others if you wish. Ask us if there is anything that is not clear or if you would like more information. Take time to decide whether or not you wish to take part.

What is the purpose of the study?

Nystagmus, which is an eye condition, where the eyes are moving constantly, can cause visual problems. Sometimes no reason can be found for the problem, or it can be related to changes in the eye or nervous system. The cause of nystagmus is poorly understood. We are inviting you to take part in this study because we would like to identify genes, which are responsible for nystagmus. This may lead to a better understanding of the causes of nystagmus.

What will be involved if I take part in the study?

Firstly, we will ask details of your medical history. We will next ask for details of your relatives who suffer from similar condition so that we can construct a family tree.

We will then invite you for an eye examination including usual examinations such as visual acuity and color vision. We may also need to put drops in your eyes to dilate pupil to examine the back of eyes. To classify exactly the form of Nystagmus, we will record your eye movements by videotape and/or with infrared cameras. We may also take photographs of the back of the eye using a scanning light with an equipment called optical coherence tomography to compare the retinal thickness at various levels. If we think that it is possible that you have an underlying eye disease, we may request for further electrophysiological examinations of the function of the retina and the optic nerve. For these examinations, electrodes are stuck on skin and you are asked to look at light flashes or pattern stimuli. We will then ask you to consider providing us with a saliva (spit) or blood sample for these studies.

The eye examination, including the eye movement recordings, will take approximately one hour and can be completed during one visit. Additional electrophysiological tests would have to be arranged in a separate visit and would also take approximately one hour.

Eye movement recordings, retinal photographs and the electrophysiological tests are entirely safe and present no hazard.

If you undergo surgical procedure to improve the symptoms which involves strengthening or weakening of muscles around the eye, a small piece of the muscle is usually removed which is discarded. We would like to ask your permission to use this piece of muscle for genetic analysis to investigate into the gene causing the nystagmus and any associated defect of the muscle.

We would also like to perform a standard neurological examination checking your reflexes, strength and balance which will take about 5 minutes. In addition we would like to examine whether nystagmus has an influence on people's learning ability. This test will last approximately 30 minutes, during this time a researcher will interview you.

What is the benefit of this study to others and me?

The primary goal of this research is to identify genes causative of nystagmus and any defects in the muscle associated with it. This may not lead to direct benefits for nystagmus patients or their relatives. However, some families may wish to consider a gene test in the future. Knowledge of the normal function of the gene may lead to new approaches to both treatment and prevention of this condition.

Will information obtained in the study be confidential?

Any personal information and individual results will be kept confidential. The tests will be recorded in your medical records and will be treated with the usual degree of confidentiality under the data protection act. You will not be identified in any documents relating to the study. Normally, your GP will be informed of your participation in this study.

What will happen to the results of the research study?

The Saliva or blood sample and if you undergo surgery the tissue sample that you provide are for research purposes only, to help us find the gene that may cause nystagmus. This study may take two to five years to complete, the results will be published in medical journals, and your general practitioner and hospital specialist will be informed.

How will DNA samples be stored and maintained?

Saliva samples or Blood samples and muscle tissue (that would normally be discarded during a surgical procedure) will only be used for the purpose of this study. An advisory group composed of representatives involved in research, specialists in the care of patients with Nystagmus, and independent and lay members will oversee maintenance of the DNA samples.

Who is organizing and funding the research?

The National Health Service is sponsoring this study. The sponsors of this study will pay the ophthalmology department for including you in this study.

Who has reviewed the study?

All research that involves NHS patients or staff, information from NHS medical records or uses NHS patients or staff, information from NHS medical records or uses NHS premises or facilities must be approved by an NHS Research Ethics Committee before it goes ahead. Approval does not guarantee that you will not come to any harm if you take part. However, approval means that the Committee is satisfied that your rights will be respected, that any risks have been reduced to a minimum and balanced against possible benefits and that you have been given sufficient information on which to make an informed decision to take part or not.

This study has been reviewed by the Leicestershire, Northamptonshire and Rutland Research Ethics Committee 1, Research & Development Directorate, and The University of Hospitals [UHL] NHS Trust.

What if I am harmed by the study?

If you are harmed by taking part in this research project, there are no special compensation arrangements. If you are harmed due to someone's negligence, then you may have grounds for a legal action but you may have to pay for it. Regardless of this, if you wish to complain, or have any concerns about any aspect of the way you have been approached or treated during the course of this study, the normal National Health Service complaints mechanisms should be available to you.

Will I receive out of pocket expenses for taking part in the study?

Return travel expenses from your home to the Leicester Royal Infirmary will be reimbursed. You will not receive any payment for the tissue. The tissue is a gift - neither you nor your relatives will benefit from any inventions that result from the use of the tissue.

What happens if I do not wish to participate in this study or wish to withdraw from the study?

You are not under any obligation to participate in these studies. If you enter the study and subsequently wish to withdraw, please inform Professor Irene Gottlob, Ophthalmology. You don't need to give any reason for doing so. Medical care of both you and other members of your family will not be affected if you decide not to participate in the study.

Who do I contact for further information?
Professor Irene Gottlob
Ophthalmology,
The Robert Kilpatrick Clinical Sciences Building,
PO Box 65,
The Leicester Royal Infirmary,
Leicester,
LE2 7LX.

Tel: 0116 258 6291
Fax: 0116 225 8810
Thank you for reading this.

C. ADULT CONSENT FORM

Centre Number:
Study Number:
Patient
Identification
Number for this
trial:

University Hospitals of Leicester



NHS Trust

Leicester Royal Infirmary

Leicester
LE1 5WW

Tel: 0116 2541414
Fax: 0116 2585631
Minicom: 0116 2586878

Clinical and genetic assessment of Nystagmus

ADULT CONSENT FORM

Name of Researcher/Principal Investigator: Professor Irene Gottlob
Professor of Ophthalmology
0116 2586291

Name of Patient:
Address of Patient:
DOB of Patient:

This form shall be read in conjunction with the Adult Information Leaflet, Version 6 – August 2010.

Please **initial** the following box(es)

1. I confirm that I have read and understand the Information sheet dated August 2010, Version 6 for the above study and have had the opportunity to ask questions. ☐
2. I understand that I may withdraw my consent to my tissue being used at any time without justifying my decision and without affecting my normal care and medical management. ☐
3. I agree to donate the tissue samples as detailed below and allow their use in medical research as described in the Adult Information Leaflet. ☐
4. I understand that the tissue is a gift and that my child will not benefit from any intellectual properties that result from the use of the tissue. ☐
5. I agree / do not agree to my saliva / blood / tissue samples being used to undertake genetic research as described in the Adult Information Leaflet. (Patient to delete as applicable) ☐

6. I understand that if research using my tissues produces information, which has immediate clinical relevance to me, I will be informed by my hospital consultant or GP and be given an opportunity to discuss the results. ☐
7. I understand that sections of any of my medical notes may be looked at by responsible individuals from the research team, [Ophthalmology, University of Leicester] or from regulatory authorities where it is relevant to my taking part in research. I give permission for these individuals to have access to my records. ☐
8. I understand that saliva/ blood/ tissue samples and associated clinical data may be transferred to non-commercial research partners of the University Hospitals of Leicester NHS Trust and Ophthalmology, University of Leicester, but that the personal information will be removed prior to transfer. ☐
9. I agree to taking part in California Verbal learning test ☐
10. I agree to taking part in neurological examinations ☐
11. I agree to taking part in the following eye examinations:
(please tick if possible in box(es) below) ☐
- Eye examination ☐
 - Video recordings ☐
 - Photography ☐
 - Eye movement recordings ☐
12. The samples which I hereby consent to donate are:
(please tick if possible in box(es) below) ☐
- Blood ☐
 - Muscle tissue from outside the eye ☐
 - Saliva ☐
13. I agree to take part in undergoing Magnetic Resonance Imaging (MRI). If you agree to take part in MRI scan you will receive supplementary information leaflet specific for MRI scan, Version 2, August 2010. ☐
14. I agree to take part in the above study.

Signature of Patient _____

(Name in BLOCK LETTERS): _____

Date: _____

I confirm I have explained the nature of the Study, as detailed in the Adult Information Sheet, in terms, which in my judgment are suited to the understanding of the patient.

Signature of investigator: _____

(Name in BLOCK LETTERS): _____ Date: _____

Clinical and Genetic Assessment of Nystagmus

INFORMATION FOR CHILDREN

D. CHILDREN'S INFORMATION LEAFLET



We would like to examine you because we want to find out more about your or your family members eye movements. We would like to find out why giggly eyes (nystagmus) run in families. We would like to find out more about the gene, which is inherited, from your parents.

In this study, we may examine your eyes and record your eye movements with videotapes or tiny cameras fixed on glasses. We may also record electrical waves from your eyes and brain. For this, we will stick small wires on your skin or on your eye lid and ask you to look at light flashes and patterns. This does not hurt and we may numb your eyes with some drops. The examination will last between one and two hours. If you are tired you can tell us and we will let you rest. If you want you can stop the examination at any time.

We will ask you to give us some Spit sample (saliva) or swab from the mouth (buccal swab) or, blood from your arm, which may pinch a bit.

If you have any operation to improve your eyes, we would ask you to give us the tissue from the operation, so we can look at it under a microscope. This tissue is otherwise not used for anything.

If you take part you may help us to understand better giggly eyes.

Thank you very much for reading this.

Clinical and Genetic Assessment of Nystagmus

PARENT INFORMATION LEAFLET

Principal Investigator: Professor Irene Gottlob, Ophthalmology

We invite your child to consider taking part in a research project. Before your child decides, it is important for your child to understand why the research is being done and what it will involve. Please take time to read the following information carefully and discuss it with others if you wish. Ask us if there is anything that is not clear or if you would like more information. Take time to decide whether or not you wish your child to take part.

What is the purpose of the study?

Nystagmus, which is an eye condition, where the eyes are moving constantly, can cause visual problems. Sometimes no reason can be found for the problem, or it can be related to changes in the eye or nervous system. The cause of nystagmus is poorly understood. We are inviting your child to take part in this study because we would like to identify genes, which are responsible for nystagmus. This may lead to a better understanding of the causes of nystagmus.

What will be involved if I take part in the study?

Firstly, we will ask details of your Childs medical history. We will next ask for details of your relatives who suffer from similar condition so that we can construct a family tree. We will then invite your child for an eye examination including usual examinations such as visual acuity and color vision. We may also need to put drops in your Childs eyes to dilate pupil to examine the back of eyes. To classify exactly the form of Nystagmus, we will record your Childs eye movements by videotape and/or with infrared cameras.

We may also take the photographs of the back of the eye using a scanning light with a equipment called optical coherence tomography to compare the retinal thickness at various levels. If we think that it is possible that your child has an underlying eye

disease, we may request for further electrophysiological examinations of the function of the retina and the optic nerve. For these examinations, electrodes are stuck on child's skin and they are asked to look at light flashes or pattern stimuli. We will then ask you to consider providing us with saliva (spit) or blood sample or mouth swabs of your child for these studies.

The eye examination, including the eye movement recordings, will take approximately one hour and can be completed during one visit. Additional electrophysiological tests would have to be arranged in a separate visit and would also take approximately one hour.

Eye movement recordings, retinal photographs and the electrophysiological tests are entirely safe and present no hazard.

If your child undergoes surgical procedure to improve the symptoms which involves strengthening or weakening of muscles around the eye. During the operation, a small piece of the muscle is usually removed which is discarded. We would like to ask your permission to use this piece of muscle for genetic analysis to investigate into the gene causing the nystagmus and any associated defect of the muscle.

We would also like to perform a standard neurological examination checking your reflexes, strength and balance which will take about 5 minutes. In addition we would like to examine whether nystagmus has any influence on people's learning ability. This test will last approximately 30 minutes, during this time a researcher will interview you.

What is the benefit of this study to others and me?

The primary goal of this research is to identify genes causative of nystagmus and any defects in the muscle associated with it. This may not lead to direct benefits for nystagmus patients or their relatives. However, some families may wish to consider a gene test in the future. Knowledge of the normal function of the gene may lead to new approaches to both treatment and prevention of this condition.

Will information obtained in the study be confidential?

Any personal information and individual results will be kept confidential. The tests will be recorded in your child's medical records and will be treated with the usual degree of confidentiality under the data protection act. Your child will not be identified in any documents relating to the study. Normally, your child's GP will be informed of your participation in this study.

What will happen to the results of the research study?

The Saliva or blood sample and if the child undergoes surgery the tissue sample that your child provides are for research purposes only, to help us find the gene that may cause nystagmus. This study may take two to five years to complete, the results will be published in medical journals, and your child's general practitioner and hospital specialist will be informed.

How will DNA samples be stored and maintained?

Saliva samples or Blood samples or mouth swaps and muscle tissue (that would normally be discarded during a surgical procedure) will only be used for the purpose of this study. An advisory group composed of representatives involved in research, specialists in the care of patients with Nystagmus, and independent and lay members will oversee maintenance of the DNA samples.

Who is organizing and funding the research?

The National Health Service is sponsoring this study. The sponsors of this study will pay the ophthalmology department for including you in this study.

Who has reviewed the study?

All research that involves NHS patients or staff, information from NHS medical records or uses NHS patients or staff, information from NHS medical records or uses NHS premises or facilities must be approved by an NHS Research Ethics Committee before it goes ahead. Approval does not guarantee that you will not come to any harm if you take part. However, approval means that the Committee is satisfied that your rights will be respected, that any risks have been reduced to a minimum and balanced against possible benefits and that you have been given sufficient information on which to make an informed decision to take part or not.

This study has been reviewed by the Leicestershire, Northamptonshire and Rutland Research Ethics Committee 1, Research & Development Directorate, and The University of Hospitals [UHL] NHS Trust.

What if I am harmed by the study?

If your child is harmed by taking part in this research project, there are no special compensation arrangements. If your child is harmed due to someone's negligence, then your child may have grounds for a legal action but your family may have to pay for it. Regardless of this, if your child wishes to complain, or have any concerns about any aspect of the way your child and your family have been approached or treated during the course of this study, the normal National Health Service complaints mechanisms should be available to you and your child.

Will I receive out of pocket expenses for taking part in the study?

Return travel expenses from your home to the Leicester Royal Infirmary will be reimbursed. Your child will not receive any payment for the tissue. The tissue is a gift - neither your child nor your relatives will benefit from any inventions that result from the use of the tissue.

What happens if I do not wish to participate in this study or wish to withdraw from the study?

Your child is not under any obligation to participate in these studies. If your child enters the study and subsequently wish to withdraw, please inform Professor Irene Gottlob, Ophthalmology. Your child does not need to give any reason for doing so. Medical care of both your child and other members of your family will not be affected if your child decides not to participate in the study.

Who do I contact for further information?
Professor Irene Gottlob
Ophthalmology,
The Robert Kilpatrick Clinical Sciences Building,
PO Box 65,
The Leicester Royal Infirmary,
Leicester,
LE2 7LX.
Tel: 0116 258 6291
Fax: 0116 225 8810

Thank you for reading this.

F. CHILDREN'S CONSENT FORM

Centre Number:
Study Number:
Patient Identification
Number for this trial:

University Hospitals of Leicester



NHS Trust

Leicester Royal Infirmary
Leicester
LE1 5WW

Tel: 0116 2541414
Fax: 0116 2585631
Minicom: 0116 2586878

Clinical and genetic assessment of nystagmus

CHILD CONSENT FORM

Name of Researcher/Principal Investigator: Professor Irene Gottlob
Professor of Ophthalmology
0116 2586291

Name of Patient:
Address of Patient:
DOB of Patient:

This form shall be read in conjunction with the Parent Information Leaflet, Version 6, dated August 2010 and the Child Information Leaflet, Version 6, dated August 2010.

Please **initial** the following box(es)

1. I confirm that my child and I have read and understand the Information sheets dated August 2010, Version 6 for the above study and have had the opportunity to ask questions.
2. I understand that I may withdraw consent to my child's tissue being used at any time without justifying my child's decision and without affecting my child's and my family's normal care and medical management.
3. I agree to donate my child's tissue samples as detailed below and allow their use in medical research as described in the Parent/Child Information Leaflets.
4. I understand that the tissue is a gift and that my child will not benefit from any intellectual property that results from the use of the tissue.
5. I agree / do not agree for my child's saliva / buccal swab / blood sample / muscle tissue samples to be used to undertake genetic research as described in the Parent/Child Information Leaflet.

☐☐☐☐☐

6. I understand that if research using my child's tissues produces information, which has immediate clinical relevance to my child and my family, I and my child will be informed by my hospital consultant or GP, and be given an opportunity to discuss the results. ☐
7. I understand that sections of any of my child's medical notes may be looked at by responsible individuals from the research team, [Ophthalmology, University of Leicester] or from regulatory authorities where it is relevant to my taking part in research. I give permission for these individuals to have access to my child's records. ☐
8. I understand that saliva / buccal swab / blood sample / tissue samples and associated clinical data of my child may be transferred to non-commercial research partners of the University Hospitals of Leicester NHS Trust and Ophthalmology, University of Leicester, but that the personal information will be removed prior to transfer. ☐
9. I agree for my child to taking part in California verbal reading test ☐
10. I agree for my child to take part in neurological examinations ☐
11. I agree to taking part in the following eye examinations:
(please tick if possible in box(es) below) ☐
- Eye examination ☐
 - Video recordings ☐
 - Photography ☐
 - Eye movement recordings ☐
12. The samples which my child hereby consents to donate are:
(please tick if possible in box(es) below) ☐
- Blood ☐
 - Muscle tissue from outside the eye ☐
 - Saliva / buccal swab ☐
13. I agree to take part in undergoing Magnetic Resonance Imaging (MRI).
If you agree to take part in MRI scan you will receive supplementary information leaflet specific for MRI scan Version 2, August 2010 ☐
14. My child agrees to take part in the above study. ☐

Signature of Patient: _____

(Name in BLOCK LETTERS): _____

Date: _____

Clinical and Genetic Assessment of Nystagmus

SUPPLEMENTARY ADULT INFORMATION LEAFLET FOR MRI SCAN

Principal Investigator: Professor Irene Gottlob, Ophthalmology

We invite you to consider taking part in a research project which is part of the study "Clinical and genetic assessment of nystagmus". This part of the study will be performed on a specialized scanner in Nottingham. Before you decide it is important for you to understand why the research is being done and what it will involve. Please take time to read the following information carefully and discuss it with others if you wish. Ask us if there is anything that is not clear or if you would like more information. Take time to decide whether or not you wish to take part.

What is the purpose of the study?

Nystagmus, which is an eye condition, where the eyes are moving constantly, can cause visual problems. Sometimes no reason can be found for the problem, or it can be related to changes in the eye or nervous system. The cause of nystagmus is poorly understood. We are inviting you to take part in this study because we would like to see whether there are any differences in the parts of the brains that control eye movements between people with and without nystagmus. This may lead to a better understanding of the causes of nystagmus.

What will be involved if I take part in the study?

Prior to or on attendance, you will be asked to complete the MRI scan safety questionnaire. Provided that there are no reasons identified in the questionnaire why you should not have the MRI scan, you will then have the MRI scan. This involves lying in the MRI scanner for a period of not more than 45 minutes while we acquire the brain scan images. While in the scanner you will have protective earplugs or earphones on as MRI scanners can be quite noisy.

Most people undergo MRI scanning without any difficulty, but if you need to you will be able to contact the MRI technician at any time during the scan via an intercom or with an emergency buzzer. Following the MRI scan your participation in the study is

complete. There are no blood tests and there is no requirement to take any medications.

What is the benefit of this study to me and others?

The primary goal of this research is to identify if there are differences in the parts of the brain responsible for eye movements in nystagmus. This may not lead to direct benefits for nystagmus patients or their relatives.

What are the possible disadvantages and risks of taking part?

Provided you do not have condition which prevents you from having an MRI scan, there are no risks associated with this scan. You will be screened for conditions preventing you from having an MRI scan before you have the scan.

The MRI scanner is a relatively enclosed space and occasionally participants can feel claustrophobic. During the scan you are able to speak to the researchers performing the scan. If you would like to come out of the scanner at any time, you can request this. If you know that you are claustrophobic, we would advise against you participating.

In the unlikely event that an unsuspected abnormality is identified on the scan by one of the researchers, the images will be reviewed by a qualified consultant neuroradiologist (a doctor who specializes in looking at brain scans) working with the research team. If the suspicion of a significant abnormality is confirmed, the research team leader (who is a practicing doctor) will contact you to let you know, and may arrange further tests or referral to another specialist, if this is required. The research team leader will also contact your GP to let them know of the findings. The finding of a significant unexpected abnormality may have benefits in that it may be possible to offer treatments earlier than would otherwise have been possible. However, participants should also be aware that the finding of significant abnormality may adversely effect employment and insurance status.

Will information obtained in the study be confidential?

Any personal information and individual results will be kept confidential. The results of the MRI scan will be recorded in your medical records and will be treated with the usual degree of confidentiality under the data protection act. You will not be identified in any documents relating to the study. Normally your GP will be informed that you take part in the study.

What will happen to the results of the research study?

The images obtained during MRI scanning will be stored safely and only available to researchers directly involved in this study. This study may take two to five years to complete, the results will be published in medical journals, and your general practitioner and hospital specialist will be informed.

Who is organizing and funding the research?

The National Health Service is sponsoring this study. The sponsors of this study will pay the ophthalmology department for including you in this study.

Who has reviewed the study?

All research that involves NHS patients or staff, information from NHS medical records or uses NHS patients or staff, information from NHS medical records or uses NHS premises or facilities must be approved by an NHS Research Ethics Committee before it goes ahead. Approval does not guarantee that you will not come to any harm if you take part. However, approval means that the Committee is satisfied that your rights will be respected, that any risks have been reduced to a minimum and balanced against possible benefits and that you have been given sufficient information on which to make an informed decision to take part or not.

This study has been reviewed by the Leicestershire, Northamptonshire and Rutland Research Ethics Committee 1, Research & Development Directorate, and The University of Hospitals [UHL] NHS Trust.

What if I am harmed by the study?

If you are harmed by taking part in this research project, there are no special compensation arrangements. If you are harmed due to someone's negligence, then you may have grounds for a legal action but you may have to pay for it. Regardless of this, if you wish to complain, or have any concerns about any aspect of the way you have been approached or treated during the course of this study, the normal National Health Service complaints mechanisms should be available to you.

Will I receive out of pocket expenses for taking part in the study?

Return travel expenses from your home to the Hospital will be reimbursed. You will not receive any payment for your time.

What happens if I do not wish to participate in this study or wish to withdraw from the study?


You are not under any obligation to participate in these studies. If you enter the study and subsequently wish to withdraw, please inform Professor Irene Gottlob, Ophthalmology. You don't need to give any reason for doing so. Medical care of both you and other members of your family will not be affected if you decide not to participate in the study.

Who do I contact for further information?

Professor Irene Gottlob
Ophthalmology,
The Robert Kilpatrick Clinical Sciences Building,
PO Box 65,
The Leicester Royal Infirmary,
Leicester,
LE2 7LX.

Tel: 0116 258 6291
Fax: 0116 225 8810

H. GP LETTER

University Hospitals of Leicester 
NHS Trust

Leicester Royal Infirmary
Leicester
LE1 5WW

Tel: 0116 2541414
Fax: 0116 2585631
Minicom: 0116 2586878

Re: Patients Name

Date

Dear Dr

The above named patient or family member of a patient with Nystagmus, has agreed to participate in a study examining the clinics and genetics of hereditary nystagmus forms.

In the study we will first obtain, by history, a family tree with affected and non-affected family members. We then would like to perform a complete ophthalmologic examination including visual acuity, color vision, pupillary reflexes, slit lamp examination and fundus examination with pupil dilation.

We may in addition record the eye movements on videotape and with infrared cameras and obtain electrophysiological examinations such as electroretinograms, electrooculograms and visual evoked potentials. These examinations are all used routinely in patients with nystagmus and are completely harmless. If all examinations are performed it will require one or two hours examination time. However, the patient may rest or stop the examinations at any time.

For genetic analysis we would like to obtain a blood sample or alternatively a mouth swab. However, blood samples will allow us better analysis.

In addition to above tests we may also perform MRI, to identify if there are differences in parts of the brain responsible for eye movements in Nystagmus, and we would like to perform a standard neurological examination and cognitive function (California Verbal Learning Test (2nd Edition)) in some patients with different subtypes of nystagmus.

Please do not hesitate to contact me if you have any questions, or would like to know more information.

Yours sincerely,

Irene Gottlob

Professor of Ophthalmology

I. MRI SAFETY QUESTIONNAIRE



The University of
Nottingham

Sir Peter Mansfield Magnetic Resonance Centre

MR Volunteer Safety Screening Questionnaire:

NAME	Date of Scan	Date of Birth
ADDRESS	Volunteer Number	
	Ethics Code	
Phone number	Weight	Height if applicable

MR scanning uses strong magnetic fields. For your own safety and the safety of others it is **very important** that you do not go into the magnet halls with any metal in or on your body or clothing. Please answer the following questions carefully and ask if anything is not clear. All information is held in the strictest confidence.

1. Do you have any implants in your body? e.g. replacement joints, drug pumps Y/N
2. Do you have aneurysm clips (clips put around blood vessels during surgery)? Y/N
3. Do you have a pacemaker or artificial heart valve? *(These stop working near MR Scanners)* Y/N
4. Have you ever had any surgery? Please give brief details over. Y/N
(We do not need to know about uncomplicated caesarean delivery, vasectomy or termination of pregnancy)
5. Do you have any foreign bodies in your body (e.g. shrapnel)? Y/N
6. Have you ever worked in a machine tool shop without eye protection? Y/N
7. Do you wear a hearing aid or cochlear implant? Y/N
8. Could you be pregnant? (Pregnancy tests are available in the female toilets) Y/N
9. Have you ever suffered from tinnitus? Y/N
10. Do you wear dentures, a dental plate or a brace? Y/N
11. Are you susceptible to claustrophobia? Y/N
12. Do you suffer from blackouts, epilepsy or fits? Y/N
13. Do you have any tattoos? (If yes, you may be asked to read and sign another form) Y/N
14. Do you have any body piercing jewellery that cannot be removed? Y/N
15. Do you have any skin patches (trans-dermal patches)? Y/N
16. Do you have a coil in place (IUD) for contraception? Do you know what type? Y/N
17. Do you have any condition that may affect your ability to control your temperature ? Y/N
(e.g. Do you have a fever, cardiovascular disease, hypertension, diabetes or cerebrovascular disease?)
18. Will you remove all metal including coins, body-piercing jewellery, false-teeth, hearing aids etc. before entering the magnet hall? *(lockers available by the changing rooms)* Y/N
19. Is there anything else you think we should know? Y/N

I have read and understood all the questions	
Signature:	Date:
Verified by: Scanner Operator/MR Assistant Signature :	Date